DOCTORAL THESIS

A systematic investigation of the asymptotic giant branches of globular clusters using multi-object spectroscopy

Author:
Benjamin MACLEAN
B.Sc. (Hons)

Supervisors:
Dr. Simon CAMPBELL
Prof. John LATTANZIO
Dr. Gayandhi DE SILVA

A thesis submitted in fulfilment of the requirements for the degree of Doctor of Philosophy

in the

School of Physics and Astronomy

May 7, 2018

Copyright Notice

© Benjamin MacLean 2018

Under the Copyright Act 1968, this thesis must be used only under the normal conditions of scholarly fair dealing. In particular no results or conclusions should be extracted from it, nor should it be copied or closely paraphrased in whole or in part without the written consent of the author. Proper written acknowledgement should be made for any assistance obtained from this thesis. I certify that I have made all reasonable efforts to secure copyright permissions for third-party content included in this thesis and have not knowingly added copyright content to my work without the author's permission.

Declaration of Authorship

I, BENJAMIN MACLEAN, hereby declare that this thesis contains no material which has been accepted for the award of any other degree or diploma at any university or equivalent institution and that, to the best of my knowledge and belief, this thesis contains no material previously published or written by another person, except where due reference is made in the text of the thesis.

This thesis includes three original manuscripts that have been published in peer reviewed journals, and one manuscript that has been submitted for publication. The core theme of the thesis is 'observations of AGB stars in globular clusters'. The ideas, development and writing up of all the papers in the thesis were the principal responsibility of myself, the student, working within the School of Physics and Astronomy under the supervision of Dr. Simon Campbell.

The inclusion of co-authors reflects the fact that the work came from active collaboration between researchers and acknowledges input into team-based research.

I have renumbered sections, equations, and figures of the published papers in order to generate a consistent presentation within the thesis. In the case of Chapters 2, 3, 4, and 5, my contribution to the work involved is described in the following table on Page v.

Student signature: [redacted] Date: May 7, 2018

The undersigned hereby certify that the above declaration correctly reflects the nature and extent of the student's and co-authors' contributions to this work. In instances where I am not the responsible author I have consulted with the responsible author to agree on the respective contributions of the authors.

Main Supervisor signature: [redacted] Date: May 7, 2018

Thesis Chapter	Publication Title	Status	Nature and % of student contribution	Co-author names, nature and % of contribution	Co-authors(s), Monash student Y/N
2	An extreme paucity of second population AGB stars in the 'normal' globular cluster M 4	Published (MNRAS, July 2016)	80% – Concept, analysing data and manuscript authoring.	Simon Campbell: 15% – Concept, result interpretation, manuscript input. Others: 5% – Research advice, manuscript input.	N
3	NGC 6752 AGB Stars Revisited: Improved AGB temperatures remove apparent overionisation of Fe I	Published (A&A, Sept 2017)	40% – Concept, data analysis, result interpretation, input into manuscript	Simon Campbell: 50% – Concept, data analysis, result interpretation and manuscript authoring. Others: 10% – Research advice, manuscript input.	N
4	AGB subpopulations in the nearby globular cluster NGC 6397	Published (MNRAS, March 2018)	85% – Concept, analysing data, result interpretation, and manuscript authoring.	Simon Campbell: 10% – Research advice/input, manuscript input. Others: 5% – Research advice, manuscript input.	N
5	On the AGB stars of M 4: A robust disagreement between spectroscopic observations and theory	Submitted (MNRAS, May 2018)	70% – Concept, data analysis, result interpretation, and manuscript authoring.	Simon Campbell: 20% – Concept, result interpretation, input into manuscript. Others: 10% – Data analysis, research advice, manuscript input.	N

Abstract

In this thesis, we investigate asymptotic giant branch (AGB) stars within Galactic globular clusters (GCs). It has been well established that GCs contain multiple populations of stars, identified by an intrinsic spread in star-to-star abundances of light elements. These populations have been observed mostly using red giant branch (RGB) stars. Recent literature has suggested that in a given GC, AGB stars may display abundance distributions that differ from those seen among the RGB stars of the cluster. While some small differences are predicted by stellar evolutionary theory, the disparity between the giant branches in some GCs is much larger than expected. Primarily using high-resolution spectra, we explore this phenomenon further by providing new observations of AGB and RGB stars in GCs, and investigating details of the spectroscopic method and its application to low-mass AGB stars.

We developed a new spectroscopic analysis pipeline for this study. Using this pipeline we determine stellar parameters and a range of elemental abundances for samples of AGB and RGB stars in three GCs: M 4, NGC 6752, and NGC 6397. Using the abundances of Na, O, Mg, and Al, we analysed the relative distributions of these species between the RGB and AGB samples for each cluster. We find that AGB stars in M 4 and NGC 6752 have significantly lower abundances of Na compared to the respective RGB samples, indicating that the most Na-enhanced stars in these clusters appear to be missing from the AGB. In contrast, we find identical distributions of elemental abundances between the AGB and RGB in NGC 6397.

It is generally accepted that Na abundance correlates with effective temperature on the horizontal branch (HB), while stellar theory predicts that very hot stars on the HB do not ascend the AGB. To quantify this precisely, we calculate a suite of stellar models, and make predictions as to the proportion of stars that are expected to avoid the AGB. For M 4 and NGC 6752, we find that the avoidance rates we infer from observations of stellar abundances are much higher than those predicted by the models. Thus we identify a disparity between observations and theoretical expectations of the distribution of abundances in GC AGB stars.

We attempt to resolve this disagreement through extensive tests of our spectroscopic method, but find Na abundances to be very robust and reliable – the discrepancy between observation and theory remains. Finally, we suggest some potential avenues for future research into this phenomenon of Na-rich AGB star deficits in GCs.

Publications

Refereed

1. **MacLean, B. T.**; Campbell, S. W.; De Silva, G. M.; Lattanzio, J.; D'Orazi, V.; Simpson, J. D.; Momany, Y. (2016). "An extreme paucity of second population AGB stars in the 'normal' globular cluster M 4", *Monthly Notices of the Royal Astronomical Society*, 460, L69.

2. Campbell, S. W.; **MacLean, B. T.**; D'Orazi, V.; Casagrande, L.; de Silva, G. M.; Yong, D.; Cottrell, P. L.; Lattanzio, J. C. (2017). "NGC 6752 AGB stars revisited – I. Improved AGB temperatures remove apparent overionisation of Fe I" *Astronomy & Astrophysics*, 605, A98.

3. **MacLean, B. T.**; Campbell, S. W.; De Silva, G. M.; Lattanzio, J.; D'Orazi, V.; Cottrell, P. L.; Momany, Y.; Casagrande, L. (2018). "AGB subpopulations in the nearby globular cluster NGC 6397", *Monthly Notices of the Royal Astronomical Society*, 475, 257.

Submitted

1. **MacLean, B. T.**; Campbell, S. W.; Amarsi, A. M. ; Nordlander, T.; Cottrell, P. L.; De Silva, G. M.; Lattanzio, J.; Constantino, T.; D'Orazi, V.; Casagrande, L. (2018). "On the AGB stars of M 4: A robust disagreement between spectroscopic observations and theory", *Monthly Notices of the Royal Astronomical Society*, Submitted.

Non-refereed

1. Kuehn, Charles A.; Stello, Dennis; Campbell, Simon; Drury, Jason; de Silva, Gayandhi; **MacLean, Ben**; Bedding, Timothy R.; Huber, Daniel (2016). "K2 and M 4: A Unique Opportunity to Unlock the Mysteries of Globular Clusters", *American Astronomical Society*, AAS Meeting #227, 144.13.

2. Campbell, S. W.; Constantino, T. N.; D'Orazi, V.; Meakin, C.; Stello, D.; Christensen-Dalsgaard, J.; Kuehn, C.; De Silva, G. M.; Arnett, W. D.; Lattanzio, J. C.; **MacLean, B. T.** (2016). "Towards 21st century stellar models: Star clusters, supercomputing and asteroseismology", *Astronomische Nachrichten*, 337, 788.

Acknowledgements

First and foremost, I would like to acknowledge my primary supervisor, Dr. Simon Campbell. I was lucky in many aspects on my Ph.D., but none more so than having Simon as my teacher, research partner, advisor, and friend. Despite being half a world away for 2.5 years of my candidature, he was never out of reach, and put a huge amount of faith in me which I will greatly appreciate. I couldn't possibly quantify the amount of my work that he has read (and re-read, and re-re-read), with seemingly unlimited patience. Simon's advice, expertise, and skill have made me a better scientist and I will always be extremely thankful that I have had the opportunity to work with, and alongside him.

I would also like to thank my co-supervisors Prof. John Lattanzio and Dr. Gayandhi De Silva. They have been my supervisors since my Honours project in 2014, and I am so glad that I have had them as an indispensable resource of scientific knowledge, advice, and friendship for several years. It was John and Gayandhi who first saw my potential, and after Honours offered to help find a Ph.D. project that was right for me – something I will always be thankful for, and will never forget.

I thank the collaborators and co-authors (both local and international) that I have worked with throughout my time at Monash, all of whom have had a part in helping me get to the end, and produce some great science: Valentina D'Orazi, Peter Cottrell, Jeffery Simpson, Anish Amarsi, Thomas Nordlander, Luca Casagrande, Thomas Constantino, and Yazan Momany.

I have been at Monash University since 2009 and throughout my time here I have interacted with, and been aided by, many academic and administrative staff. For their parts in my journey, and in no particular order, I would like to thank Michael Brown, Duncan Galloway, Andrew Casey, Alex Heger, Amanda Karakas, Jean Pettigrew, Alina Donea, and JJ Eldridge. I would also like to thank Monash University, the School of Physics and Astronomy, and the Monash Centre for Astrophysics for giving me the opportunity to achieve my goals, and the Monash Stellar Interiors and Nucleosynthesis (SINS) group for their inclusion over the years. This research was supported by an Australian Government Research Training Program (RTP) Scholarship.

Over my doctoral candidature I have forged more than a few valued friendships, whose companionship I hope to appreciate for many more years. Specifically I would like to acknowledge Vaishali Purkash, Rebecca Nealon, Tyone Woods, Cheryl Woynarski, Kate and Douglas Jackson, Athira Menon, Melanie Ham, Timothy Dolley, Adelle Goodwin, and Carolyn Doherty. I would also like to thank my family, both the one I have adopted and the one I was born into, for their ongoing love and support – especially my sistas.

Finally, and most importantly, I would like to thank my best friend, my partner in crime, certainly my better half, and the love of my life: my wife Grace. It is difficult to put into words how important Grace is to me – in fact, I can hardly envision my life without her. Without her immeasurable love, her unwavering support, and pure existence, I would never have completed this thesis. Every aspect of my life is better with Grace in it, and she has walked by my side for every step in this journey. I am thankful beyond words for the companionship we have shared, and hope to have her by my side for every journey I am yet to begin.

For Chloe.

Contents

List of Abbreviations

MS	Main sequence
RGB	Red giant branch
HB	Horizontal branch
AGB	Asymptotic giant branch
EW	Equivalent width
GC	Globular cluster
SP1/2	Subpopulation one/two
CMD	Colour-magnitude diagram
T_{eff}	Effective temperature
log g	Surface gravity
v_t	Microturbulent velocity

Recurring citations

I99	Ivans et al. (1999)
SB05	Smith and Briley (2005)
Mar08	Marino et al. (2008)
C09	Carretta et al. (2009b)
L11	Lind et al. (2011b)
C13	Campbell et al. (2013)
ML16	**MacLean et al. (2016)**
L16	Lapenna et al. (2016)
Mar17	Marino et al. (2017)
W17	Wang et al. (2017)
C17	**Campbell, MacLean, et al. (2017)**
ML18a	**MacLean et al. (2018a)**
ML18b	**MacLean et al. (2018b)**

"All that is gold does not glitter,
Not all those who wander are lost;
The old that is strong does not wither,
Deep roots are not reached by the frost."

J. R. R. Tolkien

Dedicated to my wife, Grace

Chapter 1

Introduction

An understanding of the evolution of stars, and the processes that occur during this evolution, are a vital component of our comprehension of the world around us, and our own existence within the vast universe that we see beyond our terrestrial home. Before our planet began producing life, and before the Sun and other stars lit up the sky, the universe was dominated by energy in the form of photons. Through a process known as big bang nucleosynthesis, much of this energy was then converted into protons and electrons, which in turn combined to form free hydrogen and helium nuclei. Over time, gravitational perturbations in this primordial soup drew these atoms together, first into giant clouds of gas, and later fragmenting and contracting further to form stars: spherical coalescences of hydrogen and helium, existing in a state of both hydrostatic equilibrium – a steady balance of gravitational contraction and internal pressure – and constant change – where atoms in the core violently collide to form new elements through nucleosynthesis, driving the star along a steady evolutionary path.

Through 13.5 billion years of this amazing process – whereby stars steadily convert hydrogen and helium into a vast diversity of chemical species – the universe that we experience every day came into being.

For this reason alone, to understand our own universal origin, we are motivated to scientifically investigate the stars. But to continue as humankind has for countless millennia – venturing to understand the workings of the mysterious night sky, how it came to be, and where it will take us in the future – is just as noble a pursuit.

While this thesis will investigate only a minute section of the almost endless story of the universe and its wonders, the questions asked within cover an important part of the Galaxy's history, and through these we hope to increase our broader understanding of the physics and evolution of stars.

1.1 The evolution and nucleosynthetic processes of low-mass stars

1.1.1 Formation and Main Sequence

When a cloud of gas contracts to form a star, one of the most important features to consider is the amount of gas that becomes gravitationally bound; i.e., the mass of the proto-star. This simple value – that can range from anywhere between ~ 0.08 to 300 (and potentially even up to 10^5) times the mass of our Sun (Kippenhahn and Weigert, 1990) – will be the single most important property of the star. It will determine how long it will live, which evolutionary phases the star will experience, and ultimately the way in which it will contribute to the chemical history of its host cluster and galaxy.

For the purpose of this thesis (which will be detailed in §1.2), we will consider only the formation, evolution, and chemical contributions of low-mass stars – those with a mass of $M \lesssim 8M_\odot$ – and primarily discuss stars with a mass of $M \sim 0.8M_\odot$ (representative of present day Galactic globular cluster and halo stars). These stars have much longer lives than stars with higher masses, and do not end their evolution with supernovae (Woosley et al., 2002; Heger et al., 2003). Low-mass stars vastly out-number high-mass stars, and an understanding of their evolution is vital to our understanding of the universe and its history. Note that the stellar masses indicated throughout this section are the initial mass – the stellar mass as it was at the beginning of the main sequence (stars lose mass throughout their lives).

Just as any star, one of low-mass (such as those observed in thesis) will form in the gravitational well of a contracting gas cloud (usually a smaller portion of a large gas cloud that has undergone fragmentation; Larson, 2003), composed mostly of hydrogen and helium. The mass, density and temperature at the centre of the potential well will increase, forming a proto-star that will continue to contract and accrete material from the surrounding cloud. The core will increase in temperature until it reaches $\sim$1 MK, when nuclear fusion is enabled (Eddington, 1926; Iben, 1965).

At the onset of nuclear fusion (the star will begin to combine individual protons into more complex nuclei, including hydrogen-2 and helium-3 (Clayton, 1983). This process, however, will not release enough energy to support the star against further gravitation contraction, nor prevent additional material accreting onto the star. When the core reaches $\sim$10 MK, hydrogen burning via the pp-chain, which ultimately converts hydrogen into helium-4, will overtake as the dominant source of energy and internal pressure (Hansen et al., 2004). The H-burning CNO-cycle may also begin when the core reaches slightly higher temperatures (see Figure 1.1 for H-burning energy generation at varying core temperatures).

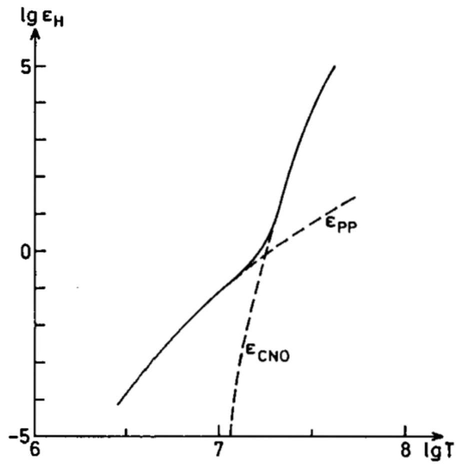

FIGURE 1.1: Energy generation rates (erg g^{-1} s^{-1}) of the pp chain and CNO cycles (dashed lines) as a function of stellar core temperature (K), and the total rate for hydrogen burning (solid line). Adapted from Kippenhahn and Weigert (1990), Figure 18.8.

At this point the stellar core will emit enough radiation to prevent further contraction and accretion – it will join the Main Sequence (MS; Figure 1.2) where the star will steadily convert hydrogen to helium in its core (Iben, 1967). The stars investigated in this thesis remain on the MS for more than 10 billion years. This is by far the longest phase of evolution, making it the most populated region of a stellar cluster's colour-magnitude diagram (CMD; see Figure 1.2).

1.1.2 Post-MS evolution

Red Giant Branch

After ~10 Gyrs of steady fusion in the core, when its innermost region has finally been exhausted of hydrogen, the low-mass star will evolve off the main sequence – the core will contract, and the star will become a continually expanding Red Giant Branch (RGB) star where hydrogen burns in an outward-moving shell[1], slowly increasing the mass of a now degenerate helium core. At the beginning of the RGB, some of the helium produced in the core (as well as any other products of H-burning that are present; e.g., nitrogen) will be carried to the surface by a deep convective region (Iben and Renzini, 1984; Lambert, 1992). This is called 'first dredge up', the first in a series of important events that can alter the composition of a stellar atmosphere. Further up the RGB, low mass stars will undergo an additional mixing event, often called 'extra mixing' or 'deep mixing", which generally

[1]Outwardly moving in mass coordinate, but not necessarily in radius

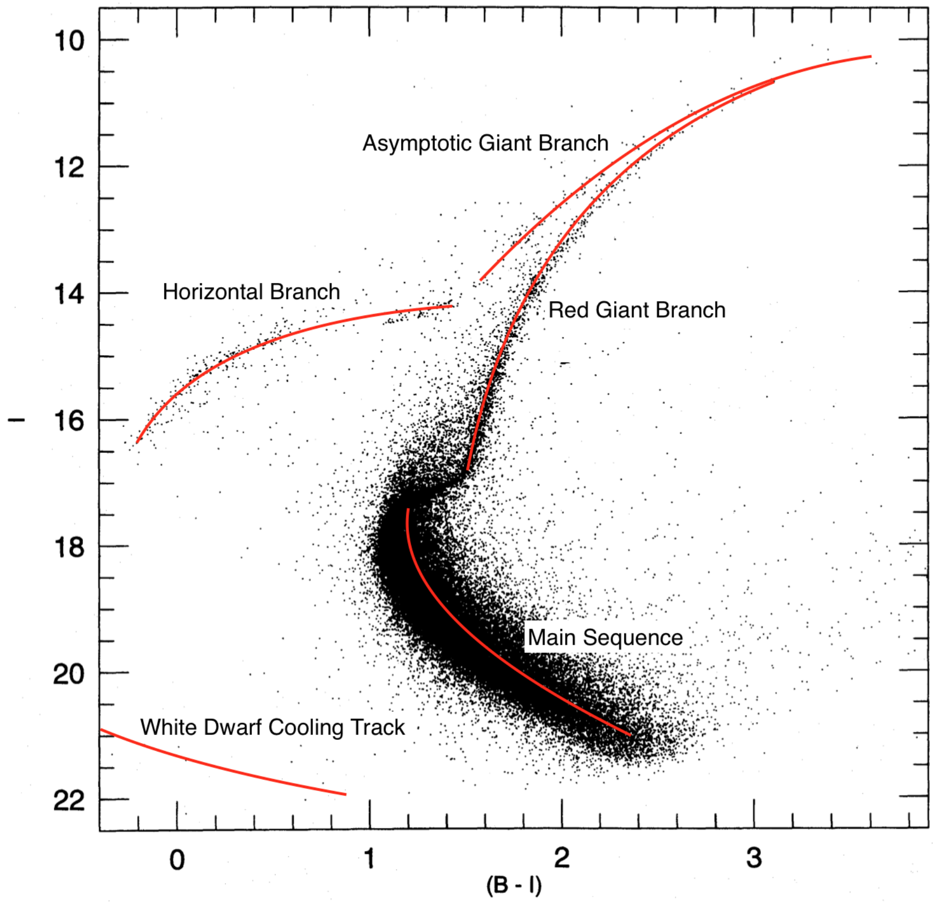

FIGURE 1.2: Colour-magnitude diagram of the globular cluster M 5 (NGC 5904), adapted from Sandquist et al. (1996), Figure 7b, with annotations indicating the main evolutionary phases of a low-mass star.

increases the atmospheric helium and nitrogen abundances while decreasing the lithium and carbon abundances (Langer et al., 1985; Eggleton et al., 2006; Henkel et al., 2017). Mixing events such as these are vital for enriching the universe with nuclear-processed material. The star will continue to expand as its H-exhausted core increases in mass. This expansion causes the surface layers to cool and become less gravitationally bound their host, resulting in substantial mass loss during the RGB phase ($\sim 0.15 M_{\odot}$; Reimers, 1975).

Horizontal Branch

By the time the H-exhausted core reaches a mass of $M \sim 0.475 M_{\odot}$ (Sweigart and Gross, 1978; Catelan et al., 1996), the star will be up to 10^3 times brighter than when it left the MS (i.e., at the tip of the RGB Iben, 1967; Bellazzini, 2008). At this mass, the helium core will reach a critical density, and gravitational contraction will have pushed the core temperature to the point ($\sim$200 MK) where the helium present can undergo its own fusion – via the triple-α and α-capture processes – into carbon and oxygen (Schönberg and Chandrasekhar, 1942; Kippenhahn and Weigert, 1990). Initially this is a runaway burning event, but expansion of the core soon allows the He burning to stabilise. The star at this time will become a Horizontal Branch (HB) star, with stable helium fusion in the core and a hydrogen burning shell (Iben and Rood, 1970).

The horizontal branch star (also known as a 'core helium burning' – CHeB – star) is largely stable through this phase. In brightness, it will reduce to around the mid-RGB level (brighter than the MS), but will be significantly hotter. During its $\sim$ 100 Myr life in the CHeB phase the HB star will only move slightly on a CMD, increasing by a small amount in radius and effective temperature as it burns helium in its core (but usually not enough to move across the entire HB range of its host cluster; e.g., Constantino et al., 2016).

The structure and evolution of HB stars, as well as the morphology of the HB in old stellar clusters (e.g., globular clusters), is one of the most uncertain of the low-mass stellar phases. In particular, treatment of the convective boundary around the helium burning core is not well understood, and can significantly alter predictions of the subsequent stellar evolution (Constantino et al., 2017, and references within). Generally, the location and distribution of stars along the HB (HB morphology, see Figure 1.2 for example) appears to be a function of stellar mass, cluster age, helium mass fraction (Y), and metallicity ([M/H]; Sandage, 1953; Lee et al., 2002; Milone, 2013).

Asymptotic Giant Branch to White Dwarf phase

Once the core of the HB star has been entirely converted to carbon and oxygen, the He-burning usually moves outward in a shell, with the H-burning shell also still burning further out. If this happens, the star will expand a second time, evolving up the Asymptotic Giant Branch (AGB) – the final phase of nuclear evolution for a low-mass star (Lattanzio, 1986; Herwig, 2005). Most AGB stars in GCs are observed to be in the early-AGB (EAGB) phase (Constantino et al., 2016, also known as the 'AGB clump'), since the upper-AGB is one of the shortest-lived phases of low-mass stars.

Not all low-mass stars, however, will ascend the AGB. If a star has a sufficiently low mass and/or high enough He mass fraction, it will retain only a thin envelope on the HB, appearing very blue and hot. The core mass at the tip of the RGB is relatively fixed at $M \sim 0.475 M_{\odot}$ for these low mass stars (this is only slightly dependent on initial mass and metallicity; Catelan et al., 1996) due to the degenerate equation of state, and only the remaining material – left over after RGB mass loss and core growth – can contribute to the envelope on the HB. If this envelope is thin enough, the star will be unable to evolve to the AGB, but will instead slowly lose its envelope via a stellar wind and become a white dwarf star, effectively truncating its evolution. First suggested by Renzini and Buzzoni (1986) and Greggio and Renzini (1990) to explain UV excesses in elliptical galaxies, these stars – known as AGB-manqué stars – only evolve from HB stars that have effective temperatures (T_{eff}) of $\gtrsim 15,000$ K (only a few GCs have HBs that extend into this T_{eff} regime; Lee et al., 1994; Lee et al., 2002). See Figure 1.3 for a sample of evolutionary tracks of HB, early AGB, and AGB-manqué stars.

As a star increases in luminosity, both on the RGB and AGB, stellar winds drive significant mass loss (usually parametrised by a scaling factor; Reimers, 1975; Vassiliadis and Wood, 1993; Schröder and Cuntz, 2005). This is the mechanism by which low-mass stars enrich the universe: first by fusing nuclei in their cores and shells via nucleosynthesis, then mixing the burning products to their surfaces through dredge up and mixing events, and finally expelling their atmospheres until only the hot, dense core remains. A series of important events occur on the AGB called 'thermal pulses' and 'third dredge up'; however we leave discussion of these for the following section.

When a low-mass star leaves the tip of the AGB (or potentially skips the phase entirely) it enters the post-AGB phase, where it sheds what little atmosphere remains and becomes a white dwarf (composed of a mass-dependent combination of degenerate helium, or carbon and oxygen), slowly cooling and never again engaging in nucleosynthesis.

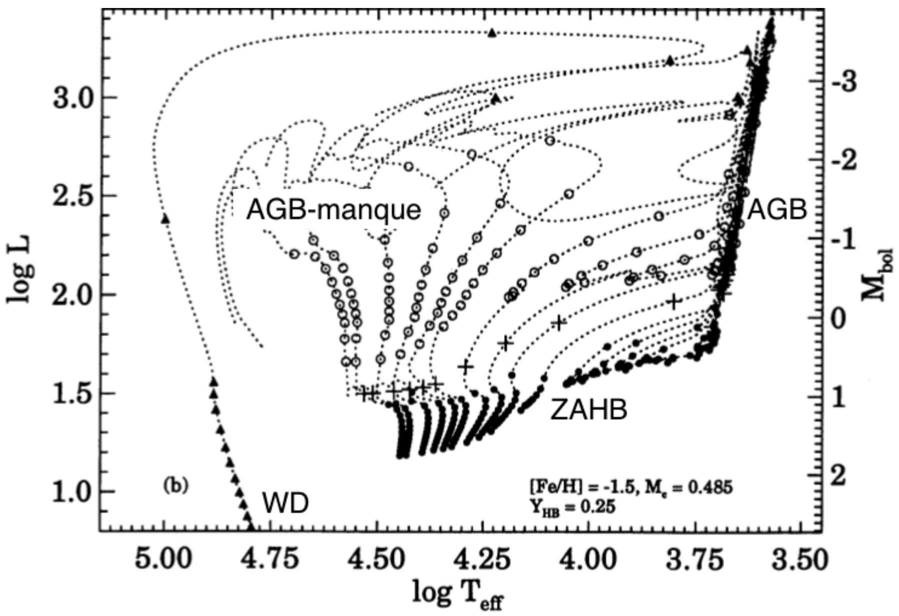

FIGURE 1.3: Horizontal branch and post-HB evolutionary tracks for a range of initial zero-age HB (ZAHB) models (varying in total ZAHB mass) with metallicities representative of many globular clusters (here [Fe/H] = -1.5). Models contain a helium core mass of 0.485 $M_\odot$ and a helium mass fraction in the envelope of Y = 0.25. Note that in these models, stars with initial ZAHB effective temperatures ($T_{\rm eff}$) of $\gtrsim 15,000$ K (log $T_{\rm eff}$ $\gtrsim 4.15$) do not join the AGB, but become AGB-manqué stars, evolving into white dwarfs. In globular clusters with extended blue HBs (to be discussed in §1.2), up to 30% of HB stars can become AGB-manqué stars, avoiding the AGB. Adapted from Dorman et al. (1993), Figure 3(b), with annotations indicating evolutionary phases.

Additional low-mass chemical enrichment

While a star of $0.8M_{\odot}$ will not undergo atmospheric chemical enrichment after the extra mixing event on the RGB, stars with masses between $1 \lesssim M/M_{\odot} \lesssim 8$ may experience a variety of mass-dependent enrichment events on the AGB that can alter their surface composition. These events are important for understanding the nature of globular clusters.

Just like at the base of the RGB, stars more massive than $M \sim 4M_{\odot}$ that begin to ascend the AGB will undergo a dredging event – 'second dredge up' – driven by a deep convective region bringing hydrogen burning products into the atmosphere (Habing and Olofsson, 2004). Further up the AGB, stars in the mass range $1 \lesssim M/M_{\odot} \lesssim 8$ will experience thermal instabilities in the He burning shell that generate a series of internal contractions and expansions – known as 'thermal pulses' – where periodic structure changes inside the star can result in neutron-capture elements (species heaver than iron) being produced and raised to the surface. This is known as 'third dredge up' (Iben, 1975; Herwig et al., 1997, see Figure 1.4). In intermediate-mass ($4 \lesssim M/M_{\odot} \lesssim 6$) AGB stars, an additional process produces and mixes hot hydrogen burning products (N, Na, and sometimes Al) directly into the atmosphere ('hot bottom burning'; Lattanzio et al., 1997).

These events make the AGB phase potentially the most important for a low-mass star and its influence on the interstellar medium (ISM) from which future generations of stars will form. This is because many chemical species are created within low-mass AGB stars, and enrich the universe in important and specific ways. They pollute the ISM with light elements such as carbon, nitrogen, and sodium; and with heavy neutron-capture species (specifically via the slow neutron-capture process) like lead, barium, and zirconium (Lugaro et al., 2003; Cristallo et al., 2009). As we will see, a complete picture of the evolution and chemical yields of low-mass stars will have an important effect on understanding the formation and chemical history of globular clusters, the Galaxy, and the Universe.

1.2 Globular clusters as stellar laboratories

Stars do not form in isolation, but in clusters. These stellar clusters range in membership from tens to millions of coeval siblings, and these members usually only vary (star-to-star) in their initial mass and binary status. Most importantly, stars born from the same burst of formation typically share identical chemical compositions, with variations to this only coming later in the evolution of each individual star (e.g., dredge up, binary interactions), or stellar cluster (e.g., subsequent star formation, gravitational disruption).

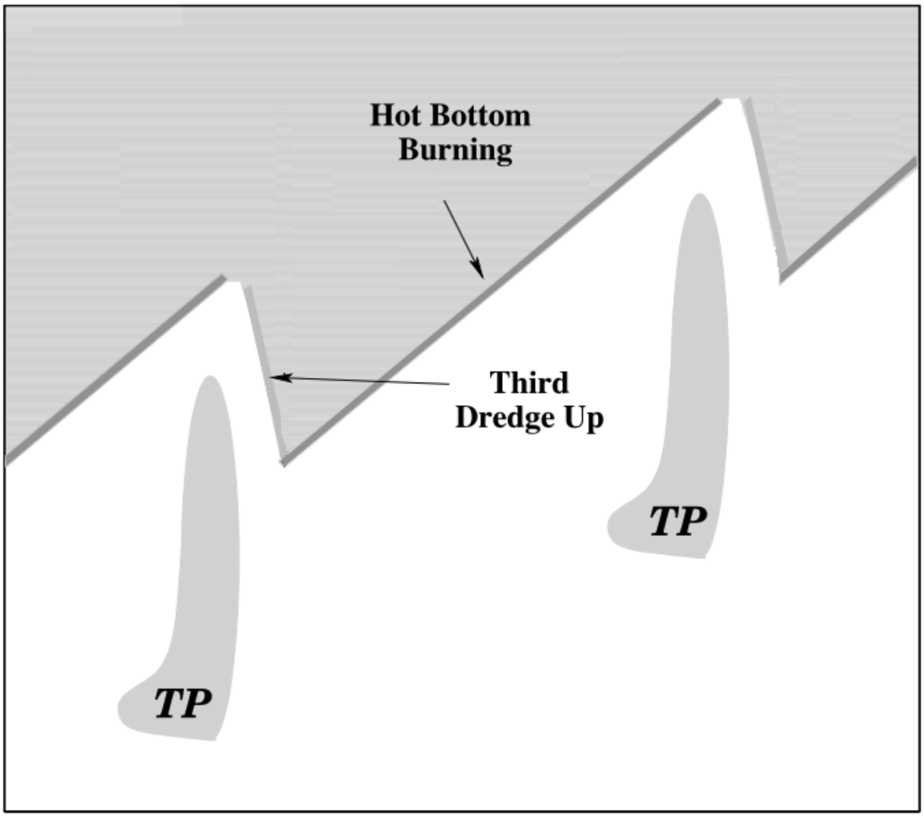

FIGURE 1.4: Schematic Kippenhahn diagram of a super-AGB star ($5 \lesssim M/M_{\odot} \lesssim 10$) during the thermally pulsing AGB phase. The light grey regions indicate convection zones, while white regions are radiative. During each thermal pulse (when the the H-free core moves inward), neutron-capture species (e.g., yttrium and barium) and H-burning products (e.g., nitrogen and sodium) may be mixed to the surface (third dredge up). The location of hot bottom burning is also indicated. Adapted from Doherty et al. (2015), Figure 3.

In this thesis, we will focus exclusively on Galactic globular clusters (GCs) – very old ($\gtrsim$10 Gyrs; Sandage, 1986; Gratton et al., 2003b) and massive ($\gtrsim 10^4$ $M_{\odot}$; Meylan and Mayor, 1986; Simpson et al., 2017) stellar clusters with wide and often eccentric Galactic orbits (Peterson, 1974). While GCs have been observed orbiting many galaxies, spectroscopic surveys of individual stars in extragalactic GCs has only become viable in recent years due to the vast distances involved (Brodie and Strader, 2006). There are, however, many Galactic GCs available for detailed observation and investigation: to date, more than 157 such GCs have been identified (Harris, 1996). In this thesis we will only discuss Galactic GCs.

Due to their age and internal uniformity, GCs provide a unique site to study low-mass stars (and their evolution) in a relatively isolated environment, as opposed to the conditions in the Galactic plane where most open clusters are gravitationally disrupted less than 1 Gyr after formation (Lada and Lada, 2003). At an average age of ∼12 Gyrs, the most evolved stars (i.e., post-MS) in a GC had an initial mass of ∼0.8 $M_{\odot}$ at the beginning of their MS lives (Salaris et al., 1997; Miglio et al., 2016). This is particularly useful because determining the masses of single stars (in the Galactic field for example) is a difficult process, whereas having a large population of coeval stellar siblings allows this parameter to be confidently constrained. The relative homogeneity of stellar mass among the evolved stars in a GC also allows for targeted surveys of specific evolutionary phases, which can be challenging to isolate in a CMD with a heterogeneous stellar sample.

Early photometric studies of Galactic GCs noted a variety of HB morphology among their targets. Differences in the average colour, and in the range of colours, of each HB were visible in the early CMDs of Arp et al. (1952). It was well understood that an older (and by correlation, lower metallicity) GC would have a generally bluer HB than younger GCs with a higher metallicity; however theoretical population synthesis studies were unable to explain the full range of HB morphologies (Sandage and Wallerstein, 1960) – see Figure 1.5 for example. It was inferred that a second, independent parameter was required to match the varying HB colour ranges (Sandage and Wildey, 1967).

1.2.1 Multiple populations

In the 1970s, advances in astronomical spectroscopy enabled the collection of low-resolution spectra from individual GC stars. Until this point, it had been generally accepted that GCs were homogeneous in their chemical abundances (Baade, 1944), and that they formed from a single burst of star formation (like Galactic open clusters; see e.g., MacLean et al., 2015).

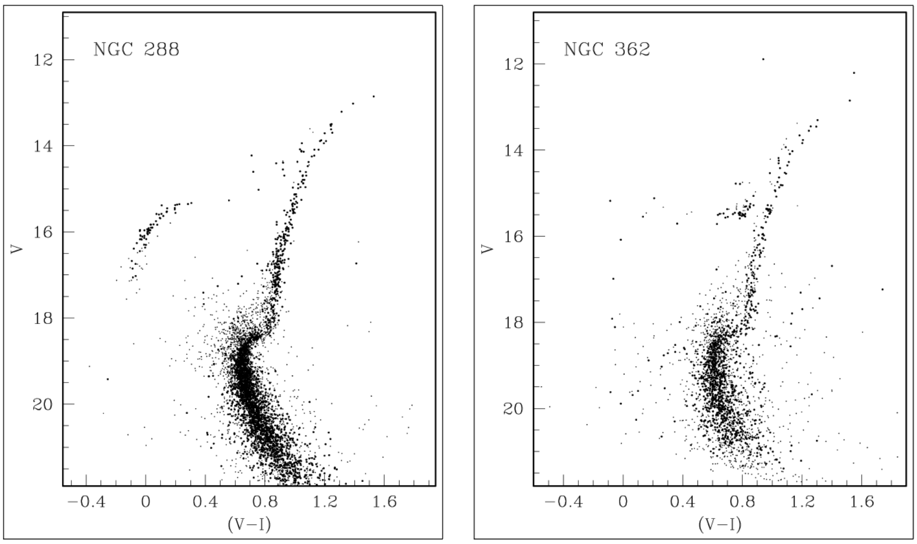

FIGURE 1.5: Photometric CMDs of NGC 288 and NGC 362, a 'second parameter pair' of GCs, which have similar metallicities ([Fe/H] = -1.32 and -1.26, respectively; Harris, 1996) but very different HB morphologies. Adapted from Rosenberg et al. (2000), Figures 5 and 6.

In a study of the spectra of 20 evolved stars in the GC M 92, Zinn (1973) found six to have very weak 'G-band' strengths (the spectral band covering the CH molecular absorption feature), indicating that many M 92 stars may be depleted in carbon. Interestingly, all six weak G-band stars were on the AGB. Mallia (1975) similarly found two AGB stars in NGC 6397 with weak G-bands, while a comprehensive study of 145 giant stars in 17 GCs by Hesser et al. (1977) found significant spreads in cyanogen (CN) band strengths in some globular clusters. Hesser et al. (1977) urgently recommended systematic surveys of GC stars to discover the cause of these anomalies. These studies, and many others published around the same time (e.g., McClure and Norris, 1977; Norris and Zinn, 1977; Mallia, 1978; Carbon et al., 1982, also see Figure 1.6), identified star-to-star heterogeneities in, and an anti-correlation between, the absorption band-strengths of CN and CH molecules (Kraft, 1979).

The originally hypothesised explanation for the results in these studies was that CN and CH variations can arise from stellar evolutionary effects, such as internal mixing on the upper-RGB known as 'extra mixing' (McClure, 1979; Smith, 1987).

In one of the first studies of GC stars using high-resolution spectra, Cottrell and Da Costa (1981) performed a study of carefully selected giant star pairs in NGC 6752 (three pairs) and 47 Tucanae (two pairs), respectively (each pair of stars had similar stellar parameters but different CN band strengths). They found that sodium abundances varied dramatically in both clusters (differences of up to 0.5 dex, correlated with CN band

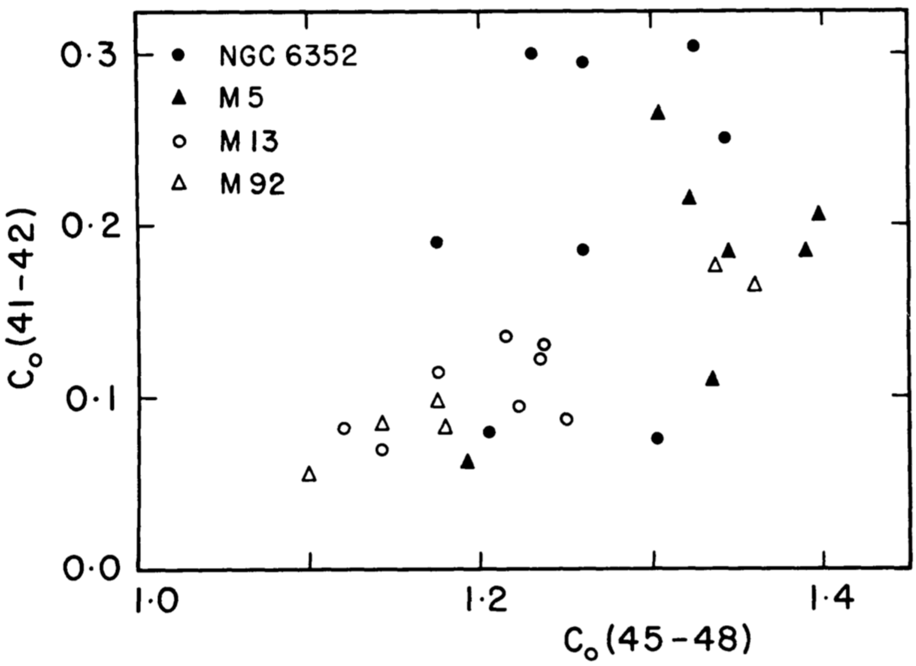

FIGURE 1.6: DDO filter system (McClure, 1973) colours of giant stars from four GCs. The C 41 filter covers the CN molecular band feature, therefore CN-strong stars exhibit a higher C_o(41-42) colour at a given C_o(45-48) colour than CN-weak stars. The clusters M 5 and NGC 6352 clearly show a large range of C_o(41-42) values at a given C_o(45-48) value, indicating a large spread in CN band strengths. Adapted from the review of Smith (1987), Figure 1, compiling data from Osborn (1971), Hesser et al. (1977), and Norris and Zinn (1977).

strengths), and that aluminium varied in NGC 6752 (differences of 0.2 dex; no difference in 47 Tuc). Similar findings of aluminium variations by Norris et al. (1981, NGC 6752) and Norris and Smith (1983, NGC 3201, M 5, ω Cen, M 22) led to the consensus that not all chemical variations in GCs can be attributed to evolutionary mixing. Since atmospheric Na and Al abundances are not thought to change during the lives of single low-mass stars (unlike carbon and nitrogen; Iben and Renzini, 1984; Gratton et al., 2004), these studies suggested that GCs are indeed chemically heterogeneous, and that the abundance variations must be inherited at birth (Freeman and Norris, 1981).

All of the elements that have been found to vary within GCs have a H-burning nucleosynthetic origin (e.g., the CNO cycle, and the Ne-Na and Mg-Al chains; Gratton et al., 2012). This contributed to a general consensus of helium mass fraction – the primary product of H-burning – as the elusive 'second parameter' driving HB morphology[2] (Sweigart, 1997; Sweigart and Catelan, 1998; Catelan, 2009). Helium abundance, however, is very difficult to measure directly in stars. The two ultra-violet He absorption lines are only detectable in very hot HB stars, while few instruments can observe the near-infrared line at 10830 Å (Da Costa et al., 1986; Dupree et al., 2011; Smith et al., 2014). Instead, helium mass fraction is often inferred from matching theoretical isochrones with GC photometry, and is generally found to correlate with N, Na and Al, and anti-correlate with C, O and Mg – in agreement with stellar evolutionary and nucleosynthetic theory (Nardiello et al., 2015; Chantereau et al., 2016).

Over the subsequent decades, as low- and high-resolution spectroscopic surveys of GCs became common in the literature (e.g., Smith and Norris, 1993; Sneden et al., 1997; Kraft et al., 1997; Ivans et al., 1999; Yong et al., 2003; Carretta et al., 2009c), GCs were regularly shown to contain distinct star-to-star abundance patterns in the form of light-element anti-correlations (Carretta et al., 2010). The most well-documented are those of C-N, Na-O, and Mg-Al, which often (but not always) present as a bimodality (see Figure 1.7 for examples). In fact, the Na-O anti-correlation is so prevalent among GCs that Carretta et al. (2009b) defined only those GCs that show the pattern to be bona-fide GCs. Additionally, most GCs have been found to be homogeneous in species heavier than Si; however exceptions exist which show heterogeneity in some iron-peak and/or neutron-capture species (Bragaglia et al., 2013). Furthermore, these anti-correlations were systematically observed on the RGB, HB, and most importantly on the MS (Briley et al., 1991; Kraft, 1994), providing further evidence that the

[2]However, as with all complex astrophysical problems, there are many factors that contribute to such phenomena – not just two.

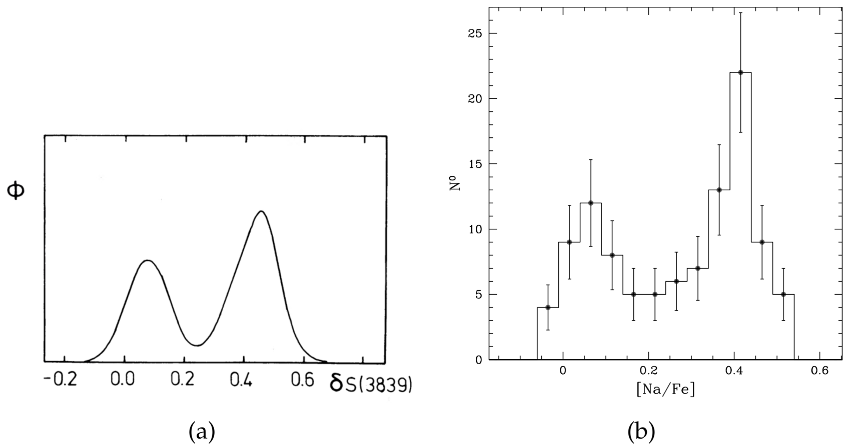

FIGURE 1.7: Histograms of (a) δS(3839) values (a proxy for inferring CN abundance, see Chapter 5) of 49 RGB stars in NGC 6752 showing a bimodality in CN band strengths (Figure 5 from Norris et al., 1981), and (b) [Na/Fe] values of 105 RGB stars in M 4 showing a bimodality in sodium abundances. Adapted from (Marino et al., 2008), Figure 6.

abundance variations are intrinsic to the stars (see the literature reviews of Sneden, 1999; Gratton et al., 2012).

In the past, the AGB has proven difficult to observe systematically due to the low number of stars in the phase[3] at any one time in a given GC, and because AGB stars can be difficult to differentiate from RGB stars in a CMD without both high quality photometry and high completeness, due to the branches having a similar range in colour and brightness, especially on the upper-RGB and upper-AGB.

A consistent and reasonable model for the phenomenon of multiple populations remains elusive. The most commonly invoked explanation requires at least two distinct bursts of star formation within a GC's early history, with pollution (from stellar ejecta) occurring between each formation episode – at each turn increasing the He, N and Na abundance of the ISM. The source and mechanism of this cluster 'self-pollution' has remained elusive, however the main suspects are intermediate mass AGB stars (4 - 7 $M_\odot$) undergoing hot bottom burning and third dredge up (Cottrell and Da Costa, 1981; Ventura et al., 2001, see § 1.1.2), and fast-rotating massive stars (20 - 120 $M_\odot$ Decressin et al., 2007; Charbonnel et al., 2014).

Additional barriers to a complete understanding of GC formation history include mass budget problems (D'Antona et al., 2002), stellar evolutionary constraints (Fenner et al., 2004), and difficulties in reproducing observed abundances (Karakas et al., 2006; Marcolini et al., 2009). Furthermore, each GC presents its own challenges: the range and morphology of

[3]This is because the AGB is a very short phase, compared to the earlier phases

the abundance patterns varies from cluster to cluster, requiring one to investigate and explain each object independently (Gratton et al., 2004). Some have also questioned the so-called 'multiple generation' hypothesis, preferring rather to consider stars with similar abundances as separate subpopulations – not necessarily indicative of a generational effect (see Renzini et al., 2015, for a recent review on the proposed scenarios).

To aid in our analysis, presentation of results, and discussions, we define Na-poor/CN-weak stars (often called the 'first generation') as SP1 – subpopulation one – while all stars that are enriched in Na/CN-strong, we define as SP2 – subpopulation two. We note that more than two subpopulations have been observed in many GCs (e.g., NGC 6752 is usually considered to contain three subpopulations, while up to six have been claimed for ω Centauri; Milone et al., 2013; Milone et al., 2017), however for simplification we have chosen to restrict our classification to this binary definition.

Carretta et al. (2009b) recommended a fixed abundance threshold for separating these subpopulations, irrespective of each GC's abundance distributions[4], however we have found that the 'population separation point' (PSP) should be determined for each cluster individually, and based on its internal abundance distributions – see Chapter 2.

While the light elemental abundance distributions vary from cluster to cluster, in general, SP1-like abundances are typically in the range of $-0.5 \lesssim [\mathrm{Na/Fe}] \lesssim 0.2$ and $0.0 \lesssim [\mathrm{O/Fe}] \lesssim 1.0$, and are typically similar in abundance to Galactic halo field stars of similar metallicities (Martell et al., 2011). SP2-like abundances typically are $[\mathrm{Na/Fe}] \gtrsim 0.2$ and $[\mathrm{O/Fe}] \lesssim 0.0$, and reaching up to $[\mathrm{Na/Fe}] \sim 1.0$ and down to $[\mathrm{O/Fe}] \sim -1.0$ in GCs with more extreme Na-O anti-correlations than most GCs (see Figure 1.8 for a composite plot of RGB stellar abundances from 19 GCs).

1.2.2 Globular cluster summary

As mentioned above, a consensus has yet to be reached as to many of the details of GC formation and chemical history – it is a very active field of research. In general, however, it is agreed that:

(i) most GCs are homogeneous in elements heavier than Si,

(ii) there are two or more chemically unique populations within each GC (identifiable using C, N, Na, O, and sometimes Mg and/or Al abundances),

(iii) all heterogeneous species lighter than iron are products of hydrogen burning,

[4]Carretta et al. (2009b) suggest that the separation in Na abundance between SP1 and SP2 should be at [Na/H] = $[\mathrm{Na/H}]_{\mathrm{min}}$ + 0.3 dex for all GCs; where $[\mathrm{Na/H}]_{\mathrm{min}}$ is the lowest Na abundance in the GC sample.

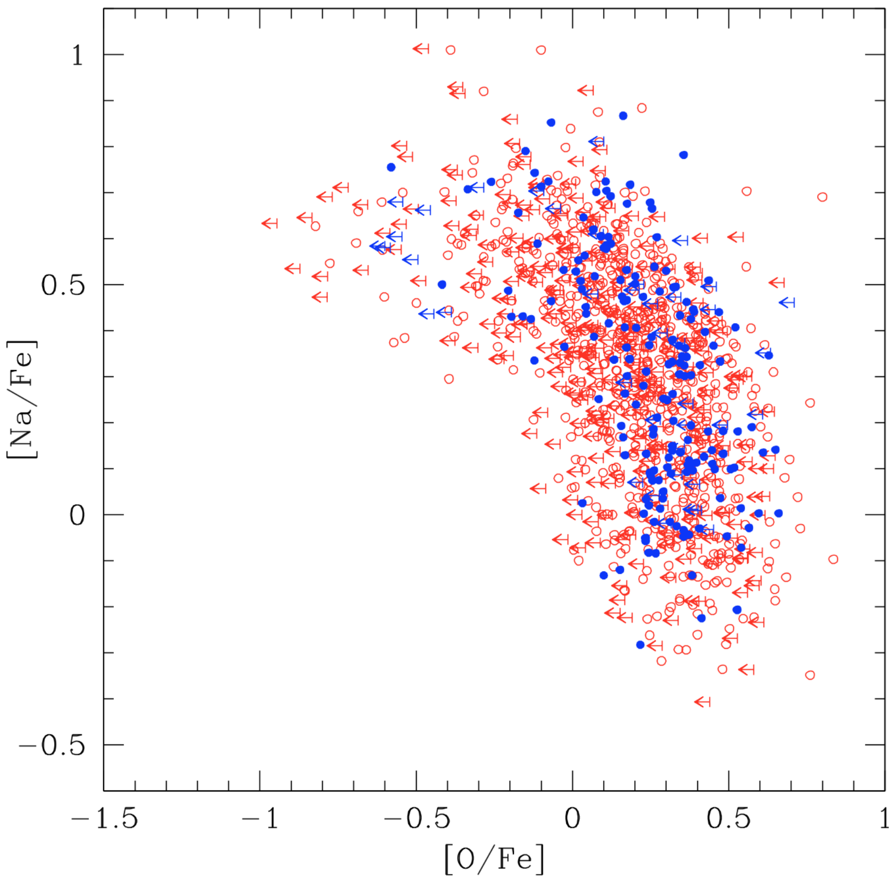

FIGURE 1.8: Composite plot of [Na/Fe] and [O/Fe] abundances of 1958 RGB stars from 19 GCs (of varying metallicities, ages, and HB morphology). Abundances from GIRAFFE spectra are shown as red circles, while abundances from UVES spectra are blue circles. Adapted from Carretta et al. (2009b), Figure 6.

(iv) inferred He mass fractions generally correlate with N, Na and Al abundances and anti-correlates with O and Mg abundance, and

(v) internal variations in He mass fraction, along with global age and metallicity, contribute to the HB morphology of a GC; therefore

(vi) an extended blue HB is usually accompanied by an extended Na-O anti-correlation. Furthermore,

(vii) these abundance variations do not arise from internal evolutionary mechanisms in individual stars (with the exception of slight evolutionary changes in C and N abundance), therefore

(viii) the light elemental abundances of GC stars have been present since their formation (although see Bastian et al., 2015, for an opposing view).

Aspects of GCs that the scientific community have yet to reach a consensus on include:

(i) the identity of the stars that contributed to GC abundance spreads,

(ii) the mechanism by which the ISM of GCs were polluted,

(iii) whether or not each population corresponds to a distinct and subsequent star formation episode, and

(iv) the impact that the abundance variations have on the evolution of the individual stars in a GC.

This final point is of core importance to this thesis, as we seek to explore the effects that these multiple populations (and their associated chemical abundances) have on the evolution of stars in GCs. In particular, we have observationally investigated whether stars with SP2-like chemical compositions appear to be avoiding the AGB phase in some globular clusters.

As we will see, the inferred proportions of stars in each subpopulation are vital for understanding the evolution of GC stars. For clarity, we define $\mathscr{R}$ to be the percentage of stars in a GC that are found to be members of SP2, specific to each phase. Typical $\mathscr{R}_{MS}$, $\mathscr{R}_{RGB}$, and $\mathscr{R}_{HB}$ values are on the order of 50-70% (Carretta et al., 2010). Furthermore, we define:

$$\mathscr{F} = (1 - \frac{\mathscr{R}_{\rm AGB}}{\mathscr{R}_{\rm RGB}})\cdot 100\%, \tag{1.1}$$

as a parametrisation of the relative proportions of AGB and RGB stars with SP2-like chemical compositions, which will be discussed in more detail in the next section.

1.3 The case of the 'missing' globular cluster AGB stars

In even the earliest spectroscopic studies of globular clusters, AGB stars were noted to have weak G-band absorption (carbon-poor), however these were attributed solely to evolutionary mixing events (first dredge up and extra mixing – where carbon abundance is reduced by the time that the star reached the RGB tip; e.g., Zinn, 1973; Mallia, 1975). More difficult to explain was the presence of both G-band strong and weak AGB stars in the studies of Norris and Zinn (1977) and Zinn (1977), indicating that some AGB stars were perhaps less affected by RGB mixing than others.

While investigating the CN band strengths of stars in NGC 6752, Norris et al. (1981) observed that the 12 AGB stars in their sample were exclusively CN-weak, whereas their RGB sample showed a significant bimodal distribution of CN band strengths (with $\mathscr{R}_{RGB} \simeq 50\%$, see Figure 1.9). They were unable to draw any conclusions from these results, and suggested a more targeted study of the AGB of NGC 6752. Ivans et al. (1999) found a sample of 11 AGB stars in M 4 to have on average higher C and O abundances, and lower N abundances, than the RGB of M 4. In contrast Smith and Norris (1993) found a sample of 8 AGB stars in M 5 to be primarily CN-strong (compared to 8 RGB stars in the same cluster). A literature review by Sneden et al. (2000) showed that the CN band strengths of AGB stars in M 13 and M 4 had been reported to be generally weaker than their RGB stars, while both they and Campbell et al. (2006) re-emphasised the extreme CN-weak characteristics of AGB stars in NGC 6752.

In each of these cases, AGB stars were not systematically targeted, and low number statistics (<10 AGB stars in most cases) prevented deeper investigation of this phenomenon. Campbell et al. (2010) performed the first spectroscopic survey of GCs that specifically targeted the AGB, and confirmed that the AGB of some clusters are indeed CN-weak – especially that of NGC 6752, and potentially also NGC 1851 and NGC 288 (Campbell et al., 2012). The formation of molecular absorption bands (e.g., CN), however, is poorly understood – molecular 'abundances' are inferred from photon counts of spectral bands and trends with stellar parameters (especially $T_{\rm eff}$ and gravity) are removed empirically (Norris et al., 1981; Ivans et al., 1999). High-resolution spectra of AGB stars in GCs were sought in order to determine more reliable elemental abundances, specifically those of Na, O, Mg, and Al, which are not altered during the evolution of a low-mass star.

1.3.1 Na abundances of NGC 6752 AGB stars

Campbell et al. (2013, hereafter C13) presented Na abundances for a sample of 24 RGB and 20 AGB stars in NGC 6752, using high-resolution spectra from the FLAMES instrument on the VLT. They found all of the observed

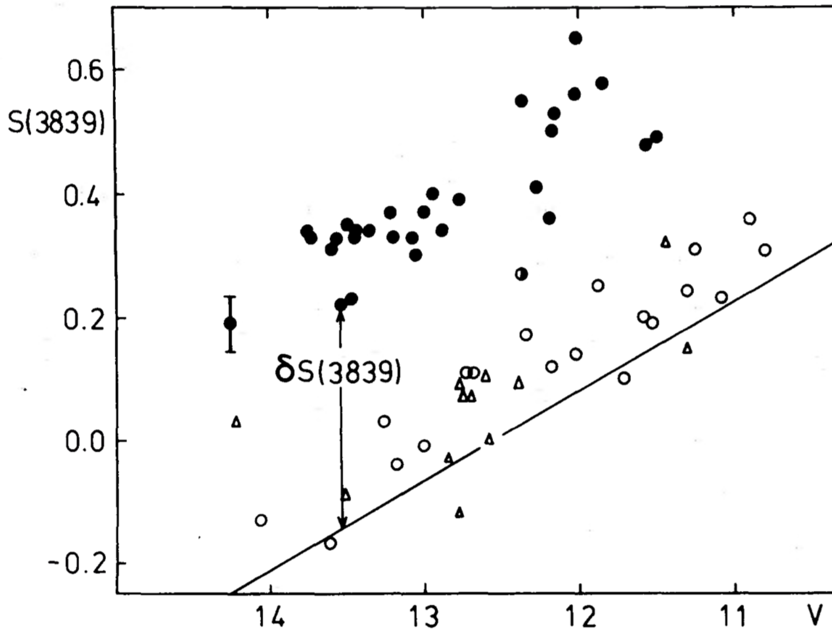

FIGURE 1.9: δS(3839) values (a proxy for inferring CN abundance) of 49 RGB stars (circles; CN weak and strong are open and closed, respectively) and 12 AGB stars (triangles) in NGC 6752, against photometric V-band magnitude. Note that every AGB star is classified as CN weak, despite nitrogen increasing on the upper RGB via extra mixing. The solid line is an empirical trend between magnitude and S(3839). Adapted from Norris et al. (1981), Figure 3.

AGB stars to have [Na/Fe] $\lesssim$ 0.12, with no intrinsic scatter (i.e., homogeneous in [Na/Fe] within an uncertainty of ~0.1), compared to their RGB sample which they found to range between -0.24 and 0.70 in [Na/Fe] (Figure 1.10). In the definition of this thesis, C13 found that NGC 6752 has SP2 proportions of $\mathscr{R}_{RGB} = 70\%$, but $\mathscr{R}_{AGB} = 0\%$.

While no theoretical explanation was found by C13, they showed that the HB stars of NGC 6752 appeared to be becoming AGB-manqué stars at a much lower $T_{\rm eff}$ (i.e., at a much redder photometric colour) than is predicted by stellar evolutionary theory – the low-metallicity models of Dorman et al. (1993) predicted AGB avoidance at $\sim 15,000$ K (see Figure 1.3). By the estimation of C13, HB stars in NGC 6752 with $T_{\rm eff} \gtrsim 11,500$ K avoid the AGB entirely and become AGB-manqué stars, potentially exposing a flaw in current low-mass stellar evolution models which do not predict AGB avoidance at this HB $T_{\rm eff}$.

To succinctly parametrise this apparent 'SP2 AGB deficit'[5], we use our $\mathscr{F}$ definition where a value of 100% indicates that no SP2 (Na-rich) stars reach the AGB, such as was reported by C13 for NGC 6752. For clusters

[5]The terminology surrounding this phenomenon is not yet consistent in the literature. The phenomenon is referred to as 'AGB failure', 'AGB avoidance', and 'AGB deficit' interchangeably.

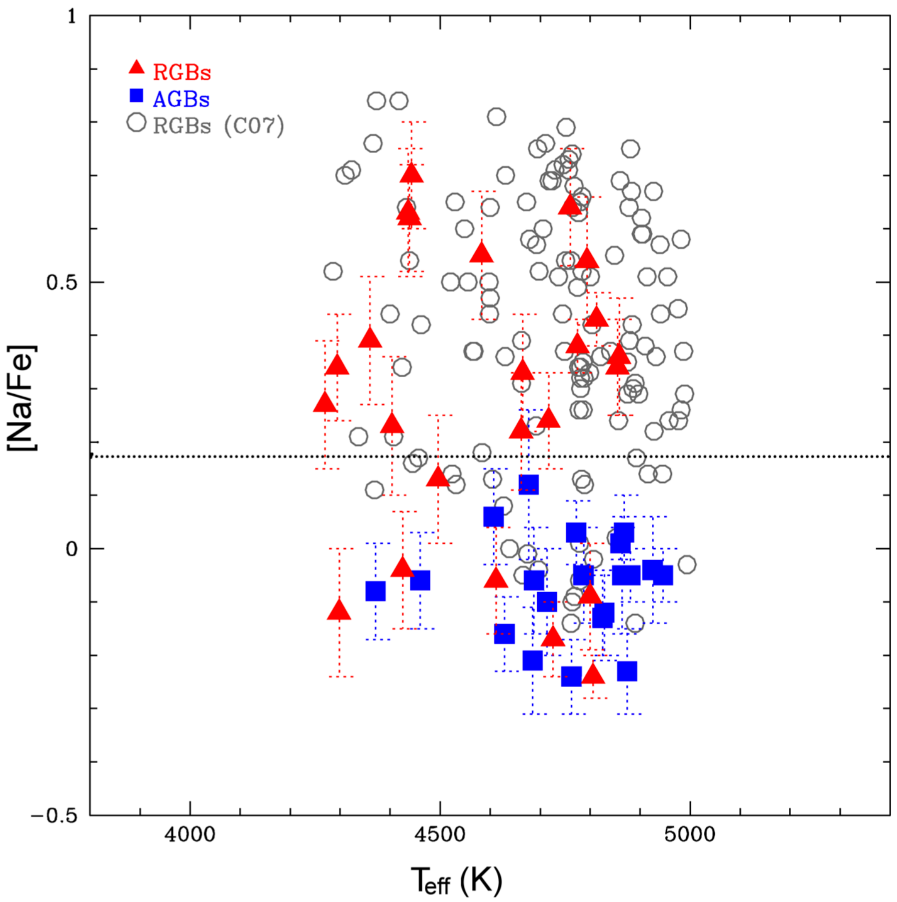

FIGURE 1.10: [Na/Fe] abundances of a sample of AGB and RGB stars in the GC NGC 6752, as presented in Campbell et al. (2013). Note that all AGB stars are reported to have [Na/Fe] values of $\lesssim 0.12$, clearly different to the distribution of Na abundances of the RGB.

with extended HBs – where the bluest stars reach a T_{eff} of over 15,000 K; (e.g., NGC 6752 and NGC 2808) – an $\mathscr{F}$ value of up to ~30% may be expected from theory (i.e., 30% of SP2 stars are predicted to become AGB-manqué stars). Clusters whose HBs do not extend into this regime (e.g., M 4 and NGC 6397) are expected to have an $\mathscr{F}$ value of zero per cent, with all stars in the cluster ascending the AGB. We use this definition throughout the thesis.

The findings of C13 ($\mathscr{F} = 100\%$, instead of the predicted 30%) sparked a new field of investigation. Efforts were made to theoretically explain the AGB distribution of NGC 6752, and reproduce the C13 results. Cassisi et al. (2014) were unable to achieve this using population synthesis models (despite successfully reproducing the low number ratio between HB and AGB stars in NGC 6752), concluding that "there is no simple explanation for the lack of [observed] second generation stars [in NGC 6752]". Charbonnel et al. (2013), using a combination of very high helium mass fraction and increased RGB mass loss, showed that it is possible to achieve a maximum AGB Na abundance of [Na/Fe] ~ 0.18 – only slightly higher than found in C13. However, the helium mass fractions (Y up to 0.37) and mass loss rates (Reimers' factor η up to 0.65) used in this study may have been physically unreasonable – for NGC 6752, Milone et al. (2013) found $Y \leq 0.275$ and McDonald and Zijlstra (2015) recommend a Reimers' factor of $\eta = 0.518$.

1.3.2 A new era of systematic surveys targeting AGB stars in GCs

Prompted by the controversial findings of C13, new observations of AGB stars in GCs were made, exploring whether the phenomenon is unique to NGC 6752. Johnson et al. (2015) observed spectra of stars in 47 Tucanae (NGC 104), and used the Na abundances of its AGB population to show that $\mathscr{F} \lesssim 20\%$ for this cluster. García-Hernández et al. (2015) reported Al abundance results for M 2, M 3, M 5, and M 13, finding SP2 AGB stars in all clusters; however in each case Al-poor AGB stars outnumber the Al-rich. A second cluster was soon found to display a similar abundance distribution to NGC 6752. Lapenna et al., 2015 derived Na, O, Al, and Mg abundances for a sample of RGB and AGB stars in M 62 (which has a similar HB morphology to NGC 6752), and found all of their AGB stars to be from SP1, providing the first confirmation that GCs other than NGC 6752 may display an SP2 AGB deficit that is higher than expected. Their AGB sample was small, however, with only five stars.

An additional method utilising photometric colour indices has been used to investigate the existence and prevalence of SP2 AGB deficits in GCs. Monelli et al. (2013) defined a new photometric index, $C_{UBI} = (U - B) - (B - I)$ which they used to separate the RGB subpopulations of 23 GCs. The Johnson photometric U-band (Johnson and Morgan, 1953) is sensitive to the CN and NH molecular absorption bands, and hence allows stellar abundance information to be inferred photometrically. The only AGB sample that Monelli et al. (2013) analysed in this way was 47 Tucanae, in which they found a bimodality similar to the RGB sample of the same cluster. García-Hernández et al. (2015) also used the C_{UBI} index to separate AGB subpopulations in their analysis of four GCs, while Milone et al. (2015a, M 2) and Gruyters et al. (2017) used similar methods to observe multiple populations in the AGB stars of other GCs (M 3, M 92, NGC 362, NGC 1851, and NGC 6752). We note here that the broadness of the UBI filter passbands means that they incorporate multiple atomic lines and molecular bands, and high-resolution spectra provide a much more precise tool to investigate subpopulations in GCs.

Observations and theoretical studies of AGB stars in GCs have increased even more in recent years, with a consensus yet to be reached. Discussion of these recent studies, and the controversy surrounding them, is reserved for Chapters 1.5 - 5. The purpose of this thesis is to contribute to the debate on GC AGB stars, and provide new observations and analyses of their abundance distributions.

1.4 The spectroscopic method

This thesis relies heavily on the analysis of stellar spectra, and especially on the determination of elemental abundances from spectral absorption features arising from the interaction of atoms and molecules with electromagnetic radiation.

While low-resolution spectra (R $\sim$ 3000, like those observed with AAOmega on the Anglo-Australian Telescope; Sharp et al., 2006), are unable to resolve narrow atomic absorption features, the broad absorption bands that arise from the formation of molecules (e.g., CN, CH, NH) in the upper atmospheres of stars are easily detectable. Despite the lack of a firm theoretical understanding of their formation, relative chemical abundances (especially those of carbon and nitrogen) can be empirically inferred by comparing photon counts inside, and adjacent to, the absorption features (e.g., Norris et al., 1981, and Figure 1.11). Measuring molecular band strengths was the method first used to observe multiple populations in GCs (e.g., Zinn, 1973; Hesser et al., 1977), and we use molecular band strengths alongside atomic abundances as a complimentary tool in Chapter 5.

Absorption features arising from the interaction between electromagnetic radiation and atoms in the upper layers of a star are much more thoroughly understood than molecular band formation, and potentially allow for a more robust abundance analysis of stellar spectra. The spectral widths of these features are typically on the order of 10^{-3} - 10^{-1}Å, and their strength and profile depend on a variety of factors including electron structure and potentials, formation depth and conditions, broadening effects, the degree to which they adhere to the Saha-Boltzmann ionization-excitation formulation (adherence is often called local thermodynamic equilibrium, or LTE), and abundance (Hubeny and Mihalas, 2014; Gray, 2005).

In order to infer a stellar chemical abundance from a particular atomic absorption line, several details must be known (or estimated) about both the star and the line. A model of the atmosphere of the star is used to determine where the line is formed, based on the optimal conditions required to form the line (temperature, density, etc.). To create this model, an estimate of the $T_{\rm eff}$, surface gravitational acceleration (log g), and metallicity ([M/H]) of the star are required; along with a free parameter called microturbulence ($v_{\rm t}$, which can be inferred from Fe I line measurements or estimated from empirical relations). Knowledge of the absorption line (e.g., species, ionisation state, excitation potential, etc.) is also required. Finally, the spectral

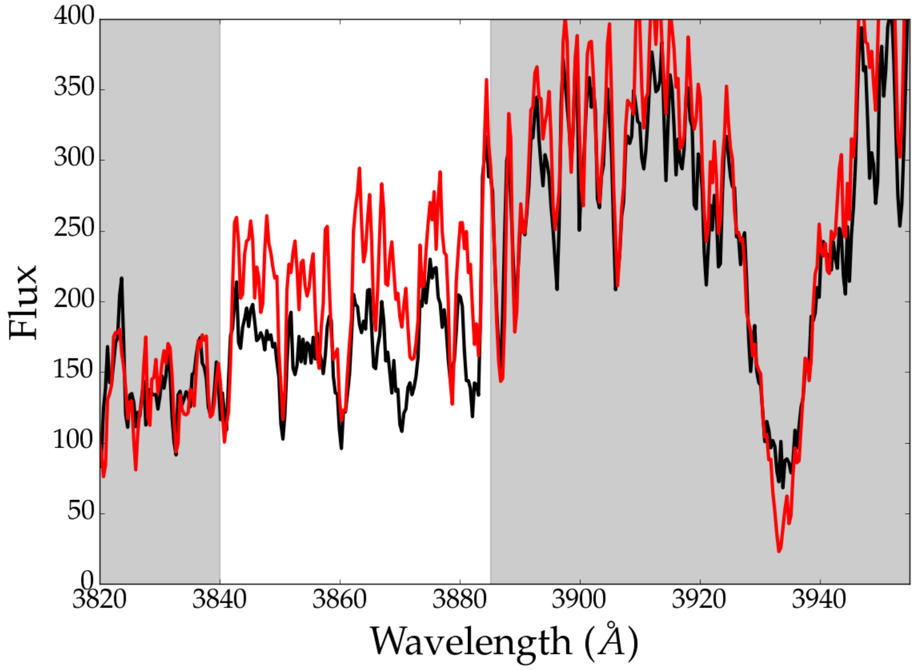

FIGURE 1.11: A low-resolution (R = 3000) spectral fragments of RGB stars 4938 (black) and 7298 (red) from our M 4 sample (see Chapter 5) showing the molecular CN absorption bands (∼3840-3885 Å) in the white region. Note that star 4938 has a generally lower flux in the CN region than star 7298, indicating it experiences more CN absorption and therefore has a higher nitrogen abundance.

line profile is parametrised with an equivalent width (EW; see Figure 1.12). The basic equations of absorption line theory (Gray, 2005) are then used to determine an abundance based on the inputs described above, usually using an LTE code such as MOOG (Sneden, 1973).

Abundances are typically expressed using the square-bracket formalism, denoting the scaled-solar logarithm of the ratio of two elemental species. For example,

$$[\mathrm{X/H}] \equiv \mathrm{A(X)} - \mathrm{A(X)}_{\odot}$$
$$\mathrm{A(X)} = \log_{10}(\frac{\mathrm{N_X}}{\mathrm{N_H}}) + 12.0^{6},$$

where N_X represents the number density of atoms of element X. While metallicity is considered to be the total stellar abundance of all elements heavier than He, in practice a proxy element is adopted that scales with global metallicity – e.g., Fe, Ni, Ca (McWilliam, 1997). In this thesis, we follow the common practice of defining the metallicity of a star as being the same as its iron abundance; i.e., [M/H] = [Fe/H].

1.4.1 Atmospheric models

There are many factors to consider when determining the chemical abundance of a star, but potentially the most difficult is obtaining an accurate model of the stellar atmosphere (where the absorption lines are formed). Computational limits restrict both the number of dimensions that can be feasibly modelled, and the level of physical detail that can be incorporated in the model. Until recently, only one-dimensional atmospheric models were available for use in spectroscopic abundance determination. The two most commonly used grids of 1D models (from which a star-specific model is interpolated) are the ATLAS9 (Kurucz, 1993; Castelli and Kurucz, 2004) and MARCS (Gustafsson et al., 1975; Gustafsson et al., 2008) grids. These models assume LTE – abundances determined using 1D models require corrections when line formation conditions diverge from LTE (non-LTE).

Efforts have been made over the last decade to create full three-dimensional, time-dependent, hydrodynamical models of stellar atmospheres. The largest and most utilised of these is The Stagger-Grid[7] (Magic et al., 2013). These 3D models cannot be interpolated in T_{eff} and log g (as with 1D models); and determining abundances is much more computationally demanding, especially when incorporating non-LTE effects (e.g., Nordlander et al., 2017). A mean 3D (<3D>, spatially and temporally averaged) grid of models is also available as part of the Stagger-Grid project, within which we can interpolate in T_{eff} and log g to our desired model, and used in the analysis of 1D line formation.

[6] A(X) can also be written as $\log_{\epsilon}(\mathrm{X})$

[7] https://staggergrid.wordpress.com/

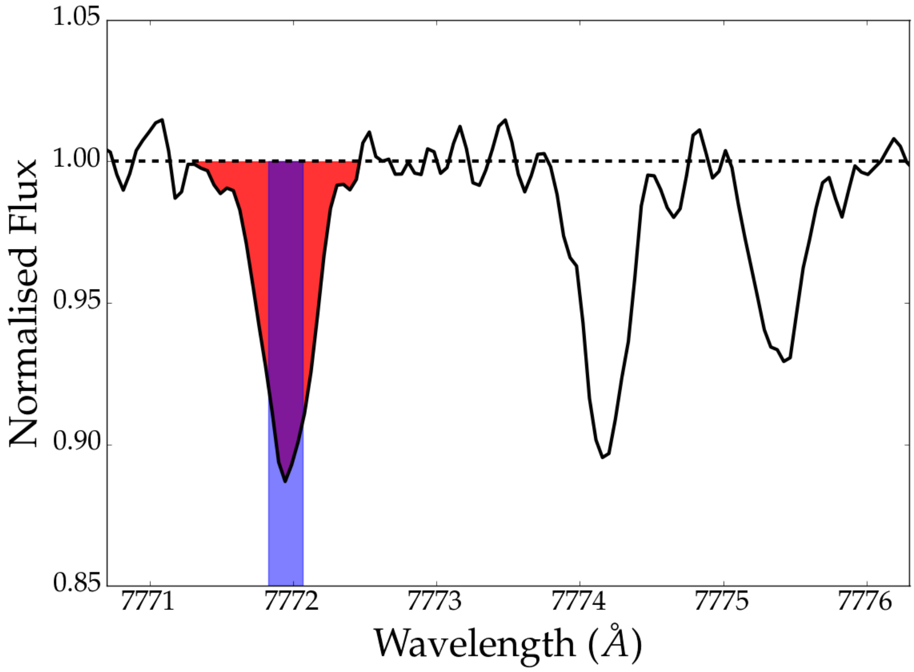

FIGURE 1.12: A high-resolution (R = 28,000) spectral fragment of AGB star 11285 from our M 4 sample (see Chapter 2) showing the 777nm oxygen triplet absorption feature. The profile of the 7771.94Å spectral line is parametrised schematically with an equivalent width (EW) – the width of a rectangle with the same area as the absorption line, and a height the same as the spectral blackbody continuum. As an illustration, the blue and red areas in this Figure have approximately the same total area (not to scale), and the width of the blue area is taken to be the EW.

The application of atmospheric models in abundance determination (while necessary) should be handled with care, since no model can be 100% accurate. We discuss and investigate this topic further in Chapter 5.

1.4.2 Stellar parameter determination

When it comes to choosing stellar parameters and interpolating 1D or <3D> atmospheric models for use in stellar abundance determination, a variety of techniques exist, and there are significant uncertainties involved in each. The choice of $T_{\rm eff}$, gravity, microturbulence and metallicity are non-trivial and critical, and many sources of error are contained within these four values. Two main methods exist for estimating these four stellar parameters: the photometric and the spectroscopic methods[8].

Photometrically, a star will be observed to have a particular brightness and colour. If the approximate age and global metallicity of its host cluster are also known, empirical relations (e.g., between colour and $T_{\rm eff}$; Alonso et al., 1999) can be used to estimate the parameters of stars from their position in a CMD. This is known at the photometric method. Despite reducing the number of variables that must be considered, the accuracy of these relations (especially between colour and $T_{\rm eff}$) is sample-dependent, and can often result in systematic offsets over a sample of stars, increasing the final abundance uncertainties. For clusters whose observation is impacted significantly by interstellar extinction, a detailed reddening map may also be required to compensate for the additional uncertainty in photometric colour indices (e.g., stars in M 4 appear to be ~ 0.4 dex redder in $B - V$ colour than they really are, and with a significant star-to-star scatter in reddening values).

The other main technique of determining stellar parameters is known as the spectroscopic method, which utilises the relative strengths of Fe I and Fe II absorption lines (other elements such as Ti and Ni can also be used) to gain a star-specific set of parameters. Once an estimated set of stellar parameters is determined (usually photometrically), and a range of Fe I and Fe II lines have been measured in the stellar spectrum, the final parameters are inferred by requiring that

(i) for $T_{\rm eff}$: the line-to-line Fe I abundances show no trend with excitation potential (E.P.),

(ii) for $v_{\rm t}$: the line-to-line Fe I abundances show no trend with reduced equivalent width (R.W. = EW/λ), and

(iii) for log g: the average Fe I and Fe II abundances are the same (i.e., ionisation balance).

[8]Other methods can also be employed – e.g., Hα absorption line fitting

Complications that exist within this process include Fe abundance uncertainties (e.g., EW measurements, atomic line data), the interdependence of parameters on the line-to-line Fe I abundances, and details of the iterative procedure used to determine the final set of parameters (local minima can exist within the parameter space for the three requirements of the spectroscopic method, see Chapter 3).

While several pre-developed codes exist within the spectroscopic community for the determination of stellar parameters using the spectroscopic method, a deeper understanding than is typically gained by using an existing code is preferred, in order to better understand the interplay between stellar parameters and line-to-line Fe abundances. To this end, a new *Python* (v2.7) code called PHOBOS was developed for this thesis that iteratively determines the optimal stellar parameters for a given set of Fe line measurements.

1.4.3 PHOBOS: A new analysis pipeline

PHOBOS, a spectroscopic analysis pipeline that has been developed for this thesis, has two main functions and purposes. The first is as a wrapper for:

(i) the LTE abundance code MOOG (Sneden, 1973),

(ii) the EW measurement algorithm ARES[9] (Sousa et al., 2015),

(iii) and an interpolation routine for 1D ATLAS9 stellar atmospheric models (Castelli and Kurucz, 2004).

The second purpose of PHOBOS is to spectroscopically determine the optimal set of stellar parameters ($T_{\rm eff}$, $v_{\rm t}$, log g, and [Fe/H]) for a given set of Fe I and Fe II absorption line measurements. An initial estimate of these parameters is necessary, and can be either calculated by PHOBOS based on photometric measurements, or input directly. Two versions of this algorithm were developed; the first used in Chapter 2, and the second in Chapter 5. Both are described below.

PHOBOS V1

Beginning with an initial estimate (from the photometric method) the first version of PHOBOS altered the atmospheric model of a star in $T_{\rm eff}$ (10K steps) and $v_{\rm t}$ (0.05 km/s steps) until the E.P. and R.W. slopes were within a pre-specified tolerance (0.015 dex/eV and 0.015 dex, respectively). PHOBOS then altered log g (0.05 dex steps) until the average Fe II abundance (strongly dependant on log g) was within 0.1 dex of the average Fe I abundance. The interdependence of parameters on the Fe I slopes and ionisation

[9]However in this thesis, many of the reported absorption lines were manually measured with IRAF

balance necessitates iteration, and PHOBOS would continue this process until all conditions were simultaneously satisfied.

While useful, this method of determining spectroscopic parameters was dependent on having accurate photometric estimates of the stellar parameters. Furthermore, the final $T_{\rm eff}$ values were found not to be independent of these estimates, with systematic offsets and trends within the photometric colour-$T_{\rm eff}$ relations still remaining evident (see Chapter 5). In other words, the final spectroscopic parameters were a function of not only the Fe linelist provided to PHOBOS, but also of the photometric estimates (the accuracy of which can vary cluster-to-cluster). See Chapter 3 for an example of the consequences of this dependence.

PHOBOS V2

A different approach to determining spectroscopic parameters was taken in the second version of PHOBOS, where the final parameters do not inherit the offsets or trends of their photometric estimates. While a starting point is still required, we have found that reliable photometric estimates are not needed – parameters indicative of entire evolutionary phases can be used (at least for M 4; see below). This also means that uncertainties from reddening can be avoided.

In this new procedure, PHOBOS determines the relationships between $T_{\rm eff}$ and the Fe I-E.P. slope, and between $v_{\rm t}$ and the Fe I-R.W slope. Assuming linear relations (which we found was reasonable on a $T_{\rm eff}$ scale of $\lesssim 1000$ K), the new $T_{\rm eff}$ and $v_{\rm t}$ values chosen are those for which slopes of zero are achieved. At each iteration, log g is calculated 'photometrically', based on an empirical relationship with V magnitude and stellar mass (from Alonso et al., 1999). In this way ionisation balance is not forced, since Fe I lines can experience significant non-LTE effects (which PHOBOS/MOOG do not account for). There have also been suggestions in the literature that AGB stars experience additional non-LTE effects that are not yet fully understood, and that forcing ionisation balance may hide this effect (Ivans et al., 1999; Lapenna et al., 2015). See Figure 1.13 for a schematic description of our method used in PHOBOS V2.

Because the adopted Fe linelist is now the only factor on which the final parameters are dependent, star-specific parameter uncertainties can be determined. At each iteration, PHOBOS measures the standard error on the Fe I slope with E.P. and R.W., and calculates the associated $T_{\rm eff}$ and $v_{\rm t}$ values that produce these slope limits.

This new method for determining spectroscopic parameters is much more robust than that of PHOBOS V1, because it is dependent entirely on the Fe linelist. An important feature of PHOBOS V2 is that its results are reproducible using a range of stellar parameters, whereas PHOBOS V2 was

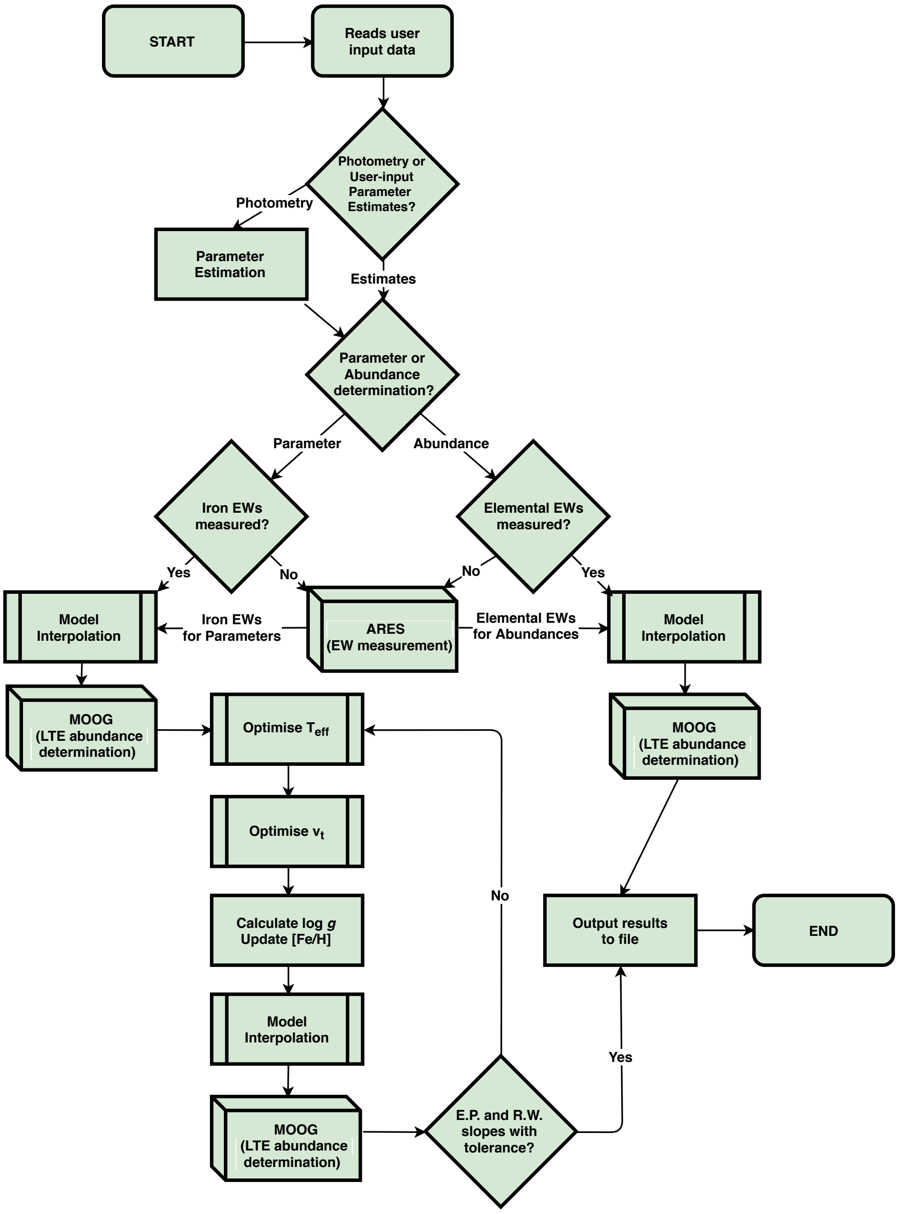

FIGURE 1.13: Flowchart describing the basic operation of PHOBOS V2. The code, plus a thorough description of its procedures, is available on GitHub (`github.com/btmaclean/PHOBOS`).

biased toward the photometric parameter estimates (see Chapter 3 for a deeper investigation into photometrically-dependent spectroscopic parameter solutions).

In Chapter 5, we describe a test where we provided our entire sample of M 4 RGB and AGB stars with identical initial values: $T_{\rm eff} = 4500$ K, $v_{\rm t}$ = 1.5, and log g = 2.5; representative of a typical globular cluster giant star. In this test, PHOBOS determined final parameters that were the same as when star-specific photometric parameters (estimated using empirical relations between colour and $T_{\rm eff}$) were used as the initial estimates (the average difference in star-to-star $T_{\rm eff}$ between the tests was 0 ± 2 K). This indicated that an initial $T_{\rm eff}$ within $\sim$1000 K (at least) of the 'true' $T_{\rm eff}$ will allow PHOBOS to determine a solution that is totally independent of the initial parameter estimates. Additionally the abundances from Fe I and Fe II lines, as determined with PHOBOS V2 for M 4, are the same as what was expected from the literature (previous spectroscopic studies of M 4) and non-LTE theory (see Chapter 5), providing strong evidence for the accuracy of our new method.

1.4.4 Data samples, quality, and details

The primary source of observational data used in this thesis was the High Efficiency and Resolution Multi-Element Spectrograph (HERMES) instrument on the 3.9 m Anglo-Australian Telescope (AAT) at the Siding Spring Observatory in NSW, Australia. HERMES utilises the 2dF facility, a multi-object fibre-fed positioning system that enables spectroscopic observation of up to 400 objects simultaneously over a 2° field of view (Lewis et al., 2002).

HERMES splits the incident light into four channels, defined by their wavelength ranges: 3700 - 4920 Å (blue), 5600 - 5930 Å (green), 6430 - 6790 Å (red), and 7540 - 10000 Å (infrared). While the spectral resolution of HERMES varies between fibres, and within the wavelength range, the resolution is typically between $25,000 < \mathrm{R} < 30,000$, allowing unblended atomic absorption lines in stellar spectra to be adequately resolved (Heijmans et al., 2012; Freeman, 2012).

Observations with HERMES were made in August 2014 and July 2015 via programmes 14B/27 and 15A/21 (PI Campbell), and reduced using the 2DFDR package (AAO Software Team, 2015). Our HERMES data had a signal-to-noise ratio ranging from 70 - 150, depending on target magnitude. Targets were selected based on the photometry of Mochejska et al. (2002, M 4; UBV from the 2.5m du Pont Telescope at Las Campanas Observatory) and Momany et al. (2003, M 4, NGC 6397; UBVI from the ESO/MPG WFI), which were used to separate the AGB and RGB of our target globular clusters. The line list that we used to determine chemical abundances was based on that of the GALAH collaboration ('GALactic Archaeology using HERMES', which is utilising HERMES exclusively; De Silva et al., 2015).

In addition to HERMES data we utilised spectra from the FLAMES/Giraffe instrument on the ESO Very Large Telescope (VLT) for Chapter 3, using the HR11 grating (spectral coverage $\lambda = 5597$ - 5840 Å, $55,000 < \mathrm{R} < 65,000$; Pasquini et al., 2002) for elemental abundance determination of NGC 6752 stars. Our FLAMES/VLT data were collected in June, 2013 (programme 089.D-0038, PI Campbell) with a signal-to-noise ratio of $\gtrsim 70$.

In Chapter 5 we used low-resolution spectra from the AAOmega/2dF multi-object spectrograph on the AAT (spectral coverage $\lambda = 3700$ - 8500 Å, $\mathrm{R} = 3,000$; Saunders et al., 2004; Sharp et al., 2006) for CN band strength determination of M 4 stars. Our AAOmega spectra were observed in September 2009 (programme 09B/15, PI Campbell), with a signal-to-noise ratio of ~ 20 to 50.

1.5 Thesis outline

Using primarily high-resolution spectra, this thesis seeks to provide both new observations of light-element abundance distributions of AGB stars in globular clusters, and fresh insight into spectroscopic abundance analysis in general.

The Chapters (published and submitted papers) described below alternate between brand new observations of GC AGB stars, and technical investigations. Chapters 2 and 4 are the first dedicated AGB studies of two clusters – M 4 and NGC 6397, respectively. Chapters 3 and 5 are technical re-analyses and comparisons to published work from other authors and research groups, in order to gain and provide deeper insights into the spectroscopic method and its utility (and caveats) for AGB stars.

Here we give an overview of each of these four Chapters, including brief statements highlighting recent relevant publications which strongly influenced the research direction of this thesis.

Chapter 2: An extreme paucity of second population AGB stars in the 'normal' globular cluster M 4 [2016, *MNRAS* 460, L69]

In this study we used high-resolution spectra from the newly operating HERMES spectrograph on the Anglo-Australian Telescope (this was the first abundance study to be performed utilising HERMES). Stellar parameters and abundances from Fe I, Fe II, Na I and O I lines were determined for a sample of RGB and AGB stars in the globular cluster M 4, using PHOBOS V1. While we confirmed the homogeneity of the cluster's metallicity, we initially expected the [Na/Fe] and [O/Fe] distributions of our AGB sample to be identical (within measurement uncertainties) to our RGB sample. This is because the bluest stars on M 4's HB have $T_{\rm eff} \sim 9,000$ K – evolutionary models predict that stars with such effective temperatures retain an envelope large enough to allow AGB evolution. We predicted $\mathscr{F} = 0\%$ for this cluster. Instead, we found that every AGB star in our sample displayed SP1-like characteristics, similar to the findings of C13 (NGC 6752). We reported that our abundances were consistent with M 4 showing an SP2 AGB deficit of $80\% \lesssim \mathscr{F} \lesssim 100\%$ – a much larger $\mathscr{F}$ value than expected. In this study we did not attempt to explain this phenomenon, but provided several potential hypotheses to guide future work. This study was published in the Letters section of the *Monthly Notices of the Royal Astronomical Society* as MacLean et al. (2016, hereafter ML16).

Chapter 3: NGC 6752 AGB Stars Revisited: Improved AGB temperatures remove apparent overionisation of Fe I [2017, *A&A* 605, A98]

With newly observed VLT-FLAMES spectra of NGC 6752 stars, Lapenna et al. (2016, hereafter L16) reported Fe, Na and O abundances for exactly the same sample of 20 AGB stars for which C13 published Na abundances. They did not, however re-observe C13's RGB sample (i.e., there were no RGB stars observed, or analysed, in L16). L16 reported a much larger range of [Na/Fe] values than C13 had found, and abundances from Fe I (but not Fe II) lines that were systematically lower, and with a larger spread, than have been typically determined for NGC 6752 (Harris, 1996; Yong et al., 2005). When L16 over-plotted their AGB stellar abundances on a sample of NGC 6752 RGB stellar abundances from Yong et al. (2003), the AGB stars covered the SP1 and intermediate SP2 abundance ranges, but not the most extreme Na-rich region. If true, this is in line with stellar evolutionary theory because a substantial amount of AGB avoidance is expected in NGC 6752 (i.e., AGB-manqué stars evolving from the cluster's extended blue HB). Indeed, L16 found an $\mathscr{F}$ value of $\sim$ 30% (which matches the theoretical study of Cassisi et al., 2014), compared to $\mathscr{F} = 100\%$ in C13. Chapter 3 describes our efforts to investigate and understand the reason why L16 reached such a different conclusion to C13, by re-analysing our sample of NGC 6752 AGB spectra and searching for potential differences in method that may have caused the contrasting results.

Upon comparing just the published abundances of C13 and L16, we discovered that the [Na/H] abundances of the two studies actually agreed very well, while it was the stellar parameters that varied significantly. A substantial difference in abundances from Fe I lines caused the disparity between reported [Na/Fe] results. L16 used Fe I lines to determine metallicity, while C13 assumed a constant value from the literature, effectively reporting on NGC 6752's [Na/H] distribution since metallicity was assumed to be homogeneous. We investigated potential explanations for this difference. Ultimately, we found that the $T_{\rm eff}$ values of the stellar atmospheric models had the largest impact on abundances from Fe I lines, and that the colour-$T_{\rm eff}$ relations that L16 adopted for photometric stellar parameter estimation gave systematically lower effective temperatures than other relations that are usually considered more reliable (we found the $V - K$ relations to be most reliable for NGC 6752). While L16 determined their final stellar parameters spectroscopically, we note that they retained the bias toward low $T_{\rm eff}$ values from the relations they adopted (similar to PHOBOS V1, which we rectified in PHOBOS V2). We further showed that with a new $T_{\rm eff}$ scale, the conclusion of a 100% SP2 AGB deficit (as in C13) could be made from both our [Na/H] and [Na/Fe] abundances, largely due to the robustness of Na I lines to systematic differences in T_{eff}. This work was published in *Astronomy & Astrophysics* as Campbell, MacLean, et al. (2017, hereafter C17).

Chapter 4: AGB subpopulations in the nearby globular cluster NGC 6397 [2018, *MNRAS* 475, 257]

In Chapter 4, we report on a new set of parameters and abundances for a sample of AGB and RGB stars in the GC NGC 6397; the first high-resolution study of AGB stars in this cluster. The spectra for these stars were observed with HERMES during the same observing run as for our M 4 sample. For this analysis, we did not use PHOBOS' spectroscopic parameter utility, but opted instead for photometrically estimated parameters (except metallicity, for which Fe I and Fe II lines were measured). The reason for this choice was largely due to the uncertainty surrounding parameter selection in the recent literature (see Chapter 3). We decided that since we had not yet developed a more reliable method for spectroscopic parameter determination (than PHOBOS V1), and since NGC 6397 does not experience differential reddening like M 4, well estimated photometric parameters were the most reliable option. We further determined Fe, Na, O, Mg, and Al abundances for our sample of AGB and RGB stars in NGC 6397.

The adopted parameters proved to be reliable: our RGB abundances from Fe I, Fe II, Na I, O I, Mg I, and Al I lines agreed well with both the existing literature, non-LTE predictions, and did not show significant trends with T_{eff}. As expected from stellar evolutionary theory (NGC 6397's HB extends only to $T_{\text{eff}} \sim 10,500$ K), our AGB and RGB samples matched very well, with the same proportions of SP2 stars on each branch – i.e., $\mathscr{F} = 0\%$, no SP2 AGB deficit. Comparing to our M 4 study, the spectra were observed with the same instrument (HERMES), and the method was almost identical: the same line list was used, and although a different method of parameter determination was used, we showed in Chapter 3 that this would be unlikely to alter our [Na/H] values significantly. Our NGC 6397 results contrast strongly with those from our M 4 study, indicating that since the phenomenon is not present in NGC 6397, our M 4 result was most likely not an artefact of our method in Chapter 2. This work was published in the *Monthly Notices of the Royal Astronomical Society* as MacLean et al. (2018a, hereafter ML18a).

Chapter 5: On the AGB stars of M 4: The mystery persists [2018, *MNRAS* Submitted]

In the time between the publication of the controversial results of ML16 (Chapter 2) and the submission of this final Chapter for publication, *three* independent studies of M 4 and its AGB were published; all responding to our ML16 results, and with new observations. The first of these, Lardo et al. (2017), used only the photometric C_{UBI} index to identify SP1 and SP2 stars on both the RGB and AGB, concluding that the spread in C_{UBI} values on both giant branches were equivalent (therefore $\mathscr{F} = 0\%$). Soon after this, both Marino et al. (2017, hereafter Mar17) and Wang et al. (2017, hereafter W17) published elemental abundances for M 4 AGB stars using independent spectroscopic observations using the FLAMES spectrograph on the VLT. Mar17 concluded the same as Lardo et al. (2017), that the [Na/Fe] and [O/Fe] distributions of their AGB sample were consistent with an RGB-like Na-O anti-correlation. Note that Mar17 (like L16) did not re-observe an RGB sample, but compared their AGB results directly to the M 4 RGB abundances of Marino et al. (2008, hereafter Mar08). W17 reported Fe and Na abundances for an AGB and RGB sample, and concluded that while their AGB sample covers a larger range in Na values than in ML16, the most-Na rich AGB stars did appear to be missing, and they concluded that there appears to be a deficit of SP2 AGB stars in M 4.

With such a disagreement regarding the AGB of M 4 now existing in the literature, we decided to take a second look at our ML16 results in an attempt to resolve the disparate conclusions in the literature, and with the aim of potentially explaining the SP2 AGB deficit phenomenon – at least in M 4. To this end, we re-analysed our HERMES spectra using our updated PHOBOS V2 spectroscopic pipeline to determine more reliable stellar parameters that are insensitive to the initial photometric estimates (see 1.4.3 for details), resolving an issue in the recent GC literature where systematic offsets in $T_{\rm eff}$ and [Fe/H] (stemming, in part, from the use of individual colour-$T_{\rm eff}$ relations for stellar parameter determination) have produced conflicting results between studies. Using our new stellar parameters, we determined updated Na and O abundances for our entire M 4 sample from Chapter 2. Additionally, we presented brand new Mg and Al abundances using our HERMES spectra, and CN band strengths using new low-resolution spectra from AAOmega/2dF. We found that our ML16 results were robust, and supported by our new Al abundances and CN band strengths, which showed the same SP2 AGB deficit that was present in our original Na abundances. Due to our large uncertainties in O abundance, we concluded that this species is homogeneous in M 4 (within errors), along with Fe and Mg.

We then compared our new abundance results with those of Mar17 (and Mar08 for the RGB), W17, and Ivans et al. (1999, hereafter I99), and compared our CN results with the compiled CN band strengths from Smith and Briley (2005, hereafter SB05). We found the Na, Al, and CN results in each of these studies agreed with our conclusion that AGB stars in M 4 contain, on average, less H-burning products than RGB stars in the cluster, and are generally representative of SP1 stars – i.e., M 4 displays a significant deficit of SP2 AGB stars. In order to establish a precise, quantitative theoretical expectation of the abundances of AGB stars in M 4, we calculated a range of stellar models with the Monash University stellar structure code MONSTAR, using observational constraints on M 4 stars from the literature. All models whose HB T_{eff} matched the observed values from Marino et al. (2011) and Villanova et al. (2012) ascended the AGB, while only stars with a $T_{\mathrm{eff}} \sim 6000$ K higher than the bluest HB stars in M 4 avoided the AGB. We predicted, using these models, that the distribution in light-elemental abundances on the AGB should be identical to that of the RGB.

In an attempt to reconcile the disparity between the theoretical predictions and the observations of AGB stars in M 4, we investigated the likelihood that we misidentified Na-rich AGB stars as being Na-poor due to systematic and random uncertainties in our high-resolution spectroscopic method. We found that our conclusion of an SP2 AGB deficit in M 4 is insensitive to a range of factors, including: large T_{eff} uncertainties, the effects of including a He-enhancement in the atmospheric models of SP2 stars, the abundance determination pipeline utilised, the choice of 1D and mean-3D atmospheric models, and full-3D non-LTE effects on absorption lines.

Thus, in summary, while we established that, en-large, all observational studies of M 4's AGB agree that there is a discrepancy between the light-elemental abundance distributions of RGB and AGB stars, we were unable to reconcile these observations with the theoretical predictions. The mystery persists. In this Chapter, we suggested avenues of future research on this topic. This work has been submitted to the *Monthly Notices of the Royal Astronomical Society* for publication (MacLean et al., 2018b, hereafter ML18b).

TABLE 1.1: A summary of the subpopulation membership percentages of RGB and AGB stars in GCs as reported in the literature, by publication date. Also included are metallicities as reported in each study, HB-morphology ('R' indicates the presence of a red-HB, 'B' a blue-HB, and 'EB' an extended blue-HB), and the elemental inhomogeneities used to separate the subpopulations. Sample sizes are the total number of RGB and AGB stars analysed in each respective study. The percentages of RGB and AGB stars in a GC that are found to be members of SP2 are written as $\mathscr{R}_{RGB}$ and $\mathscr{R}_{AGB}$, while $\mathscr{F} = (1 - \mathscr{R}_{\mathrm{AGB}}/\mathscr{R}_{\mathrm{RGB}}) \cdot 100\%$, which we use throughout as our 'SP2 AGB deficit' parameter (see 1.2.2). Included are the studies of C13, Johnson et al. (2015, J15), García-Hernández et al. (2015, GH15), Lapenna et al. (2016, L16), Wang et al. (2016, W16), Mar17, W17, Mucciarelli et al. (2018, Muc18), and Chapters 2, 3, 4, and 5, from this thesis. This is a reworking and update of Table 2.4.

Study	NGC	Other ID	[Fe/H]	Sample size RGB	Sample size AGB	$\mathscr{R}_{\mathrm{RGB}}$	$\mathscr{R}_{\mathrm{AGB}}$	$\mathscr{F}$	HB morphology	Elements used
C13	6752	-	-1.54[1]	24	20	70	0	100	B+EB	Na
J15	104	47 Tuc	-0.68	113	35	55	37	33	R	Na
L15	6266	M 62	-1.10[2]	13	5	46	0	100	R+B+EB	Na, O, Al
GH15	7089	M 2	-1.65	12	5	80	40	50	B+EB	Al
GH15	5272	M 3	-1.50	46	9	50	33	34	R+B	Al
GH15	5904	M 5	-1.29	107	15	50	31	38	R+B+EB	Al
GH15	6205	M 13	-1.53	67	14	70	28	60	B+EB	Al
ML16	6121	M 4	-1.15	106	15	55	0	100	R+B	Na, O
L16	6752	-	-1.58[2]	37[3]	20	73	63	14	B+EB	Na, O
W16	2808	-	-1.11	40	31	52	55	-6	R+B+EB	Na
Mar17	2808	-	-1.27	140	7	54	57	-6	R+B+EB	Na, O, Mg, Al

Mar17	6121	M 4	-1.20	105[4]	17	60	47	22	R+B	Na, O, Al
C17	6752	-	-1.43[2]	24	20	70	0	100	B+EB	Na
W17	104	47 Tuc	-0.82	27	40	67	40	40	R	Na
W17	6121	M 4	-1.14	68	19	76	53	30	R+B	Na
W17	6809	M 55	-1.86	77	23	66	65	2	B	Na
W17	6752	-	-1.60	24	20	75	15	80	B+EB	Na
ML18a	6397	-	-2.15	47	8	60	60	0	B	Na, O, Mg, Al
Muc18	5824	-	-2.11[2]	87	30	40	23	43	B+EB	Mg, Al
ML18b	6121	M 4	-1.20	106	15	55	20	64	R+B	Na, O, Al, CN

[1] Adopted value.

[2] RGB stars only.

[3] RGB abundances adopted from Yong et al., 2003.

[4] RGB abundances adopted from Mar08.

Chapter 2

An extreme paucity of second population AGB stars in the 'normal' globular cluster M 4

Published in *MNRAS* 460, L69, July 2016.

Abstract

Galactic Globular clusters (GCs) are now known to harbour multiple stellar populations, which are chemically distinct in many light element abundances. It is becoming increasingly clear that asymptotic giant branch (AGB) stars in GCs show different abundance distributions in light elements compared to those in the red giant branch (RGB) and other phases, skewing toward more primordial, field-star-like abundances, which we refer to as subpopulation one (SP1). As part of a larger program targeting giants in GCs, we obtained high-resolution spectra for a sample of 106 RGB and 15 AGB stars in Messier 4 (NGC 6121) using the 2dF+HERMES facility on the Anglo-Australian Telescope. In this Letter we report an extreme paucity of AGB stars with [Na/O] > -0.17 in M 4, which contrasts with the RGB that has abundances up to [Na/O] $= 0.55$. The AGB abundance distribution is consistent with all AGB stars being from SP1. This result appears to imply that all subpopulation two stars (SP2; Na-rich, O-poor) avoid the AGB phase. This is an unexpected result given M 4's horizontal branch morphology – it does not have an extended blue horizontal branch. This is the first abundance study to be performed utilising the HERMES spectrograph.

2.1 Introduction

It has been well established that Galactic GCs are typically homogeneous in the iron peak species (Carretta et al., 2009a), but are chemically inhomogeneous in elements affected by proton-capture reactions (e.g., C, N, O, Na). These inhomogeneities are generally thought to arise from nucleosynthesis in the first generation of stars (Gratton et al., 2004). Correlations exist in the star-to-star scatter of some elemental abundances within each cluster, and can be used as tracers of GC formation (see Gratton et al. 2012 for an extensive review). One well-documented chemical pattern is the sodium and oxygen anti-correlation (Na-O), seen in all GCs (Carretta et al., 2010), but not in open clusters (De Silva et al., 2009; MacLean et al., 2015). The Na-O anti-correlation has been documented across both evolved and unevolved stars in many GCs, indicating that this pattern must be imprinted on the stars at their birth. While GC stars can often be separated into more than two distinct subpopulations in chemical space, for the sake of clarity here we use just two. Stars with near primordial abundances (Na-poor, O-rich) we designate as subpopulation one (SP1) and those enriched in sodium and depleted in oxygen as subpopulation two (SP2). We also define the percentage of RGB and AGB stars in a GC that are found to be members of SP2 as $\mathscr{R}_{RGB}$ and $\mathscr{R}_{AGB}$, respectively. In studies targeting the RGB in GCs, typical $\mathscr{R}_{RGB}$ values are found to be on the order of $\sim$60 (see Figure 16 in Carretta et al., 2010).

It is becoming clear that the light element abundance distributions of AGB stars are significantly different to those of stars in other phases of evolution in many GCs. Norris et al. (1981) found no examples of cyanogen (CN) strong AGB stars in NGC 6752 despite the bimodality of CN strengths in the RGB (see also Campbell et al., 2010). Campbell et al. (2013) observed Na abundances of AGB stars in the same cluster, and no Na-rich AGB stars were found ($\mathscr{R}_{AGB} = 0$, compared to $\mathscr{R}_{AGB} = 70$). They concluded that the most likely explanation was that all Na-rich stars (SP2) fail to reach the AGB phase. M 62 was similarly observed to have a value of $\mathscr{R}_{AGB} = 0$ (Lapenna et al., 2015), while for 47 Tucanae Johnson et al. (2015) found that $\mathscr{R}_{AGB} = 37$, indicating that a smaller, but significant proportion of SP2 stars are avoiding the AGB phase.

We define the 'AGB failure rate' $\mathscr{F}$ of a GC to be the percentage of SP2 stars that avoid the AGB (as inferred by its $\mathscr{R}_{\rm RGB}$ value), given by

$$\mathscr{F} = (1 - \frac{\mathscr{R}_{\rm AGB}}{\mathscr{R}_{\rm RGB}}) \cdot 100\%, \tag{2.1}$$

where a value of 100 indicates that no SP2 stars reach the AGB (as in NGC 6752), and a value of zero indicates that $\mathscr{R}_{\rm AGB} = \mathscr{R}_{\rm RGB}$. We provide an up-to-date summary of this 'AGB avoidance' phenomenon in Table 2.4.

While theoretical simulations struggle to quantitatively reproduce the Na distributions of AGB stars in GCs, it likely results from the He-enrichment of SP2 (Charbonnel et al., 2013; Cassisi et al., 2014; Charbonnel and Chantereau, 2016). This results in a smaller envelope mass in the horizontal branch (HB) phase, giving rise to higher surface temperatures. The most extreme of these stars fail to reach the AGB phase and evolve directly to the white dwarf phase and are known as AGB-manqué ('failed') stars (Greggio and Renzini, 1990). Gratton et al. (2010a) showed that a large He-enrichment can result in an extended blue-HB (e.g. NGC 6752 and M 62), suggesting that an extended blue-HB may be indicative of a high $\mathscr{F}$ value. The recently reported slight AGB failure rate of 47 Tucanae (Johnson et al., 2015), which contains only a red HB, further supports this link between HB morphology and AGB avoidance.

The GC Messier 4 (NGC 6121), considered archetypal, is moderately metal-poor and shows well-populated and distinct red- and blue-HBs with no significant blue extension (Mochejska et al., 2002). Norris (1981) first documented the bimodality of the CN band strength of giant stars in M 4 (although we note that Smith and Norris, 1993 reported a CN-strong monomodality on the RGB), and Carretta et al. (2013) suggested that it only contains two distinct subpopulations (unlike many GCs which contain three or more). While the high resolution abundance study of Ivans et al. (1999) first hinted at a disparity between $\mathscr{R}_{RGB}$ and $\mathscr{R}_{AGB}$, AGB stars have never been systematically studied. M 4 has been observed to show a bimodal distribution in Na and O on the RGB (Marino et al., 2008, hereafter Mar08) and the HB, with all red-HB stars belonging to SP1 (Marino et al., 2011).

In this paper we present results from the first systematic study of the AGB of M 4, including Na and O abundances for a sample of 106 RGB stars and 15 AGB stars. This work is part of a larger study of AGB abundances in GCs (Campbell et al., 2010; Campbell et al., 2013), and presents the first abundance results from the HERMES spectrograph on the AAT.

2.2 Observations and membership

For target selection we used photometry of M 4 from two sources; UBV from Mochejska et al. (2002, with an 8.8′x8.8′ field of view) and UBVI from the ESO/MPG Wide Field Imager (WFI, with a 34′x33′ field of view; Momany et al., 2003). The RGB and AGB were separated in both V−(B−V) (see Figure 2.1) and U−(U−I), allowing for an accurately selected sample of AGB stars. We applied a correction of a constant value $E = 0.37$ (Hendricks et al., 2012) because M 4 is affected by significant reddening.

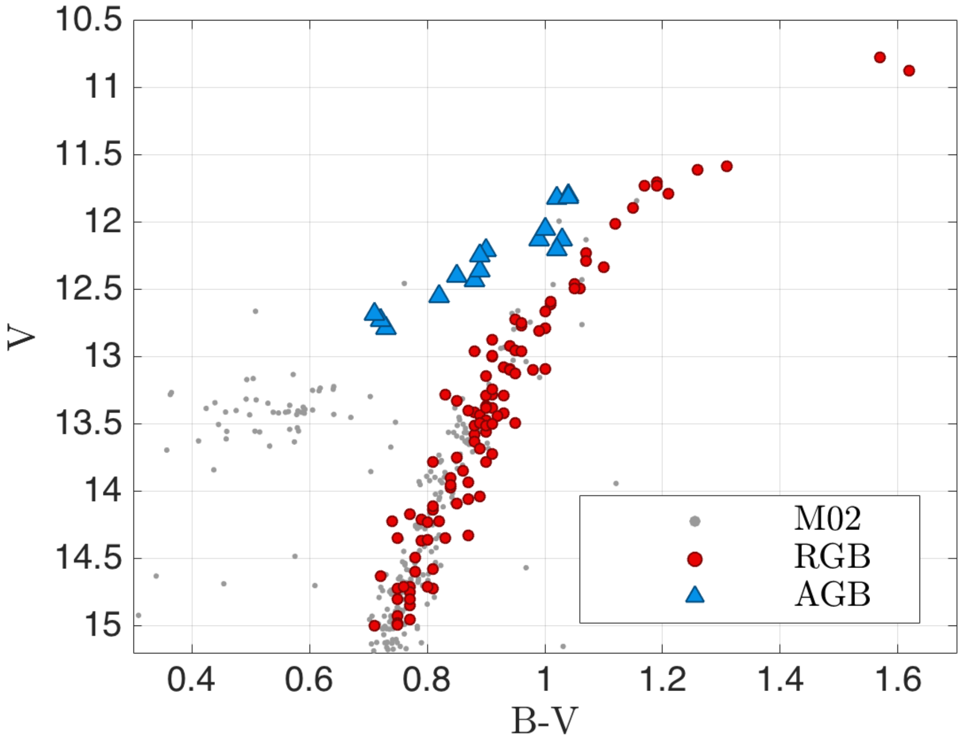

FIGURE 2.1: Final sample of RGB and AGB stars used in this work are displayed over the larger photometric sample of Mochejska et al. (2002, M02). A value of B−V = $+0.05$ was added to the WFI data due to a systematic offset between the two photometric data sets.

Spectra were collected in August 2014 and July 2015 using 2dF+HERMES on the AAT which provides $R = 28,000$ resolution spectra in 4 narrow spectral windows (Sheinis et al., 2015). In total 121 targets were observed with average SNR of 70. The software package 2DFDR (AAO Software Team, 2015, v6.5) was used to reduce the spectral data for analysis.

Radial velocities for the HERMES spectra were measured with the IRAF *fxcor* package (Tody, 1986), using a solar reference template. We considered all stars with radial velocities above 90 km/s or below 50 km/s to be non-members. Our average radial velocity after non-member elimination was <v> = 70.62 ± 0.31 km/s ($\sigma = 3.45$ km/s), agreeing well with Malavolta et al. (2015), who report <v> = 71.08 ± 0.08 km/s ($\sigma = 3.97$ km/s). Individual stellar radial velocities are in Table 2.1. Stellar metallicities (discussed in §2.3.1) were used as a further test of cluster membership, with one AGB star and two RGB stars possessing metallicities that were farther than 2σ from the mean, leaving a sample of 106 RGB and 15 AGB stars. A colour-magnitude diagram of the final sample is presented in Figure 2.1.

2.3 Method and Results

2.3.1 Atmospheric parameters

BV photometry was used to calculate initial estimates of the stellar parameters for each star. Effective temperature ($T_{\rm eff}$) was estimated using the calibrated scale of Ramírez and Meléndez (2005), while surface gravity (log g) and microturbulence ($v_{\rm t}$) were estimated using empirical relations from Alonso et al. (1999) and Gratton et al. (1996), respectively.

Final $T_{\rm eff}$, log g and $v_{\rm t}$ values (Table 2.1) were determined spectroscopically by measuring the equivalent widths (using the ARES package, Sousa et al., 2015) of neutral and singly-ionized iron (Fe I & II, respectively) absorption lines and calculating the one-dimensional local thermodynamic equilibrium (LTE) abundance from each line with the MOOG code (Sneden, 1973, June 2014 release) and model atmospheres interpolated from the Castelli and Kurucz (2004) grid. Final spectroscopic parameters were found by requiring excitation and ionisation balance (with tolerances of 0.015 in slope and 0.1 dex, respectively), as per Sousa (2014) and using our newly developed code PHOBOS, to be detailed in MacLean et al. (2016, in preparation). We found the average metallicity of the cluster to be <[Fe/H]> = -1.15 ± 0.01 ($\sigma = 0.05$).

2.3.2 Chemical abundances & Analysis of results

We determined LTE abundances for Na and O by measuring the equivalent widths of a selection of absorption lines. It is well known that many sodium and oxygen lines deviate from LTE, with systematic offsets that have been a subject of much research (e.g., Asplund, 2005; Lapenna et al., 2014). The sodium 568 nm doublet was measured for each star, and the abundances of each line were corrected for non-LTE effects as described in Lind et al. (2011a) by using the web-based INSPECT interface[1], and adopting the provided Δ[Na/Fe]$_{\mathrm{NLTE}}$ corrections which were around -0.15 dex.

In the case of oxygen, the 777 nm triplet was measured and corrected for non-LTE effects following Takeda (2003). Recently, Amarsi et al. (2015) calculated a fine grid of oxygen corrections for both non-LTE effects and the effects of using 3D stellar atmosphere models; however the grid range is $T_{\mathrm{eff}} > 5000$K and log $g > 3.0$; outside the range of most of our stars.

Final [Na/Fe] and [O/Fe] abundances for all confirmed cluster members are contained in Table 2.1. Also included are uncertainties based on line-to-line scatter, which are in the range ~ 0.10 to 0.15 dex. The abundance sensitivities due to the uncertainty in stellar parameters are given in Table 2.2. These are on the order of 0.02 to 0.15 dex.

[1]http://inspect-stars.net

TABLE 2.1: Stellar parameters, radial velocities and chemical abundances for each star. Abundance errors reflect line-to-line scatter, and do not take atmospheric sensitivities into account (see Table 2.2 and text for discussion). Included are the stellar designations used by Mar08. We adopt the Asplund et al. (2009) solar abundance values. See Appendix A, Table A.1 for complete table.

Star	Type	RV (km/s)	$T_{\rm eff}$ (K)	log g (cgs)	$v_{\rm t}$ (km/s)	[Fe/H]	[O/Fe]	[Na/Fe]	ID Mar08
25	RGB	66.6	5028	2.64	1.09	-1.14 ± 0.12	0.30 ± 0.12	0.43 ± 0.13	-
907	RGB	69.4	5047	2.69	0.94	-1.18 ± 0.11	0.42 ± 0.12	0.37 ± 0.11	-
1029	RGB	72.2	4936	2.45	1.41	-1.10 ± 0.09	0.09 ± 0.11	0.49 ± 0.11	22089
1129	RGB	69.6	4886	2.20	1.20	-1.11 ± 0.10	0.35 ± 0.12	0.10 ± 0.10	-
1474	RGB	70.4	5159	2.78	0.92	-1.06 ± 0.11	0.12 ± 0.12	0.39 ± 0.12	-

TABLE 2.2: Abundance uncertainties due to the atmospheric sensitivities of a representative sub-sample of RGB and AGB stars in our M 4 data set. Parameter variations (in parentheses) are the expected uncertainties in the respective parameters.

				[O/Fe]				[Na/Fe]			
Star	Type	$T_{\rm eff}$	log g	$\Delta T_{\rm eff}$ (±50K)	Δlog g (±0.2)	$\Delta v_{\rm t}$ (±0.1)	Total	$\Delta T_{\rm eff}$ (±50K)	Δlog g (±0.2)	$\Delta v_{\rm t}$ (±0.1)	Total
16547	AGB	4847	1.90	∓0.07	±0.07	∓0.01	±0.10	±0.04	∓0.01	∓0.02	±0.03
16788	RGB	3954	0.36	∓0.10	±0.11	∓0.01	±0.15	±0.05	∓0.04	∓0.04	±0.02
47603	RGB	5251	3.01	∓0.06	±0.06	∓0.01	±0.08	±0.03	∓0.02	∓0.01	±0.02

TABLE 2.3: The average differences in parameters and abundances between this work, Mar08, and C09. Uncertainties are the errors on the mean. There are no major offsets in the Na and O abundances of our work and that of Mar08.

Parameter	This study − Mar08	This study − C09
$\Delta T_{\rm eff}$	53.9 ± 1.1	154.8 ± 1.5
$\Delta\log g$	-0.210 ± 0.004	0.080 ± 0.003
$\Delta v_{\rm t}$	-0.071 ± 0.004	0.049 ± 0.007
Δ[Fe/H]	-0.092 ± 0.001	0.054 ± 0.002
Δ[O/Fe]	0.014 ± 0.003	0.197 ± 0.004
Δ[Na/Fe]	-0.044 ± 0.002	-0.126 ± 0.003

There is significant overlap between our RGB sample, that of Mar08 (51 stars in common), and Carretta et al. (2009b, hereafter C09, 46 stars in common). We made a detailed comparison of this intersecting sample, which revealed that while there are slight offsets between each study in several stellar parameters, the scatter among the parameters is consistent with uncertainties quoted in this work. The results of this comparison are provided in Table 2.3.

The [Na/Fe] and [O/Fe] values of our RGB and AGB samples are plotted along with the RGB sample of Mar08 in Figure 2.2. The larger scatter in our abundances compared to Mar08 is due the lower signal-to-noise ratio of our data. We attempted to define a population separation point (PSP) in our RGB sample by identifying a minimum between the two subpopulations (see Fig. 7 in Mar08; however the uncertainties in our abundances combined with the relatively small spread in Na and O in M 4 did not allow us to define one reliably. We have instead included the Mar08 PSP at [Na/O] $= -0.16$ in the figure. Using this PSP we find $\mathscr{R}_{\rm RGB} = 55$, which is consistent with that found by Mar08. It is also close to $\mathscr{R}_{\rm RGB} = 62{\pm}4$, as determined for the double main sequence using photometric star counts (Milone et al., 2014).

The usual Na-O anticorrelation can be seen in the RGB sample, with a spread of $\sim$$0.8$ dex in [Na/Fe] and $\sim$$0.6$ dex in [O/Fe]. In contrast, the AGB distribution is heavily skewed to SP1 compositions, with the spread in AGB abundances being restricted to $\sim$$0.4$ dex in [Na/Fe] and $\sim$$0.3$ dex in [O/Fe]. There are no AGB stars above the Mar08 PSP, giving $\mathscr{R}_{\rm AGB} = 0$ and $\mathscr{F} = 100$.

2.4 Discussion and conclusions

The novel feature of this work is the AGB sample. This is the first time that the AGB has been specifically targeted in M 4. We found that our sample of AGB stars has a much smaller spread in Na and O abundances than the

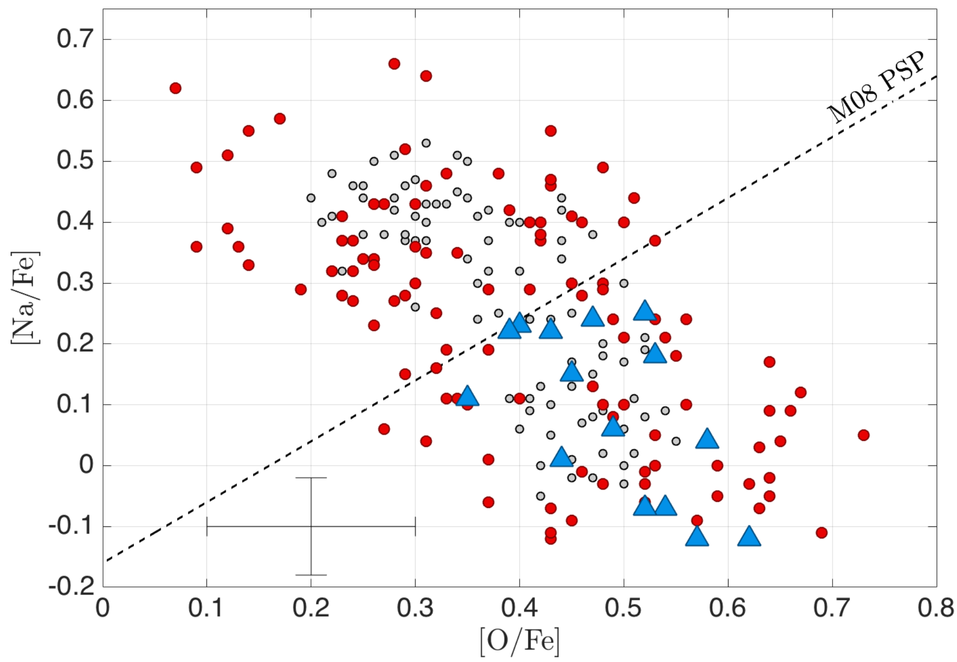

FIGURE 2.2: Final Na and O abundances for our RGB stars (solid red circles) and AGB stars (solid blue triangles; also see CMD in Fig. 2.1). Shown for comparison is the RGB sample of Mar08 (open grey circles). The Na-O anticorrelation is evident. The AGB distribution is clearly different from the RGB, showing a paucity of SP2 stars. Typical errors in individual abundances are shown in the bottom left, while the population separation point (PSP) from Mar08 is indicated by the dashed diagonal line (M08, see text for details).

RGB sample. Following the population separation point from Mar08, the AGB distribution is consistent with $\mathscr{R}_{\mathrm{AGB}} = 0$ and $\mathscr{F} = 100$. However, given (i) that the tails of the SP1 and SP2 RGB distributions appear to overlap in [Na/O] (cf. Fig. 7 in Mar08), and (ii) the uncertainties in our data, it is possible that the higher-Na (lower-O) AGB stars actually lie in the tail of the SP2 distribution. This would increase the value of $\mathscr{R}_{\mathrm{AGB}}$ from zero. Thus, until better data are obtained for the AGB stars, some uncertainty remains as to the exact failure rate ($\mathscr{F}$) of M 4. It is clear however that the majority of AGB stars in M 4 have compositions typical of SP1 stars (Fig. 2.2). A further uncertainty lies in the NLTE corrections, which may not be accurate for AGB stars. This was suggested by Lapenna et al. (2015) as a possible risk to determining subpopulation membership based on NLTE-affected Na lines; however there is growing evidence from a number of studies (including the Lapenna et al., 2015 M 62 study) that SP2 AGB avoidance is common in GCs. These studies are based on various elements and atomic lines (Table 2.4).

TABLE 2.4: A summary (including our current M 4 results) of the subpopulation membership percentages of RGB and AGB stars in GCs as reported in the literature. Also included are metallicities, HB-morphology ('R' indicates the presence of a red-HB, 'B' a blue-HB, and 'EB' an extended blue-HB), and the elemental inhomogeneities used to separate the subpopulations. Sample sizes are the total number of RGB and AGB stars analysed in each respective study.

NGC	Other	[Fe/H]	ΔY	Sample size		$\mathscr{R}_{\mathrm{RGB}}$	$\mathscr{R}_{\mathrm{AGB}}$	$\mathscr{F}$	HB	Elements
				RGB	AGB				morphology	used
104	47 Tuc	-0.68	0.02[2]	113[3]	35	55	37	33	R	Na
5272	M 3	-1.50	0.02[4]	46[5]	9	50	33	34	R+B	Al
5904	M 5	-1.29	-	107[5]	15	50	33	34	R+B+EB	Al
6121	M 4	-1.15	0.01[6]	106[7]	15	55	0	100	R+B	Na-O
6205	M 13	-1.53	0.06[8]	67[5]	14	70	27	61	B+EB	Al
6266	M 62	-1.10	0.08[9]	13[10]	5	46	0	100	R+B+EB	Na-O, Mg-Al
6752	-	-1.54	0.03[11]	24[12]	20	70	0	100	EB	Na
7089	M 2	-1.65	0.07[13]	12[5]	5	80	40	50	B+EB	Al

[2] Milone et al. (2012b) [3] Johnson et al. (2015) [4] Valcarce et al. (2016) [5] García-Hernández et al. (2015)
[6] Valcarce et al. (2014) [7] This study [8] Dalessandro et al. (2013) [9] Milone (2015) [10] Lapenna et al. (2015)
[11] Milone et al. (2013) [12] Campbell et al. (2013) [13] Milone et al. (2015a)

To put this finding in context we provide a summary of AGB and RGB subpopulation membership in Table 2.4 for the GCs for which $\mathscr{F}$ values have been determined. The table also includes HB morphology descriptions. As previously mentioned, recent observational and theoretical work has suggested a close link between HB morphology, He-enrichment, and $\mathscr{R}_{\mathrm{AGB}}$ values in GCs. For example, helium enrichment in NGC 6752 and M 62 – both of which have $\mathscr{F} = 100$ – has been inferred to be relatively high, with $\Delta Y \simeq 0.03$ and 0.08, respectively (Milone et al., 2013; Milone, 2015). Both these GCs also have extended blue HBs. In Table 2.4 the GC with the closest HB morphology to M 4 is M 3. The helium spread in M 3 has been reported to be up to $\Delta Y \sim 0.02$ (Valcarce et al., 2016). In terms of AGB stars, García-Hernández et al. (2015) report that M 3 has $\mathscr{F} = 34$, as is (qualitatively) expected from its HB morphology and moderate He enrichment. Given M 4's low He enrichment ($\Delta Y \simeq 0.01$, Valcarce et al., 2014), and its lack of an extended blue-HB, it would be expected that the AGB abundance distribution should be similar to M 3 or 47 Tucanae (red-HB only, $\mathscr{F} = 33$). It should be noted that age is a critical parameter in HB morphology, and that the differences in ages between these three clusters (M3, M 4 and 47 Tuc) are up to $\sim$1.2 Gyr (Carretta et al., 2010; Charbonnel and Chantereau, 2016). Instead of showing a low to moderate AGB failure rate, as may be expected, M4 is consistent with a GC with an extended blue-HB and a higher SP2 He abundance. Furthermore, a comparison between the HB morphologies of M 4 and NGC 6752 shows that the M 4 blue HB ends approximately where the NGC 6752 HB starts (around Teff $\sim$7000 K). Using star counts Campbell et al. (2013) report that it is only the stars hotter than $\sim$11500 K (the Grundahl Jump) that fail to reach the AGB, ie. far beyond the bluest HB stars in M 4. Models predict AGB avoidance only at even higher temperatures (see eg. Fig. 3 in Campbell et al. 2013). This suggests that there is one (or more) extra parameters that determine AGB avoidance, and that the HB stellar models cannot reproduce the observations, particularly for M 4.

The extreme paucity (or possible total lack, $\mathscr{F} = 100$) of SP2 AGB stars in the 'normal' globular cluster M 4 imposes further constraints upon the theory of the evolution of low-mass metal-poor stars, in particular the evolution of SP2 stars through the giant phases of evolution, and how this may be tied to their initial He abundances, mass-loss histories, and other factors. Finally, this result (i) demonstrates that star counts using the AGB to test stellar evolution time-scales may be unreliable because of altered CMD number statistics, (ii) could help to understand the source of excess UV flux in the spectra of elliptical galaxies due to the high surface temperatures of AGB-manqué stars, and (iii) may provide indirect clues to the formation history of globular clusters and their HB morphologies.

Acknowledgements

Based in part on data acquired through the AAO, via programs 14B/27 and 15A/21 (PI Campbell). VD acknowledges support from AAO distinguished visitor program 2016.

Chapter 3

NGC 6752 AGB Stars Revisited: Improved AGB temperatures remove apparent overionisation of Fe I

Published in *Astronomy & Astrophysics* 605, A98, September 2017.

Abstract

A recent study reported a strong apparent depression of Fe I, relative to Fe II, in the AGB stars of NGC 6752. This depression is much greater than that expected from the neglect of non-local thermodynamic equilibrium effects, in particular the dominant effect of overionisation. The iron abundances derived from Fe I were then used to scale all other neutral species in the study. Here we attempt to reproduce the apparent Fe discrepancy, and investigate differences in reported sodium abundances. We compare in detail the methods and results of the recent study with those of an earlier study of NGC 6752 AGB stars. Iron and sodium abundances are derived using Fe I, Fe II, and Na I lines. We explore various uncertainties to test the robustness of our abundance determinations. We reproduce the large Fe I depression found by the recent study, using different observational data and computational tools. Further investigation shows that the degree of the apparent Fe I depression is strongly dependent on the adopted stellar effective temperature. To minimise uncertainties in Fe I we derive temperatures for each star individually using the infrared flux method (IRFM). We find that the T_{eff} scales used by both the previous studies are cooler, by up to 100 K; such underestimated temperatures amplify the apparent Fe I depression. Our IRFM temperatures result in negligible apparent depression, consistent with theory. We also re-derived sodium abundances and, remarkably, found them to be unaffected by the new temperature scale. [Na/H] in the AGB stars is consistent between all studies. Since Fe is constant, it follows that [Na/Fe] is also consistent between studies, apart from any systematic offsets in Fe. We recommend the use of $(V - K)$ relations for AGB stars, based on comparisons with our individually-derived IRFM temperatures, and their inherently low uncertainties. We plan to investigate the effect of the improved temperature scale on other elements, and re-evaluate the subpopulation distributions on the AGB, in the next paper of this series.

3.1 Introduction

Due to their relatively homogeneous stellar populations, Galactic globular clusters (GCs) have long been used to constrain stellar evolution models of low-mass stars (eg. Castellani and Renzini 1968; Schwarzschild 1970; Iben 1971; Zinn 1974; Norris 1974; Sweigart 1997; Baraffe et al. 1997; Salaris et al. 2016). The colour-magnitude diagrams of GCs generally exhibit well-populated sequences corresponding to most phases of stellar evolution. Additionally, most GCs are chemically homogeneous in heavy elements, for example the star-to-star variation of iron is usually smaller than the observational uncertainties. Main sequence observations indicate that the age differences between the subpopulations are undetectable, or small ($\lesssim 10^8$ years), as compared to total ages of up to 13 Gyr (eg. Piotto et al. 2007). For most purposes, the stars in each GC can be considered coeval.

In contrast to this homogeneity, observations of the light elements have revealed a consistent picture of subpopulations within each GC. Supported also by photometry, these subpopulations are most clearly seen in multi-dimensional chemical space, for example in the Na-O plane. Indeed Carretta et al., 2010 suggest that a negative/anti-correlation in Na-O is the defining feature of a GC, clearly separating them from open clusters which show light element homogeneity (De Silva et al. 2009; MacLean et al. 2015). In addition to the well studied variation in the elements such as C, N, O, Na, Mg, Al, there is a growing body of evidence that helium also varies (eg. D'Antona et al. 2005; Milone 2015; Valcarce et al. 2016). This is qualitatively consistent with proton-capture nucleosynthesis, whereby H is burned to He through the CNO cycle (converting C and O to N), and Al and Na are produced through the Mg-Al and Ne-Na cycles. We refer the reader to Gratton et al., 2012 for a complete review of multiple populations in globular clusters.

Whilst the now well-established existence of multiple subpopulations in GCs adds significant complexity to understanding GCs and their formation, it opens up new opportunities in constraining stellar evolution models since each GC has (at least) two populations practically identical in age and heavy element composition, but different in light element composition. Thus GCs can provide differential comparisons between models of different initial light element constitutions, and in particular, helium content, which is a dominant factor in a star's evolution (eg. D'Antona et al. 2002; Karakas et al. 2014; Charbonnel and Chantereau 2016).

Until recently chemical abundance studies of the GC multiple populations have mainly focused on red giant branch (RGB) stars. Studies of earlier phases of evolution such as the main sequence and sub giant branch have shown that the proportions of stars making up each subpopulation within a GC are generally constant through the colour-magnitude diagram. It has also been shown that the subpopulations occupy different locations on the horizontal branch (HB; see eg. Marino et al. 2011; Gratton et al. 2015).

The phase of evolution directly after the HB, the asymptotic giant branch (AGB), has only recently started to be investigated systematically. The AGB is particularly interesting because it should contain information about the previous phase, the HB, which is one stage of evolution that is predicted to diverge significantly between He-rich and He-normal stars[1]. Evolutionary models of HB stars are also known to have very substantial uncertainties (eg. Constantino et al. 2015; Campbell et al. 2016; Constantino et al. 2016). Early low-resolution spectroscopic work on GC giant stars sometimes contained a few AGB stars (usually tentatively identified, see Campbell et al. 2006 for a summary). In some cases these early studies showed possible differences in subpopulation ratios between the AGB and RGB. For example Norris et al., 1981 found a lack of AGB stars with strong cyanogen (CN) band strengths in NGC 6752, as compared to their RGB sample, and Mallia, 1978 found a dominance of CN-strong stars on the AGB of 47 Tuc. Cyanogen (roughly) tracks N content, such that CN-weak stars are first generation/subpopulation (hereafter SP1) and CN-strong stars are second subpopulation (hereafter SP2). These studies were however hampered by low resolution, imprecise photometry (required for separating the RGB and AGB stars), and small samples of AGB stars. Decades later the quality of photometry had improved such that Sneden et al., 2000 and Campbell et al., 2006 argued that it should now be possible to study the AGB stars of GCs in a systematic way. Campbell et al., 2010 presented some early CN results for a systematic study of AGB stars in 9 GCs, based on medium resolution spectra ($R \sim 3000$). The findings were mixed, with a range of interpretations being possible. This was due to the uncertainties in molecular band formation, which is dependent on temperature, as well as the interrelated abundances of C, N, O. One GC did appear to be a clear case though – NGC 6752. Its AGB was dominated by CN-poor giants, in agreement with Norris et al., 1981. Norris et al., 1981 had speculated that this may imply that all of the SP2 stars avoid the AGB phase. This is however not expected from stellar theory – about 50% of the AGB stars are predicted to be SP2 (CN-strong, Na-rich; Cassisi et al. 2014). Such a claim of strong discordance between observation and theory required stronger evidence. This was provided by Campbell et al., 2013 with sodium abundance measurements from high-resolution spectroscopy of 24 RGB and 20 AGB stars in NGC 6752. The

[1]Due to the more rapid evolution of He-rich stars they have lower stellar masses at a given age. Since the HB core masses do not change significantly between He populations, the envelope masses on the HB are reduced, and the T_{eff} increased, giving rise to blue extensions in the observed HBs.

Na results confirmed the CN results, and Campbell et al., 2013 inferred that all of the Na-rich (SP2) stars were avoiding the AGB phase in NGC 6752.

Since the NGC 6752 study a number of research groups have investigated the AGB stars of many other GCs, with high-resolution spectroscopy – 47 Tuc: Johnson et al., 2015; M 2, M 3, M 5, M 13: García-Hernández et al., 2015; M 62: Lapenna et al., 2015; M 4: MacLean et al., 2016; NGC 2808: Wang et al., 2016; NGC 6752: Lapenna et al., 2016. So far no consistent picture of subpopulation ratios on the AGB has emerged. Interestingly, for the two GCs that have been studied more than once so far, conflicting evidence has been reported. In the case of M 4 photometric inferences of population proportions (Lardo et al. 2017) disagree with the spectroscopic results (MacLean et al. 2016). The conflicting spectroscopic evidence for the other case, NGC 6752 (Campbell et al. 2013; Lapenna et al. 2016) is the topic of the current study. Adding to the debate, a photometric study on NGC 6752 AGB stars has very recently been accepted for publication (Gruyters et al. 2017). We refer the reader to MacLean et al., 2016 for a more detailed summary of the literature thus far.

Conflicting results for NGC 6752

The Campbell et al., 2013 study (hereafter C13) found that the sodium abundances in their sample of NGC 6752 AGB stars were consistent with a single value – the standard deviation of [Na/Fe] was $\sigma = 0.10$, comparable to the internal errors of $\sim \pm 0.1$ dex. They reported that the single value corresponds to that of the O-rich/Na-poor subpopulation of NGC 6752 (SP1, often referred to as 'first generation'). We note that there have been at least three subpopulations identified in NGC 6752, one with field-star-like composition, and the other two with enhanced Na and reduced O (amongst other light element variations, see Carretta et al. 2012). For simplicity we divide them here into just two groups: SP1 and SP2.

In contrast to the C13 result, Lapenna et al., 2016 (hereafter L16) report a distinctly different distribution in [Na/Fe]. In particular they find that about 50% of their sample have enhanced [Na/Fe] – and corresponding (anti-) correlations with [C, N, O, Al/Fe] (see their Fig. 2). As they state, this result is much more consistent with current stellar evolution predictions (C13; Cassisi et al. 2014). L16 re-observed the AGB stellar sample of C13 (20 stars) with a different instrument, the UVES spectrograph on the VLT. C13 used data collected using FLAMES (Pasquini et al. 2003), also on the VLT. Thus the spectra and analysis methods are independent, but the AGB stellar samples are identical.

The L16 study did not investigate why the results of the two studies differ so much. The study also did not observe or homogeneously re-analyse RGB stars, which are very useful as a control sample, since they have been

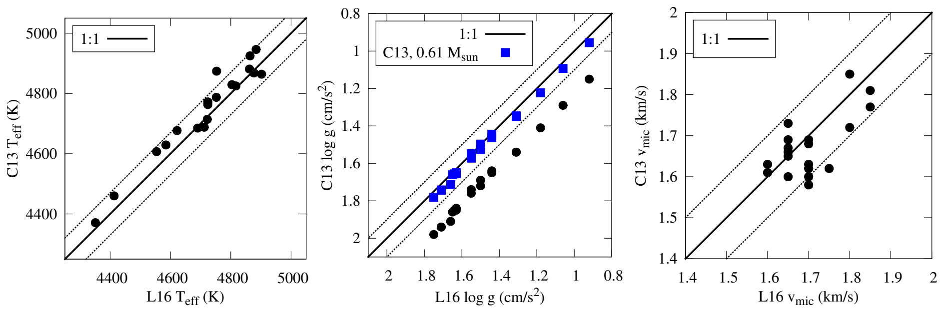

FIGURE 3.1: Comparison of T_{eff} (left), $\log g$ (centre), and v_{mic} (right) values adopted for the AGB sample by C13 and L16. Dotted lines show typical uncertainties in each of the parameters (T_{eff}, from colour-T_{eff} relation: ± 70 K; $\log g$: ± 0.1 km/s; v_{mic}: ± 0.1 dex). The centre panel also shows our new $\log g$ values calculated using a more appropriate mass estimate for the AGB stars (0.61 $M_\odot$, blue squares; see text for details).

well studied in NGC 6752, and they show the full range of Na-O dispersion for the particular analysis methodology that one adopts (C13 included 24 RGB stars). Here we explore the methods, uncertainties, and assumptions of both studies with an aim to finding a robust result for [Na/Fe]. We will investigate other elements in the next paper of the series. We begin by directly comparing the key parameters and results of the two studies.

3.2 Comparisons between C13 and L16

3.2.1 Stellar parameter comparison

The stellar parameters – effective temperature T_{eff}, surface gravity $\log g$, microturbulent velocity v_{mic}, and global metallicity [M/H] – are central to the spectroscopic determination of abundances. They are the parameters that define the stellar atmosphere model one uses to infer the strength of each line. The parameters are well known to have degeneracies, for example a change in $\log g$ can mimic a change in [Fe/H]. It is therefore imperative to compare the stellar parameters of C13 and L16[2].

L16 derived T_{eff} by requiring no trend between iron abundances and excitation potential, which is usually referred to as 'spectroscopic' T_{eff}. On the other hand C13 used 'photometric' T_{eff}, which is derived from colour-T_{eff} relations. The left panel of Figure 3.1 shows that the T_{eff} values compare well, with virtually all temperatures being the same within the uncertainties given by the colour-T_{eff} relations (C13 used the Alonso et al. 1999 relations). It is interesting that there is agreement despite the different methods used to arrive at the final temperatures (although see Sec. 3.4.2).

[2]These comparisons are in the context of 1D LTE abundance analyses.

The centre panel of Figure 3.1 shows that there is a constant offset of about 0.2 dex in surface gravity ($\log g$) between C13 and L16, with the L16 gravities being lower. This was noted by L16, who suggested that it could be due to the adopted distance modulus or stellar mass. C13 used the same distance modulus as L16 ($(m-M)_V = 13.13$; Harris 1996). However C13 neglected to account for mass loss between the RGB and AGB. They adopted the same mass for AGB stars as used for the RGB stars, 0.84 $M_\odot$, which is clearly incorrect. Following L16 we adjusted the mass for the AGB stars to 0.61 $M_\odot$, the median HB mass inferred for NGC 6752 by Gratton et al., 2010b, and recalculated $\log g$. It can be seen that this removes the offset between L16 and C13, bringing the gravities in to near perfect agreement (blue squares in Fig. 3.1).

In C13 the microturbulent velocity v_{mic} was determined using the relation of Gratton et al., 1996, whilst in L16 it was obtained spectroscopically, by requiring no trend between the reduced equivalent widths and abundances derived from Fe I lines. The right panel of Figure 3.1 shows that the L16 values are quantised, in 0.05 km/s steps. This is most likely due to 0.05 km/s steps being taken to arrive at a spectroscopic solution, a reasonable approach given the uncertainty in this parameter. The values cover a small range (1.60 to 1.85 km/s), and the two studies agree considering the characteristic uncertainty of ± 0.1 km/s.

With regards to the global metallicity used for atmospheric modelling, L16 used $[\mathrm{M/H}] = -1.50$ whilst C13 used $[\mathrm{M/H}] = -1.54$. This is a small difference and is not expected to affect the results significantly.

In summary, apart from the gravity offset, all other stellar parameters show no significant difference between the two studies. Amongst the species under investigation here (Fe I, Fe II, Na I), gravity should mainly affect Fe II. Na I is expected to be largely unaffected[3] and for this reason we continue with the comparison using the published C13 Na abundances.

3.2.2 [Na/H] comparison

To derive abundances of sodium both studies used the equivalent width (EW) method. C13 utilised the strong Na I doublets at 5682/5688 Å and 6154/6160 Å, although only the first doublet was usually measurable in the AGB stars. As far as we are aware L16 used the same doublet for their AGB sample (see their Fig. 1). The L16 data has a moderately higher resolution (UVES, $R = 40,000$) than that obtained by C13 (FLAMES, $R = 24,000$).

[3]This is due to Na I being the minority species (in these stars sodium is predominantly in the form of Na II) and thus its line formation is insensitive to pressure. Since the atmospheric pressure is primarily determined by gravity, it follows that the formation of Na I lines is not sensitive to changes in gravity (see eg. the discussion in Chapter 13 of Gray 2005).

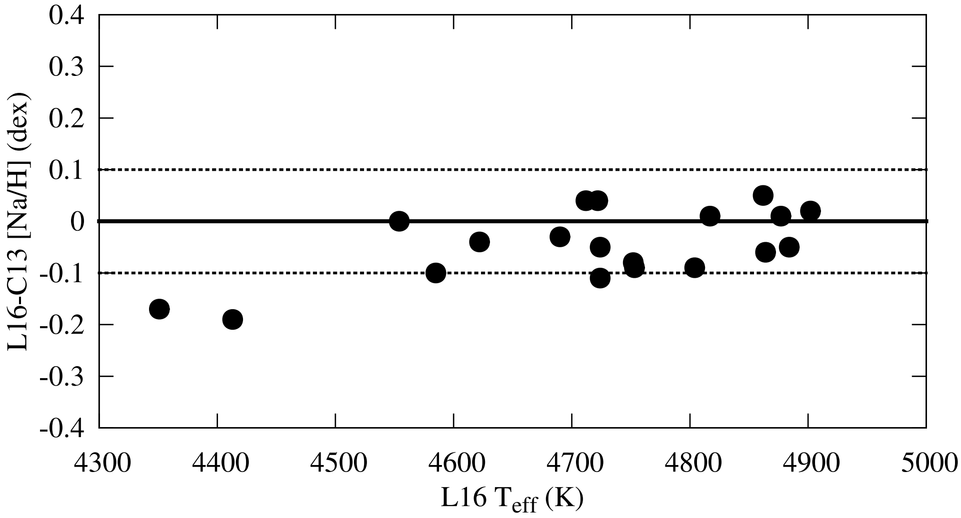

FIGURE 3.2: Difference in [Na/H] between the two studies. Dotted lines indicate typical uncertainties.

In Figure 3.2 we show the difference between the C13 and L16 [Na/H] results[3]. Apart from the two coolest stars, which have *lower* Na in L16 (we discuss these stars further in Sec. 3.6), there is no significant difference in [Na/H]. There is a slight systematic offset to lower [Na/H] in L16 (~ -0.05 dex). Adding in the uncertainties from L16, and considering that the uncertainties quoted are *internal* only, the agreement is remarkable. This strongly suggests that a range of factors have no significant effect on the Na I abundance derivation, including the following:

- Gravity offset in C13 (as expected, see footnote 3)
- Increase in resolution in L16 over C13
- Small differences in model atmospheres and their inputs (eg. [M/H])
- Small differences between the spectroscopically derived temperatures (L16) and the photometric temperatures (C13)
- Scatter in the microturbulent velocities

The result of this comparison is reassuring and gives confidence in the methods used to derive [Na/H]. C13 argued that their Na results are consistent with a single value, given the uncertainties, and that the value corresponds to SP1 of NGC 6752. This conclusion is however at odds with the L16 study, which concluded that the slightly larger spread found for [Na/H] ($\sigma = 0.13$ dex versus 0.10 dex in C13) is significant. Based on the uncertainty estimates of L16 (~ 0.06 dex, judging from [Na/H] in their Fig. 2), which are somewhat smaller that those of C13 (~ 0.10 dex), this conclusion may be correct – assuming the L16 error estimates are realistic. We

[3]We adopt the Grevesse and Sauval, 1998 solar Na value $\log \epsilon = 6.33$ for scaling.

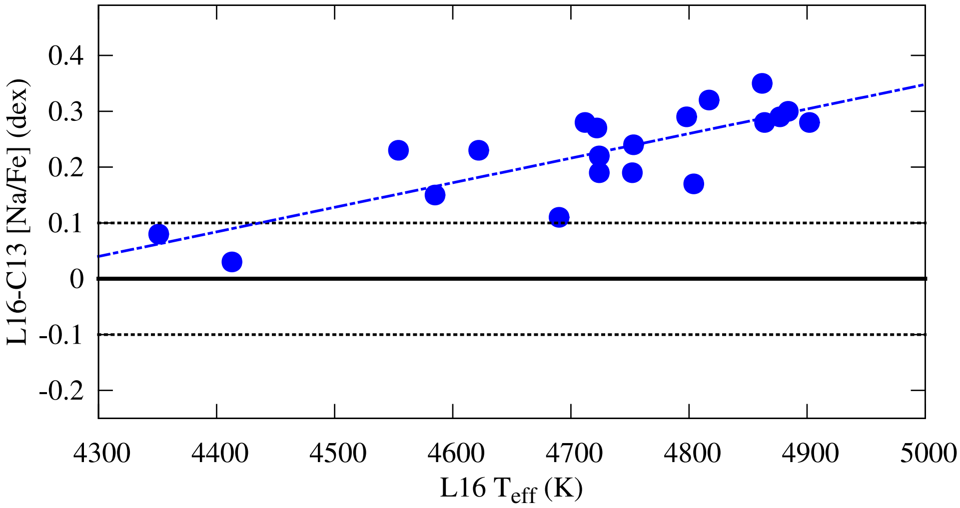

FIGURE 3.3: Difference in [Na/Fe] results between L16 and C13. The dash-dotted line is a linear fit. Differences much larger than the typical uncertainties (dashed lines) are present.

explore various sources of uncertainty in Section 3.4 and Section 3.5.2. We now investigate the considerable differences in [Na/Fe] between the two studies.

3.2.3 [Na/Fe] comparison

In Figure 3.3 we show the difference in [Na/Fe] between the two studies. Differences of up to $+0.35$ dex can be seen, although they range from zero to this very high value. Interestingly there is a temperature trend, with stars with the highest $T_{\rm eff}$ having the largest differences in [Na/Fe]. A linear regression analysis shows that the Pearson correlation coefficient $r^2 = 0.63$ and that the slope is highly significant (t-statistic = 5.6σ). This was described in L16 as a systematic offset of 0.25 dex.

Given our conclusion about [Na/H], that the results are practically identical between studies, the [Na/Fe] differences must be wholly driven by the denominator, i.e. the Fe distribution must give rise to the difference in [Na/Fe] distribution.

With respect to the methodology used to derive [Na/Fe] for the NGC 6752 AGB stars the two studies diverge considerably. C13 did not derive Fe abundances. They instead assumed a single Fe abundance for all stars in their sample ([Fe/H] $= -1.54$, Carretta et al. 2007). This assumption is discussed further at the beginning of Section 3.3. In contrast, L16 did derive Fe abundances, based on both Fe I and Fe II. An important part of their methodology was that they did not derive $\log g$ spectroscopically, at least not in the common meaning of spectroscopically (we set out the steps in their method in Sec. 3.3). This was done specifically to avoid 'forcing'

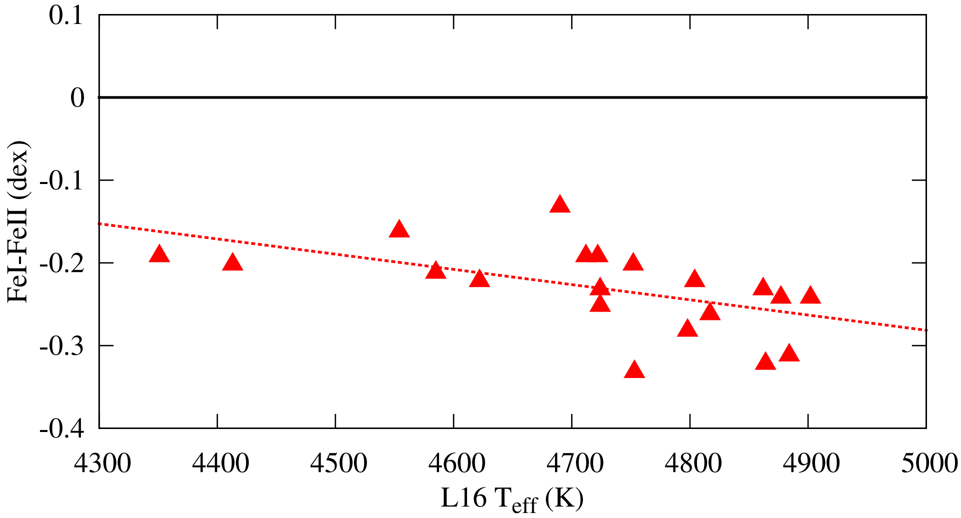

FIGURE 3.4: Depression of Fe I relative to Fe II in the L16 study. The dashed line is a linear fit.

the abundances of Fe I and Fe II to be equal. To motivate this choice L16 cite some studies that have reported Fe differences, δFe $=$ Fe I $-$ Fe II, in globular cluster RGB and AGB stars (Ivans et al. 2001; Lapenna et al. 2014; Lapenna et al. 2015; Mucciarelli et al. 2015). Certainly not requiring that Fe I = Fe II is necessary for detecting any possible δFe, which would most likely be due to overionisation of Fe I (Lind et al. 2012), but, as we show later (Sec. 3.4), care is required in order to be confident of the quantitative results. In particular there needs to be a high level of confidence in the stellar parameters used, otherwise an *apparent overionisation* can be misinterpreted as a real physical phenomenon[4].

Crucially, to obtain [Na/Fe] L16 decided to use only Fe abundances derived from Fe I lines in the denominator, following the original suggestion of Ivans et al., 2001 (see also Lapenna et al. 2014; Lapenna et al. 2015; Mucciarelli et al. 2015). Moreover, abundances for all other elements that were determined from neutral species were also scaled by Fe I. We discuss the basis and validity of this choice in Section 3.7.

In Figure 3.4 we show the run of δFe in the L16 data. Apart from the extra scatter added because of the (small, up to 0.03 dex) differences in Fe II, this shows the same trend as the [Na/Fe] differences in Figure 3.3. A linear regression analysis shows the slope is significant ($t = 2.7\sigma$). The δFe values range up to ~ -0.35 dex. Also of note is that there are no stars with an absolute value of δFe less than 0.1 dex. The L16 Fe abundances are based on many lines and have very small reported uncertainties (± 0.01 dex, Table 1 of L16). Thus the entire sample appears to have highly significant δFe. L16 conclude that there is currently no complete explanation of this δFe effect but it "seems to be a general feature of AGB stars in GCs". This conclusion

[4]That is, a physical phenomenon that is not captured by the LTE treatment.

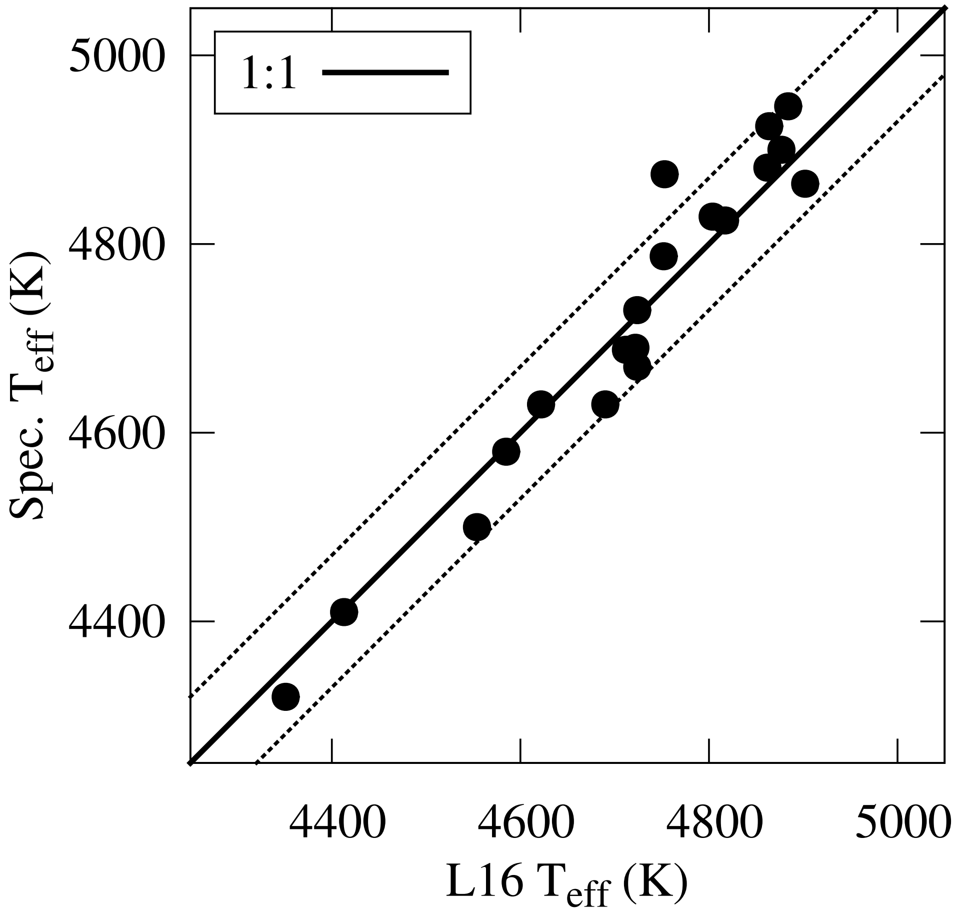

FIGURE 3.5: Spectroscopically determined T_{eff} for the C13 data using the L16 method (Sec. 3.3), compared to the L16 temperatures. The two sets of temperatures were derived using different photometry for initial T_{eff} estimates. Dashed lines indicate typical uncertainties (± 70 K).

does however rely on the reported uncertainties being realistic. We address this fundamental condition in Sections 3.4 and 3.5.2.

In summary, we conclude that *the differences in [Na/Fe] between L16 and C13 are driven wholly by the Fe I depression* relative to Fe II reported by L16.

Our next step in the comparison is to see if we can reproduce the L16 δFe from the C13 FLAMES data.

3.3 Fe I and Fe II from C13 data using C13 parameters

As noted earlier, C13 did not derive Fe abundances. A single Fe abundance was assumed for all stars in their sample, based on a detailed RGB study ([Fe/H] $= -1.54$, Carretta et al. 2007). This was considered a reasonable assumption since it is well established that NGC 6752 is mono-metallic in Fe (Gratton et al. 2005; Carretta et al. 2009a; Yong et al. 2015). However it meant that any unexpected deviation in Fe I or Fe II in the AGB stars would have been missed.

Here we present newly calculated Fe I and Fe II abundances using the C13 FLAMES data, in order to compare directly with the L16 Fe results.

We derive LTE Fe abundances using the EW method, as in the L16 study. While C13 used the MOOG stellar line analysis program (Sneden 1973), here we use the WIDTH3 program (Gratton 1988; Gratton and Sneden 1988). We aim to reproduce the L16 results, so we follow the specific methodology of that study, which comprises the following steps:

(i) T_{eff} is calculated 'spectroscopically', i.e. by requiring no trend between Fe I abundances and excitation potential.

(ii) Gravity is adjusted from the initial photometric values by recalculating it using the T_{eff} from Step 1. Iteration back to Step 1 may be required if the changes in $\log g$ are significant. Ionisation balance is ignored.

(iii) Microturbulent velocity is then adjusted by requiring no trend between Fe I abundances and line strengths.

We used Kurucz, 1993 model atmospheres, adopting the same $[\mathrm{M/H}] = -1.50$ value as L16. Photometrically-derived values of T_{eff} and $\log g$ were adopted as initial estimates (those in Fig. 3.1). The initial temperatures are identical to those used in C13, based on the Strömgren photometry from Grundahl et al., 1999 and using the $(b-y)$ relation of Alonso et al. (1999, their eqn. 15). NGC 6752 suffers from minor reddening; we corrected the b and y magnitudes for reddening using the relations of Schlegel et al., 1998, adopting $E(B-V) = 0.04$ mag (Harris 1996). The initial $\log g$ values (blue squares in Fig. 3.1) were calculated using a stellar mass of 0.61 $M_{\odot}$, and a distance modulus of $(M-m)_V = 13.13$ (Harris 1996), consistent with L16. We used the bolometric correction relation of Alonso et al. (1999, their eqns. 17 and 18).

Using Step 2 above for gravity estimation one avoids Fe I being forced to be equal to Fe II (i.e. ionisation balance is not enforced). In iterating back to Step 1 we found that the $\log g$ values are insensitive to the $\sim 0 \rightarrow 100$K modifications in T_{eff}, with the average change in $\log g$ being $\sim +0.03$ dex. Our initial microturbulence values were estimated using the relation from Gratton et al., 1996. Most of these values were unchanged in Step 3, with four AGB stars changing by $\sim \pm 0.1$ km/s, so they are still consistent with those in the right panel of Figure 3.1. Our final spectroscopic T_{eff} values are consistent with the L16 spectroscopic temperatures (Fig. 3.5). Finally, our linelist is based on that of Gratton et al., 2003a. We explore line list differences in Sec. 3.5.2.

With these parameters, and assuming a solar abundance for Fe of $\log \epsilon = 7.50$ (Grevesse and Sauval 1998), we find for the AGB stars:

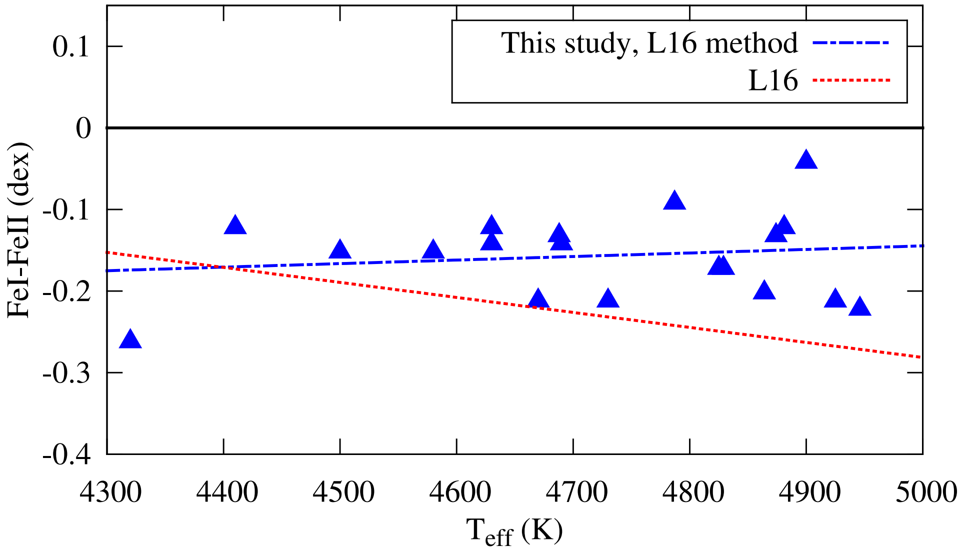

FIGURE 3.6: Depression of Fe I relative to Fe II we find when using the method of L16 and the C13 data (blue triangles). The blue dot-dashed line is a linear fit to our results, and the dashed red line is the fit to the L16 results (from Fig. 3.4). The temperatures used for this analysis are displayed in Fig. 3.5.

$$[\mathrm{Fe\,II/H}]_{AGB} = -1.48 \pm 0.01 \text{ dex } (\sigma = 0.04; \text{L16: } -1.58 \text{ dex})$$

$$[\mathrm{Fe\,I/H}]_{AGB} = -1.63 \pm 0.01 \text{ dex } (\sigma = 0.04; \text{L16: } -1.80 \text{ dex}).$$

Thus we confirm a significant Fe I-Fe II difference, at least qualitatively. Unlike the L16 δFe results our results show no substantial trend with $T_{\rm eff}$ (Fig. 3.6), with the significance of the slope being $< 1\sigma$, and $r^2 = 0.03$. The average value of the offset in our results is $\delta\mathrm{Fe} = -0.15 \pm 0.01$ dex ($\sigma = 0.05$), as compared to -0.22 dex in L16. Using the C13 parameters and the L16 spectra, L16 found an average offset of -0.27 dex. Thus there is a systematic difference of order 0.1 dex between the studies even if using the same stellar parameters. This may be related to the 0.1 dex lower [Fe II/H] found by L16, which could be due to the adoption of different oscillator strengths between the studies (we explore this as an uncertainty in Sec. 3.5.2).

3.4 The origin of δFe

The qualitatively similar finding of a definite δFe in both sets of data is in one way reassuring – it shows that, given a particular methodology, the results of L16 are reproducible with independent data and tools. However, the L16 study did not investigate the robustness of this result. An obvious question arises – is there some systematic problem(s) in the method mimicking this phenomenon?

To investigate this possibility we explore the uncertainties in the abundance analysis process. We begin by noting that it is well known that (i) offsets in Fe II can be caused by offsets in gravity, (ii) offsets in Fe I can be caused by offsets in T_{eff}, and (iii) the magnitude of non-LTE effects is predicted to be small in these stars. We explore the first two sources of uncertainty in the next two subsections and the third in Section 3.5.2.

3.4.1 Gravity check: Fe II abundance comparison with RGB stars

One way to check if there is a gravity offset problem is to compare the Fe II abundance of the AGB stars to that of the RGB stars – they should be identical for Fe II since NLTE effects are predicted to be negligible for Fe II in late-type stars (eg. Lind et al. 2012). Due to its dependence on gravity, a difference in Fe II may indicate systematic problems with $\log g$ that would require investigation.

C13 included RGB stars in their study, as a control sample. For the Fe determination in the RGB stars we again used the same methodology of L16, as described for the AGB sample above. In this case our results show no evidence of an Fe I-Fe II discrepancy:

$$[\text{Fe II/H}]_{RGB} = -1.47 \pm 0.01 \text{ dex } (\sigma = 0.06)$$

$$[\text{Fe I/H}]_{RGB} = -1.48 \pm 0.04 \text{ dex } (\sigma = 0.06).$$

Formally we measure $\delta\text{Fe} = -0.01 \pm 0.02$ ($\sigma = 0.08$).

Importantly, the AGB [Fe II/H] is perfectly in agreement with the RGB measurement. This suggests that Fe II is not the source of the AGB δFe phenomenon. Although not a definitive proof, it also suggests that the AGB $\log g$ values are reasonable. Assuming this is correct we now investigate the sensitivity of Fe to T_{eff}.

3.4.2 Temperature check: Fe I behaviour with varying T_{eff}

L16 derived surface temperatures spectroscopically, i.e. by requiring no trend between iron abundances and excitation potential. In this procedure it is usual to use photometric T_{eff} as an initial estimate. L16 did not specify if this was done, but we assume it was. We also assume the same BV photometry (Stetson, 2000) that was used for the $\log g$ derivation was also used for T_{eff}. Regardless of the source of photometry, and the method to arrive at the final temperatures, it can be seen in Figure 3.1 that the L16 temperatures agree with the C13 temperatures, within the uncertainties. Here we explore the uncertainties, to ascertain whether systematic problems with T_{eff} could

[5] We use 2σ uncertainties due to the fact that AGB stars are not significantly represented in the stellar samples on which the colour-T_{eff} relations are based.

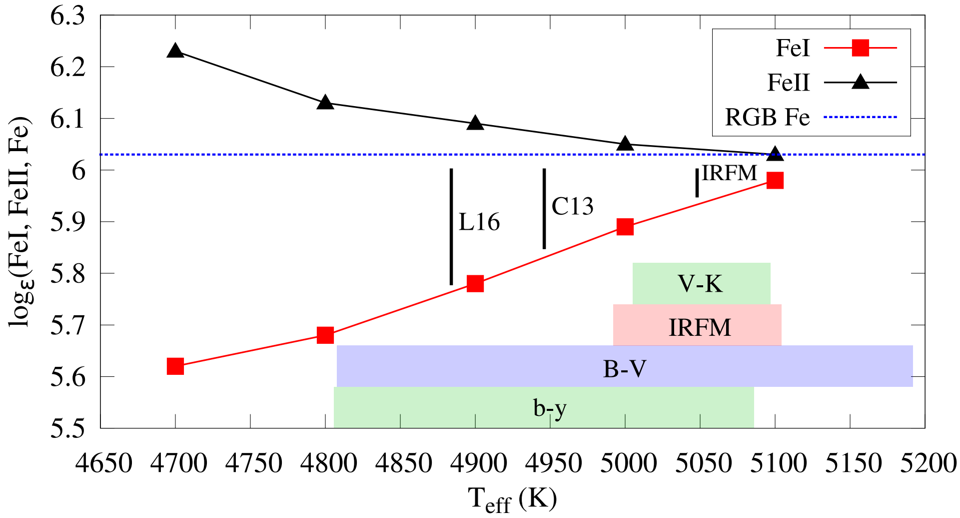

FIGURE 3.7: Testing the effect of adopted $T_{\rm eff}$ on the derived Fe I and Fe II abundances in the AGB star 97. Horizontal bars show the 2σ uncertainty ranges[5] for each of the $T_{\rm eff}$-colour relations, centred on the $T_{\rm eff}$ prediction of each relation (see text for details). The temperatures used in the C13 study (4946 K) and the L16 study (4884 K) are indicated by vertical lines, highlighting the magnitude of δFe at each $T_{\rm eff}$. Also shown is our IRFM $T_{\rm eff}$ (5048 K) and associated uncertainty. The $(V-K)$ $T_{\rm eff}$ is 5051 K. The dashed line shows the average iron abundance of the RGB stellar sample.

be giving rise to the δFe phenomenon present in both studies (Figs. 3.4 and 3.6).

AGB star test case

To investigate the sensitivity of Fe I and Fe II to the adopted $T_{\rm eff}$ we chose one star as a case study: AGB star 97. This star was chosen because it displays a strong δFe signal in both L16 and the current study, with $\delta\mathrm{Fe} = -0.31$ and -0.22, respectively. In L16 the adopted surface temperature for this star was 4884 K. In the current study we found the photometric $T_{\rm eff}$ of C13 to require no change (4946 K). The difference of 62 K is within the 1σ (±70 K) uncertainties of the Strömgren relation which we used to derive $T_{\rm eff}$ (Alonso et al. 1999).

For the test we varied $T_{\rm eff}$ and attempted to find spectroscopic 'solutions' (i.e. no trend between iron abundances and excitation potentials) at each $T_{\rm eff}$. During this process $\log g$ was kept constant, at the photometric value. In Section 3.3 we showed that the $\log g$ adjustment is negligible within the $T_{\rm eff}$ uncertainty ranges considered here.

In Figure 3.7 we show the results of the test. Interestingly, we were able to find spectroscopic 'solutions' for a wide range of temperatures, even outside the uncertainties of the colour-$T_{\rm eff}$ relations, although no solution was found above 5100 K[6]. Multiple solutions were possible because of the uncertainty in the abundance-excitation potential slope, combined with the poorly constrained microturbulence parameter, which was adjusted to reduce the slope in the usual procedure (Sec. 3.3). The slope uncertainty in this case was ± 0.03 dex/eV[7]. Over the the $T_{\rm eff}$ range of $4800 \rightarrow 5100$ K the range of microturbulence values we found spanned $1.20 \rightarrow 1.65$ km/s, with the microturbulent velocity increasing with temperature. Apart from the very low $T_{\rm eff}$ end, which is very unlikely to be representative of the true temperature (Sec. 3.4.2), these appear to be reasonable values, as compared to those reported by C13 and L16 (Fig. 3.1). It is also useful to remember that 'microturbulent velocity' is essentially a free parameter, i.e. it has little physical basis (see eg. the four listed points in Sec. 1 of Mucciarelli 2011, and references therein). For all solutions there was no trend between Fe abundances and line strength, within the uncertainties.

The δFe variation over the $T_{\rm eff}$ test range shows a consistent trend: δFe decreases with increasing $T_{\rm eff}$. Ignoring the $T_{\rm eff}$ values outside the photometric $T_{\rm eff}$ uncertainties, δFe ranges from -0.46 (at 4820 K) to -0.05 (at 5100 K). This final value is consistent with zero given the 1σ scatter in δFe of 0.08 dex that we found in the RGB sample (Sec. 3.3).

Also marked in Figure 3.7 are the temperatures used by C13 and L16. Importantly the δFe value at the L16 $T_{\rm eff}$ is very similar to that reported by L16 (their -0.31 dex versus -0.34 dex here). Considering that different spectra and tools have been used, and that both the L16 and C13 δFe values fit the δFe-$T_{\rm eff}$ trend, this is a strong confirmation of the δFe phenomenon, and its dependence on $T_{\rm eff}$, both qualitatively and quantitatively.

The gradient δFe/$T_{\rm eff}$ is ~ 0.002 dex/K. Given a typical 1σ $T_{\rm eff}$ uncertainty of $\pm$100K for the $(B-V)$ colour, this translates to a possible δFe range of 0.40 dex. This is a very substantial uncertainty and consistent with the up to 0.35 dex found by L16.

Ramifications of the δFe dependence on $T_{\rm eff}$

This result shows clearly that significant δFe values can arise even within the photometric $T_{\rm eff}$ uncertainties. Crucially it appears that the initial $T_{\rm eff}$ estimate (usually photometric) is central in determining the final δFe value. This is because there is a continuum of spectroscopic 'solutions' across the $T_{\rm eff}$ uncertainty range, so that *the spectroscopically determined $T_{\rm eff}$ will usually be close to the photometric estimate*. Figure 3.7 then implies that, if there is a systematic trend or offset in the inferred photometric temperatures, a similar trend or offset should be present in δFe – even if the temperatures are

[6]Within our test procedure. Varying $\log g$ may allow solutions at higher $T_{\rm eff}$.

[7]Across the AGB sample the average uncertainty was ± 0.02 dex/eV.

determined spectroscopically. Given this, an investigation into the sources of the adopted temperatures is mandatory, and is our next step.

Temperature scales and the case for $(V-K)$

In Figure 3.7 we also show the predictions of three colour-$T_{\rm eff}$ relations for our AGB test star: Strömgren $(b-y)$ (Alonso et al. 1999 eqn. 15, with a quoted uncertainty of $1\sigma = 70$ K), Johnson $(B-V)$ (Alonso et al. 1999 eqn. 4, $\sigma = 96$ K), and Johnson-2MASS $(V-K_{\rm s})$ (Table 5 of González Hernández and Bonifacio 2009, $\sigma = 23$ K). Reddening was corrected for in $(V-K_{\rm s})$ using the relation of Fitzpatrick and Massa (2007, their Eqn. 8) assuming $R_V = 3.1$ and $E(B-V) = 0.04$.

As a cross-check we have also calculated our own $T_{\rm eff}$ for this star using the Casagrande et al., 2010 implementation of the infrared flux method (IRFM). The IRFM estimates $T_{\rm eff}$ by comparing the ratio of the observed bolometric flux to a monochromatic IR flux with the ratio predicted by theory (synthetic spectra). Since the synthetic spectra have a very mild dependency on stellar parameters in the IR, this method is only weakly dependent on the models. The Casagrande et al., 2010 scale is calibrated absolutely, using a set of solar twins. For further details of our IRFM procedure we refer the reader to Casagrande et al., 2010. We used the 2MASS JHK (Skrutskie et al. 2006) and BV photometry for this $T_{\rm eff}$ determination (and for all the IRFM temperatures in this study). The temperature we derived has an internal uncertainty of ± 30 K, and is also included in Figure 3.7. The BV photometry we use in this study is from Momany et al., 2002. These data are of high quality, for example the average error on the V magnitudes for the AGB sample is 0.008 mag.

Immediately obvious from Figure 3.7 is that the $(V-K)$ relation gives the most precise $T_{\rm eff}$ estimate. It is also in perfect agreement with our IRFM-derived $T_{\rm eff}$, which has a similar degree of precision. Interestingly, both of these $T_{\rm eff}$ estimates give much lower δFe values than obtained using either the C13 or L16 temperatures, with δFe approaching zero at the higher end of the 2σ uncertainty bands.

That $(V-K)$ has a small uncertainty for late-type stars is well known and is due to it being (i) only marginally sensitive to metallicity/line blanketing, and (ii) having a negligible dependence on surface gravity (Alonso et al. 1999; Ramírez and Meléndez 2005). Importantly for our study, the $(V-K)$ colour is particularly suited to giants. Indeed Alonso et al., 1999 suggest that it is "probably the best temperature indicator for giant stars". Furthermore, Ramírez and Meléndez, 2005 report that, due to the colour being so insensitive to gravity, particularly in the range 4800 K $> T_{\rm eff} >$ 6000 K, it makes $(V-K)$ suitable for stars of unknown luminosity class. This is important for studies of (early) AGB stars because many of them lie in this T_{eff} range (our sample: $4500 \rightarrow 5050$ K) and it is a class of stars that have only recently started to be investigated in detail, so their surface gravities are less certain than RGB star gravities.

Temperature scales: Ensemble comparisons

As a further check of the T_{eff} 'scales' we now perform ensemble comparisons between the T_{eff} predictions from the same three colour-T_{eff} relations detailed above but across our entire NGC 6752 RGB and AGB samples. We also present our IRFM temperatures for all the stars.

The RGB sample comparison is displayed in Figure 3.8. Although small offsets and small temperature trends are present, it is clear that all three relations give temperatures that are consistent with each other, within the quoted 1σ uncertainties (Alonso et al., 1999; González Hernández and Bonifacio, 2009). This is true across the whole T_{eff} range of our RGB sample. This confirms the well-constrained nature of the parameters for GC RGB stars, as expected from much previous work on these types of stars.

The AGB on the other hand has not been well studied. In Figure 3.9 we show T_{eff} for the AGB stars. Here the $(B-V)$, $(V-K)$, and IRFM temperatures are consistent with each other, similar to the RGB case. However the Strömgren $(b-y)$ temperatures (used by C13) are offset by about -60 K. This is particularly true at higher T_{eff} (> 4700 K), where the majority of the temperatures are outside the 2σ uncertainties of the IRFM T_{eff}. Also displayed are the temperatures from L16. These are offset even more, by about -100 K on average.

Given that we have showed in Figure 3.7 that δFe is is strongly correlated with a reduction in T_{eff}, this is very suggestive that the large δFe reported by L16 (Fig. 3.4) is driven by the T_{eff} scale of that study. It also explains our own finding of significant δFe using the Strömgren $(b-y)$ temperatures adopted by C13. That the temperature scale of C13 is slightly warmer than that of L16 also shows why our δFe values are generally smaller in magnitude than those of L16 (Sec. 3.3; Fig. 3.6).

The next logical step is to use the more appropriate temperatures in deriving Fe abundances. The change in T_{eff} scale may also affect Na I, which we also re-derive in Section 3.6.

3.5 Iron from C13 data using new T_{eff} scale

3.5.1 Reanalysis method and results

In our final reanalysis of the C13 spectra we chose to use photometric parameters (IRFM) only, because (i) the temperature scale appears quite accurate so we want to avoid additional uncertainties by using the spectroscopic

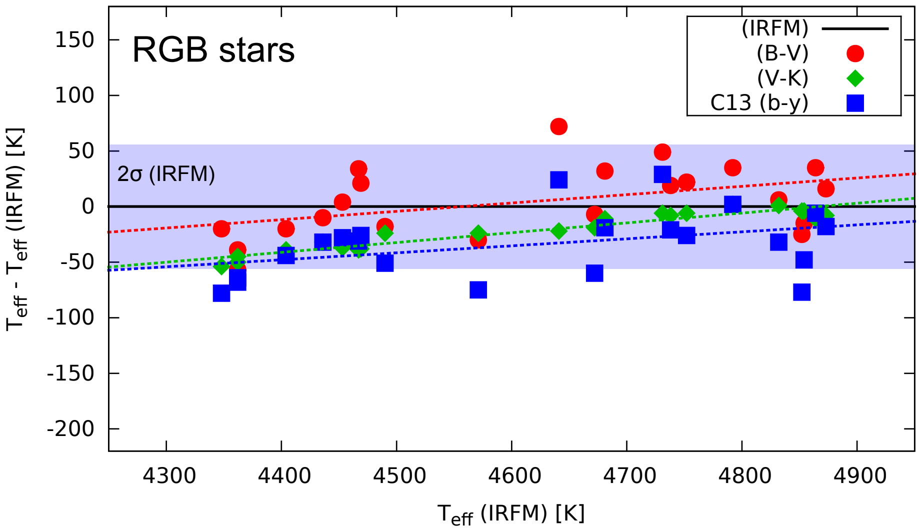

FIGURE 3.8: Comparison of $T_{\rm eff}$ derived for the RGB stars using four different methods: three different colour-$T_{\rm eff}$ relations and our IRFM (see text for details). The $T_{\rm eff}$ from the colour-$T_{\rm eff}$ relations are shown as differences from the IRFM temperatures. Dashed lines are linear fits to each $T_{\rm eff}$ set, and the shaded area shows the average 2σ internal uncertainty of the IRFM scale (± 56 K). The 2σ uncertainties of the $(b-y)$ and $(B-V)$ relations are much larger than for our IRFM, being ± 140 and ± 192 K, respectively (Alonso et al., 1999). The $(V-K)$ uncertainties ($2\sigma = 46$ K; González Hernández and Bonifacio 2009) are similar to the IRFM uncertainties.

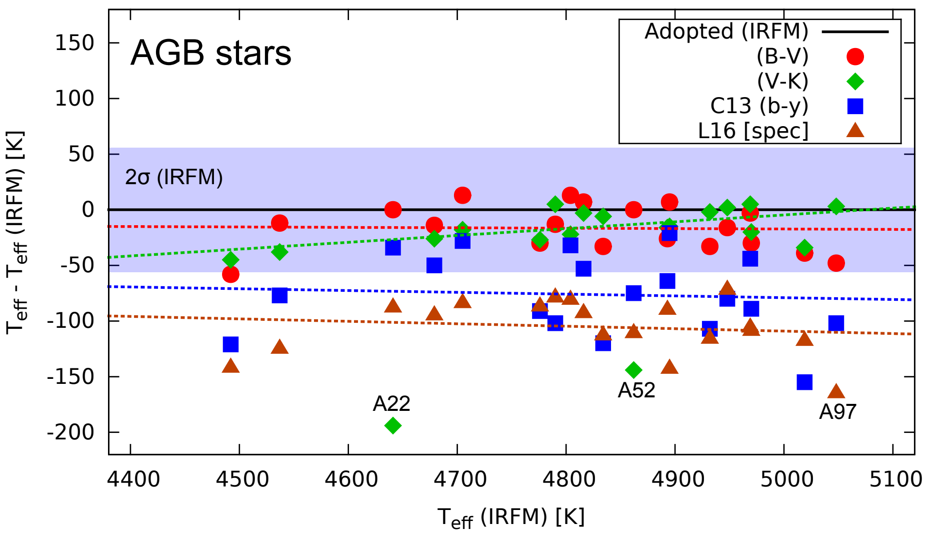

FIGURE 3.9: Comparison of five $T_{\rm eff}$ determinations for the AGB star sample. Symbols and shading are the same as Fig. 3.8, except for the addition of the L16 temperatures (L16 did not study RGB stars). Three stars are highlighted with labels: AGB star 97 was the subject of our δFe tests (Fig. 3.7), whilst A22 and A52 have uncertain IRFM and $(V-K)$ $T_{\rm eff}$ due to suspect 2MASS K magnitudes. These latter two stars have not been included in the linear regression lines for $(V-K)$ or IRFM, and we adopt the $(B-V)$ temperatures for them.

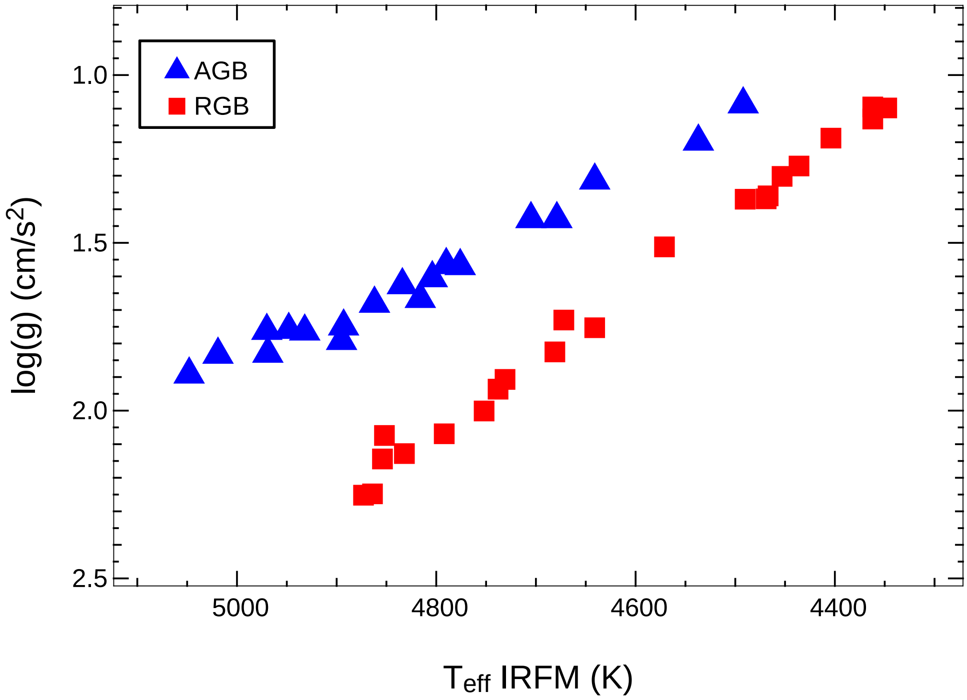

FIGURE 3.10: Our final stellar parameters for the NGC 6752 AGB and RGB stars. All are 'photometric' – based on the IRFM temperatures calculated for this study, except for 2 AGB stars (see Fig. 3.9).

T_{eff} method, and (ii) following L16, we do not want to force Fe I = Fe II by obtaining $\log g$ spectroscopically. We adopt the same distance modulus as C13 and L16, a mass of 0.78 $M_\odot$ for RGB stars and 0.61 $M_\odot$ for AGB stars. Microturbulent velocities were estimated using the Gratton et al., 1996 relation. Our final stellar parameters are plotted in the $\log g$-T_{eff} plane in Figure 3.10, and listed in Table A.2. Note that there are 19 AGB stars rather than 20, since for one star we did not have all three sets of photometry (star 89 of C13 and L16).

In Figure 3.11 we show the final iron results for our whole sample of RGB and AGB stars. Fe I and Fe II are shown separately for each star. Immediately obvious in this figure is that all abundances fall within the expected uncertainty range characterised by $1\sigma \sim 0.1$ dex. Final Fe abundances are also listed in Table A.2.

The main effect of the new stellar temperatures is to raise the Fe I values in the AGB sample, as expected from Figures 3.7, 3.8, and 3.9. Table 3.1 shows that the average increase in Fe I is $+0.11$ dex, as compared to our results using the C13 stellar parameters (Sec. 3.3). Fe II is unchanged, so this translates directly into a reduction of average δFe, reducing it from -0.15 to -0.04 dex. Figure 3.12 shows visually that δFe in the AGB sample is now negligible. A weak trend appears to be visible though, with δFe increasing

TABLE 3.1: Summary of iron abundances derived from Fe I & Fe II using different input parameters. Abundances are scaled based on a solar Fe abundance of $\log\epsilon = 7.50$ dex. Also shown is the difference $\delta\mathrm{Fe} = \mathrm{Fe\,I} - \mathrm{Fe\,II}$. The first line shows the L16 AGB results. The second set of results were obtained using the C13 temperatures (Sec. 3.3). The 3rd set of results were obtained using our new IRFM T_{eff} scale but adopting the L16 $\log gf$ values. Our final results, using the IRFM temperatures and our $\log gf$ values, are in the last two rows. The typical number of Fe I lines analysed was 20-40, and 2-3 for Fe II. The σ values are the 1σ star-to-star scatter only.

Analysis run	[Fe I/H] (dex)	σ (dex)	[Fe II/H] (dex)	σ (dex)	δFe (dex)	σ (dex)
AGB L16	-1.80	0.05	-1.58	0.02	-0.22	0.05
RGB (C13 T_{eff})	-1.48	0.06	-1.47	0.06	-0.01	0.08
AGB (C13 T_{eff})	-1.63	0.04	-1.48	0.04	-0.15	0.05
RGB (L16 gfs)	-1.43	0.05	-1.52	0.05	$+0.09$	0.07
AGB (L16 gfs)	-1.52	0.06	-1.53	0.04	$+0.01$	0.08
RGB (Final)	-1.43	0.05	-1.47	0.06	$+0.04$	0.07
AGB (Final)	-1.52	0.06	-1.48	0.04	-0.04	0.07

in magnitude in the hotter stars ($T_{\text{eff}} > 4800$ K). The average δFe is however only about -0.1 dex in this subset of AGB stars, and the trend mostly lies within the error band. We speculate that this possible trend may be due to either residual underestimation of T_{eff}, or due to NLTE effects being stronger in the hotter AGB stars (although the latter is not supported by current theory, see Sec. 3.5.2).

The main feature in the average Fe I and Fe II values (Table 3.1, final set) is that Fe I is lower in the AGB stars than in the RGB stars, by 0.11 dex. This difference is just within the combined 1σ dispersions of each sample (0.05 and 0.06, respectively; Table 3.1), so it is marginally significant. The difference becomes even less significant when considering other uncertainties (Sec. 3.5.2).

Averaging Fe abundances from Fe I and Fe II in the AGB and RGB samples to arrive at total [Fe/H] values shows that the difference between the two evolutionary phases is -0.06 dex, which is comparable to the star-to-star scatter. Visually the closeness of all the Fe determinations can be seen in Figure 3.11.

We also computed abundances for the AGB stars using the $(V-K)$ temperatures. We found this temperature scale to give identical δFe to the IRFM scale. This was expected since the temperatures are very similar, as seen in Fig. 3.9. We now explore other uncertainties in the method.

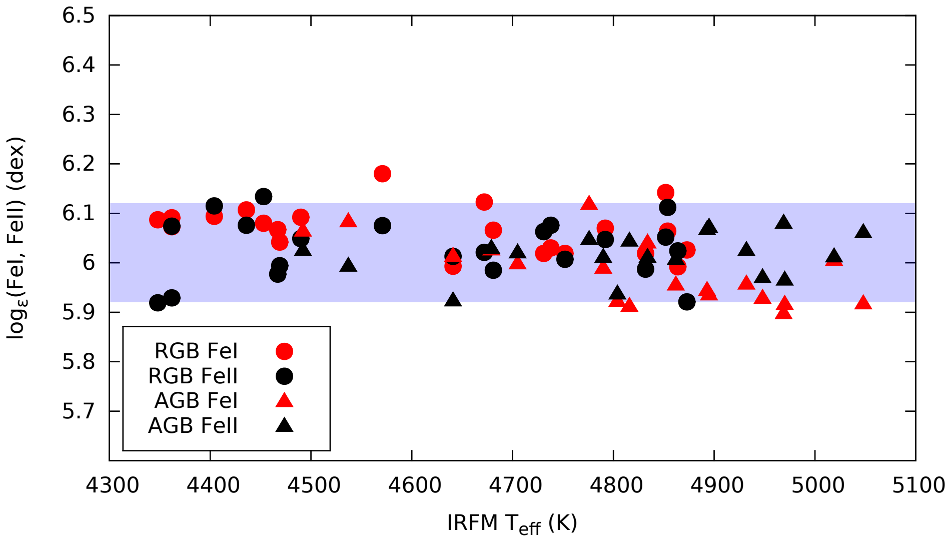

FIGURE 3.11: Iron results using our new IRFM temperatures. All RGB stars (dots) and AGB stars (triangles) are shown for comparison, with iron abundances derived using Fe I and Fe II highlighted by colour (red and black respectively). The shaded region indicates a typical uncertainty of $\sim \pm 0.10$ dex, centered around the average Fe II abundance ($\log \epsilon = 6.02$, from RGB and AGB stars).

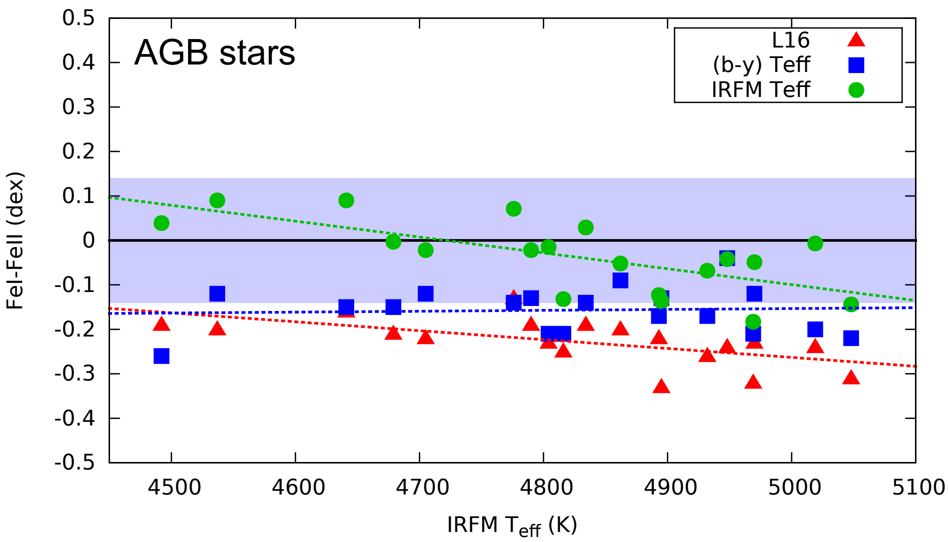

FIGURE 3.12: AGB δFe $=$ Fe I $-$ Fe II results for the current study obtained using our IRFM temperatures, and the $(b-y)$ temperatures. Also shown are the L16 values. The shaded region indicates a quadratic sum of typical (1σ) Fe I and Fe II uncertainties (± 0.14 dex).

3.5.2 Sensitivity of Fe to other uncertainties

Weighted oscillator strengths

The weighted oscillator strength ($\log gf$)[8] adopted for each line is a known source of uncertainty in spectroscopic abundance determination (eg. Gray 2005). Since oscillator strength quantifies the transition probability of a species from one level to the next, a change in $\log gf$ has a systematic effect on derived abundances, shifting them to higher or lower values. This is another possible source of difference between our study and L16 that could directly affect δFe, and thus it requires investigation.

As a first step we directly compared our Fe I and Fe II $\log gf$ values with those used by L16[9]. For Fe I we found the average difference for our 40 lines to be $\Delta \log gf = -0.02$ dex ($\sigma = 0.09$; in the sense L16 – this study). Since final abundances are taken as an average over the abundances inferred from each line, and considering other uncertainties, this difference is insignificant[10]. For the Fe II lines the average difference is slightly larger, being $\Delta \log gf = +0.05$ dex. However, for Fe II we only used two or three lines, so in the cases where only two lines were available, even one significantly deviant $\log gf$ value would be expected to alter the derived abundances tangibly – and thus alter δFe by offsetting Fe II. To check the sensitivity of our results to this difference we re-derived Fe abundances for our entire stellar sample using the L16 $\log gf$ values for Fe II. The Fe II lines ($\Delta \log gf$) we used were: 6149.23 Å ($+0.04$ dex), 6247.56 Å ($+0.02$ dex), and 6369.46 Å ($+0.10$ dex). All else was kept constant.

The results of this analysis are presented in Table 3.1. The slightly increased Fe II oscillator strengths led to an average decrease of [Fe II/H] of 0.05 dex in both the RGB and AGB samples. As Fe I is unchanged, this leads to correspondingly minor changes in δFe. For the RGB sample δFe becomes marginally significant ($+0.09$ dex), albeit in the opposite sense to the original problem in the AGB sample. In the AGB stars δFe remains insignificant, with δFe changing from -0.04 to $+0.01$ ($\sigma = 0.08$).

Thus the adopted $\log gf$ values appear to contribute to the uncertainty in δFe only to a small degree. Additionally, the lower abundance derived from Fe II using the L16 oscillator strengths most likely explains part of the ~ 0.1 dex lower average [Fe II/H] value found by L16.

[8] Where f is the oscillator strength and g is the statistical weight of the lower level.

[9] L16 used the Kurucz/Castelli line list for all species except for Fe II, for which they used values from Meléndez and Barbuy, 2009

[10] We also compared our Fe I $\log gf$ values to those used by the Gaia-ESO Survey (Ruffoni et al. 2014). Here also the average difference is minor, with $\Delta \log gf = 0.02$ dex ($\sigma = 0.09$). There are however only five lines in common (out of 40).

NLTE effects

Our final δFe results appear to show a weak trend toward higher values at higher $T_{\rm eff}$ in the AGB sample (Fig. 3.12). This could be due to a real overionisation of Fe I, but the overionisation effect would have to be stronger in stars in this particular temperature range ($T_{\rm eff} > 4800$ K).

The magnitude of non-LTE effects in atmospheres of cool stars has been recently studied by Lind et al., 2012 and Mashonkina et al., 2016. Figure 2 of Lind et al., 2012 shows that, at the metallicity of NGC 6752, the NLTE corrections for Fe I are expected to be small for AGB and RGB stars.

As a check we computed the expected NLTE corrections for a range of Fe I lines at some characteristic parameters of our AGB and RGB stars using both the Lind et al., 2012 and Mashonkina et al., 2016 web-based interpolation routines[11]. We found that corrections were consistent between the two compilations. The corrections were also almost constant, varying by just ± 0.01 dex, so they are basically offsets. The constancy across the AGB temperature range implies that the marginal δFe trend in Figure 3.12 is not explained by current NLTE theory. The magnitude of the corrections are however slightly different across each set of stars, with Δ_{NLTE} averaging $+0.05$ dex for the RGB stars and $+0.09$ dex for the AGB stars. The slightly higher value for AGB stars is expected due to their higher temperatures[12].

The NLTE offsets increase the average δFe to $+0.09$ in the RGB sample, and to $+0.05$ (from -0.04) in the AGB sample. Considering other uncertainties, these offsets are small. It is important to recognise that the NLTE corrections themselves also have uncertainties. Lind et al., 2011a showed that model atmosphere choice alone can alter the predicted NLTE corrections by up to ~ 0.1 dex (their Figure 8, for Na I). This is comparable to the magnitude of the predicted offsets we have reported here. To be consistent with L16, and considering the small effect on the results, we did not apply the NLTE offsets to our final Fe I results. This also avoids adding in the extra uncertainty of the corrections themselves.

Model Atmospheres

The choice of model atmosphere has an effect on abundance determinations. This is due to the fact that different physical stratifications are predicted by different stellar atmosphere codes – for the same set of stellar parameters. It is the differences in adopted physical descriptions in each set of theoretical models that gives rise to the different stratifications. For example, some use 'pure MLT' to describe convection, whilst some use modified

[11]The INSPECT interface: `http://www.inspect-stars.com` (Lind et al. 2011a), and the interface by Mashonkina et al., 2016: `http://spectrum.inasan.ru/nLTE`

[12]The lower gravity of the AGB stars compared to RGB stars at the same temperature reduces the difference marginally.

MLT formalisms. Overshoot (see eg. Castelli et al. 1997) and the adopted treatment of opacity are other model variables.

We ran some tests to gauge the effect of using different model grids on the derived Fe I and Fe II abundances. For the tests we used four different grids: a MARCS grid[13] (Gustafsson et al. 2008), and three different Kurucz/Castelli grids[14] (their NOVER, OVER, and AODFNEW grids; Kurucz 1993; Castelli and Kurucz 2004). The four grids differ in terms of overshoot (or lack of), treatment of convection, and treatment of opacity, for example. The parameters and EWs of one RGB star (star 12) and one AGB star (star 97) were used.

We found differences of 0.04 to 0.12 dex in the derived Fe I and Fe II abundances, with Fe I consistently at the upper end. This is consistent with the uncertainty due to adopted model atmospheres reported by Lind et al., 2011a in relation to NLTE corrections. This ~ 0.1 dex uncertainty is especially important when considering species that are very temperature sensitive, here Fe I, since the temperature stratification changes significantly. This test also indicates that uncertainties of this order must be allowed for when comparing between independent studies, even if they are based on the same data, since the model grid choice affects the results. Variations in tools/pipelines that make use of the model grids must also add to these uncertainties.

Two other possible sources of uncertainty from model atmospheres are (i) the choice of plane parallel or spherical (but still 1D) models, and (ii) the choice of model stellar mass. Traditionally, 1 $M_\odot$ stellar atmospheres are used for GC stars, since there is negligible effect in changing the mass by small amounts. However, due to the particularly low masses of AGB stars (~ 0.6 $M_\odot$), models with mass of 0.5 $M_\odot$ may be more appropriate. Due to their low envelope mass, the atmospheres of these stars are expected to be more extended than those of RGB stars, and thus spherical effects may be important. To check these two factors we made a test using the MARCS 0.5 $M_\odot$ spherical models, for which only a small grid exists (Gustafsson et al. 2008). We compared the Fe I and Fe II abundances derived using MARCS models with mass of 1 $M_\odot$ with those derived using 0.5 $M_\odot$ models, for a star with characteristic AGB parameters. We found that the differences were negligible, being of the order 0.01 dex. This indicates that mass and sphericity are not important in the case of these AGB stars.

Finally we note that the discussion above has only involved 1D model atmospheres. Three dimensional model atmospheres are now becoming available and have been shown to have significantly different stratifications as compared to 1D models (eg. Magic et al. 2013). Thus the use of 3D

[13]Downloaded from `http://marcs.astro.uu.se`
[14]Downloaded from `http://kurucz.harvard.edu/grids.html`

model atmospheres would be expected to introduce further differences in abundance determinations.

Distance

The cluster distance is a fundamental parameter that has a direct impact on the gravity scale through the derivation of the stellar bolometric magnitudes. All of the studies (C13, L16 and this study) used the Harris, 1996 catalogue value of $(m-M)_V = 13.13$. A literature search showed that this is at the lower end of the values published, which range from 13.13 to 13.38 (just in the studies we consulted, the range may be greater; Renzini et al. 1996; Gratton et al. 2003b; Yong et al. 2005). Taking the maximum of these values systematically decreases gravity by 0.1 dex. This uncertainty in $\log g$ translates to a systematic shift of the microturbulent velocity scale by an insignificant amount ($+0.03$ dex, based on the Gratton et al. 1996 relation). Nevertheless, we tested the effect of these small systematic shifts using the parameters of AGB star 97 and RGB star 12. As expected, Fe I was unaffected and Fe II was reduced by ~ 0.05 dex. This reduced $\delta\mathrm{Fe}$ in the AGB star, from -0.14 to -0.10 dex, and increased it in the RGB star since Fe I was already greater than Fe II. Again these are small changes but they do add to the many other small uncertainties.

Effect of AGB stellar mass on gravity

Another uncertainty affecting gravity determination is the adopted stellar mass for the AGB stars. The median HB stellar mass was estimated at 0.61 $M_\odot$ for NGC 6752 by Gratton et al., 2010b. This was adopted by L16 and the current study. According to theory, lower masses are possible. For example, Dorman et al., 1993 find a minimum envelope mass for AGB ascension of 0.035 $M_\odot$, at the metallicity of NGC 6752. Adding their core mass of 0.48 $M_\odot$ suggests that the minimum mass for an AGB star should be 0.52 $M_\odot$. This difference of ~ -0.1 $M_\odot$ would systematically reduce the gravity of the AGB stars by 0.07 dex. Importantly this would only affect AGB stars, leaving the RGB gravities unchanged. However the AGB masses may also be higher. Assuming a normal distribution of AGB masses around 0.61 $M_\odot$ we thus (roughly) estimate a 1σ error of $\sim \pm 0.05$ dex on the surface gravity due to the uncertainty in total stellar mass. As discussed above this can cause small changes in abundance results, particularly in the Fe abundance derived from Fe II.

Summary of uncertainties

Here we have only explored some of the uncertainties inherent in spectroscopic abundance determination. From this investigation it is clear that,

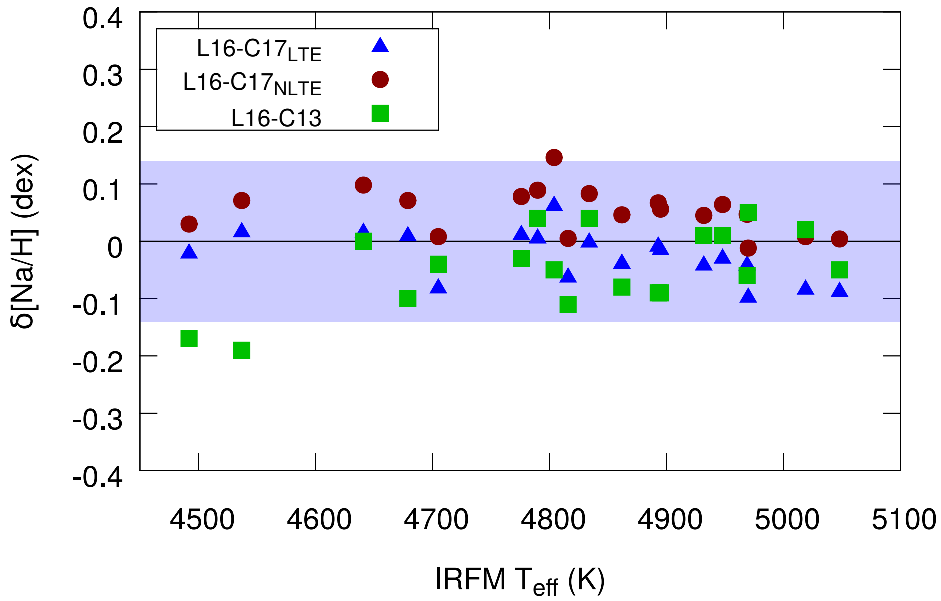

FIGURE 3.13: Comparison between our new AGB Na abundances (labelled C17), the C13 abundances, and those of L16. All abundance sets are corrected for NLTE effects except $\mathrm{C17_{LTE}}$, which is included to highlight the magnitude of the corrections. The shaded region denotes typical uncertainties of 0.1 dex, added in quadrature ($\sigma = 0.14$ dex in total). The two coolest stars are discussed in the text.

apart from the large uncertainty in $T_{\rm eff}$ given by some colour-$T_{\rm eff}$ relations, and the uncertainties in measuring EWs, there are many other sources of uncertainty that lead to additional abundance differences of the order $0.01 \rightarrow 0.10$ dex. All the uncertainties must combine, probably in a non-linear way, to create 'noise' and systematic shifts in the results, increasing the uncertainty of our final abundances. It is also clear that each source of uncertainty (including $T_{\rm eff}$) affects Fe I and Fe II to different degrees. It would thus be expected that each ion of each element would also be affected to different degrees. For a broader view of uncertainties in spectroscopic abundance determination we refer the interested reader to the detailed empirical study of Hinkel et al., 2016.

3.6 Sodium from C13 data using new $T_{\rm eff}$ scale

Of primary interest to the argument of C13 (and to a lesser extent L16) is the distribution of sodium amongst the AGB stars. It is possible that the new IRFM/$(V-K)$ temperature scale (Fig. 3.9) could remove the good agreement between [Na/H] between studies (Fig. 3.2), given that the offset is ~ 100 K.

Na I is predicted to suffer NLTE effects in giant stars such as those studied here. C13 and L16 both used the Gratton et al., 1999 corrections to LTE abundances. For the current study we have chosen to use the more recent NLTE corrections calculated by Lind et al., 2011a. As noted by Lind et al., 2011a the Gratton et al., 1999 corrections differ from most tabulations in the literature, especially at low temperatures and gravities. The Na I lines we have used are: 5682.6 Å, 5688.2 Å, 6154.2 Å, and 6160.7 Å. The last two of these lines were generally not detectable in the AGB stars, but a total of three or four lines were usually detectable in the RGB stars.

We computed NLTE corrections for all available Na lines for all stars using the INSPECT web interface[15] (Lind et al. 2011a). The corrections were not large, with an average of -0.08 dex in the AGB sample, and -0.10 dex for the RGB sample. In both sets of stars this was essentially an offset, with the standard deviation of the corrections being just $\sigma = 0.01$ dex (AGB) and 0.02 dex (RGB). All corrections and final abundances are listed in Appendix A, Table A.2.

In the RGB sample the average standard deviation of the line-to-line abundance scatter, σ_{ave}, was reduced from 0.08 dex (LTE) to 0.06 dex (NLTE). In the AGB stars σ_{ave} reduced from 0.04 dex to 0.03 dex. Although these are small changes this is reassuring as it is what is expected if the corrections are of the correct sign and magnitude. We note that since the AGB stars usually only have two lines measured, the abundances in the AGB stars shouldn't be taken as more accurate than those of the RGB stars. Indeed, we find the average line-to-line scatter increases with the number of lines measured in the AGB stars, with $\sigma_{ave} = 0.10$ dex in the stars with three detectable lines (the RGB stars generally have three or four lines measurable). This is an important point – it is common practice to report standard deviations of very small samples of lines as uncertainties in abundances. This can lead to overconfidence in results.

In Figure 3.13 we compare our new [Na/H] values with those of L16 and C13. Somewhat surprisingly, it can be seen that practically all stars have essentially the same abundances in all three studies, within the uncertainties. The only exceptions are the two coolest stars: the current study and L16 find substantially higher Na than C13 for these stars. This appears to be a minor error in C13, although it has no effect on the conclusions of that study.

The average difference in Na abundance between L16 and the current study, in the sense L16$-$this study, is $+0.05$ dex ($\sigma = 0.04$). Between L16 and C13 it is -0.05 dex ($\sigma = 0.07$), excluding the 2 coolest stars. It is interesting that the increase in temperature of ~ 100 K (above the scale of L16) has no significant effect on the Na abundances. This does concur with the

[15] http://www.inspect-stars.com

observation that a roughly 40 K temperature difference between C13 and L16 also had no significant effect (Fig. 3.2). Adding to this that different tools, model atmospheres, different stellar mass assumptions, and different spectra were used between the studies strongly suggests that the Na abundances are very robust, at least within the current analysis framework.

Our RGB sample has an average abundance of $[\mathrm{Na/H}] = -1.38$ dex, with a standard deviation of $\sigma = 0.27$ dex. In contrast, the AGB sample has an average abundance of $[\mathrm{Na/H}] = -1.71$ dex, with a standard deviation of $\sigma = 0.13$ dex. While the spread in the RGB sample is much larger than the uncertainties, the scatter in the AGB sample is low, and similar to the 0.10 dex reported by C13. Indeed, C13 noted that this level of scatter was similar to their uncertainties and therefore consistent with a single abundance of Na. We explore this topic further in the Discussion.

3.7 Discussion and Conclusion

We have investigated the differences between the NGC 6752 AGB star abundance studies of C13 and L16. In this paper we have focused on Fe and Na, since L16 reported a very strong apparent overionisation of Fe I, and argued that all neutral species, including Na I, should be scaled by Fe I, thus altering the distribution of [Na/Fe] as compared to C13 (Fig. 3.3).

By dividing all neutral species by Fe derived from Fe I, L16 essentially made the assumptions that:

(i) Overionisation affects *all* neutral species

(ii) They are affected by *exactly the same magnitude* of overionisation

While (1) is possible, (2) is highly unlikely, since the magnitudes of NLTE effects are known to vary between species, and indeed between lines of the same species. There are also variations with T_{eff}, gravity, and abundance of the element (see eg. Lind et al. 2011a; Lind et al. 2012 for the cases of Na and Fe).

The scaling to Fe I for neutral species in GC AGB stars was originally suggested by Ivans et al., 2001. They however proposed it as one of *three* options to reconcile Fe I and Fe II in the AGB stars of the globular cluster M 5. These options were arrived at after an extensive investigation into the many possible causes of the Fe discrepancy. The rationale behind the Fe I scaling option was due to the observation that: "Whenever Fe appears to be overionized ... Si, Ti, and V are excessively ionized by essentially the same amount..." (Ivans et al. 2001). This was then generalised to include *all neutral species*. As Ivans et al., 2001 state, this was an extrapolation – it was not based on any theoretical calculations, since they weren't available at that time. These calculations are now available, in particular for Fe I and

Na I. In the case of Fe I the predicted NLTE corrections (Sec. 3.5.2) are much smaller than the depression of Fe I reported by L16 (Fig. 3.4). This has created a 'tension' between theory and observations (see also Lapenna et al. 2014).

During our comparison tests we immediately reproduced a strong apparent depression of Fe I, similar to L16. Significantly, this was achieved with different input data and computational tools. However further investigation showed that this is primarily driven by the adopted stellar temperatures. By deriving more reliable temperatures specifically for our stellar sample via the IRFM method we found that the putative Fe I overionisation became insignificant. By comparing temperatures derived with colour-Teff relations to our IRFM temperatures it was found that $(V-K)$ relations are the most reliable (they have a much smaller uncertainties than $(B-V)$ relations), and we suggest that they be used for future (early) AGB studies. Previous AGB studies that have reported strong apparent Fe I overionisation will need to be checked.

Interestingly, one of the possibilities canvassed by Ivans et al., 2001 to remove the Fe discrepancy was indeed to "arbitrarily increase the values of T_{eff} above the Alonso et al. scale by 60 K on the RGB and 120 K on the AGB". By investigating other options for temperature scales they found that there were scales that were systematically hotter (see their Section 3.3 for details). They concluded that this avenue to resolve the Fe discrepancy "remains an option".

Related to this is the study of 47 Tuc by Lapenna et al., 2014. Noting that their finding of a strong depression of Fe I in the AGB stars was at odds with theoretical predictions, they made a detailed investigation into the uncertainties affecting δFe. They excluded T_{eff} as a significant source of uncertainty because the excitation balance was "well satisfied" in their sample. Our result – that spectroscopically determined temperatures tend to lie close to the initial estimates (usually photometric) – may be the reason that Lapenna et al., 2014 could not reconcile the 47 Tuc AGB Fe I and Fe II abundances. An indication that this may be the case is given by one of the tests performed by Lapenna et al., 2014. They found that δFe became negligible if parameters from a higher mass star (1.2 $M_{\odot}$) were used. The T_{eff} increase above the nominal value was $\sim +100$ K. The fact that this was a positive T_{eff} offset that reduced δFe matches with our findings (Fig. 3.7). The magnitude of this T_{eff} offset is similar to the offsets we have found here (Fig. 3.9), so we would expect a greater increase in Fe I, of the order ~ 0.2 dex as compared to ~ 0.1 dex found by Lapenna et al., 2014. However the much higher metallicity of 47 Tuc may reduce the effect.

L16 also discussed their results in terms of [X/H], noting that using Fe in the denominator may have skewed the results (they report that it did not). However the different T_{eff} scale presented here[16] means that all elements need reanalysis, since the effects are uncertain and most likely vary from element to element, as our investigation of Fe and Na has shown. As molecular band formation is highly dependent on temperature, abundances for elements based on molecules (C, N, and indirectly, O, in L16) are likely to be altered. We are unsure how the results of the L16 study will be affected. The effects may or may not alter the conclusions on the topic of AGB subpopulations, but it clearly requires investigation.

After the reconciliation of Fe I and Fe II, we checked the effect of the new temperature scale on derived sodium abundances and found that it had no significant effect. Interestingly the [Na/H] abundances across the three studies (C13, L16, and the current study) all agree, within the uncertainties. It is also remarkable that such large differences in temperatures, gravity, input data, and tools, have such little effect on the Na abundances. This suggests they are very robust – at least in the current paradigm of 1D stellar atmosphere abundance determinations and NLTE modelling. We speculate that either (i) significant changes in the (currently small) predicted NLTE corrections, or (ii) 3D atmosphere effects, would be the most likely factors that could alter the Na abundances. Since Fe is constant in NGC 6752 then [Na/Fe] must also be consistent between all studies, aside from possible systematic offsets in Fe.

We found that the Na abundance spread in the AGB sample is slightly larger than that found by C13 ($\sigma = 0.13$ dex versus 0.10 dex). This compares with a spread of $\sigma = 0.27$ dex in the RGB sample. As shown in C13 the AGB distribution is centered over the RGB SP1 distribution. However we are cautious to assign significance to the slight increase in the AGB dispersion, especially given the exploration of the many sources of uncertainty in Section 3.5.2. In particular we note the uncertainties in NLTE corrections that could amount to 0.1 dex, but which are generally ignored in abundance studies. We also recall that the Na abundances in the AGB stars are usually based on just two lines, so the line-to-line scatter uncertainty is not well constrained. Indeed, we found that the line-to-line scatter *increases* in the stars with more Na lines measured, to a an average value of 0.10 dex in the AGB stars with three detectable lines[17]. As this is just one source of uncertainty, it should be taken as a *minimum* for the total abundance uncertainty. That said, our empirical result in Figure 3.13, which shows that the Na abundances appear very robust between the three studies (all within ± 0.05 dex,

[16]Gravity should be only slightly affected, with changes most likely smaller than the L16 uncertainty of ~ 0.1 dex (Sec. 3.3).

[17]This compares with the LTE (NLTE) average scatter of 0.08 (0.06) dex in the RGB stars, which mostly have three or four lines measured.

on average), may suggest that the spread is significant[18]. If it is, this could be considered a small signal of the tail of the second population distribution being present on the AGB, similar to that found for M 4 (see Discussion in MacLean et al. 2016). However, given the small magnitude of the signal, it is advisable to attempt to identify the subpopulations in multi-dimensional chemical space instead, as noted by others (eg. L16; MacLean et al. 2016). Thus we leave the further discussion of AGB subpopulations to our next paper in the series, where we will investigate other elements given the improved AGB temperatures. What appears certain is that the Na spread in the AGB stars is very restricted compared to the RGB stars.

We conclude by noting that care must be taken in deriving AGB star temperatures, and, more generally, that uncertainty reporting in abundance analysis papers should be more robust – there are many sources of uncertainty that can significantly alter the results. The relevant example here is the standard procedure of testing the abundance results' sensitivity to temperature. Both C13 and L16 used an estimated uncertainty of $\sim \Delta T_{\text{eff}} \pm 30 K$. This uncertainty is small compared to the T_{eff} differences of $\sim 60 - 100$ K found here. If more realistic uncertainties were included, the error bars on Fe I would have been large[19] – and the results consistent with theory and other abundance studies.

Acknowledgements

The spectroscopic observations were carried out with the Very Large Telescope under ESO programme 089.D-0038 (PI Campbell). Part of this work was supported by the DAAD (PPP project 57219117) with funds from the German Federal Ministry of Education and Research. DY acknowledges funding from the Australian Research Council (FT140100554). BTM acknowledges the financial support of the Australian Postgraduate Award scholarship. We thank Yazan Momany and Frank Grundahl for providing their photometric datasets, and Yue Wang and Francesca Primas for helpful discussions. This work made extensive use of the SIMBAD, Vizier, 2MASS, and NASA ADS databases. It also made use of the open-source software packages MOOG (Chris Sneden; `http://www.as.utexas.edu/~chris/moog.htmland`) and $q2$ (Ivan Ramirez; `https://github.com/astroChasqui/q2`). We thank the anonymous referee for their constructive comments, which improved the paper.

[18] Although it may instead reflect that usually the same two Na lines are used in every AGB study, and, as we have shown, that these particular lines are insensitive to many factors.

[19] See final paragraph of Section 3.4.2.

Chapter 4

AGB subpopulations in the nearby globular cluster NGC 6397

Published in *MNRAS* 475, 257, March 2018.

Abstract

It has been well established that Galactic Globular clusters (GCs) harbour more than one stellar population, distinguishable by the anti-correlations of light element abundances (C-N, Na-O, and Mg-Al). These studies have been extended recently to the asymptotic giant branch (AGB). Here we investigate the AGB of NGC 6397 for the first time. We have performed an abundance analysis of high-resolution spectra of 47 RGB and 8 AGB stars, deriving Fe, Na, O, Mg and Al abundances. We find that NGC 6397 shows no evidence of a deficit in Na-rich AGB stars, as reported for some other GCs – the subpopulation ratios of the AGB and RGB in NGC 6397 are identical, within uncertainties. This agrees with expectations from stellar theory. This GC acts as a control for our earlier work on the AGB of M 4 (with contrasting results), since the same tools and methods were used.

4.1 Introduction

It is well known that Galactic globular clusters (GCs) show star-to-star spreads in the abundances of proton-capture elements (primarily He, C, N, O and Na), while most GCs remain homogeneous in the iron peak species (Carretta et al., 2009a). This spread often presents as multi-modal (as in the early low-resolution cyanogen (CN) studies of Norris, 1981; Cottrell and Da Costa, 1981), with two or more distinct subpopulations being identified. One of these subpopulations is always chemically similar to Galactic halo stars of the same metallicity – designated here as SP1 and which is inferred to contain primordial He abundances – with one or more further subpopulations found to have higher N and Na (and lower C and O) abundances – here designated collectively as SP2 (see Gratton et al., 2012, for an extensive review). These are the ubiquitous C-N and Na-O (and Mg-Al in some GCs) anti-correlations (Carretta et al., 2009b). This spread in light elemental abundance can also be inferred from narrow and intermediate band photometric data, seen as multiple red- or sub-giant branches, or multiple main sequences in a GC's colour-magnitude diagram (e.g., Milone et al., 2008; Milone et al., 2014).

The peculiar abundance signature of SP2 stars has been observed in both evolved and unevolved stars in many clusters (Gratton et al., 2001), indicating that this pattern is likely to have been inherited at birth. Furthermore, the pattern is generally not observed elsewhere, such as the (less massive) open clusters of the Galaxy (De Silva et al., 2009; MacLean et al., 2015); however very recently it has been suggested that the Galactic bulge may contain SP2-like stars (Schiavon et al., 2017). The most common explanation for this light-elemental inhomogeneity is the self-pollution hypothesis where the ejecta of more massive SP1 stars mixed with an early dense interstellar medium, from which SP2 stars were formed (Cannon et al., 1998; Gratton et al., 2004).

Importantly, the relative fractions of each subpopulation remain the same through all these phases of evolution, as expected from stellar evolutionary theory. However, until recently there were no systematic surveys of asymptotic giant branch (AGB) stars. Some early (e.g., Norris et al., 1981) and more recent (Campbell et al., 2010; Campbell et al., 2013) low-resolution spectroscopic studies of GCs found that the distribution of cyanogen band strengths varies greatly between the RGB and AGB of several GCs. In particular, they found no CN-strong (i.e., SP2) AGB stars in NGC 6752, which has an extended blue horizontal branch (HB). These results hinted at differences in evolution between stars of different light elemental abundances, which are not fully predicted in standard stellar evolution theory – only stars with extreme He abundances are expected to avoid the AGB phase due to smaller envelopes in the HB phase (Dorman et al., 1993; Campbell et al., 2013; Cassisi et al., 2014).

In this paper we use the prescription as described in MacLean et al. (2016, hereafter ML16), where the percentages of RGB and AGB stars in a GC that are found to be members of SP2 are written as $\mathscr{R}_{RGB}$ and $\mathscr{R}_{AGB}$, respectively (typical $\mathscr{R}_{RGB}$ values are ∼50-70%; Carretta et al., 2010); and the SP2 AGB deficit is given by

$$\mathscr{F} = (1 - \frac{\mathscr{R}_{\mathrm{AGB}}}{\mathscr{R}_{\mathrm{RGB}}})\cdot 100\%, \tag{4.1}$$

where a value of 100% indicates that no SP2 stars reach the AGB – as reported for NGC 6752 and M 62 by Campbell et al. (2013) and Lapenna et al. (2015), respectively. For clusters with extended HBs (where the bluest stars reach T_{eff} over 15,000 K; e.g., NGC 6752, NGC 2808), an $\mathscr{F}$ value of up to ∼30% may be expected due to the well-established existence of AGB-manqué stars (which evolve directly from the HB to the white dwarf phase, avoiding the AGB; Greggio and Renzini, 1990; Dorman et al., 1993; Cassisi et al., 2014). Clusters whose HBs do not extend into this regime (e.g., M 4, NGC 6397) are expected to have an $\mathscr{F}$ value of zero per cent, with all stars in the cluster ascending the AGB.

There has been much debate as to the level and existence of GC SP2 AGB deficits in recent years as more evidence has been gathered, but a definitive conclusion has yet to be reached. In fact, contradictory evidence has been presented for both NGC 6752 and M 4. For example, in Campbell et al. (2013) we found that the measured Na abundances in all NGC 6752 AGB stars were consistent with SP1, indicating $\mathscr{F} \sim 100\%$. Lapenna et al. (2016) conducted an independent study of the same GC, and found that with [Na I/Fe I] abundances, $\mathscr{F}$ dropped to the predicted value of ∼30%. The assumption that dividing by Fe I is more accurate has recently been disputed by (Campbell et al., 2017, hereafter C17). Recent studies of AGB stars in other GCs such as Johnson et al. (2015), García-Hernández et al. (2015), and Wang et al. (2016) have found varying values of $\mathscr{F}$ – see Table 4 of ML16 for a summary of $\mathscr{F}$ values as of July 2016.

Attempts to theoretically explain SP2 AGB deficits have been outpaced by the numerous observational studies that have painted a complex picture, both technically (e.g., the treatment of non-LTE) and empirically (e.g., contradictory results). If high SP2 AGB deficits are real, rather than being an artefact of the spectroscopic analysis (see §4.5 for discussion), then the most likely explanation comes from the He-enrichment of SP2 stars. This results in smaller envelope masses on the HB (Gratton et al., 2010a; Cassisi et al., 2014; Charbonnel and Chantereau, 2016) and such stars are known to evolve directly to the white dwarf phase (AGB-manqué stars). SP2 AGB deficits above $\mathscr{F} \simeq 30\%$ suggest that the location along the HB where this alternative evolutionary path begins to occur may be incorrectly predicted by theory, and/or dependent on more factors than previously thought.

Similar to the debate on AGB abundances in NGC 6752, recent studies on the archetypal GC M 4 have presented starkly different conclusions on the nature of its AGB. ML16 presented [Na/Fe] and [O/Fe] abundances for both AGB and RGB stars in M 4, reaching the conclusion that all AGB stars are consistent with being SP1 stars (i.e., $\mathscr{F} \simeq 100\%$). In contrast, Lardo et al. (2017) and Marino et al. (2017) – using photometric indices and spectroscopic analysis, respectively – concluded that the spread of light elemental abundances in the AGB of M 4 is similar to the RGB (however, both studies found that their AGB samples were offset toward SP1-like abundances). If true, this is consistent with the theoretical prediction of $\mathscr{F} = 0\%$. However, the very recent study of Wang et al. (2017) showed that the spread in Na abundances of M 4's AGB is significantly narrower than the RGB, qualitatively similar to the findings of ML16, but not as extreme. It is clear that further study of this GC is required.

If high SP2 AGB deficits are reliably demonstrated, this may impose new and important restrictions on low-mass, low-metallicity stellar evolution and/or atmospheric models; impacting the field of globular clusters, stellar evolution, and Galactic formation and archaeology.

In the current study we aim to derive AGB subpopulation ratios for the GC NGC 6397 for the first time. NGC 6397 is an old and metal-poor GC with a well documented Na-O anti-correlation on the RGB, the range of which is smaller than many other clusters (no 'extreme population' in the classification of Carretta et al., 2009a, which is associated with high He abundance). NGC 6397 also displays a Mg-Al anti-correlation (Lind et al., 2011b, hereafter L11). The short (but blue) HB of NGC 6397 extends between $8000K < T_{\text{eff}} < 10,500K$, suggesting that no stars in the cluster should evolve into AGB-manqué stars (Lovisi et al., 2012). In order to determine if this is the case, we have performed an analysis of spectra from a sample of AGB and RGB stars in NGC 6397. For each star we have derived radial velocities, stellar parameters, and abundances of Fe, Na, O, Mg and Al.

4.2 Sample selection, observations and membership

Our stellar targets were selected from the NGC 6397 photometric dataset of Momany et al. (2003, UBVI from the ESO/MPG WFI, see Table 4.1). For the bright stars considered here the photometric completeness is 100%, for all colours. The photometry covers the entire cluster out to at least 9 arcmin from the cluster centre (in some directions reaching to $\sim$ 22 arcmin). This compares with the cluster's half-light radius of 2.9 arcmin (Harris, 1996). To avoid crowding problems in the core with multi-object fibre placement the sample was limited to stars outside ~ 0.5 arcmin of the cluster centre.

The RGB and AGB are separated in V−(B−V) and U−(U−I) space (Figure 4.1). AGB stars were conservatively selected – only early-AGB stars were included so as to avoid the mislabelling of stars since the AGB and RGB colours become similar at brighter magnitudes. We then cross-matched our selection with the 2MASS database to take advantage of the high quality astrometry and JHK photometry. 2MASS IDs and JHK photometric magnitudes for the whole sample are included in Table 4.1. In total our initial target sample included 9 AGB stars and 64 RGB stars. Importantly for the science goal of this study the RGB and AGB samples are spatially coincident.

High-resolution spectra were collected in July 2015 using 2dF+HERMES on the Anglo-Australian Telescope which provides $R = 28,000$ spectra in four narrow windows; blue (4715 - 4900Å), green (5649 - 5873Å), red (6478 - 6737Å), and infrared (7585 - 7887Å) (for more details on the HERMES instrument, see De Silva et al., 2015; Sheinis et al., 2015). Due to restrictions on 2dF fibre positioning, we were able to collect spectra for only 60 of the 73 targets. This down-sampling is random, except that priority was given to obtaining the largest possible sample of AGB stars, since the number of AGB stars is inherently low compared to RGB stars (see Fig 4.1, black dots). In total we collected spectra for 8 of the 9 identified AGB stars, and 52 RGB stars.

The spectra had an average signal-to-noise ratio of 70. The software package 2DFDR (AAO Software Team, 2015, v6.5) was used to reduce the data for analysis. Radial velocities were measured with the IRAF *fxcor* package (Tody, 1986), using a solar reference template. The mean radial velocity for NGC 6397 after non-member elimination was found to be <v> = 19.30 ± 0.48 km/s ($\sigma = 3.71$km/s), consistent with Lind et al. (2009), who report <v> = 18.59 ± 0.16 km/s ($\sigma = 3.61$ km/s). Individual stellar radial velocities are listed in Table 4.1. Iterative 3-σ clipping of radial velocities and metallicities (discussed in §4.3.2) reduced the final RGB sample to 47 stars. All of the 8 observed AGB stars were found to be members.

Apart from not sampling the inner core of the cluster we do not identify any sample bias. Moreover we have collected spectra for almost all of the AGB stars in the very wide field of view of the source photometry. The 47 RGB stars offer a solid basis for comparison. The final observed samples can be seen visually in the colour-magnitude diagrams of Figure 4.1, overplotted against the full photometry sample.

TABLE 4.1: NGC 6397 target details including data from Momany et al. (2003, UBVI photometry and target IDs) and 2MASS (Skrutskie et al., 2006, JHK photometry – gaps in data represent targets with low quality flags), radial velocities (km/s), and Lind et al. (2011b, L11) IDs. See Appendix A, Table A.3 for complete table.

ID	Type	2MASS ID	L11 ID	V Mag	B Mag	U Mag	I Mag	J Mag	H Mag	K Mag	RV (km/s)
56897	AGB	17400665-5335001	-	11.83	12.76	10.59	13.11	9.76	9.25	9.13	17.17
60609	AGB	17402547-5347570	-	11.65	12.62	10.37	12.97	-	-	-	20.68
70509	AGB	17405254-5341049	-	11.98	12.90	10.75	13.17	9.95	9.48	9.31	19.38
70522	AGB	17404076-5341046	-	11.16	12.24	9.79	12.80	8.94	8.37	8.26	18.93
73216	AGB	17403510-5339572	-	11.83	12.76	10.57	13.11	-	-	-	16.00
⋮	⋮	⋮	⋮	⋮	⋮	⋮	⋮	⋮	⋮	⋮	⋮

4.3 Method

4.3.1 Atmospheric parameters

For this study we have used several photometric relations to determine effective temperatures for all stars.

Typically with spectroscopic studies (such as ML16), stellar parameters are determined by requiring the excitation and ionisation balance of abundances from neutral and singly-ionised iron (Fe I & Fe II, respectively) absorption lines (e.g., Sousa, 2014). While a significant strength of this method is that the parameters are unaffected by photometric reddening, there are also many weaknesses. Many solutions can be found for a single star, largely depending on the choice of initial parameter estimates (see C17). Additional spectroscopic uncertainties such as EW measurements, choice of atmospheric model, atomic line data, and parameter interdependence can compound this problem.

To further complicate the picture, Lapenna et al. (2014) and Lapenna et al. (2016) have provided evidence that the Fe I lines of AGB stars may experience a higher degree of non-LTE effects than RGB stars at the same metallicity and effective temperature. If true, then assuming ionisation balance may artificially and preferentially lower the derived surface gravity of AGB stars (Lind et al., 2012). In C17 we suggested that this so-called 'AGB iron over-ionisation problem' does not exist (at least in NGC 6752), but may be the result of systematic offsets in photometrically-derived $T_{\rm eff}$. Regardless, Fe I lines are well known to experience some non-LTE effects (on both the RGB and AGB, and especially at low metallicities, see Bergemann et al., 2012), so forcing ionisation balance prior to the correction of non-LTE effects may result in systematically incorrect gravities and metallicities in all stars.

We have used the B−V and V−K relations from Ramírez and Meléndez (2005), González Hernández and Bonifacio (2009) and Casagrande et al. (2010) to determine $T_{\rm eff}$ estimates. Additionally, we have calculated $T_{\rm eff}$ without relying on colour calibrations, by implementing the infrared flux method (IRFM) at an estimated log g of each AGB and RGB star, as described in Casagrande et al. (2010) and Casagrande et al. (2014) using BVI and 2MASS JHK photometry. Thus we have seven $T_{\rm eff}$ estimates for each star. These methods are dependent on metallicity, for which a value of [Fe/H] $= -2.00$ was assumed for NGC 6397. To account for interstellar extinction we applied a constant correction of $E(B-V) = -0.19$ to all stars (Gratton et al., 2003b). NGC 6397 does not suffer from significant differential reddening (Milone et al., 2012a).

Four stars were flagged for low quality and/or contamination in the 2MASS database so only the B−V relations were used to determine $T_{\rm eff}$ for

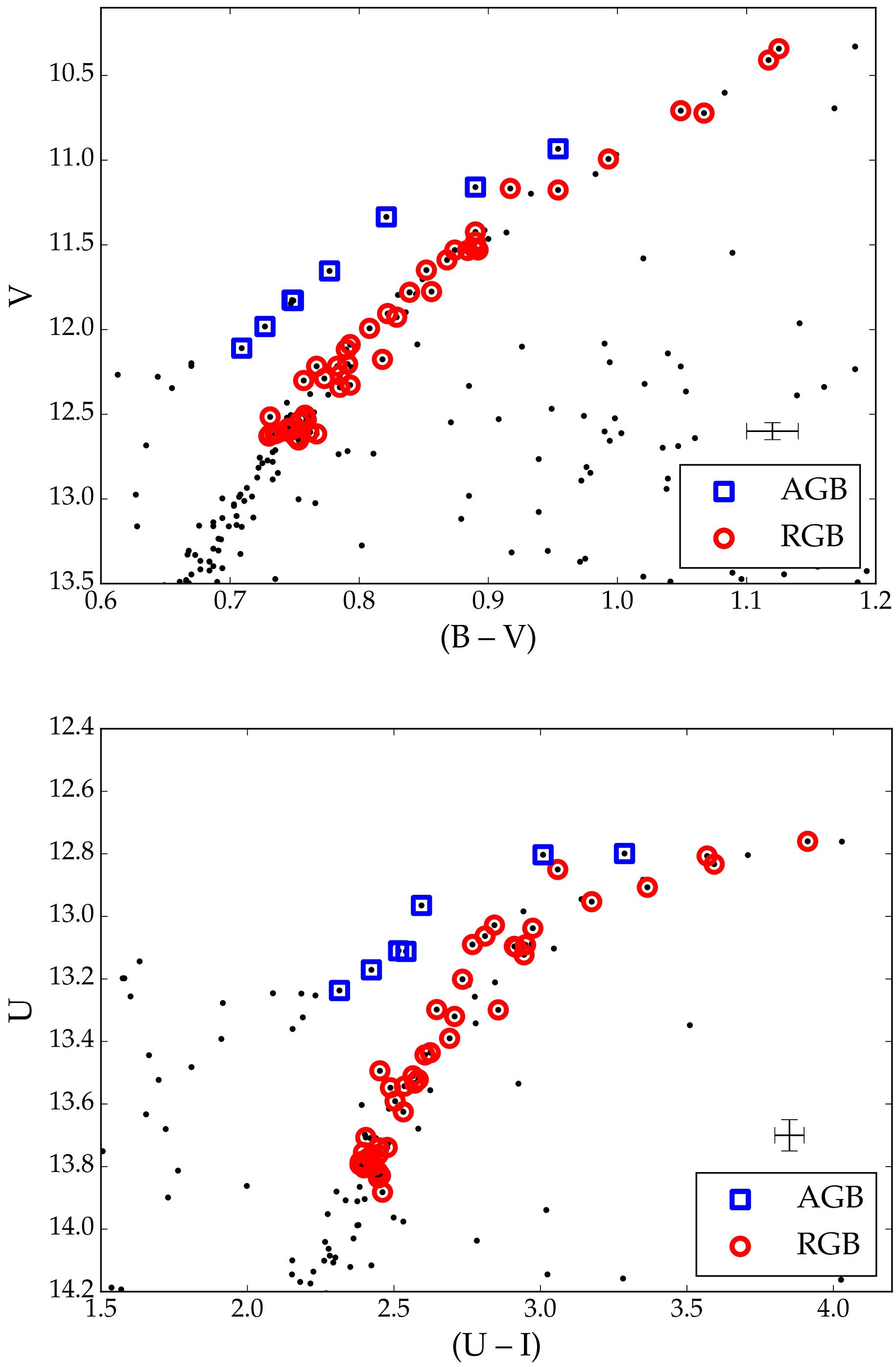

FIGURE 4.1: V−(B−V) and U−(U−I) colour-magnitude diagrams of the observed NGC 6397 RGB and AGB stars (open circles and squares, respectively), displayed over the full photometric sample of Momany et al. (2003, black points). In the top panel, a constant reddening correction value of (B−V) = −0.19 was applied to all photometric data. No reddening correction was applied to the (U−I) photometry (bottom panel). We note that there are only 7 AGB stars in the U−(U−I) diagram because one star (AGB 80621) does not have a reliable U-band magnitude and was selected based only on its B- and V-band magnitudes.

TABLE 4.2: Average differences in T_{eff} between the adopted value and each photometric estimate. Uncertainties are the 1σ standard deviations of the cluster samples. The average σ value in the last row is indicative of the spread of T_{eff} estimates for each star.

Method	ΔT_{eff} (K)
Ram (B−V)[1]	94 ± 45
Gonz (B−V)[2]	-17 ± 42
Casa (B−V)[3]	22 ± 98
Ram (V−K)[1]	69 ± 35
Gonz (V−K)[2]	-34 ± 34
Casa (V−K)[3]	-33 ± 32
IRFM	-108 ± 47
Average σ	± 48

[1]Ramírez and Meléndez (2005)

[2]González Hernández and Bonifacio (2009)

[3]Casagrande et al. (2010)

these stars. For all other stars, the mean of the seven $T_{\rm eff}$ estimates was adopted. Table 4.2 shows the variation between the final adopted $T_{\rm eff}$ values and those of the photometric relations and IRFM. Surface gravities (log g) and micro-turbulences (v_t) were determined using the empirical relations from Alonso et al. (1999) and Gratton et al. (1996), respectively, and assuming a mass of 0.8 $M_\odot$ and 0.7 $M_\odot$ for the RGB and AGB, respectively (Lovisi et al., 2012; Miglio et al., 2016). We adopt a 1σ uncertainty of ±50K for T_{eff} (see Table 4.2), ±0.1 dex for log g, and ±0.2 km/s for v_t. Final stellar parameters for each star are included in Table 4.5 and represented visually in Figure 4.2.

4.3.2 Chemical abundance determination

Chemical abundances were determined for Fe (using Fe I and Fe II), Na (Na I), O (O I), Mg (Mg I), and Al (Al I) using the equivalent width (EW) method. EWs of absorption lines were measured using a combination of the ARES (Sousa et al., 2015, v2) and IRAF *onedspec* packages, while one-dimensional LTE abundances were determined using the MOOG code (Sneden, 1973, June 2014 release) and model atmospheres that were interpolated from the Castelli and Kurucz (2004) grid. The line list and atomic data used for this analysis are specified in Table 4.3. The LTE assumption has been known for many years to be an inaccurate approximation for the abundances of many elemental species. In fact, all elements determined in this work are affected by non-LTE effects which must be accounted for if the abundances are to be reliable. Fortunately, grids of non-LTE corrections now exist for all of these elements in the parameter space occupied by our stellar sample.

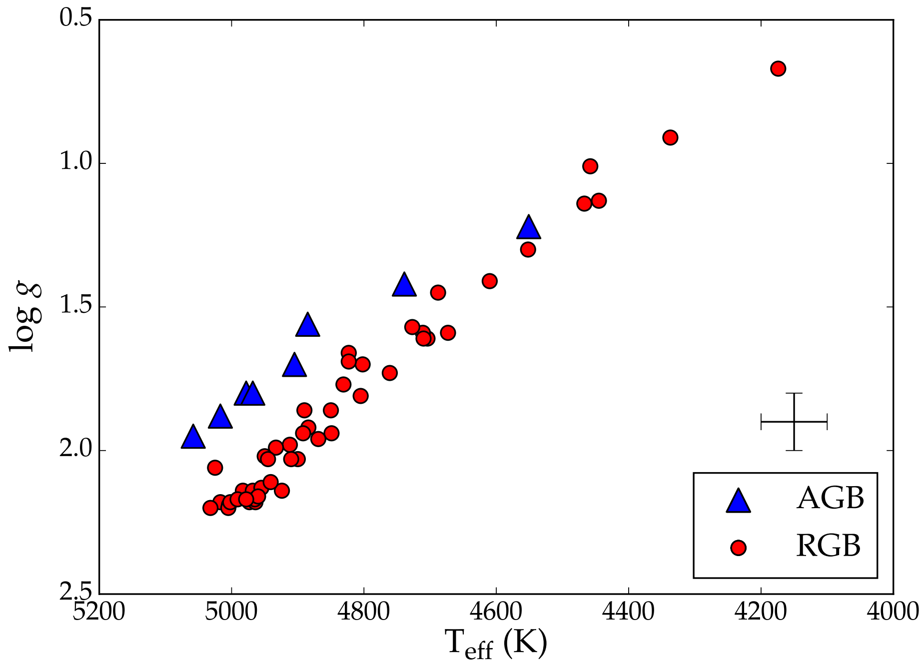

FIGURE 4.2: Final stellar parameters of NGC 6397, determined from photometric relations. The method of parameter determination is described in the text. Typical uncertainties are indicated, and are the same as in Table 4.6.

Iron abundances determined from neutral absorption lines are known to be systematically lower than those determined using singly-ionised lines (for which LTE is a realistic approximation; Lind et al., 2012). However, due to the large number of Fe lines in a stellar spectrum, it can prove difficult to perform a complete line-by-line non-LTE analysis using published grids. For this reason, we performed a test to gauge the magnitude of the offsets on a subset of stars and lines. For our test, we selected a representative subsample of three RGB and three AGB stars from NGC 6397, and interpolated corrections from Amarsi et al. (2016a) for five Fe I lines[1] and two Fe II lines[2]. The results of this test are summarised the first two rows of Table 4.4. We did not apply these average corrections, but compare them to our LTE Fe results in Section 4.4.

Non-LTE corrections were applied to all Na, O, Mg and Al abundances line-by-line using the most recent grids. As in ML16, Na abundances were determined using the 568 nm doublet and corrected for non-LTE effects as described in Lind et al. (2011a) by using the web-based INSPECT interface[3], and adopting the provided Δ[Na/Fe]$_{\mathrm{NLTE}}$ corrections. The oxygen 777 nm triplet was measured and non-LTE corrections were determined by

[1] 4788.8Å, 4839.5Å, 5701.6Å, 5753.1Å and 7748.3Å
[2] 6516.1Å and 7711.7Å
[3] http://inspect-stars.net

the interpolation of the recent Amarsi et al. (2016b) grid of corrections. For Mg, the measured EWs of the 571 nm and 769 nm lines were used for non-LTE determinations as described in Osorio and Barklem (2016), using the INSPECT interface. The average of these two values was then used to correct the 473 nm Mg line. Finally, both the 669 nm and 783 nm doublets were used to determine Al abundances, while non-LTE adjustments were interpolated from the new results of Nordlander and Lind (2017). Average non-LTE corrections, and associated spreads are listed in Table 4.4.

4.4 Abundance results & analysis

Final elemental abundances are presented in Table 4.5. Uncertainties cited in the table are based only on the line-to-line scatter of each abundance and do not consider additional sources of error. Using our estimated 1σ uncertainties of each stellar parameter (±50K in $T_{\rm eff}$, ±0.1 in log g, ±0.2 km/s in $v_{\rm t}$), an atmospheric sensitivity analysis was performed on a representative sub-sample and results are summarised in Table 4.6. Finally, in Table 4.7 we present a summary of all identified sources of uncertainties and adopted total abundance uncertainties.

TABLE 4.3: Adopted line list used for EW measurements. Based on the line list of the GALAH collaboration (De Silva et al., 2015).

Wavelength (Å)	Species	Excitation Potential (eV)	log gf
7771.94	O I	9.146	0.369
7774.16	O I	9.146	0.223
7775.39	O I	9.146	0.002
5682.63	Na I	2.100	−0.706
5688.20	Na I	2.100	−0.404
4730.03	Mg I	4.350	−2.347
5711.09	Mg I	4.350	−1.724
7691.53	Mg I	5.750	−0.783
6696.02	Al I	3.140	−1.569
6698.67	Al I	3.140	−1.870
7835.31	Al I	4.020	−0.689
7836.13	Al I	4.020	−0.534
4788.76	Fe I	3.237	−1.763
4839.54	Fe I	3.270	−1.820
4890.75	Fe I	2.875	−0.394
4891.49	Fe I	2.849	−0.111
5701.56	Fe I	2.559	−2.220
5753.12	Fe I	4.260	−0.690
5859.59	Fe I	4.549	−0.419
5862.36	Fe I	4.549	−0.127
6498.94	Fe I	0.958	−4.687
6518.37	Fe I	2.831	−2.440
6592.91	Fe I	2.727	−1.473
6593.87	Fe I	2.433	−2.420
6609.11	Fe I	2.559	−2.691
6677.99	Fe I	2.690	−1.420
7748.27	Fe I	2.949	−1.751
7780.56	Fe I	4.473	−0.010
4731.45	Fe II	2.891	−3.100
6516.08	Fe II	2.891	−3.310
7711.72	Fe II	3.903	−2.500

TABLE 4.4: Summary of average non-LTE corrections for each element, with 1σ standard deviations over the stellar sample.

Species	Average non-LTE Correction	
	RGB	AGB
Fe I	$+0.08 \pm 0.04$	$+0.08 \pm 0.03$
Fe II	< 0.01	< 0.01
O	-0.05 ± 0.01	-0.06 ± 0.01
Na	-0.06 ± 0.02	-0.06 ± 0.01
Mg	$+0.02 \pm 0.01$	$+0.02 \pm 0.01$
Al	-0.06 ± 0.03	-0.05 ± 0.05

TABLE 4.5: Stellar parameters, and derived chemical abundances for each star in NGC 6397. Abundance uncertainties reflect line-to-line scatter (1σ), and do not take atmospheric sensitivities into account (see Table 4.6, and text for discussion). The last two rows are the cluster average abundances with error on the mean, and standard deviation to indicate observed scatter. We adopt the Asplund et al. (2009) solar abundance values. See Appendix A, Table A.4 for complete table.

ID	Type	$T_{\rm eff}$ (K)	log g (cgs)	$v_{\rm t}$ (km/s)	[Fe I/H]	[Fe II/H]	[O/H]	[Na/H]	[Mg/H]	[Al/H]
56897	AGB	4978	1.80	1.64	-2.13 ± 0.06	-2.00 ± 0.02	-1.64 ± 0.01	-1.92 ± 0.01	-1.84 ± 0.04	-1.32 ± 0.03
60609	AGB	4905	1.70	1.67	-2.23 ± 0.07	-2.06 ± 0.01	-1.45 ± 0.04	-1.98 ± 0.01	-2.02 ± 0.01	-1.37 ± 0.01
70509	AGB	5017	1.88	1.61	-2.18 ± 0.06	-2.07 ± 0.04	-1.49 ± 0.04	-2.15 ± 0.01	-1.79 ± 0.05	-1.53 ± 0.04
70522	AGB	4739	1.42	1.76	-2.24 ± 0.05	-2.06 ± 0.03	-1.63 ± 0.02	-1.94 ± 0.04	-1.99 ± 0.08	-1.48 ± 0.06
73216	AGB	4968	1.80	1.64	-2.16 ± 0.05	-2.04 ± 0.00	-1.39 ± 0.06	-2.29 ± 0.04	-1.73 ± 0.05	-1.67 ± 0.03
⋮	⋮	⋮	⋮	⋮	⋮	⋮	⋮	⋮	⋮	⋮
Mean					-2.15 ± 0.01	-2.02 ± 0.00	-1.52 ± 0.02	-2.06 ± 0.02	-1.87 ± 0.01	-1.49 ± 0.02
σ					0.05	0.03	0.12	0.19	0.11	0.16

TABLE 4.6: Typical abundance uncertainties due to the (1σ) atmospheric sensitivities of a representative sub-sample of three RGB and two AGB stars in our NGC 6397 data set. Parameter variations (in parentheses) are the expected uncertainties in the respective parameters.

	$\Delta T_{\rm eff}$ ($\pm$50 K)	Δlog g ($\pm$0.1 dex)	$\Delta v_{\rm t}$ ($\pm$0.2 km/s)	**Total**
[Fe I/H]	$\pm$0.06	$\mp$0.01	$\mp$0.04	$\pm$**0.04**
[Fe II/H]	$\mp$0.01	$\pm$0.04	$\mp$0.01	$\pm$**0.04**
[O/H]	$\mp$0.06	$\pm$0.04	$\pm$0.00	$\pm$**0.07**
[Na/H]	$\pm$0.03	$\mp$0.01	$\pm$0.00	$\pm$**0.03**
[Mg/H]	$\pm$0.03	$\mp$0.00	$\pm$0.00	$\pm$**0.03**
[Al/H]	$\pm$0.03	$\pm$0.00	$\pm$0.00	$\pm$**0.03**

A comparison of our results was made with that of Lind et al. (2011b, L11) and Carretta et al. (2009b, C09), with which we had a total of 5 and 21 RGB stars in common, respectively. The results of the detailed comparison of all stellar parameters and abundances are presented in Table 4.8, which shows good agreement in all stellar parameters and slight to moderate offsets in abundance results (0.03 to 0.18 dex) between the studies. These offsets arise from different methods in analysis.

In the cases of assumed stellar mass, atmospheric model parameters, adopted non-LTE corrections, and adopted solar abundances, we were able to quantify the effects since the previous studies published their values for these inputs. These sources of uncertainty combine to total possible offsets of up to $+0.10$ dex in each abundance. Other sources of uncertainty which we could not quantify (because we do not have the relevant information from the related studies) – for example different line lists, EW measurements and instrumentation differences – most likely explain the remaining offsets. We note that the scatter around these offsets is typically considered a better indication of the agreement between abundance analysis studies, and is consistent with the uncertainties quoted in this work. We find very good agreement between our study and that of L11. A curiosity here is the lack of agreement on micro-turbulence values with C09. While we adopted photometric $v_{\rm t}$ (and therefore had a relatively small spread in values, ranging from 1.52 km/s to 1.71 km/s), C09 determined micro-turbulence spectroscopically and had a very large spread in $v_{\rm t}$ values (ranging from 0.11 km/s to 2.73 km/s in the overlapping sample). This may explain the increased offsets and scatter between C09 and our study.

The difference between our mean LTE [Fe I/H] and [Fe II/H] abundances[4] (from Table 4.5) across our sample is $<\delta$Fe$>= -0.14\pm0.01$ ($\sigma = 0.05$). This is 0.06 dex lower lower than value predicted by non-LTE theory (-0.08 ± 0.05 dex, see §4.3.2 and Fig 4.3). While this could indicate slight systematics in

[4] δFe = [Fe I/H] − [Fe II/H]

TABLE 4.7: Summary of typical abundance uncertainties (1σ) from each source identified in the text, and the total uncertainties (added in quadrature). The first column are the average line-to-line uncertainties of all stars, values in the second column are the total uncertainties from atmospheric sensitivities (Table 4.6), and the third column represents the typical uncertainties quoted in each non-LTE source (see §4.3.2 for citations). Note that individual Fe abundances were not corrected for non-LTE (see text for details).

Species	Line-to-Line	Atmospheric	non-LTE	**Total**
Fe I	±0.07	±0.04	-	$\pm$**0.08**
Fe II	±0.03	±0.04	-	$\pm$**0.05**
O	±0.03	±0.07	±0.05	$\pm$**0.09**
Na	±0.04	±0.03	±0.04	$\pm$**0.06**
Mg	±0.04	±0.03	±0.03	$\pm$**0.06**
Al	±0.04	±0.03	±0.06	$\pm$**0.08**

TABLE 4.8: The average differences in parameters and abundances between this work and that of Lind et al. (2011b, L11) and Carretta et al. (2009b, C09). Uncertainties are standard deviations, and indicate the scatter around the offsets. While significant offsets exist between our work and the works of L11 and C09, the scatter around the offsets are consistent with the uncertainties quoted in this work (see text for discussion).

Parameter	This study − L11	This study − C09
$\Delta T_{\rm eff}$	-4.3 ± 20.9	19.5 ± 29.9
$\Delta\log g$	0.08 ± 0.01	0.07 ± 0.02
$\Delta v_{\rm t}$	0.04 ± 0.03	0.21 ± 0.64
Δ[Fe I/H]	-0.08 ± 0.03	-0.13 ± 0.05
Δ[Fe II/H]	0.12 ± 0.03	0.05 ± 0.05
Δ[O/H]	0.06 ± 0.08	0.18 ± 0.14
Δ[Na/H]	-0.03 ± 0.06	-0.17 ± 0.14
Δ[Mg/H]	-0.09 ± 0.03	-
Δ[Al/H]	0.17 ± 0.12	-

either our $T_{\rm eff}$ estimates or the non-LTE corrections, the uncertainty range of our <δFe> value overlaps with that of the the non-LTE predicted δFe value, indicating broad agreement. Our Fe abundances are consistent with literature values (<[Fe/H]>$_{\rm L11}$ = -2.08 ± 0.02). Furthermore, the difference between the average RGB and AGB δFe values is less than 0.015 dex for NGC 6397, indicating that there are no significant offsets in δFe between the two giant branches, as has been disputed for NGC 6752 (Lapenna et al., 2016; Campbell et al., 2017). This is presented visually in Figure 4.3, where the overall homogeneity of Fe abundances can be seen, especially between the AGB and RGB.

Abundances of elements other than iron are presented in Figures 4.4, 4.5, and 4.6. NGC 6397 was shown by L11 to have both Na-O and Mg-Al anti-correlations, which we find on both the RGB and AGB, along with a Na-Al correlation (Fig 4.6). The abundance distributions of the two giant branches in NGC 6397 are remarkably similar – we find that $\mathscr{R}_{RGB} \simeq \mathscr{R}_{AGB} \simeq 60\%$ (compared with $\mathscr{R}_{RGB} \simeq 75\%$ in L11), indicating no SP2 AGB deficit, i.e.; $\mathscr{F} \simeq 0\%$. This is in agreement with current stellar evolutionary theory, which predicts that there should be no AGB-manqué stars in NGC 6397, due to a HB that only extends to $T_{\rm eff} \simeq 10,500$ K (Greggio and Renzini, 1990; Dorman et al., 1993; Lovisi et al., 2012).

Finally, in Figure 4.7, we present Gaussian kernel density estimations (KDEs) of our AGB and RGB samples. We also plot KDEs of the RGB samples from L11 and C09 for comparison. Constant corrections of -0.03 dex and -0.17 dex, respectively, were applied to the data of these studies based on the systematic [Na/H] offsets determined (Table 4.8). Figure 4.7 shows excellent agreement between the [Na/H] abundances of our current RGB and AGB samples, as well as between our RGB results and the RGB results of L11 and C09.

4.5 Discussion and conclusions

The primary goal of this study was to determine the proportion of SP2 stars in NGC 6397 that evolve through to the AGB phase. Since the work of Campbell et al. (2013), the nature of AGB stars in GCs has been debated in the literature, with eight high-resolution spectroscopic studies (Johnson et al., 2015; García-Hernández et al., 2015; Lapenna et al., 2015; MacLean et al., 2016; Lapenna et al., 2016; Wang et al., 2016; Marino et al., 2017; Wang et al., 2017) and five photometric studies (Monelli et al., 2013; Milone et al., 2015a; Milone et al., 2015b; Lardo et al., 2017; Gruyters et al., 2017) targeting the AGB directly, along with five theoretical studies seeking to explain the anomalous observations (Charbonnel et al., 2013; Cassisi et al., 2014; Charbonnel et al., 2014; Charbonnel and Chantereau, 2016).

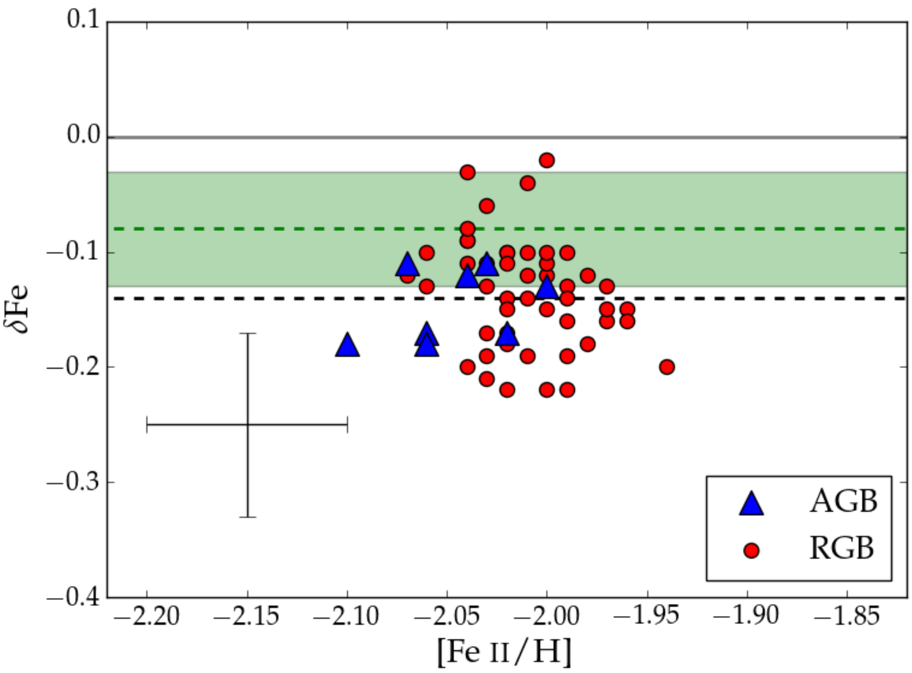

FIGURE 4.3: LTE Fe abundances for our NGC 6397 sample. Here, δFe ([Fe I/H] − [Fe II/H]) is plotted against [Fe II/H] abundance to highlight departures from LTE in Fe I, and the similarity between the Fe abundances of the AGB and RGB. The error bars indicate typical 1σ total uncertainties on individual abundances (see Table 4.7), while the black dashed line represents the sample average δFe value of -0.14 dex. The green dashed line represents the expected δFe value (-0.08 dex) from our non-LTE test (see §4.3.2) and the shaded region indicates the non-LTE uncertainties quoted in Amarsi et al. (2016a, $\pm$0.05 dex).

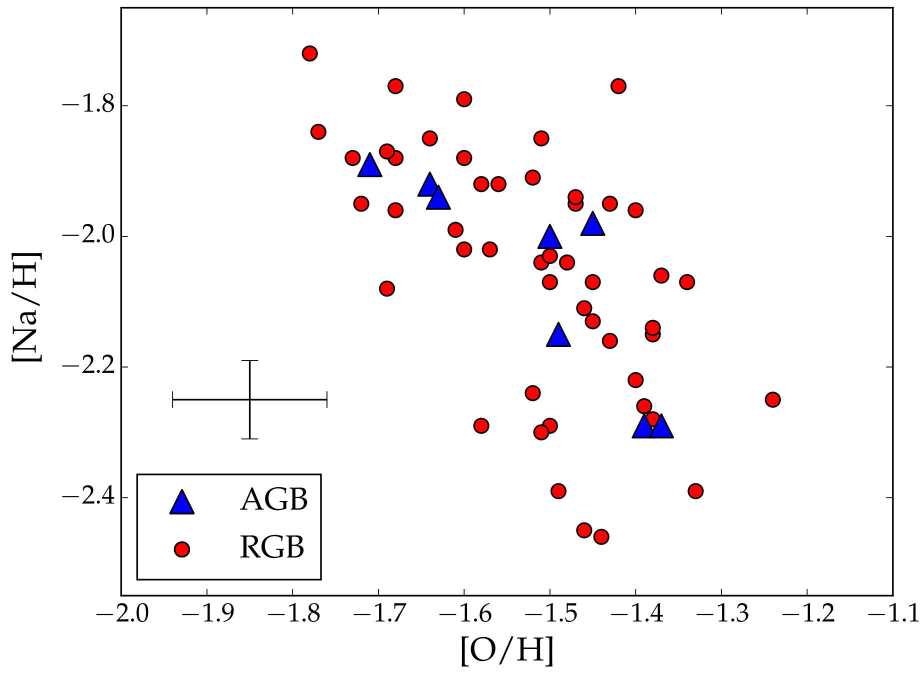

FIGURE 4.4: Na and O abundances for our NGC 6397 sample. The error bars indicate typical 1σ total uncertainties on individual abundances (see Table 4.7).

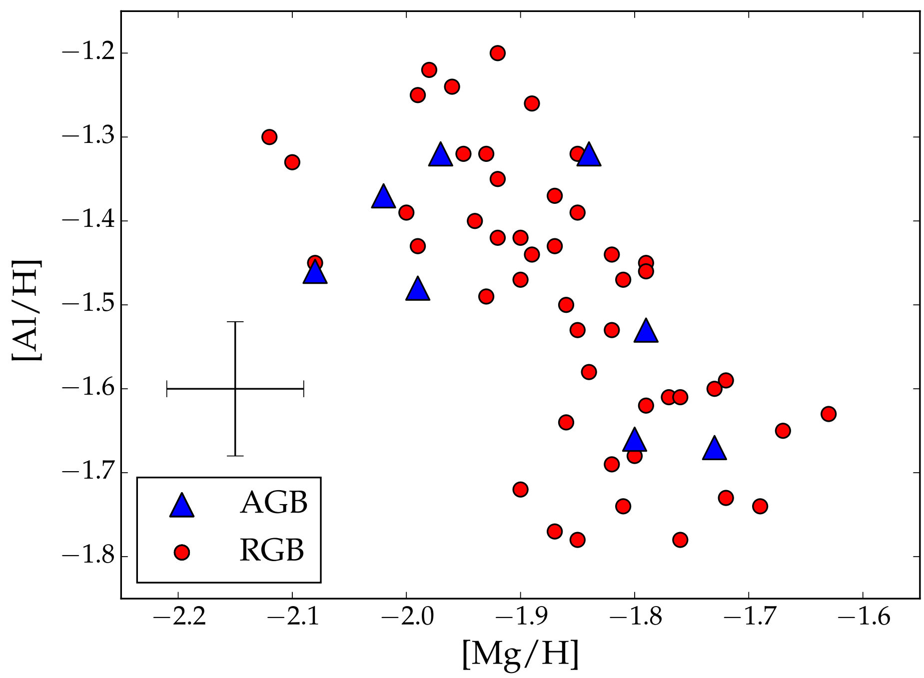

FIGURE 4.5: Same as Figure 4.4, but for Mg and Al.

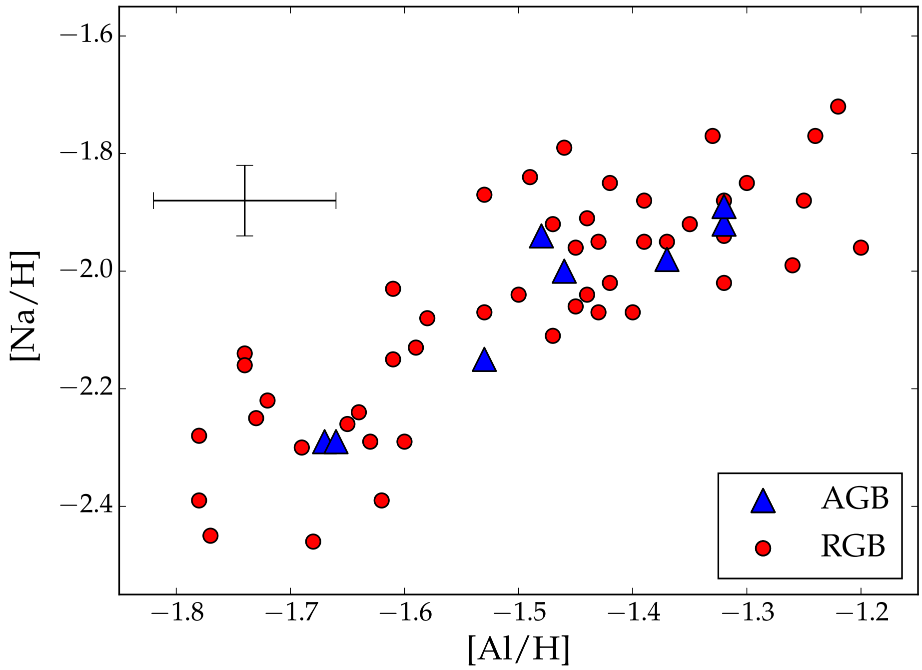

FIGURE 4.6: Same as Figure 4.4, but for Na and Al.

Since only HB stars with effective temperatures above ∼15,000 K are predicted to evolve directly to the white dwarf phase, the AGBs of clusters that lack an extended blue HB are expected to contain distributions in Na, O, Mg and Al abundances that are statistically indistinguishable from those of the RGB – all cluster stars should evolve through both giant branches (i.e., $\mathscr{F} \simeq 0\%$). Only in clusters with extended blue HBs should the distribution be different, and only with the ∼30 per cent most extreme (Na-rich/O-poor/Al-rich) AGB stars missing (i.e., $\mathscr{F} \simeq 30\%$ Dorman et al., 1993; Cassisi et al., 2014).

Despite a rapidly expanding literature sample of GC AGB studies, the picture is still far from clear. To date, eleven GCs have had their AGB systematically probed with high-resolution spectrographs[5], with mixed results in $\mathscr{F}$ values (see ML16, Table 4). However, only three clusters have been reported to have $\mathscr{F} \simeq 100\%$: NGC 6752 (Campbell et al., 2013, C17), M 62 (Lapenna et al., 2015) and M 4 (ML16). Of these, only M 62 has not been disputed by subsequent studies, but we note that this GC has not yet been studied a second time.

Lapenna et al. (2016) reported that the Fe I abundances of AGB stars in NGC 6752 are lower than predicted by standard non-LTE theory. If extrapolated to Na abundance, (i.e., if Na is assumed to follow this trend), the AGB [Na I/Fe I] abundance distribution moves to be in line with stellar

[5]NGC 2808, NGC 6397, NGC 6752, 47 Tucanae, M 2, M 3, M 4, M 5, M 13, M 55 & M 62

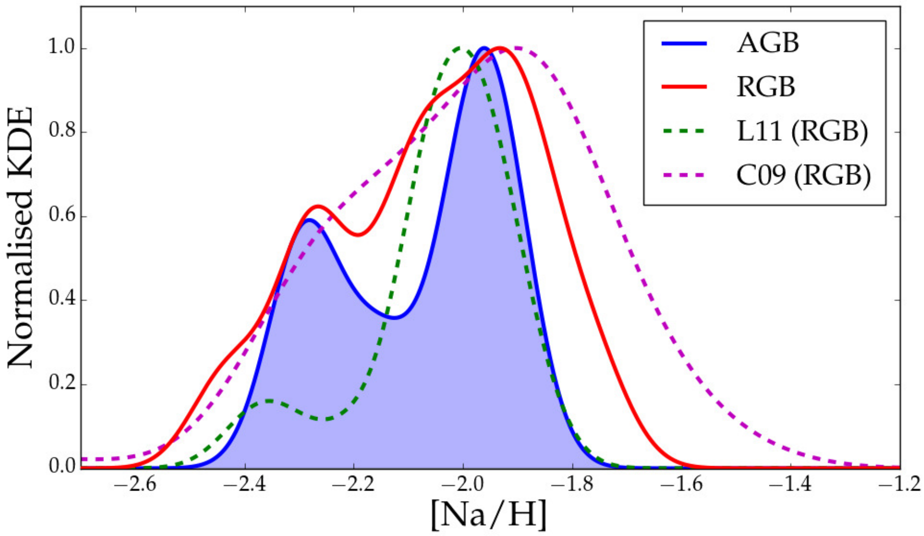

FIGURE 4.7: Gaussian kernel density estimations (KDEs) of our NGC 6397 [Na/H] abundances, along with those of Lind et al. (2011b, L11) and Carretta et al. (2009b, C09), with systematic offsets removed (see text for details). A smoothing bandwidth of 0.06 dex (total Na uncertainty, see Table 4.7) was applied to each of our RGB and AGB data sets, while for C09 we used a bandwidth of 0.11 dex, matching their total error calculations (see C09, Appendix A). L11 did not quote total abundance uncertainties, however their average measurement uncertainty in Na was the same as in our sample (0.04 dex), therefore we applied an identical bandwidth of 0.06 dex. The discrepancy between the relative heights of the two peaks in the L11 sample, compared to those of the other samples, may be due to the low number of stars observed in L11 (21 RGB stars).

theory ($\mathscr{F} \simeq 30\%$, as expected in GCs with an extended blue HB), contradicting the conclusions of Campbell et al. (2013) who claimed $\mathscr{F} \simeq 100\%$. However, in a detailed re-analysis of their data, C17 reported that there was no iron abundance discrepancy in NGC 6752 when more reliable $T_{\rm eff}$ scales were used, therefore concluding that the original Na results of Campbell et al. (2013) are reliable. Furthermore, for NGC 6397 we have found no significant δFe offset between the AGB and RGB, and that the Fe abundances are internally homogeneous (at the level of our uncertainties). This allows [X/H] abundances to be used for the elemental distribution analyses of the giant branches, because using [X/Fe] would introduce additional scatter (through measurement uncertainties), but no new information.

The abundances of NGC 6397 (Figs 4.4-4.7) contain no evidence of a SP2 AGB deficit, with the relative distributions of the RGB and AGB being identical in all abundance planes ($\mathscr{F} \simeq 0\%$).

It is interesting to compare this result with that of M 4 by ML16, since the methods and tools we have used are almost identical. The only difference between the NGC 6397 analysis performed in this study and that of ML16 is the method of determining atmospheric parameters. In ML16, $T_{\rm eff}$, log g and $v_{\rm t}$ values were determined spectroscopically by requiring excitation and ionisation balance (as per Sousa, 2014), whereas for NGC 6397 these parameters were estimated through photometric relations. As shown in C17, NaI abundances are quite robust, that is they are not as sensitive to systematic shifts in $T_{\rm eff}$ as FeI abundances. We have also shown that our Fe results are consistent with non-LTE theory, and show homogeneous abundances in both ionisation states, indicating that our $T_{\rm eff}$ scale is accurate. For these reasons, we consider that the different method of parameter determination between our two studies should have little consequence on the reliability of our [Na/H] abundances.

Thus our NGC 6397 result further strengthens the conclusions of ML16 whose analysis was almost identical, but whose results are in contradistinction. We therefore suggest that our original M 4 conclusions ($\mathscr{F} \simeq 100$, but with some uncertainty) are sound, and that our NGC 6397 results show – by providing a control sample – that our method of analysis does not artificially shift AGB abundances toward SP1-like distributions.

As stated in ML16, our M 4 result ($\mathscr{F} \simeq 100$) is in clear contradiction with stellar theory – we can think of no reason why SP2 stars in M 4 should avoid the AGB phase, since the maximum $T_{\rm eff}$ of its HB is ~9000 K (Marino et al., 2011). This is especially true in light of our result for NGC 6397 – which has a bluer HB than M 4, but $\mathscr{F} \simeq 0\%$. In the search for a possible explanation of our results, and those of Campbell et al. (2013) and Campbell et al. (2017, NGC 6752) and Lapenna et al. (2015, M 62), we consider three possible causes of the low-Na signature of AGB stars in M 4, NGC 6752 &

M 62:

(i) The low-Na signature is intrinsic – HB stars are becoming AGB-manqué stars at a much lower HB $T_{\rm eff}$ than predicted. This is the most commonly cited explanation in the literature.

(ii) The atmospheric models of some AGB stars are incorrectly determined, but only in particular sections of the GC AGB parameter space. This would result in incorrectly predicted absorption line profiles, and represent a significant 'blind spot' in the standard spectroscopic method.

(iii) All Na-rich stars in these three GCs are undergoing an unknown burning or mixing process, between the HB and AGB, that acts to deplete Na in the envelope and leave only a low-Na signature by the early AGB phase.

Investigating these hypotheses is beyond the scope of the present work. However, we note that (iii) is almost certainly impossible since there is no known mechanism that can destroy Na, while simultaneously creating O, in the interior conditions found in these stars.

More generally we note that, of the GCs which have been analysed for SP2 AGB deficits, not a single deficit (or lack thereof) claim has been confirmed by a different working group, or with independently selected targets. This suggests that the methods that are used require detailed investigation and checking, such as performed in C17. This is especially pertinent for M 4, for which the three existing studies all give different values of $\mathscr{F}$. We will aim to resolve this issue in a forthcoming study. Finally, we suggest another potential next step in investigating this problem could be a controlled spectroscopic study of an 'HB second parameter' pair or trio of clusters with similar metallicity and age, but different HB-morphology (such as NGC 288, NGC 362, and NGC 1851), in an attempt to disentangle the effect of global GC parameters on apparent AGB deficits.

Acknowledgements

Based in part on data acquired through the AAO, via program 15A/21 (PI Campbell). Part of this work was supported by the DAAD (PPP project 57219117) with funds from the German Federal Ministry of Education and Research (BMBF). BTM acknowledges the financial support of his Australian Postgraduate Award scholarship. SWC acknowledges federal funding from the Australian Research Council though the Future Fellowship grant entitled "Where are the Convective Boundaries in Stars?" (FT160100046). VD acknowledges support from the AAO distinguished visitor program 2016. LC gratefully acknowledges support from the Australian Research

Council (grants DP150100250, FT160100402). We thank Anish Amarsi and Thomas Nordlander for providing non-LTE corrections, and Michael Brown, Alexander Heger, and the referee for useful conversations, comments, and advice.

Chapter 5

On the AGB stars of M 4: A robust disagreement between spectroscopic observations and theory

Submitted to *MNRAS*, May 2018.

Abstract

Several recent spectroscopic investigations have presented conflicting results on the existence of Na-rich asymptotic giant branch (AGB) stars in the Galactic globular cluster M 4 (NGC 6121). The studies disagree on whether or not Na-rich red giant branch (RGB) stars evolve to the AGB. For a sample of previously published HERMES/AAT AGB and RGB stellar spectra we present a re-analysis of O, Na, and Fe abundances, and a new analysis of Mg and Al abundances; we also present CN band strengths for this sample, derived from low-resolution AAOmega spectra. Following a detailed literature comparison, we find that the AGB samples of all studies consistently show lower abundances of Na and Al, and are weaker in CN, than RGB stars in the cluster. This is similar to recent observations of AGB stars in NGC 6752 and M 62. In an attempt to explain this result, we present new theoretical stellar evolutionary models for M 4; however, these predict that all stars, including Na-rich RGB stars, evolve onto the AGB. We test the robustness of our abundance results using a variety of atmospheric models and spectroscopic methods; however, we do not find evidence that systematic modelling uncertainties can explain the apparent lack of Na-rich AGB stars in M 4. We conclude that an unexplained, but robust, discordance between observations and theory remains for the AGB stars in M 4.

5.1 Introduction

In early GC studies stars were observed at the same evolutionary stage but with different CN strengths, which cannot be explained only with evolutionary effects (e.g. Hesser et al., 1977; Norris et al., 1981). These and other findings led to the general consensus that Galactic GCs contain multiple populations of stars, identified by variations in light elemental abundances that are *intrinsic* – inherited at birth – to the stars. Variations are typically observed in the abundances of C, N, Na, and O, and sometimes Mg and Al (see the extensive reviews of Sneden 1999; Gratton et al. 2012 and references therein; but see Bastian et al. 2013 for an opposing view). In this paper we designate those GC stars with halo-like abundances (CN-weak, Na poor) as subpopulation one (SP1), and all stars enriched in Na (or that present as CN-strong) as subpopulation two (SP2).

Over the decades since the first spectroscopic studies of Galactic GCs, stars in each evolutionary phase have been targeted to evaluate the consistency of the light-elemental abundance distributions along the stellar evolutionary tracks. While systematic observations of the asymptotic giant branch (AGB, the final phase of nuclear burning) have only been performed relatively recently, AGB stars had previously been included among the GC stellar samples of last century. The literature reviews of Sneden et al. (2000) and Campbell et al. (2006) noted that the distribution of CN band strengths of AGB stars in certain globular clusters are very different to those seen in RGB stars – most strikingly that the AGB stars of NGC 6752 are exclusively CN-weak. This is in contradiction to the theoretical prediction that the N abundance of a star, which is traced by the CN band strength, should *increase* as a result of 'deep mixing' on the RGB (Langer et al., 1985; Henkel et al., 2017).

Seeking a more reliable diagnostic tool, Campbell et al. (2013) measured Na abundances for a sample of 20 AGB and 24 RGB stars in NGC 6752. Just as in the earlier low-resolution CN studies of the cluster, they found homogeneity in their entire sample of AGB stars: the [Na/Fe] values were all within ± 0.1 dex and very low ([Na/Fe] $\lesssim 0.12$ dex). This contrasted greatly with their RGB sample for which a variation in [Na/Fe] of ~ 0.9 dex was reported. While this result was challenged observationally (Lapenna et al., 2016), a detailed reanalysis by Campbell et al. (2017, hereafter C13) supported the original conclusion: that up to 100% of the Na enhanced stars (SP2; which represent 70% of the total RGB population) in NGC 6752 appear to be avoiding the AGB entirely.

It is generally agreed that stars enriched in N and Na are also enriched in He (Dupree et al., 2011; Nardiello et al., 2015). Stars with a He-enhancement evolve faster and thus have lower initial masses than stars of the same age but normal helium. Assuming these stars experience the same amount of mass loss on the RGB, they will retain less envelope on the horizontal branch (HB) and appear bluer (Sweigart, 1997; Catelan, 2009).

The results of Campbell et al. (2013), and subsequently Lapenna et al. (2015) who found the AGB of M 62 to be similarly SP1 dominated, conflict with the prediction of stellar evolutionary theory that only HB stars with extremely thin envelopes avoid the AGB, becoming AGB-manqué stars (Renzini and Buzzoni, 1986; Greggio and Renzini, 1990). At the metallicities of GCs this only occurs in stellar models with effective temperatures ($T_{\rm eff}$) higher than $\sim 15,000$ K (Dorman et al., 1993), corresponding to ∼30% of the most helium enhanced stars in NGC 6752 and M 62. Efforts to explain these observations have not been able to reproduce the results – see for example Cassisi et al. (2014), who could not reproduce the NGC 6752 observations using population synthesis (also see Campbell et al., 2013; Chantereau et al., 2016).

Adding to the debate on this topic, MacLean et al. (2016, hereafter ML16) reported O, Na, and Fe abundances for a sample of 15 AGB and 106 RGB stars in M 4 (NGC 6121), which contains no HB stars predicted to become AGB-manqué stars – M 4's HB extends only to ~ 9000 K in $T_{\rm eff}$. Surprisingly, all 15 AGB stars were found to have SP1-like O and Na abundances despite a significantly larger spread in the RGB abundances. This is the third such finding (after NGC 6752 and M 62) of a paucity of SP2 AGB stars in a globular cluster; but the first for a GC without an extended blue HB. While AGB stars have been included within stellar samples of spectroscopic M 4 studies in the past (Norris 1981; Suntzeff and Smith 1991; Ivans et al. 1999; and the literature reviews of Sneden et al. 2000; Smith and Briley 2005), ML16 was the first study that specifically targeted the AGB to investigate stellar evolution using the multiple population phenomenon of M 4.

Due to the controversial nature of the discovery of ML16, and uncertainties regarding the separation of the subpopulations in [Na/O] space, caveats to the conclusions arising from the study were noted. M 4 is a moderately metal-poor ([Fe/H] $= -1.16$; Harris, 1996) cluster that displays a distinctly bimodal HB (Marino et al., 2011) and a well established Na-O anti-correlation on the RGB and HB. While M 4 does not exhibit a Mg-Al anti-correlation (Mg has been observed to be homogeneous in M 4), Al correlates with Na (Marino et al., 2008).

The conclusions of ML16 motivated the publication of three additional studies (to date) of AGB stars in M 4 by three separate research groups. Using the photometric index C_{UBI} (which has been shown to correlate with light-elemental abundances in RGB stars; Monelli et al., 2013), Lardo et al. (2017) determined the spread in C_{UBI} values to be quantitatively similar between the AGB and RGB in M 4, in contradiction to the spectroscopic findings of ML16. Using high-resolution spectra, Marino et al. (2017, hereafter Mar17) came to the same conclusion as Lardo et al. (2017) by showing that a sample of 17 AGB stars had a similar range in [Na/Fe] values as the RGB sample from Marino et al. (2008, hereafter Mar08). However, with similar data, Wang et al. (2017, hereafter W17) found that M 4 AGB stars have lower [Na/H] values than stars on the RGB, and that the most Na-rich stars did appear to be missing from the AGB, but not to the extreme degree that ML16 had concluded. Thus a significant uncertainty exists within the literature with regard to the nature of M 4's AGB population.

The mixed and contradictory results of recent studies into the light-elemental abundances of M 4's AGB population call for a detailed, quantitative reinvestigation of the available data in order to idenitify why the results differ. In this paper we adopt the $\mathscr{F}$ parametrisation of SP2 AGB deficits[1] that was used in ML16 and MacLean et al. (2018a, hereafter ML18a).

This paper is structured as follows. In Section 5.2 we re-analyse our previously published sample of high-resolution M 4 stellar spectra in order to test the robustness of our earlier study on M 4 (ML16). In Section 5.3 we calculate CN band strengths from previously unpublished low-resolution spectra of M 4 stars. In an attempt to resolve the conflicting conclusions in recent (and historical) spectroscopic studies, we compare our abundance and CN results with M 4 AGB and RGB data from the literature in Section 5.4. In Section 5.5 we use 1D stellar evolution models to establish a precise, quantitative theoretical expectation of the abundance distribution of the AGB of M 4. In Section 5.6 we investigate possible explanations for the AGB results found in this study (and throughout the literature) including a series of tests utilising a range of stellar atmospheric models. Finally, we summarise our results and conclusions in Section 5.7.

5.2 High-resolution spectra re-analysis

In order to be confident in our earlier results, which have been challenged in the literature, we re-analysed our sample of M 4 stellar spectra upon which our ML16 results were based. The motivation behind this re-analysis was to i) check the ML16 results in light of recent debate on stellar parameter determination for AGB stars in GCs (see Lapenna et al., 2016; Campbell et al., 2017), and ii) increase the number of elements available for use as a diagnostic of multiple populations. Specifically, we redetermined the stellar parameters ($T_{\rm eff}$, v_t, log g, and [Fe/H]) and abundances (Na and O) that

[1] $\mathscr{F} = (1 - \frac{\mathscr{R}_{\rm AGB}}{\mathscr{R}_{\rm RGB}})\cdot 100\%$, where the percentages of RGB and AGB stars in a GC that are found to be members of SP2 are written as $\mathscr{R}_{RGB}$ and $\mathscr{R}_{AGB}$. For example, Campbell et al. (2013) reported $\mathscr{R}_{RGB} = 70\%$ and $\mathscr{R}_{AGB} = 0\%$ for NGC 6752.

were published in ML16. We also determined abundances of Mg and Al for our full sample of 15 AGB and 106 RGB stars.

5.2.1 Targets and data

The reduced M 4 high-resolution spectra and photometry used in this study are the same as those used in ML16. M 4 suffers from significant differential reddening, however constant reddening values were used in ML16. Here we improve upon this, with each star corrected using the reddening map of Hendricks et al. (2012). Individual corrections are included in Table 5.1. We found an average reddening value of $E(B-V)=0.37$ and a 1σ star-to-star scatter of ± 0.02. This differential reddening map, however, does not cover our entire sample, and some stars were only adjusted according to the average reddening value.

The M 4 targets included in this study are presented in Figure 5.1. In total, 24 AGB stars were identified in the photometry of Momany et al. (2003). Seven of these were not observable due to 2dF fibre positioning restrictions, and two were found in ML16 to be non-members, leaving a final sample of 15. Due to the randomness of stellar astrometry within a GC, we did not identify any sources of selection bias.

TABLE 5.1: M 4 target details including data from Momany et al. (2003, $UBVI$ photometry and target IDs) and 2MASS (Skrutskie et al., 2006, JHK photometry), and differential reddening corrections. Gaps in 2MASS data represent targets with low quality flags. Stars for which no reddening value is listed were outside the reddening map of Hendricks et al. (2012), and were corrected according to the average reddening value of $\mathrm{E}(B-V) = 0.37$. See Appendix A, Table A.5 for complete table.

ID	Type	2MASS ID	V	B	U	I	J	H	K	$\mathrm{E}(B-V)$
788	AGB	16235772-2622557	12.21	13.43	14.14	10.69	9.64	9.00	8.82	-
3590	AGB	16232184-2630495	12.48	13.64	14.37	10.92	-	-	-	0.36
10092	AGB	16233067-2629390	12.61	13.74	14.39	11.09	-	-	-	0.36
11285	AGB	16233195-2631457	12.84	13.90	14.42	11.40	10.35	9.77	9.58	0.37
13609	AGB	16233477-2631349	12.76	13.81	14.25	11.31	10.21	9.65	9.48	-
⋮	⋮	⋮	⋮	⋮	⋮	⋮	⋮	⋮	⋮	⋮

5.2.2 Atmospheric parameters

For the determination of surface gravity (log g), we did not adopt the standard spectroscopic approach, wherein ionisation balance between abundances determined from neutral and singly-ionised Fe lines is enforced. This is because such an approach can be biased by not accounting for non-LTE effects on Fe I lines (Ivans et al., 1999; Lapenna et al., 2016; Sitnova et al., 2015). Therefore, we instead calculated log g using estimates of T_{eff}, luminosity and mass. The luminosity was computed from de-reddened V magnitudes, with bolometric corrections from Alonso et al. (1999). We assumed a mass of 0.8 $M_{\odot}$ and 0.7 $M_{\odot}$ for the RGB and AGB, respectively (Miglio et al., 2016).

We investigated different approaches to determining the effective temperatures (T_{eff}) of our stars. T_{eff} determinations can be subject to significant uncertainties, both random and systematic. Incorrect modelling assumptions, and degeneracies in the stellar spectra with respect to different stellar parameters, can lead the standard spectroscopic method (requiring a balance of line-by-line Fe I abundances over a range of excitation potentials) to give unreliable and/or significantly offset T_{eff} values. Similarly, the photometric method (utilising empirical relations between T_{eff} and photometric magnitudes) can potentially produce large uncertainties (up to ± 200 K); for example, see Campbell et al. (2017, C17) for a detailed investigation of T_{eff} determination using the photometric method, and its effect on Fe and Na abundances determined for AGB and RGB stars.

Due to i) the high level of differential reddening in M 4 (and the fact that our sample is not fully covered by the reddening map of Hendricks et al., 2012), and ii) the debate within the literature as to appropriate selections of colour-T_{eff} empirical relationships (see C17), we endeavoured to further improve the spectroscopic T_{eff} determination from our spectroscopic code PHOBOS. Version one of this code (PHOBOS V1) was used in ML16 to determine parameters spectroscopically, but it was dependent on having accurate initial photometric estimates of T_{eff}. In C17 we noted that spectroscopic codes and methods appear to give effective temperatures that inherit some of the biases/trends in colour-T_{eff} relations (see §4 in C17). We investigated this problem in PHOBOS V1 and found that, in our case, this bias was due to the choice of the numerical scheme employed to iterate to a solution.

In principle, the choice of photometric estimate should have no bearing on the spectroscopic parameters that the code determines – that is, the spectroscopic parameters should only be a function of the Fe absorption line-list, and not the initial photometric estimates. We have improved the numerical scheme in PHOBOS V2 to search for global minima in the stellar parameter space, so that the initial T_{eff} estimates only require an accuracy of ~ 1000 K, and so that the code is 'agnostic' about the initial T_{eff} estimate.

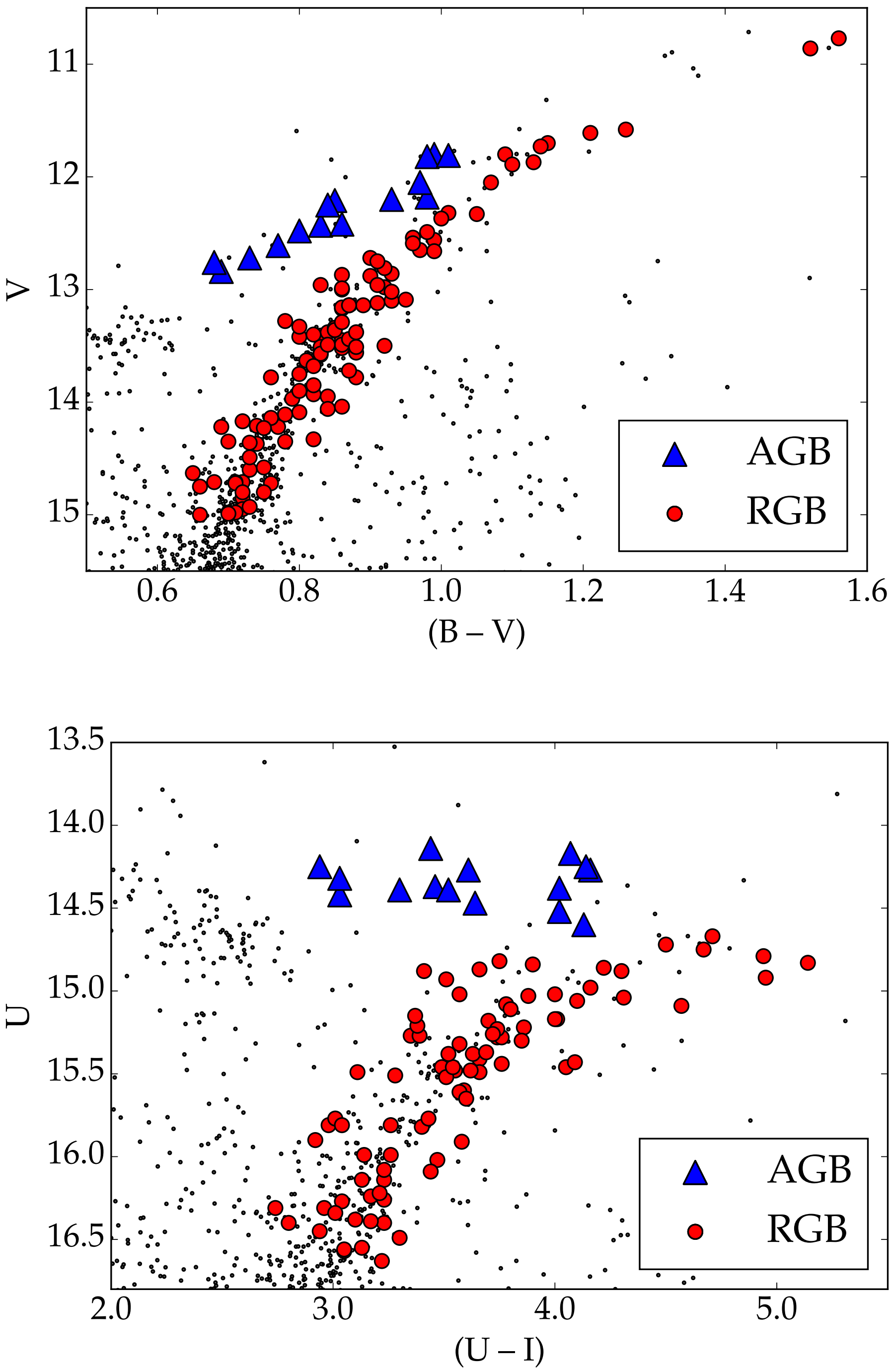

FIGURE 5.1: V - $(B - V)$ and U - $(U - I)$ colour-magnitude diagrams of M 4 RGB and AGB target stars, displayed over the full photometric sample of Momany et al. (2003, black points). In the top panel, targets have been corrected for extinction according to the differential reddening map of Hendricks et al. (2012), and a constant value of $(B - V) = 0.37$ was applied to the non-target photometric data. No reddening correction has been applied to the $(U - I)$ photometry in the bottom panel.

PHOBOS V2 determines $T_{\rm eff}$ by requiring no trend between the excitation potential of Fe I absorption lines and the abundances calculated from those lines. Initial microturbulence (v_t) estimates were determined using the empirical relation from Gratton et al. (1996), while final spectroscopic values are required to have no trend between the reduced wavelength of Fe I lines and their associated line-by-line abundances.

To test the efficacy of our improved code (PHOBOS V2), we conducted two tests, using our entire M 4 sample of 121 giant stars, to determine spectroscopic parameters primarily based on two very different sets of photometrically estimated initial-guess $T_{\rm eff}$ values. The first set of initial guesses ($T_{\rm eff,ph}$) are an average of six predictions from the empirical $B - V$ and $V - K$ relations of Ramírez and Meléndez (2005), González Hernández and Bonifacio (2009), and Casagrande et al. (2010), and one direct calculation by implementing the infrared flux method (IRFM) at an estimated log g of each star using BVI and 2MASS JHK photometry (Casagrande et al., 2014). For stars that were flagged for low quality and/or contamination in the 2MASS database, only the $B - V$ relations were used to determine $T_{\rm eff,ph}$, while for all other stars, the mean of the seven estimates was adopted as $T_{\rm eff,ph}$. These methods are mildly dependent on metallicity, for which a value of [Fe/H] $= -1.10$ was assumed (a change in adopted metallicity of 0.1 dex alters $T_{\rm eff,ph}$ values by ~ 10 K). Table 5.2 summarises the average difference between the adopted $T_{\rm eff,ph}$ values and those of the individual photometric relations and IRFM – the systematic differences between the relations highlight that individual photometric relations are often poor choices for determining stellar parameters. Individual $T_{\rm eff,ph}$ values are listed in Table 5.3. For the second, and extreme, test of PHOBOS V2, the initial $T_{\rm eff}$ guesses of every star (regardless of evolutionary phase) were assumed to be identical: $T_{\rm eff} = 4500$ K, log g = 2.5, and v_t = 1.5 – broadly representative of a giant GC star. We designate this second set of initial guesses as $T_{\rm eff,4500}$.

We used PHOBOS V2 to determine spectroscopic parameters twice, once using the parameter set $T_{\rm eff,ph}$, and again using the $T_{\rm eff,4500}$ set of parameters for the initial guess. As seen in Figure 5.2, the differences between the spectroscopically determined effective temperature values using the two different initial estimates ($T_{\rm eff,sp,ph}$ and $T_{\rm eff,sp,4500)}$) are extremely small, with $\Delta T_{\rm eff} = 0 \pm 2$ K, while the the average difference between the photometric ($T_{\rm eff,ph}$) and spectroscopic ($T_{\rm eff,sp}$) values is $\Delta T_{\rm eff} = 12 \pm 76$ K. This indicates that no information from the photometric $T_{\rm eff}$ estimates is retained within the spectroscopic results. This is beneficial because the final stellar parameters are independent of the choice of colour-$T_{\rm eff}$ relation, and are therefore reproducible and consistent.

In summary, we adopt the spectroscopic parameters included in Table 5.3 and presented in Figure 5.3. The subsequent elemental abundance

TABLE 5.2: Average differences between the average $T_{\mathrm{eff,ph}}$ values and each photometric estimate ($T_{\mathrm{eff,ph}} - T_{\mathrm{eff,estimate}}$) for our first PHOBOS test. Uncertainties are the standard deviations of the stellar sample, with the quoted uncertainty of each relation in brackets (except for IRFM, which is the average IRFM uncertainty of our sample).

Method	ΔT_{eff} (K)
Ram $(B-V)^1$	0 ± 71 (51)
Gonz $(B-V)^2$	-49 ± 70 (57)
Casa $(B-V)^3$	-74 ± 89 (73)
Ram $(V-K)$	132 ± 52 (28)
Gonz $(V-K)$	24 ± 48 (23)
Casa $(V-K)$	-2 ± 54 (25)
IRFM^3	-5 ± 62 (33)
Average σ	64

[1]Ramírez and Meléndez, 2005

[2]González Hernández and Bonifacio (2009)

[3]Casagrande et al. (2010)

determinations were based on these stellar parameters. PHOBOS V2 now also calculates star-to-star T_{eff} and v_t uncertainties based on the standard error of the slope between excitation potential and reduced wavelength, and line-to-line Fe I abundances. These uncertainties are included in Table 5.3. The typical 1σ T_{eff} and v_t uncertainties of our sample are 65 K and 0.1 km/s, respectively, and we adopt a 1σ log g uncertainty of 0.2 dex.

5.2.3 Chemical abundance determination

With our improved stellar parameters, we adopted the method of ML18a for the determination of chemical abundances. This is mostly the same as the method previously used for this sample (ML16), but with an updated line list (that includes Mg and Al) and non-LTE corrections from more recent sources where available. In brief, the equivalent width (EW) method was used in combination with the ARES (Sousa et al., 2015, v2), IRAF *onedspec*, and MOOG (Sneden, 1973, June 2014 release) packages, with α-enhanced (+0.4 dex) 1D model atmospheres interpolated from the Castelli and Kurucz (2004) grid. Although the M 4 spectral data is unchanged from ML16, for consistency all Na I and O I EWs were remeasured (with little change), while Mg I, and Al I EWs are new, since these abundances were not determined in ML16.

All absorption lines measured are known to suffer from non-LTE effects (Bergemann and Nordlander, 2014). Abundances of O, Na, and Al were corrected for these non-LTE effects by interpolation of the grids from Amarsi et al. (2016b, O), Lind et al. (2011a, Na), and Nordlander and Lind (2017, Al). Mg was not corrected for non-LTE because it is known (and confirmed

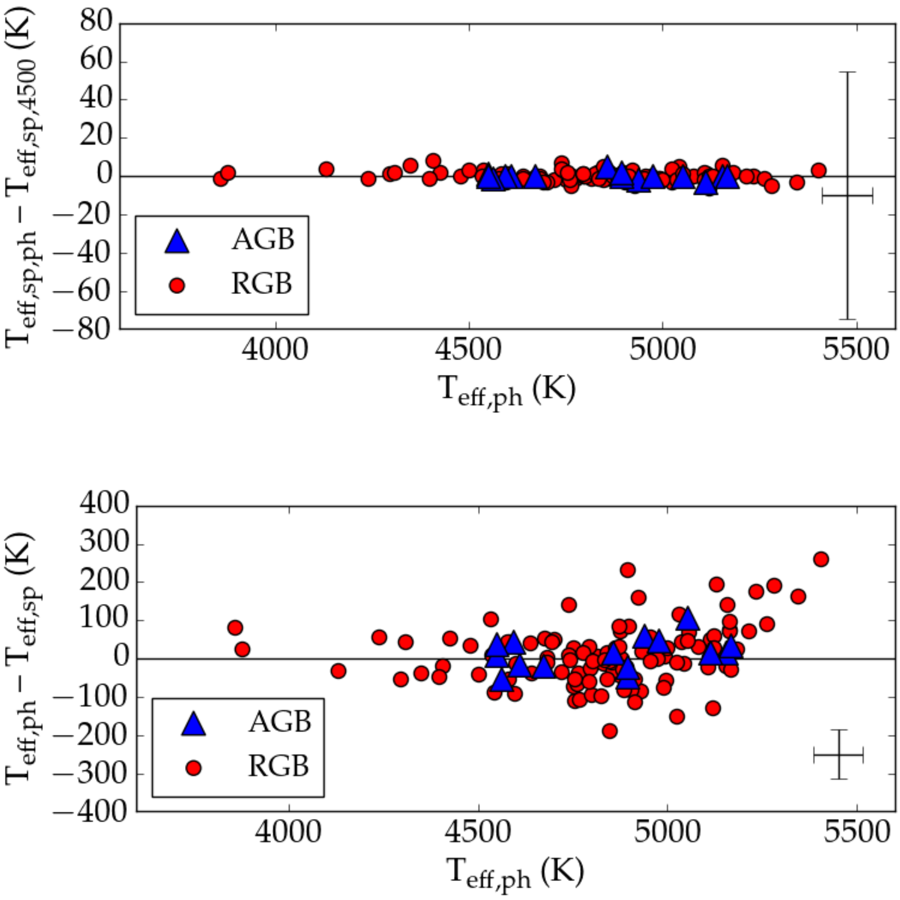

FIGURE 5.2: **Top panel:** The star-to-star differences between the spectroscopic $T_{eff,sp}$ values determined (using PHOBOS V2) based on initial estimates from i) photometrically estimated stellar parameters ($T_{eff,ph}$), and ii) a single T_{eff} of 4500 K ($T_{eff,4500}$). The average difference between the spectroscopic values of the two tests is $\Delta T_{\rm eff} = 0 \pm 2$ K. **Bottom panel:** The star-to-star differences between our photometrically estimated $T_{eff,ph}$ values and final adopted spectroscopic $T_{eff,sp}$ values. Error bars in both panels are our typical $T_{eff,sp}$ uncertainties – ~ 65 K, as determined by PHOBOS V2 (see text for more detail).

TABLE 5.3: Stellar parameters for each star in our M4 sample. Spectroscopic effective temperatures ($T_{eff,sp}$), microturbulence values (v_t), and uncertainties were determined using PHOBOS V2, while log g values were calculated based on the empirical relation from Alonso et al. (1999). These were adopted as our final parameters. $T_{eff,ph}$ values are the effective temperatures estimated from photometric colour-T_{eff} relations, were used in the PHOBOS test, and are included for comparison (also see Figure 5.2). See Appendix A, Table A.6 for complete table.

Star ID	Evolutionary phase	$T_{eff,sp}$ (K)	log g (cgs)	v_t (km/s)	$T_{eff,ph}$ (K)
788	AGB	4877 ± 52	1.71	1.56 ± 0.07	4937
3590	AGB	4929 ± 36	1.84	1.68 ± 0.06	4975
10092	AGB	4944 ± 29	1.90	1.45 ± 0.04	5051
11285	AGB	5137 ± 69	2.08	1.73 ± 0.19	5154
13609	AGB	5131 ± 67	2.05	1.21 ± 0.10	5166
⋮	⋮	⋮	⋮	⋮	⋮

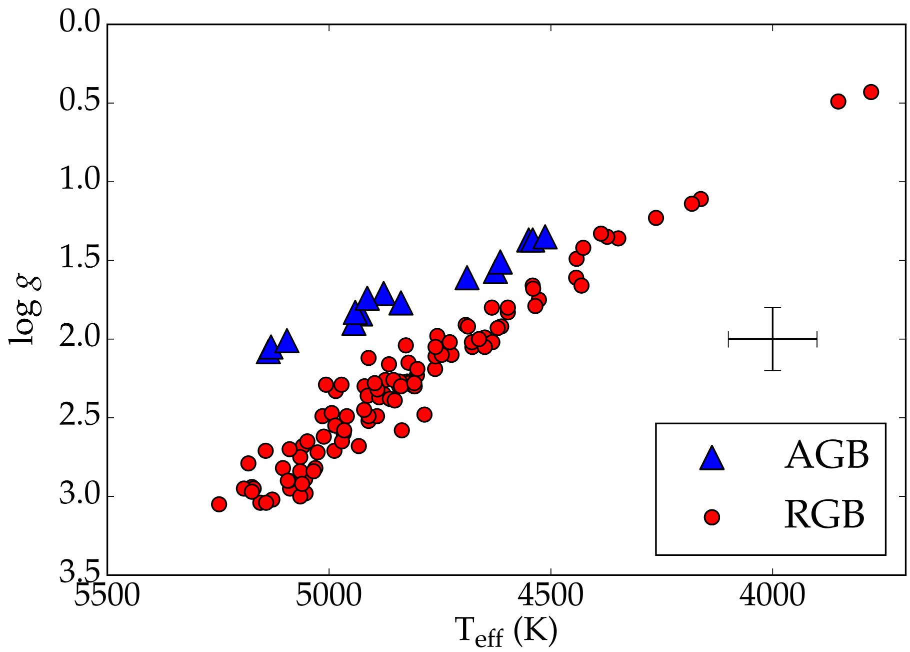

FIGURE 5.3: Final T_{eff} and log g values of our M4 stellar sample, determined spectroscopically using PHOBOS V2. Typical uncertainties are indicated (see Table 5.6).

TABLE 5.4: Summary of average non-LTE corrections for each chemical species.

Species	Average non-LTE Correction AGB	RGB
Fe I	$+0.00 \pm 0.03$	-0.01 ± 0.07
Fe II	-0.01 ± 0.00	-0.01 ± 0.01
O I	-0.16 ± 0.04	-0.10 ± 0.02
Na I	-0.11 ± 0.03	-0.14 ± 0.03
Al I	-0.13 ± 0.03	-0.10 ± 0.03

in this study) to be homogeneous in M 4. More detail of this method, and our adopted line list, can be found in ML18a.

As in ML18a, we were unable to correct our derived Fe abundances for non-LTE effects on a line-by-line basis due to the large number of Fe I lines in the stellar spectrum. We have therefore performed a test on a representative subset of three RGB and three AGB stars from M 4, using corrections interpolated from the Amarsi et al. (2016a) grid for five Fe I lines[2] and two Fe II lines[3]. For our sample of M 4 stars the non-LTE effects on Fe I and Fe II are negligible considering our uncertainty in individual abundances (discussed in §5.2.4), thus we do not apply them to our final abundances. The O, Na, Al non-LTE corrections for our sample are largely systematic with minimal star-to-star scatter. However, the average corrections for the three species are slightly different ($\Delta_{\rm corr} \sim 0.03$ to 0.06) for the AGB and RGB. We summarise the results of our Fe non-LTE test along with the non-LTE corrections of Na and Al abundances in Table 5.4.

5.2.4 Abundance results

Chemical abundances using the new stellar parameters from this study are presented in Table 5.5. Individual uncertainties cited in these tables are based only on the line-to-line scatter of each abundance. Using the 1σ uncertainties of each stellar parameter (± 65 K in $T_{\rm eff}$, ± 0.2 in log g, ± 0.1 km/s in v_t), an atmospheric sensitivity analysis was performed on a representative sub-sample and the results are summarised in Table 5.6. The uncertainty in abundances due to atmospheric uncertainties is $\leq \pm 0.05$ for all species, except for Fe II and O I which are ± 0.10 and ± 0.13, respectively.

The use of elemental ratios with respect to Fe can be problematic, especially in globular clusters that are homogeneous in Fe abundance at the level of uncertainty in the relevant studies (i.e. when not using differential analysis methods such as in Yong et al., 2013). In these cases, dividing

[2] 4788.8Å, 4839.5Å, 5701.6Å, 5753.1Å and 7748.3Å

[3] 6516.1Å and 7711.7Å

star-to-star elemental abundances by Fe abundance adds noise from the imperfect measurement of [Fe/H] and thereby degrades the signal in star-to-star abundance distributions (see C17 for a detailed analysis). Throughout this paper we present all abundances in the form $\log_\epsilon(\mathrm{X})$[4], which eliminates many systematic offsets that may exist in [X/Fe] and [X/H] ratios – for example adopted solar abundances, and the sensitivity of Fe I to T_{eff}.

A detailed comparison to recent high-resolution spectroscopic studies of M 4 is not only warranted, but crucial for this cluster. We reserve this analysis and discussion for §5.4, except for a comparison with our previous results (ML16), which is presented in Table 5.8. The only change of note is in log g. In ML16 we assumed a mass of 0.8 $M_\odot$ for all stars, while here we assumed a mass of 0.7 $M_\odot$ for our AGB sample, which accounts for -0.10 dex of the -0.15 difference in log g values for the AGB stars. No other significant changes occurred in the re-analysis, with T_{eff}, $\log_\epsilon(\mathrm{Fe\,I})$, $\log_\epsilon(\mathrm{O})$, and $\log_\epsilon(\mathrm{Na})$ showing very little change. The scatter is indicative of our parameter uncertainties[5] and estimated total abundance errors (Table 5.7).

[4]$\log_\epsilon(\mathrm{X}) = \log_{10}(\mathrm{N_X}/\mathrm{N_H}) + 12.0$, where N_X represents the number density of atoms of element X.

[5]An exception is the scatter in v_t differences, which has little effect on elemental abundances – see Table 5.6.

TABLE 5.5: Chemical abundances for each star in our M 4 sample. Abundance uncertainties reflect line-to-line scatter (1σ), and do not take atmospheric sensitivities into account (see Table 5.6). The last four lines show the cluster average abundances (for the AGB and RGB) with standard error of the mean, and standard deviation to indicate observed scatter. O, Na, and Al abundances were corrected for non-LTE effects. See Appendix A, Table A.7 for complete table.

ID	Type	$\log_\epsilon$(Fe I)	$\log_\epsilon$(Fe II)	$\log_\epsilon$(O)	$\log_\epsilon$(Na)	$\log_\epsilon$(Mg)	$\log_\epsilon$(Al)
788	AGB	6.24 ± 0.08	6.24 ± 0.03	8.26 ± 0.05	4.93 ± 0.01	6.79 ± 0.03	5.56 ± 0.02
3590	AGB	6.27 ± 0.06	6.29 ± 0.04	8.07 ± 0.01	5.15 ± 0.03	6.73 ± 0.04	5.67 ± 0.03
10092	AGB	6.33 ± 0.04	6.35 ± 0.01	8.29 ± 0.06	4.95 ± 0.02	6.72 ± 0.03	5.53 ± 0.03
11285	AGB	6.32 ± 0.07	6.31 ± 0.04	8.10 ± 0.04	5.19 ± 0.02	6.80 ± 0.02	5.71 ± 0.06
13609	AGB	6.32 ± 0.09	6.38 ± 0.06	8.12 ± 0.04	5.02 ± 0.11	6.76 ± 0.05	5.57 ± 0.05
⋮	⋮	⋮	⋮	⋮	⋮	⋮	⋮
Mean	AGB	6.30 ± 0.01	6.31 ± 0.01	8.18 ± 0.02	5.11 ± 0.03	6.76 ± 0.01	5.62 ± 0.02
σ		0.03	0.04	0.09	0.12	0.03	0.08
Mean	RGB	6.33 ± 0.01	6.34 ± 0.01	8.10 ± 0.01	5.33 ± 0.02	6.78 ± 0.01	5.76 ± 0.01
σ		0.05	0.06	0.12	0.19	0.05	0.09

TABLE 5.6: Typical abundance uncertainties due to the (1σ) atmospheric sensitivities of a representative sub-sample of three RGB and two AGB stars in our M 4 data set. Parameter variations (in parentheses) are the adopted uncertainties in the respective parameters. Note the direction of signs.

	$\Delta T_{\rm eff}$ (± 65 K)	$\Delta \log g$ (± 0.2)	Δv_t (± 0.1)	**Total**
$\log_\epsilon(\rm Fe\,I)$	± 0.05	± 0.00	∓ 0.02	$\pm$**0.05**
$\log_\epsilon(\rm Fe\,II)$	∓ 0.05	± 0.09	∓ 0.02	$\pm$**0.10**
$\log_\epsilon(\rm O)$	∓ 0.10	± 0.08	∓ 0.01	$\pm$**0.13**
$\log_\epsilon(\rm Na)$	± 0.05	∓ 0.01	∓ 0.02	$\pm$**0.04**
$\log_\epsilon(\rm Mg)$	± 0.03	± 0.00	∓ 0.01	$\pm$**0.03**
$\log_\epsilon(\rm Al)$	± 0.04	± 0.00	± 0.00	$\pm$**0.04**

Abundances from Fe II lines were not published in ML16, but are included here as part of our re-analysis. In Figure 5.4 we plot $\log_\epsilon(\rm Fe\,I)$ against δFe (ionisation balance; δFe = $\log_\epsilon(\rm Fe\,I) - \log_\epsilon(\rm Fe\,II)$). Our non-LTE test (see §5.2.3) predicted a theoretical δFe value of 0.00 ± 0.07, while our observed sample has an average δFe of -0.01 ± 0.05. This high level of agreement is strong evidence that our PHOBOS V2 spectroscopic method is reliable, and that our stellar parameters are accurate.

As in ML16, M 4 shows a significant spread in Na abundance among RGB stars ($\sigma = \pm 0.19$ dex; see Figure 5.5). However, considering the uncertainty in O abundance we cannot resolve the Na-O anti-correlation that has been reported elsewhere (e.g. Marino et al., 2008). In fact, given the total uncertainty in our O abundances of ± 0.15 dex (Table 5.7) – compared to the O spread on the RGB of ± 0.12 dex (Table 5.5) – we cannot say that M 4 actually shows heterogeneity in O abundance, formally it appears to be homogeneous. This uncertainty in $\log_\epsilon(\rm O)$ comes from the large sensitivity of the 777nm triplet to $T_{\rm eff}$ and log g, and is typically smaller for other O lines that we could not observe with HERMES/AAT. Na, on the other hand, shows a significant star-to-star scatter in both the RGB, and (to a smaller degree; $\sigma = \pm 0.12$ dex) the AGB.

We find a correlation between Na and Al abundance, but no evidence of a Mg-Al anti-correlation (Figure 5.6), in agreement with previous results (e.g. Mar08). A clear outlier is the star AGB18573 which appears to have a low Na abundance but a high Al abundance. We have not been able to provide an explanation for this anomalous star, however, it was reported by Mar17 to be similarly Na-poor and Al-rich. We find Mg to be homogeneous in M 4 ($\sigma = \pm 0.05$ dex on the RGB), while Al is difficult to classify because the star-to-star scatter ($\sigma = \pm 0.09$ and ± 0.08 dex on the RGB and AGB, respectively) is similar to our total uncertainties in the abundance (± 0.08 dex). We note however, that for the AGB, the 1σ spread in Al abundance reduces to ± 0.06 dex when the Al-rich outlier AGB18573 is discounted, and can be

TABLE 5.7: Summary of typical abundance uncertainties (1σ) from each source identified in the text, and the total uncertainties (when added in quadrature). The first column are the average line-to-line uncertainties of all stars, values in the second column are the total uncertainties from atmospheric sensitivities (Table 5.6), and the third column represents the typical uncertainties in non-LTE corrections, as reported in the relevant sources (see §5.2.3). Note that individual Fe abundances were not corrected for non-LTE (see text for details).

Species	Line-to-Line	Atmospheric	non-LTE	**Total**
Fe I	±0.09	±0.05	-	$\pm$**0.10**
Fe II	±0.04	±0.10	-	$\pm$**0.11**
O	±0.05	±0.13	±0.05	$\pm$**0.15**
Na	±0.04	±0.04	±0.04	$\pm$**0.07**
Mg	±0.04	±0.03	-	$\pm$**0.05**
Al	±0.03	±0.04	±0.06	$\pm$**0.08**

TABLE 5.8: The average differences in parameters and abundances between this study and MacLean et al. (2016, ML16). Uncertainties are standard deviations, and indicate the scatter between the studies, if the offsets were removed. The significant change in log g values is discussed in the text. Note that abundances from Fe II lines were not published in ML16.

Parameter	This study $-$ ML16 (AGB)	(RGB)
ΔT_{eff}	-21 ± 44	-20 ± 57
$\Delta\log g$	-0.15 ± 0.12	-0.04 ± 0.10
Δv_t	$+0.12 \pm 0.18$	$+0.12 \pm 0.15$
$\Delta\log_\epsilon(\mathrm{Fe\,I})$	-0.02 ± 0.04	-0.02 ± 0.05
$\Delta\log_\epsilon(\mathrm{O})$	$+0.06 \pm 0.07$	$+0.04 \pm 0.09$
$\Delta\log_\epsilon(\mathrm{Na})$	-0.03 ± 0.06	$+0.00 \pm 0.06$

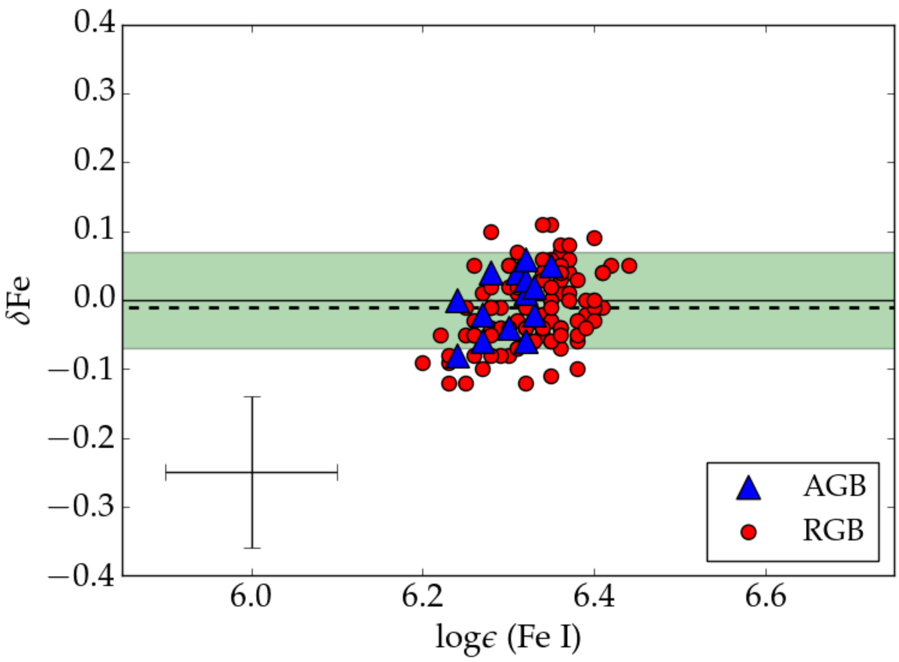

FIGURE 5.4: Fe abundances for this study. Here, ionisation difference (δFe = $\log_{\epsilon}$(Fe I) − $\log_{\epsilon}$(Fe II)) is plotted against $\log_{\epsilon}$(Fe I) abundance to highlight departures from LTE in Fe I, and the similarity between the Fe abundances of the AGB and RGB. The error bar indicates typical 1σ total uncertainties in individual abundances (i.e. the line-to-line uncertainties and the 1σ atmospheric sensitivity uncertainties added in quadrature), while the black dashed line represents the sample average δFe value of -0.01. The shaded green region indicates the non-LTE uncertainties quoted in Amarsi et al. (2016a, ±0.05 dex), around the expected δFe value ($+0.00$ dex, solid black line) from our non-LTE test (see §5.2.3).

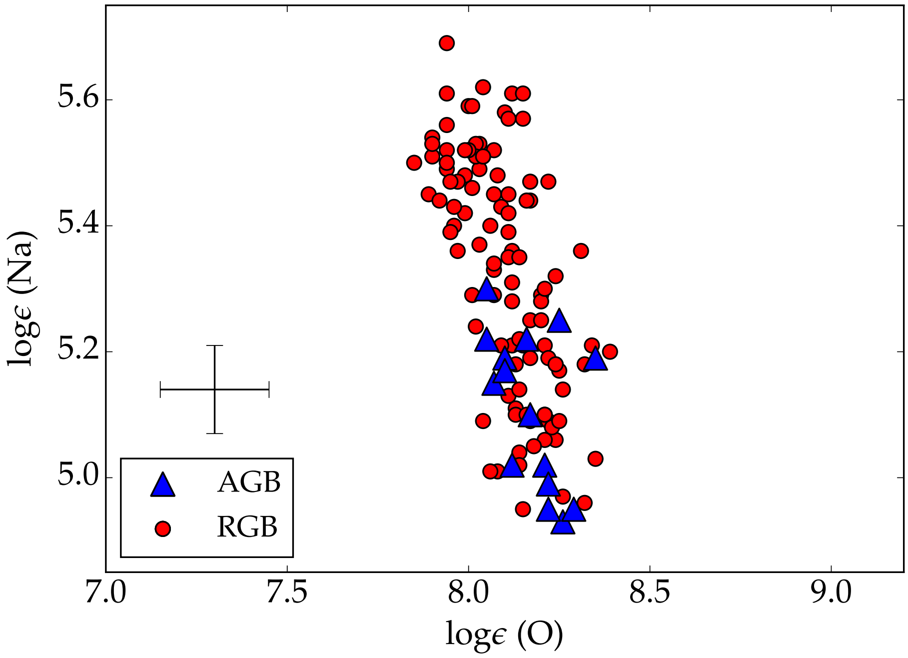

FIGURE 5.5: O and Na abundances for our M 4 sample. The error bar indicates typical 1σ total uncertainties in individual abundances (i.e. the line-to-line uncertainties and the 1σ atmospheric sensitivity uncertainties added in quadrature).

seen in Figure 5.6 to have a smaller spread than our RGB sample.

As in ML16, the average Na, O, and Al abundances of AGB stars in M 4 are clearly different to that of the RGB, being heavily weighted toward SP1-like abundances. Our Fe and Mg abundances are constant, and the average RGB and AGB abundances agree. These results are consistent with our claim in ML16 that M 4 may not contain SP2 AGB stars ($\mathscr{F} = 100\%$). Due to the spread in AGB Na abundances, and our abundance uncertainties, we conclude that $\mathscr{F} \gtrsim 65\%$ – i.e. less than 20% of AGB stars, or 3 out of 15, have SP2-like abundances. This compares with 55% on the RGB. This value is considerably higher than that expected from stellar evolutionary theory ($\mathscr{F} = 0\%$) for a cluster with a HB extending only to $T_{\rm eff} \simeq 9000$ K.

5.3 Cyanogen band strengths from low-resolution spectra

As a further observational check of the relative abundance distributions of M 4's AGB and RGB, we determined CN band-strengths for a sample of M 4 stars. The bimodality of CN band strengths in M 4 is well established (Norris, 1981; Ivans et al., 1999), and can be used to identify to which sub-population (SP1 or SP2) a star belongs because CN band strengths have

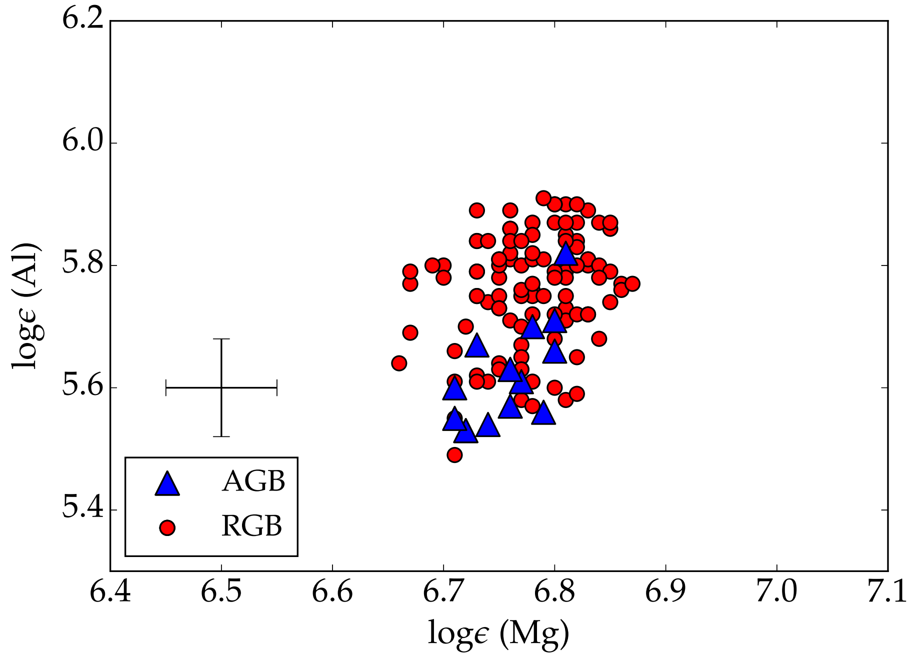

FIGURE 5.6: Same as Figure 5.5, but for Mg and Al abundances.

been shown to correlate with Na abundance[6] (Cottrell and Da Costa, 1981; Campbell et al., 2012; Smith, 2015).

In addition to our sample of high-resolution spectra, low-resolution spectra of M 4 stars were collected in September 2009 (Campbell et al., 2010) using the AAOmega/2dF multi-object spectrograph on the Anglo-Australian Telescope ($R \simeq 3000$; Lewis et al., 2002; Saunders et al., 2004; Sharp et al., 2006). We used the 1700B grating which gave a spectral coverage from 3755 Å to 4437 Å, while the signal-to-noise ratio for all targets was $\gtrsim 20$. The software package 2DFDR (AAO Software Team, 2015, v3.211) was used to reduce the data in preparation for analysis. This is new and unpublished data, and is included to provide an additional avenue for the investigation of M 4 abundance distributions. A total of 7 AGB and 19 RGB stars were observed with AAOmega; all but two of which (stars 25133 and 17999) were included in our HERMES target list.

To quantify the CN band strengths we use the S3839 CN index from Norris (1981) which compares a spectral segment where the CN molecule absorbs light with a neighbouring pseudo-continuum:

$$S3839 = -2.5 \log \frac{\int_{3846}^{3883} I_\lambda d\lambda}{\int_{3883}^{3916} I_\lambda d\lambda}. \tag{5.1}$$

[6]CN band strengths are primarily indicative of atmospheric N abundance, which correlates with Na

IRAF was used to measure the integrated fluxes of our low-resolution spectra. Target data, S3839 values, and δS3839 excess values are given in Table 5.9. CN band strengths are presented in Figure 5.7.

Even without adjusting for the trend with V band magnitude (called the baseline in Norris, 1981; Ivans et al., 1999), it can be seen that the RGB stars display a significant spread in S3839 values, and that our AGB sample are heavily weighted to low S3839 index values. The green fiducial line in Figure 5.7 was used to empirically correct for the trend between V band magnitude and S3839 value (δS3839 excess is the vertical distance of each star to the green fiducial), and as a reference we include the baseline used by Norris (1981) which is qualitatively similar.

We adopt the characteristic S3839 uncertainty of ± 0.02 from Campbell et al., 2012, which was based on the typical differences between S3839 measurements from two separate observations of the same star in the GC NGC 1851 (the spectra of which were obtained during the same observing program and with the same technical specifications as the M 4 spectra used in this study), and a typical δS3839 uncertainty of 0.08 dex due to assumptions in determining the trend with V band magnitude. We discuss our CN results further in the next section, in comparison with previous CN studies on M 4.

5.4 Literature comparison of AGB abundances

After determining reliable elemental abundances and CN band strengths, we compiled and compared spectroscopic results from the literature in order to investigate the conflicting conclusions regarding M 4's AGB abundances.

While ML16 was the first study that systematically targeted the AGB of M 4, AGB stars had been included previously in several spectroscopic studies of the cluster: Norris (1981), Suntzeff and Smith (1991), and Ivans et al. (1999, hereafter I99). CN band strengths and abundances from these three studies were compiled and merged into the data set of Smith and Briley (2005, hereafter SB05) who reported on six AGB stars (two of which they classified as CN-strong, one as CN-intermediate, and the remaining three as CN-weak). I99 reported that their AGB abundances show less evidence of H-burning than their RGB sample, and described their AGB results as "puzzling".

Soon after the publication of ML16, Lardo et al. (2017) disputed our conclusion by utilising the photometric index $C_{UBI} = (U - B) - (B - I)$, which has been used to separate the RGB (and the AGB more recently) subpopulations of GCs (e.g. Monelli et al., 2013; García-Hernández et al., 2015). They demonstrated that the spread in C_{UBI} for their sample of AGB stars is statistically similar to that of the RGB. Although C_{UBI} has been used to

TABLE 5.9: S3839 CN index values for the low-resolution M 4 sample, along with V-band magnitudes and δS3839 excess values. The last four lines show the cluster average abundances (for the AGB and RGB) with standard error of the mean, and standard deviation to indicate observed scatter. Note that all but two (stars 25133 and 17999) of the low-resolution targets were also observed with HERMES in high-resolution. V-band magnitudes and IDs are from Momany et al. (2003).

ID	Type	V	S3839	δS3839
3590	AGB	12.48	0.47	0.17
10092	AGB	12.61	0.23	-0.04
11285	AGB	12.84	0.30	0.06
13609	AGB	12.76	0.09	-0.17
20089	AGB	12.72	0.35	0.05
25133	AGB	12.45	0.17	-0.13
46676	AGB	12.05	0.34	-0.02
1029	RGB	13.14	0.66	0.46
3114	RGB	13.38	0.54	0.37
4361	RGB	13.51	0.67	0.52
4806	RGB	13.16	0.22	0.03
4938	RGB	12.86	0.71	0.46
6978	RGB	13.34	0.67	0.50
7298	RGB	13.42	0.13	-0.03
8803	RGB	11.87	0.72	0.34
9040	RGB	12.32	0.57	0.25
10801	RGB	12.54	0.76	0.45
10928	RGB	11.80	0.70	0.30
12387	RGB	13.14	0.37	0.17
13170	RGB	13.52	0.18	0.04
14037	RGB	12.05	0.31	-0.05
14350	RGB	12.65	0.69	0.42
14377	RGB	12.81	0.58	0.33
15010	RGB	12.37	0.33	0.01
17999	RGB	11.84	0.64	0.24
23196	RGB	13.02	0.72	0.50
Mean	AGB	-	0.28 ± 0.03	-0.01 ± 0.03
σ			0.13	0.12
Mean	RGB	-	0.51 ± 0.02	0.23 ± 0.02
σ			0.21	0.25

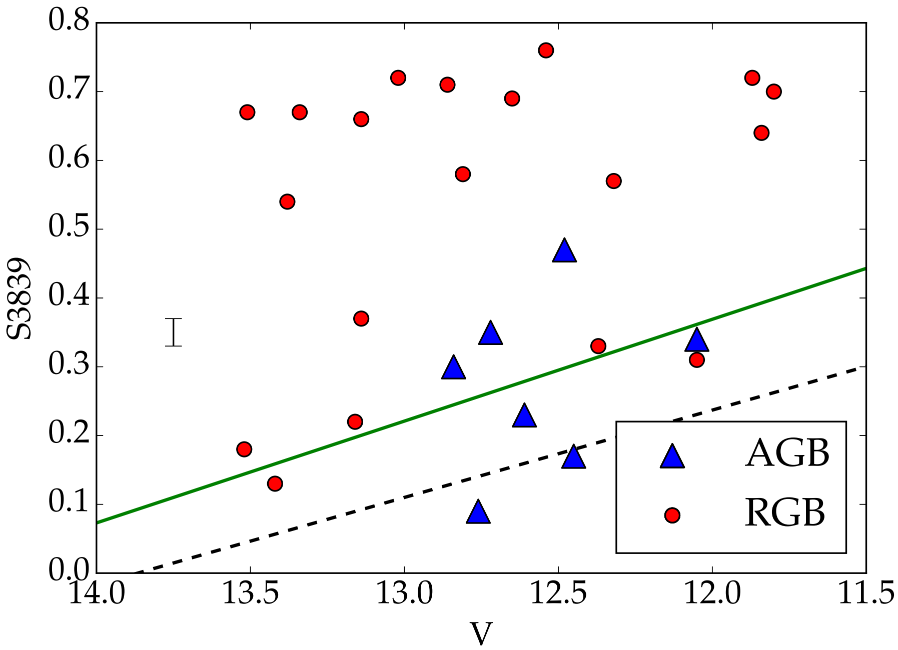

FIGURE 5.7: S3839 CN index values versus V-band magnitudes for our M 4 low-resolution sample. The green trend-line is a linear best fit for the five RGB stars with the lowest CN band strengths ($S3839 = -0.148V + 2.145$), while the dashed trend-line is the baseline from Figure 3 of Norris (1981, $S3839 = -0.127V + 1.761$). The typical S3839 uncertainty is represented on the left.

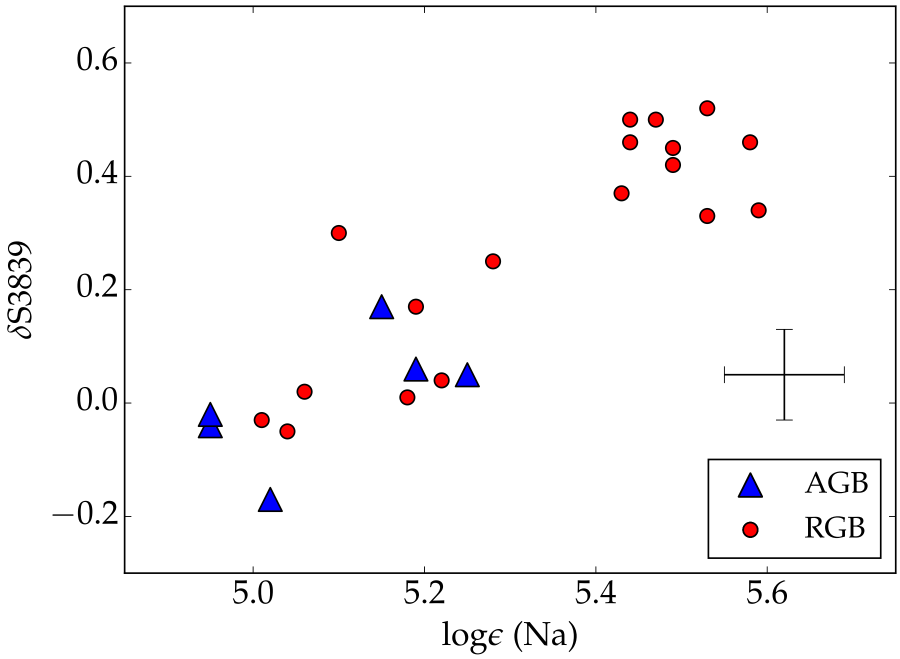

FIGURE 5.8: δS3839 (excess CN index values) versus Na abundances for stars in both our M 4 HERMES and AAOmega samples. δS3839 values are the distance a star is above the green trend-line in Figure 5.7. The error bar represents typical uncertainties. Note that for two stars (25133 and 17999) only low-resolution spectra were observed, and they are therefore not included in this plot.

infer this result, the broadness of the UBI filter pass-bands means that they incorporate a multitude of atomic lines and molecular bands, which makes abundance information that has been inferred from photometric bands difficult to interpret, and can only be used to infer the collective differences that may be the result of a range of spectroscopic features. In an era where medium to high-resolution spectroscopic data is available, these spectra provide a much more definitive answer to the discussion of subpopulations. We therefore focus on spectroscopic data in this investigation.

In response to the unexpected findings of ML16, two high-resolution spectroscopic studies – both using VLT/FLAMES spectra – have been performed on M 4 AGB stars: Mar17 and Wang et al. (2017, W17). Mar17 determined the abundances of a range of species (most relevant to this comparison are the abundances of O, Na, Mg, Al, and Fe) for a sample of 17 AGB stars, but did not re-observe or redetermine abundances for RGB stars. They reported that their AGB sample showed similar [Na/Fe] and [O/Fe] values to a sample of RGB abundances from Mar08 – on average their AGB sample had [Na/Fe] values only 0.08 dex lower than the RGB sample – thereby challenging the conclusion of ML16 by reporting the discovery of both SP1 and SP2-like AGB stars in M 4.

W17 observed a sample of 19 AGB and 68 RGB stars in M 4, and determined Fe and Na abundances for each star. They reported that their AGB sample shows, on average, lower [Na/H] values than their RGB sample (by 0.14 dex). This was in broad agreement with ML16, however they reported a larger spread in Na abundances on the AGB – $\sigma = 0.17$ dex compared to 0.14 dex in ML16; however their uncertainties in [Na/H] are larger than those determined for our Na abundances (± 0.16 dex compared to ± 0.11 dex). They also noted a smaller difference in maximum [Na/H] between the RGB and AGB (Δ[Na/H]$_{max}$ = 0.26 dex compared to 0.40 dex in ML16). Curiously, the [Na/H] results of W17 also agreed well with an overlapping sub-sample of Mar17, confusing the situation further since the conclusions of Mar17 and ML16 are in contradiction.

In summary, for our comparison we have collated:

(i) the O, Na, Mg, Al, and Fe abundances from I99,

(ii) the CN band strengths from SB05,

(iii) the O, Na, Mg, Al, and Fe abundances from Mar17 and Mar08,

(iv) the Na and Fe abundances from W17,

(v) the O, Na, Mg, Al, and Fe abundances from this study, and

(vi) CN band strengths from this study.

The evolutionary-phase designation of targets in I99 was questioned in SB05, who reclassified several of the I99 AGB targets. Star 4633 was determined by SB05 and Suntzeff and Smith (1991) to be on the RGB, and here we adopt this classification. Targets 2519, 4201, 1701, and 4414 are listed in SB05 as 'uncertain', and we did not include them in our comparison for this reason (we note that their exclusion does not affect the result). For our analysis of the CN band strengths from SB05, we redetermined δS3839 excess values using the green fiducial from Figure 5.7 to ensure consistency with the CN results of this study.

The studies of Mar08, Mar17, and W17 included many of the same stars in M 4 as ML16, and a direct comparison of the adopted stellar parameters and reported abundances is possible for the overlapping samples. For our comparisons, we use the $\log_{\epsilon}(\mathrm{X})$ notation in order to avoid including systematic offsets such as solar abundance choice and dividing abundances by Fe abundance. Differences between the values determined in this study and those published in Mar08, Mar17, and W17 are summarised in Table 5.10.

The AGB stellar parameters adopted in this study are largely similar to those in Mar17, while the RGB sample in Mar08 has, on average, higher log g values by 0.25 dex than our RGB sample, which is likely connected to their Fe I abundances which are systematically larger by 0.09 dex[7]. There are significant offsets between our abundances and those in Mar08 and Mar17 (up to an average difference of 0.25 dex), however the scatter around these offsets – typically considered a better indication of the agreement between abundance analysis studies – is consistent with the uncertainties quoted in this study. A detailed investigation of the differences in Na abundance between our work and Mar17 (AGB EWs were kindly provided by A. F. Marino via priv. comm.) revealed that all offsets were able to be accounted for by quantifiable differences in stellar parameters, non-LTE corrections, choice of atmospheric models, atomic line data, and EWs. The measured EWs for lines in common (the 568nm doublet) were quite similar, with typical differences of the order of 5 mÅ, corresponding to $\Delta\log_{\epsilon}(\mathrm{Na}) \sim 0.09$ dex.

Comparing our work with that of W17, we note that while the adopted T_{eff} values are quite different (~ 100 K difference), the abundances agree more closely than with Mar08/Mar17. There is still a notable offset in AGB Na abundance ($\Delta\log_{\epsilon}(\mathrm{Na})$ = 0.14 dex), however the large uncertainties quoted in W17 (± 0.16 dex) make it difficult to determine its significance.

We were unable to identify overlapping sample stars with SB05 and I99, and therefore could not directly compare the CN band strengths and elemental abundances from these studies in the same manner.

[7]Ionisation balance was forced in Mar08, which is controlled primarily by log g.

TABLE 5.10: The average star-to-star differences in parameters and abundances between the published results of Marino et al. (2017, Mar17, AGB only), Marino et al. (2008, Mar08, RGB only), Wang et al. (2017, W17), and those of this study. Uncertainties are standard deviations, and indicate the scatter between the studies, if the offsets were removed. While significant offsets exist between our work those of Mar17, Mar08 and W17, the scatter around the offsets are consistent with the uncertainties quoted in this study (see text for discussion).

Parameter	Mar17 - this study (AGB)	Mar08 - this study (RGB)	W17 - this study (AGB)	W17 - this study (RGB)
ΔT_{eff}	-30 ± 64	-37 ± 61	-94 ± 57	-113 ± 88
$\Delta\log g$	$+0.06 \pm 0.21$	$+0.25 \pm 0.13$	-0.06 ± 0.03	$+0.00 \pm 0.06$
Δv_t	$+0.15 \pm 0.17$	-0.07 ± 0.13	-0.10 ± 0.21	-0.17 ± 0.20
$\Delta\log_\epsilon(\mathrm{Fe\,I})$	-0.02 ± 0.06	$+0.09 \pm 0.07$	$+0.05 \pm 0.09$	$+0.07 \pm 0.11$
$\Delta\log_\epsilon(\mathrm{Fe\,II})$	$+0.03 \pm 0.06$	-	-0.01 ± 0.06	$+0.03 \pm 0.10$
$\Delta\log_\epsilon(\mathrm{O})$	-0.10 ± 0.07	-0.03 ± 0.12	-	-
$\Delta\log_\epsilon(\mathrm{Na})$	$+0.19 \pm 0.06$	$+0.21 \pm 0.09$	$+0.14 \pm 0.09$	$+0.06 \pm 0.11$
$\Delta\log_\epsilon(\mathrm{Mg})$	$+0.10 \pm 0.06$	$+0.22 \pm 0.08$	-	-
$\Delta\log_\epsilon(\mathrm{Al})$	$+0.13 \pm 0.04$	$+0.18 \pm 0.08$	-	-

In order to facilitate comparisons both between the AGB and RGB, and each individual study, we present kernel density estimation (KDE) histograms of the O, Na, Mg, Al, and Fe abundances in Figures 5.9, 5.10, 5.11, 5.12, and 5.13, respectively, and KDEs of CN band strengths in Figure 5.14. The published abundance uncertainties in each study were adopted, and used for the smoothing bandwidths applied to the KDE histograms. We now discuss each element individually.

Iron

The $\log_\epsilon(\mathrm{Fe\,I})$ values as published in Mar08, Mar17, W17, and the Fe abundances determined in this study (§5.2.4) are presented in Figure 5.9. In the cases of this study, W17, and I99, the respective samples of RGB and AGB stars were observed simultaneously and analysed in a consistent manner, and the reported Fe abundances agree very well internally, with average differences between the AGB and RGB no larger than 0.04 dex.

In contrast, Mar17 did not observe an RGB sample at the same time as their AGB sample was observed, nor did they re-analyse the results of Mar08 (in which a sample of 105 RGB stars was observed and analysed spectroscopically). Instead, they compared their AGB results directly with their RGB abundances from Mar08. A significant difference in [Fe/H] of 0.14 can be seen between their AGB and RGB samples, larger than the total [Fe/H] uncertainty quoted in either publication. This difference can cause significant problems if elements are scaled by Fe abundance as it implicitly assumes that all other elemental abundances are offset by the same amount. As discussed earlier, we have chosen not to scale abundances with Fe in this study. The reason that the Fe abundances do not agree for these samples is likely to be changes in the adopted spectroscopic method (that, for example, produce systematic offsets in T_{eff} or log g), however we cannot determine the true cause with the available data.

The Fe abundances from neutral lines are very consistent between these studies, except for the disagreement between Mar08 and Mar17. The average abundance for all five studies is [Fe/H] $= -1.14 \pm 0.07$ (assuming a solar Fe abundance of 7.50).

Oxygen

The O abundances of this study, Mar17, Mar08, and I99 are presented in Figure 5.10. Both our re-analysed AGB sample and that of I99 show, on average, slightly higher O abundances than the respective RGB samples ($\Delta\log_\epsilon(\mathrm{O}) = 0.08$ for both studies), while the AGB abundances of Mar17 are slightly *lower* than the RGB values from Mar08 ($\Delta\log_\epsilon(\mathrm{O}) = -0.08$). The moderate systematic offsets between studies (up to 0.14 dex) can be

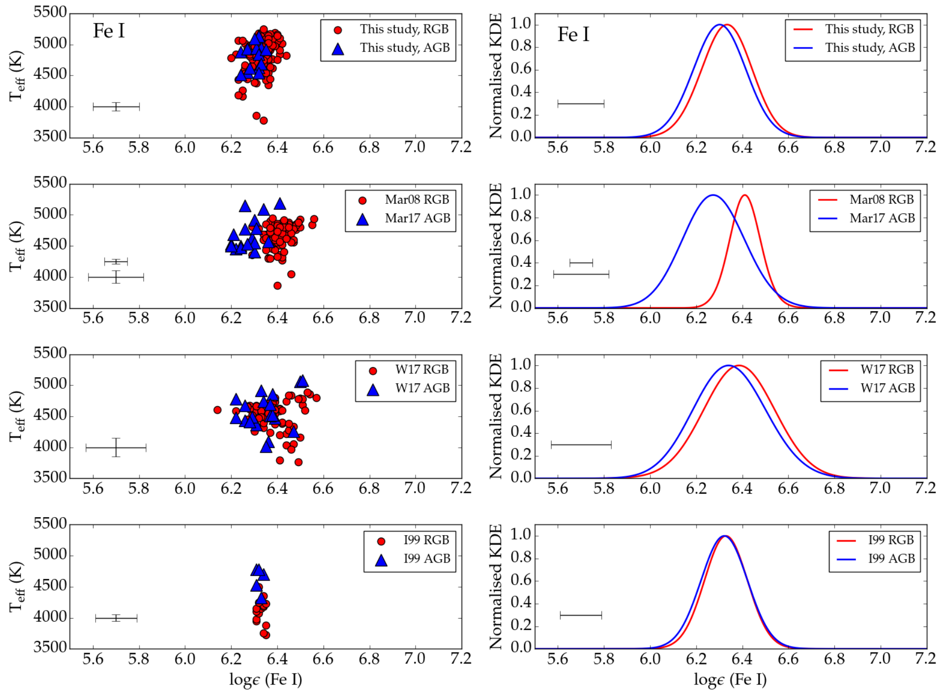

FIGURE 5.9: Abundances determined from Fe I absorption lines from this study, Mar17, Mar08, W17, and I99 are presented in the left-hand panels, with kernel density estimations (KDEs) of these data presented in the right-hand panels. Typical abundance errors are shown, as published in the relevant studies (in the Mar17/Mar08 panel the top error bars are those of the RGB sample in Mar08), and were used as the bandwidths of the KDEs in the right-hand panels.

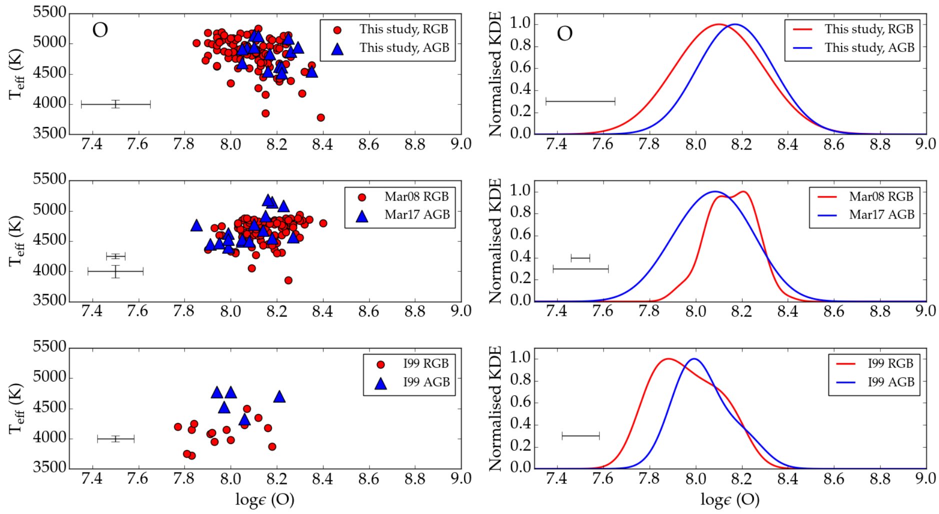

FIGURE 5.10: Same as Figure 5.9, but for the abundances determined from O I absorption lines from this study, Mar17, Mar08, and I99.

largely accounted for by line-list differences (in this study we used the 777nm triplet, while Mar08, Mar17 and I99 used the 630nm forbidden line), however these offsets are still smaller than our uncertainty in $\log_\epsilon(\mathrm{O})$.

In our work, the difference between the branches ($\Delta\log_\epsilon(\mathrm{O}) = 0.08$) is smaller than the total uncertainty in our O abundances (±0.15, see Table 5.7), and the scatter in our RGB O abundances (±0.12). We therefore do not make any conclusions about the AGB of M 4 from these data. Similarly for the results of Mar17 and I99, the differences between the O abundances of the giant branches are of the order of the uncertainties (±0.12 and ±0.08, respectively), and are therefore too small to claim any significant variation.

These O abundances shed little light on the nature of AGB stars in M 4 due to the large uncertainties and relatively small spread in values. Most notable are the O abundances of our work and that of Mar17, whose scatter in $\log_\epsilon(\mathrm{O})$ (±0.12 for Mar17) is of the order of the total reported uncertainty. Furthermore, we detect no bimodality in O abundance, and it is possible that the bimodality seen in the RGB abundances of Mar08 is an artefact of the very small uncertainty of ±0.04, which is less than half the magnitude of the O uncertainty in Mar17, which utilised the same method and absorption lines. This casts doubt on the confidence with which a Na-O anti-correlation can be claimed, and it cannot be confirmed that a heterogeneity in O abundance exists within M 4 giant stars (Carretta et al. 2009b similarly reported a formal homogeneity in O for M 4).

Sodium

The Na abundances reported by Mar17, Mar08, W17, I99, and this study are presented in Figure 5.11. A significant spread larger than the uncertainties exists within all abundance samples, with many showing strong evidence of bimodality.

In all AGB studies of M 4, there is an apparent absence on the AGB of the most Na-rich stars, when compared to the corresponding sample of RGB stars. The various data sets are surprisingly similar, with only one AGB star having $\log_\epsilon(\mathrm{Na}) > 5.5$ (in the sample of Mar17); while in all RGB samples, the largest density of $\log_\epsilon(\mathrm{Na})$ values is between 5.5 and 5.7. The RGB and AGB of W17 overlap to a larger extent than those of the other studies, but the lack of the most Na-rich stars on the AGB is clear (as noted by W17). The differences between the giant branches in this work, and that of Mar08/Mar17, W17, and I99 are $\Delta\log_\epsilon(\mathrm{Na}) = -0.22$, -0.21, -0.14, and -0.20, respectively (these values are all larger than the respective uncertainties in Na abundance, except for that of W17).

It is important to note that in all cases there is also evidence of heterogeneity in the Na abundances of M 4's AGB population (in this study we found a spread of $\sigma = 0.12$ dex, compared to a total Na uncertainty of ± 0.07 dex). This may indicate that stars that have some Na enrichment (i.e. SP2 stars) are indeed present on the AGB, but that there is a limiting factor that is preventing stars with the highest Na abundances from either evolving to the AGB, or appearing as Na-rich on the AGB as they would have on the RGB. We also note (especially among our abundances, and those of Mar17) that some AGB stars in M 4 appear to have lower Na abundances than the most Na-poor RGB stars of the cluster. This suggests that there may be a systematic offset in Na abundance between the two giant branches. We explore this possibility in Section 5.6.

Finally, we note that the Na abundance uncertainty of W17 (± 0.16 dex) appears to be overestimated, most likely due to the selection of stellar parameters which resulted in an uncertainty in T_{eff} of ± 150 K. The uncertainty in Na abundance in the study of I99 (± 0.04 dex) appears to be underestimated – the structure seen in the I99 KDE is unlikely to be real, but is more likely an artefact of both small uncertainties and a small sample size – however we chose to adopt the published uncertainties.

Magnesium

Mg abundances from our work, Mar17, Mar08, and I99 are presented in Figure 5.12. Previous studies have concluded that M 4 is homogeneous in Mg, and we find this for all samples included here.

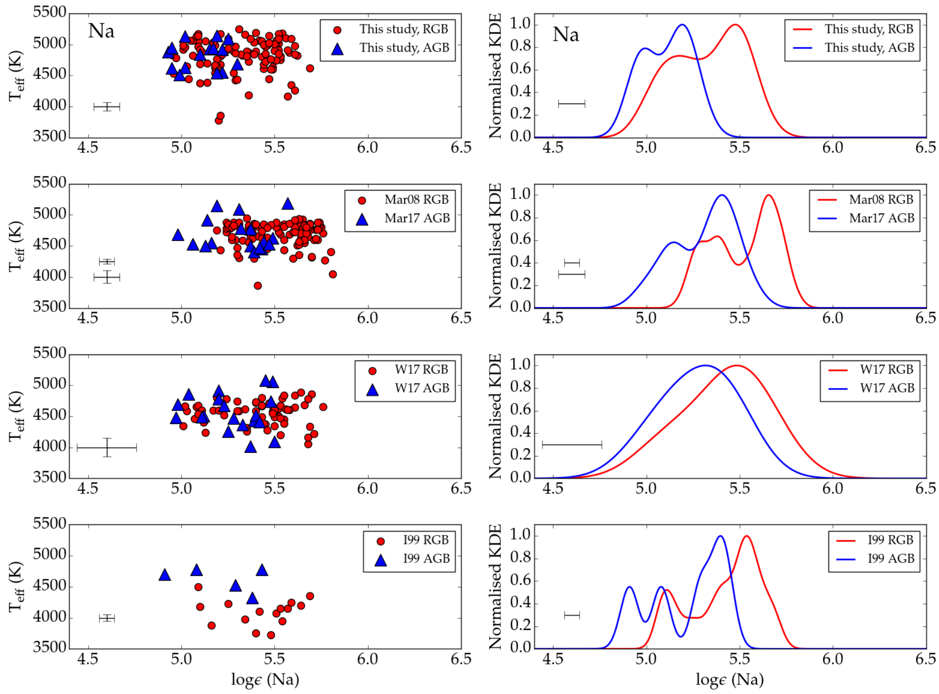

FIGURE 5.11: Same as Figure 5.9, but for the abundances determined from Na I absorption lines from this study, Mar17, Mar08, W17, and I99.

Due to the homogeneity of Mg, we do not expect any significant difference between the $\log_\epsilon(\mathrm{Mg})$ values of AGB and RGB stars in the cluster. While this is the case with the results of this study and those of I99 ($\Delta\log_\epsilon(\mathrm{Mg}) = -0.02$ and 0.00, respectively), the abundances of Mar08 and Mar17 indicate that AGB stars in M 4 present as significantly more Mg-poor than the RGB ($\Delta\log_\epsilon(\mathrm{Mg}) = -0.14$). We consider this to be unlikely, and it may be related to the discrepancy in Fe abundance between the two studies.

Aluminium

Figure 5.13 presents the Al abundances of this study, Mar17, Mar08, and I99. The spread in RGB $\log_\epsilon(\mathrm{Al})$ values, while significant in each sample at the 1σ level (± 0.09, ± 0.12, and ± 0.12 for our work, Mar08, and I99, respectively) is quite small and there is no evidence of bimodality. The spread in AGB Al abundances, however, is even smaller than for each of the respective RGB samples, and shows potentially homogeneous abundances (except for the single Al-rich outlier in this study and Mar17; 2MASS ID 16234085-2631215).

The similarity between the Al abundances of this study, Mar17, and I99 is noteworthy, with the AGB samples in all cases being significantly offset to lower values ($\Delta\log_\epsilon(\mathrm{Al}) = -0.14$, -0.18, and -0.18, respectively), indicating that M 4 stars on the AGB are more Al-poor, on average, than those

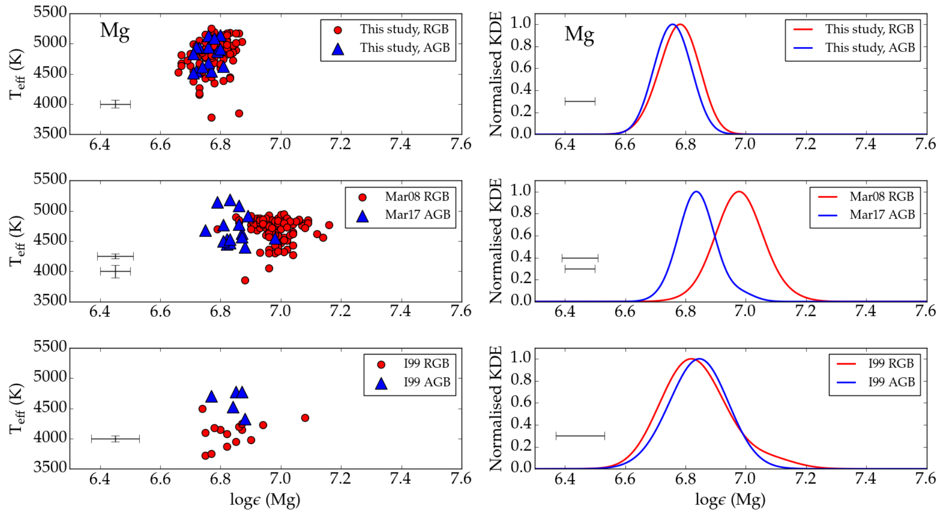

FIGURE 5.12: Same as Figure 5.9, but for the abundances determined from Mg I absorption lines from this study, Mar17, Mar08, and I99.

on the RGB.

While the Al abundance uncertainty reported in I99 (± 0.03 dex) appears to be underestimated (as with Na), we adopt this value for our comparison while noting that the structure in the bottom right panel of Figure 5.13 is likely an artefact of this underestimation.

Cyanogen

In Figure 5.14, the compiled CN band strengths of SB05 and the results from this study (from §5.3) are presented. A clear bimodality in δS3839 values is visible in the RGB samples of both studies (albeit with a larger spread of ± 0.25 in the results from this study, compared to ± 0.19 in SB05), which has been noted in previous CN studies of M 4 (Norris, 1981; Suntzeff and Smith, 1991).

Both studies strongly suggest an extreme paucity of CN-strong AGB stars in the cluster: $\Delta\delta$S3839 $= -0.20$ and -0.14 for this study and SB05, respectively. In both AGB samples, however, there is a significant spread in δS3839 values (± 0.12 and 0.11, respectively), with an apparent bimodality in the AGB sample of SB05 (although there are only 6 stars in this sample). This striking similarity between the independently observed and analysed CN results provides significant weight to our Na and Al abundance results, along with the strong correlation between δS3839 and $\log_\epsilon(\text{Na})$ values (see Figure 5.8).

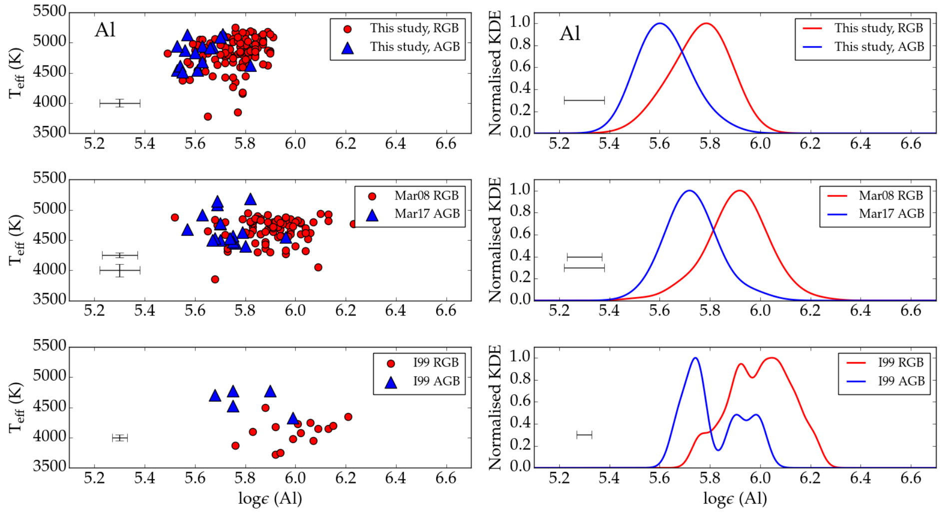

FIGURE 5.13: Same as Figure 5.9, but for the abundances determined from Al I absorption lines from this study, Mar17, Mar08, and I99.

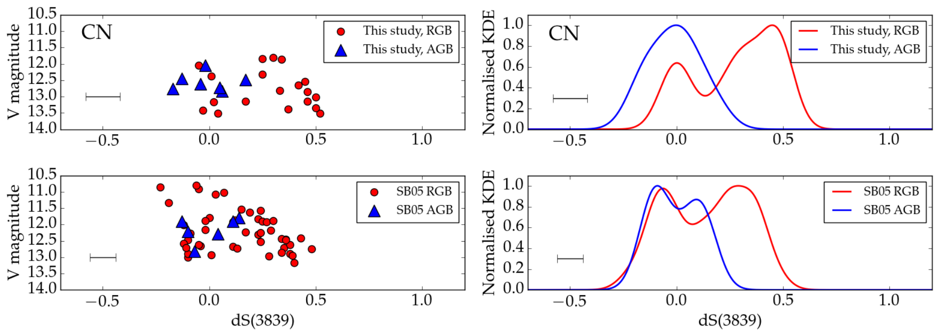

FIGURE 5.14: Same as Figure 5.9, but for the CN band strengths (δS3839 values) from this study and SB05.

Comparison Summary

In summary, we have identified four main conclusions from the literature comparison:

(i) there is no systematic offset between the Mg and Fe abundances of AGB and RGB stars in M 4,

(ii) the AGB of M 4 is systematically offset to lower values in Na and Al abundances, and CN band strength compared to the RGB,

(iii) no conclusions can be drawn concerning differences in the O abundances of AGB or RGB stars in M 4, and

(iv) due to (iii) there may be no Na-O anti-correlation in M 4.

Three of the most common diagnostic tools of multiple populations in M 4 – Na abundances, Al abundances, and CN band strengths – consistently indicate a significant difference between the light-elemental distributions of AGB and RGB stars in this globular cluster, with an apparent deficit of AGB stars enhanced in H-burning products. The only exception to this are the O abundances, from which no conclusion can be consistently drawn. Indeed, we detect little evidence of a spread in O abundance for M 4. Thus, taken at face value, most of the results presented in this section show that, in general, the AGB stars in M 4 contain less H-burning products than RGB stars in the cluster. It is possible that the stars currently on the AGB have experienced less of the 'self-pollution' that M 4 (and other Galactic GCs) is thought to have experienced early in its life (D'Orazi and Marino, 2010).

We can see only two possible explanations for the results presented here:

(i) The most Na-enhanced – and by correlation, He-enriched (D'Antona et al., 2002; Chantereau et al., 2016) – stars in M 4 are not evolving to the AGB, but are becoming AGB-manqué stars, evolving directly from the HB to the WD phase.

(ii) Systematic errors are affecting both the high-resolution spectroscopic method of abundance determination *and* the calculation of S3839 index values of AGB stars across several studies, consistently resulting in AGB samples appearing more Na-poor, Al-poor, and CN-weak than they are in reality.

We investigate i) in §5.5 with 1D stellar evolution models, and ii) in §5.6 by conducting tests on the impact of using a range of different atmospheric models for the determination of elemental abundances.

5.5 Expectations from theoretical stellar evolution models

In the stellar evolutionary models of Dorman et al. (1993), at the approximate metallicity of M 4 ([Fe/H] ~ -1.15), stars with zero-age HB (ZAHB) effective temperatures of $15,000 \lesssim \mathrm{T_{eff}} \lesssim 19,000$ K have short early-AGB lives and evolve to the white dwarf cooling phase without fully ascending the AGB. These stars may not be detectable on the AGB due to the short time-scale of this phase of evolution. Stars with $\mathrm{T_{eff}} \gtrsim 19,000$ K at the ZAHB become AGB-manqué stars and never join the AGB. If applied to M 4, this implies that *all* stars in M 4 should evolve to and ascend the AGB. This is because the hottest HB stars in the cluster have $\mathrm{T_{eff}} \sim 9500$ K (Villanova et al., 2012).

The spectroscopic abundances of M 4's AGB population, as presented in this study, appear to suggest that the most Na-rich stars (these stars populate the blue-HB due to the correlation between He and Na abundance; Marino et al., 2011; Chantereau et al., 2016) either do not evolve to the early-AGB, or spend a very short amount of time in this phase[8].

To establish a precise, quantitative theoretical expectation of M 4's AGB abundances we have calculated a range of theoretical stellar model tracks for M 4 stars. We have done this in order to determine the likelihood of the blue HB stars in the cluster avoiding the AGB, thereby intrinsically creating the abundance distributions observed in this study – where the most Na-rich stars are present on the HB, but missing on the AGB. The stellar models were calculated using the Monash University stellar structure code MONSTAR (Lattanzio, 1986; Campbell and Lattanzio, 2008) with Spruit (2015) overshooting in the core helium-burning phase, as described in Constantino et al. (2017). The code has been updated with low temperature opacity tables which follow variations in C, N and O (Marigo and Aringer, 2009; Constantino et al., 2014). The Reimers (1975) mass loss prescription was used for the RGB.

Our aim was to determine the optimal parameters for M 4 stars that allowed us to most accurately match the observed bimodal HB, and to identify whether these stars evolve to the AGB. We then sought to determine the approximate HB $\mathrm{T_{eff}}$ required for M 4 stars to avoid the AGB phase. At a given age and metallicity, the HB $\mathrm{T_{eff}}$ of a star is a function of both initial mass[9] and helium mass fraction – a higher Y value decreases the time on

[8] Such that no such Na-rich stars are in the AGB phase at the present time.

[9] Since the core mass at the onset of helium burning is relatively fixed at $\sim 0.475 M_{\odot}$ due to the degenerate equation of state (Sweigart and Gross, 1978), the amount of leftover envelope after the core helium flash directly influences the HB $\mathrm{T_{eff}}$.

TABLE 5.11: A summary of M 4 observational constraints for helium enrichment (ΔY), age, and RGB mass loss parameter (Reimers η). The values adopted for use in our theoretical models are listed in the last row.

Reference	ΔY	Age (Gyr)	Reimers η
H02[1]	-	12.70 ± 0.70	-
MF09[2]	-	12.65 ± 0.64	-
V12[3]	0.04	-	-
Val14[4]	$\lesssim 0.01$	-	-
MZ15[5]	-	11.81 ± 0.66	0.40 ± 0.08
N15[6]	0.02	-	-
Adopted	0.03	12.45 ± 0.7	0.40 ± 0.08

[1]Hansen et al., 2002; [2]Marín-Franch et al., 2009
[3]Villanova et al., 2012; [4]Valcarce et al., 2014
[5]McDonald and Zijlstra, 2015; [6]Nardiello et al., 2015

the main sequence, so for a coeval cluster with a helium abundance variation, a star enhanced in He will have a lower initial mass, and therefore have a higher HB $T_{\rm eff}$.

We began by identifying the most important observational and theoretical constraints that affect HB morphology, and created a range of parameters over which to test. We tested three parameters: helium enrichment (ΔY), cluster age, and RGB mass loss rate. Cluster metallicity also has an effect on HB morphology, however, this value is well constrained for M 4 – therefore we assumed [Fe/H]$= -1.15$ for all evolutionary models. Published estimates of these constraints from the literature, and the values adopted for our evolutionary models, are summarised in Table 5.11.

For the helium mass-fraction of SP1 stars in M 4 we adopted Y = 0.245 (Valcarce et al., 2014), and for SP2 stars we adopted Y = 0.275 (so ΔY = 0.03, see Table 5.11). For C, N and O abundances, we adopted the values reported by Villanova et al. (2012) for the N-poor (SP1) and N-rich (SP2) populations[10]. We calculated models over a range of ages (determined primarily by initial mass and Y, for which the dependence was controlled) and RGB mass loss rates. We compared the maximum $T_{\rm eff}$ reached on the HB – our primary observational constraint – with observed values reported in the literature, as determined by Marino et al. (2011, maximum red-HB $T_{\rm eff} = 6250$ K) and Villanova et al. (2012, maximum blue-HB $T_{\rm eff} = 9500$ K). A summary of our model tracks is presented in Table 5.12.

We found that in order to match the HB morphology of M 4, based on spectroscopic HB $T_{\rm eff}$ values and helium mass-fractions in the literature, we required a Reimers mass loss rate of $\eta = 0.44 \pm 0.04$ and initial masses of

[10]SP1: [C/Fe] = -0.20, [N/Fe] = $+0.16$, [O/Fe] = $+0.42$.
SP2: [C/Fe] = -0.36, [N/Fe] = $+0.80$, [O/Fe] = $+0.25$.

TABLE 5.12: A summary of theoretical stellar models calculated for M 4. The last column indicates the highest T_{eff} that was reached in the HB phase of each model track, our primary observational constraint. The first ten models listed are representative of SP1 stars, with a T_{eff} constraint on the red-HB from Marino et al. (2011). The next ten models are representative of SP2 stars, with a T_{eff} constraint on the blue-HB from Villanova et al. (2012). The final nine models are tests using extreme values of RGB mass loss, age, and helium enrichment, to explore AGB-manqué evolution. In Figure 5.15 we show tracks of the three models in bold text, which we found to best match the red-HB (Y = 0.245), the blue-HB (Y = 0.275), and also the lowest HB T_{eff} required to produce an AGB-manqué star (Y = 0.325).

Y	Age (RGB-tip) (Gyr)	Initial Mass ($M_\odot$)	Reimers η	HB Max T_{eff} (K)
SP1 (Observed HB Max T_{eff} = 6250 K)				
0.245	11.83	0.839	0.32	5375
0.245	11.83	0.839	0.40	5540
0.245	11.83	0.839	0.47	6030
0.245	12.45	0.827	0.32	5425
0.245	12.45	0.827	0.40	5675
0.245	**12.45**	**0.827**	**0.44**	**6120**
0.245	12.45	0.827	0.47	6960
0.245	13.24	0.813	0.32	5510
0.245	13.24	0.813	0.40	6050
0.245	13.24	0.813	0.47	8250
SP2 (Observed HB Max T_{eff} = 9500 K)				
0.275	11.79	0.796	0.32	5720
0.275	11.79	0.796	0.40	7250
0.275	11.79	0.796	0.47	9370
0.275	12.40	0.785	0.32	6025
0.275	12.40	0.785	0.40	8150
0.275	**12.40**	**0.785**	**0.44**	**9400**
0.275	12.40	0.785	0.47	10390
0.275	13.22	0.771	0.32	6950
0.275	13.22	0.771	0.40	9380
0.275	13.22	0.771	0.47	11870
Tests of extreme η values				
0.275	12.40	0.785	0.55	13530
0.275	12.40	0.785	0.58	15200
0.275	12.40	0.785	0.60	17000
Tests of extreme ages				
0.275	14.59	0.750	0.44	13070
0.275	15.70	0.735	0.44	16000
Tests of extreme Y values				
0.295	12.40	0.757	0.44	11840
0.315	12.40	0.729	0.44	14500
0.325	**12.40**	**0.715**	**0.44**	**15500**
0.350	12.40	0.680	0.44	19200

0.827 ± 0.013 and 0.785 ± 0.013 $M_\odot$ for SP1 and SP2, respectively; which gave a cluster age of 12.4 ± 0.6 Gyr. Uncertainties given here are the ranges in each value for which the HB morphology was able to be reproduced.

In Figure 5.15 we present model tracks with the mean mass loss rates and initial masses required to match the HB of M 4 (according to the maximum T_{eff} reached on the HB), which are indicated in bold text in Table 5.12. Included for reference are the stellar parameters (reported T_{eff} and photometric log g) of HB stars determined by Marino et al. (2011) and Villanova et al. (2012), and AGB stars determined with PHOBOS V2 in this study. As an example of an AGB-manqué star, we also included a stellar model with a very large helium enhancement (Y = 0.32 and ΔY = 0.08, see Table 5.12), for which we adopted the mean age and mass loss rate that we determined for M 4 (12.4 Gyr, $\eta = 0.44$).

All stellar models whose maximum T_{eff} on the HB closely matched the values in the literature (6250 K for the red-HB, and 9500 K for the blue-HB) evolved to the AGB. In fact, all models with a maximum HB $T_{\text{eff}} \lesssim 15,500$ K spend enough time on the early-AGB to potentially be observed. This provides a very strong prediction that every star in M 4 should evolve to (at least) the early-AGB, and that the light elemental abundance distribution of the AGB should match that of the HB and RGB. Furthermore, we find that only HB stars with a maximum $T_{\text{eff}} \gtrsim 15,500$ K are likely to avoid the AGB, or have short enough AGB-lifetimes to avoid detection – this agrees well with the HB models of Dorman et al. (1993). We note that there is a difference of 6000 K in T_{eff} between the observed blue end of M 4's HB and the values required for the evolution of AGB-manqué stars. Comparing to the reported uncertainty in T_{eff} of ± 50 K in Marino et al. (2011) and Villanova et al. (2012), this is a very large difference. This shows that there is a very clear expectation that *all* stars on the M 4 blue-HB should become AGB stars.

In chemical space, this implies that the Na, Al, and CN distributions should be identical on the AGB and RGB. Given the abundance results from multiple spectroscopic studies (see §5.4), which indicate that these abundance distributions are *not* identical, there is a clear discordance between the observations of M 4 stars and theoretical expectations.

In the next section, we investigate various uncertainties and assumptions that may affect the abundances of AGB stars in M 4, to see whether aspects of the spectroscopic method may be responsible for the contradictory results found thus far.

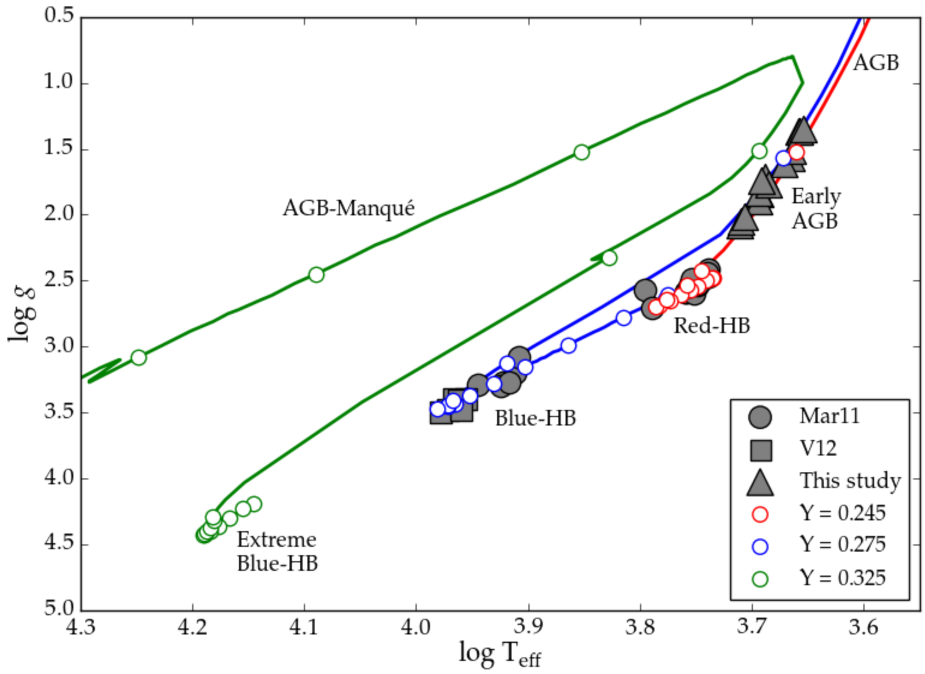

FIGURE 5.15: Evolutionary tracks of the three models found to best match the red-HB (red track, Y = 0.245), the blue-HB (blue track, Y = 0.275), and the lowest HB T_{eff} required to produce an AGB-manqué star (green track, Y = 0.325) – see Table 5.12 and text for model details. While each model was evolved from the beginning of the main sequence, we show the evolution of each model from the ZAHB. Points along the evolutionary tracks are separated in age by 10 Myr to give an indication of time spent in each phase, and hence the likelihood of observing stars in each phase. Also included are the T_{eff} and log g values for our AGB sample (from §5.2), and the T_{eff} values of HB stars from Marino et al. (2011, Mar11) and Villanova et al. (2012, V12) for which we redetermined log g photometrically (using the empirical relation from Alonso et al., 1999, so that all observations are on the same log g scale). Also note that the blue-HB model begins on the red-HB before quickly moving to canonical blue-HB temperatures, possibly indicating that some red-HB stars may in fact be SP2 stars that are still in the early HB phase. While Marino et al. (2011) did not report on any Na-rich stars on the red-HB, they did find a larger spread of Na abundances among red-HB stars than blue-HB stars.

5.6 Atmospheric model tests

5.6.1 Stellar parameter test

Determining precise effective temperatures for stars can be difficult – random and systematic errors are often of the order of $100-200$ K (e.g. Ramírez and Meléndez, 2005; Wang et al., 2017, also see Table 5.2, Figure 5.2, and Table 5.10). While the random errors in our work that are associated with uncertainties in atmospheric parameters are presented in Table 5.6, we conducted an additional test of stellar parameters, in an effort to investigate the effects of systematic errors in $T_{\rm eff}$ on our sample of M 4 stars.

We redetermined LTE Na and Fe abundances for our M 4 stellar sample using three different empirical colour-$T_{\rm eff}$ relations (see §5.2.2), chosen to maximise the systematic differences between the estimated effective temperatures. These relations are the $B-V$ relation from Alonso et al. (1999), the $B-V$ relation from Casagrande et al. (2010), and the $V-K$ relation from Ramírez and Meléndez (2005, note that some stars do not have reliable 2MASS magnitudes and were therefore not included here). The average differences between the $T_{\rm eff}$ values determined from these relations and those adopted for our final $T_{\rm eff,sp}$ results in § 5.2 are 1 ± 67 K, -83 ± 105 K and 129 ± 109 K, respectively. The star-to-star differences are presented in Figure 5.16, showing individual $T_{\rm eff}$ differences of up to 500K and a total 1σ scatter of 127 K for the entire sample. Values of log g and v_t were determined using the same method as in §5.2.2.

The LTE Fe and Na abundances determined using the stellar parameters from these three relations (the line-list and method are the same as in §5.2) are presented in Figures 5.17 and 5.18. Systematic differences in $T_{\rm eff}$ have a large effect on the spread and distribution of Fe abundances, with the Casagrande et al. (2010) and Ramírez and Meléndez (2005) relations producing significant trends between $T_{\rm eff}$ and $\log_\epsilon(\text{Fe I})$ (also see C17). Our adopted $T_{\rm eff,sp}$ values (included in the bottom panels for comparison) produce the tightest distribution of Fe abundances ($\sigma = 0.05$).

In contrast to the effect on Fe abundance, large systematic variations in $T_{\rm eff}$ appear to have little impact on the distribution of Na abundances, despite some stars' $T_{\rm eff}$ varying by up to nearly 500 K between the three empirical relations and those adopted in this study. As seen in Figure 5.18, the Na-poor nature of our AGB sample is present irrespective of the $T_{\rm eff}$ scale adopted. This demonstrates that conservative systematic changes in stellar atmospheric parameters have virtually no bearing on our results, and that $\log_\epsilon(\text{Na})$ is much more robust to sample-wide $T_{\rm eff}$ variations than $\log_\epsilon(\text{Fe I})$ (which we also found to be the case for NGC 6752; see C17). Next, we investigated the effect of including helium enhancement in atmospheric models.

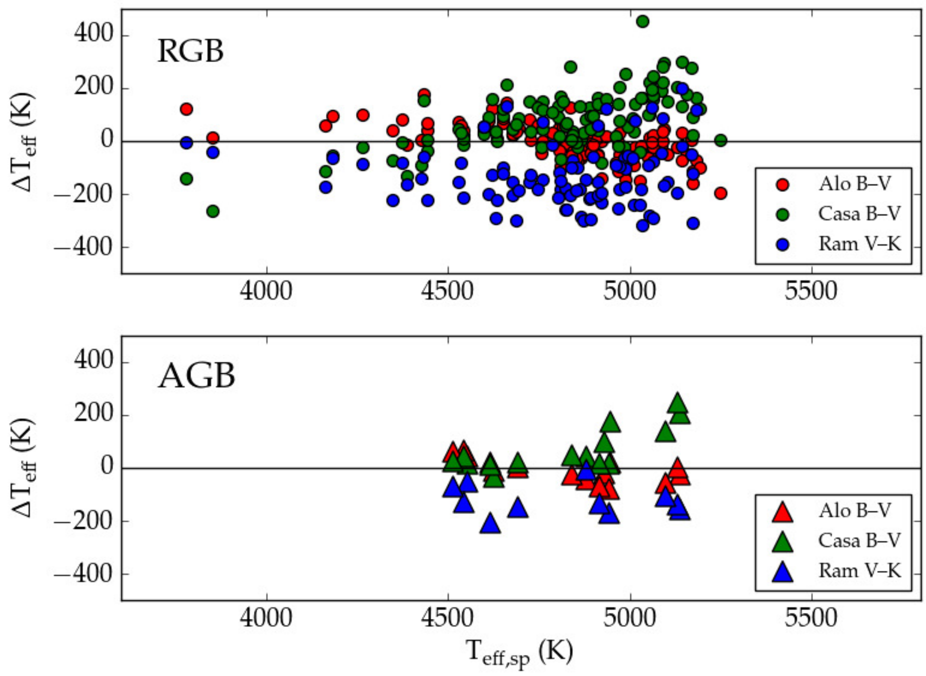

FIGURE 5.16: The star-to-star differences in T_{eff} between our $T_{eff,sp}$ values and those of three empirical colour-T_{eff} relations: Alonso et al. (1999, $B-V$), Casagrande et al. (2010, $B-V$), and Ramírez and Meléndez (2005, $V-K$), where $\Delta T_{eff} = T_{eff,relation} - T_{eff,sp}$. The top panel shows our sample of RGB stars in M 4, while the bottom panel presents our AGB sample.

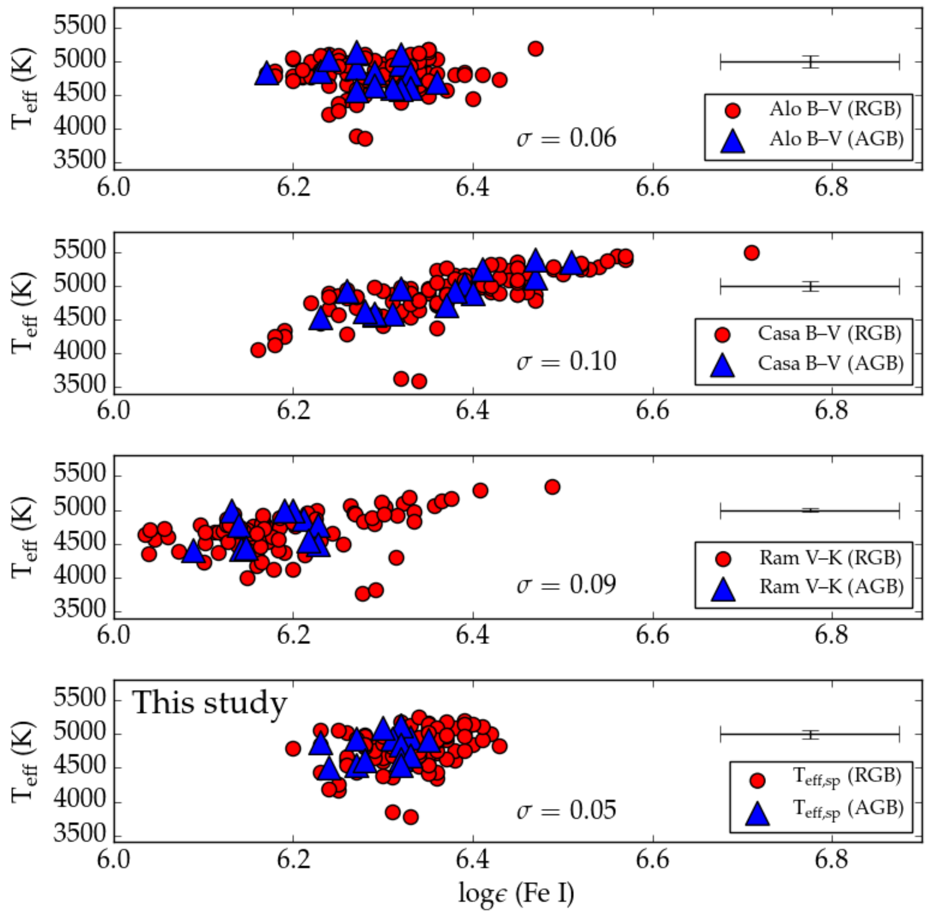

FIGURE 5.17: Fe abundances plotted against T_{eff}, as determined using three different empirical colour-T_{eff} relations (top three panels) – Alonso et al. (1999, $B-V$), Casagrande et al. (2010, $B-V$), and Ramírez and Meléndez (2005, $V-K$) – and our spectroscopic stellar parameters ($T_{eff,sp}$, using PHOBOS; bottom panel). The total uncertainty in $\log_\epsilon(\mathrm{Fe\,I})$ is indicated (see Table 5.7), along with the relevant quoted uncertainties in T_{eff} for each relation.

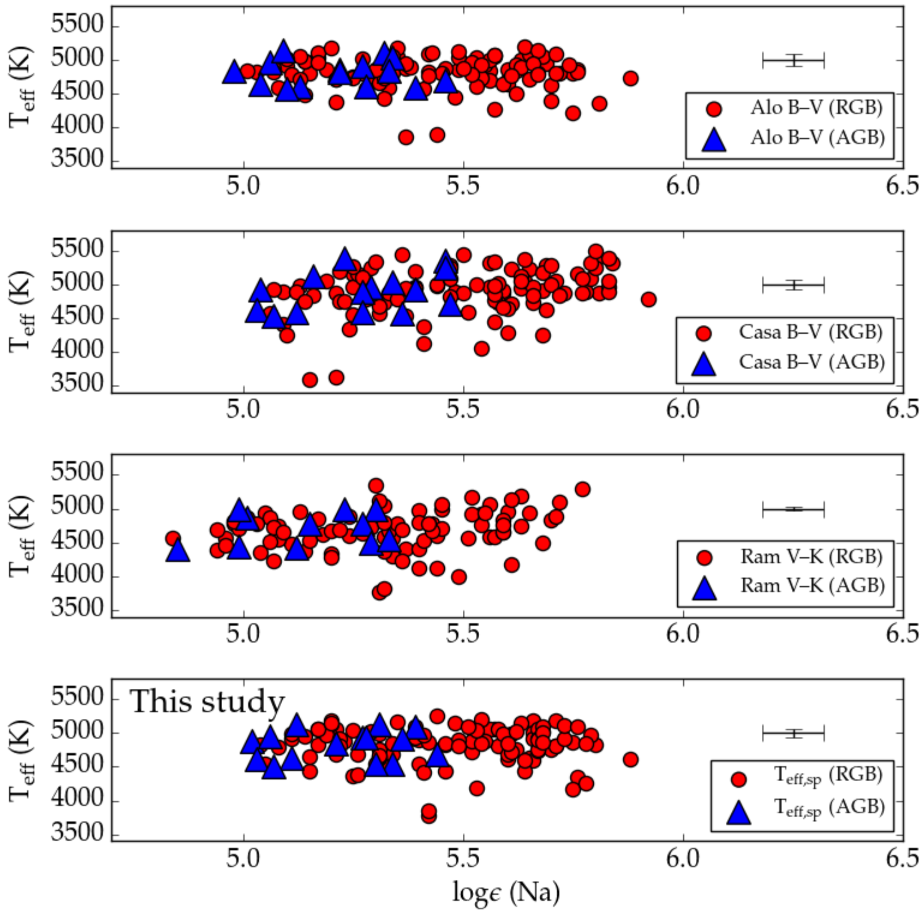

FIGURE 5.18: Same as Figure 5.17, but for Na abundance.

5.6.2 Helium enriched model test

The KURUCZ/ATLAS9 atmospheric models used in the determination of abundances in this study adopt the solar abundances of Grevesse and Sauval (1998) – with a helium mass fraction of Y $= 0.248$, which is similar to the primordial value assumed for SP1 stars in M 4 (Y ~ 0.245; Valcarce et al., 2014). It is accepted that some GC stars are significantly enriched in helium (by more than ΔY $= 0.15$ in some clusters, for example NGC2808; D'Antona et al., 2005). Villanova et al., 2012 determined helium abundances for a sample of blue HB stars in M 4 (assumed to represent the most He-rich stars in the cluster), and found ΔY to be of the order of 0.03-0.04, while Valcarce et al. (2014) and Nardiello et al. (2015) determined ΔY values of $\lesssim 0.01$ and 0.02, respectively.

Here we investigate the effects of including a He-enhancement in the atmospheric models used in chemical abundance determination. We redetermined the LTE abundances of O, Na, Mg, Al, and Fe for a sub-sample of M 4 stars using a representative helium rich model available in the ATLAS9 database. Few He enhanced models have been computed for the ATLAS9 grid, so we conducted this test using the model with parameters closest to our M 4 sample: [Fe/H]$= -1.5$, T$_{\rm eff}$ $= 5000$ K, log $g = 1.5$, $v_t = 2.0$ km/s, and ΔY$= +0.1$ (Y $= 0.352$). Due to the restriction of model selection, only a small subset of stars in our sample have stellar parameters similar to this model; therefore only a representative test was possible.

For a sub-sample of four AGB and eight RGB stars (which cover the entire range of Na abundance as determined with PHOBOS V2), we determined LTE abundances using: i) the He enhanced model ('Y-enh/α-norm') which has scaled solar abundances for all other species, ii) a model with scaled solar abundances and Y $= 0.248$ ('Y-norm/α-norm'), and iii) a model with Y $= 0.248$ and an α-element element enhancement of +0.4 dex ('Y-norm/α-enh'). With these three models[11], we were able to quantify the effect of increased He on elemental abundances while controlling for α-enhancement (α-enhanced atmospheric models were adopted for our abundance determination in §5.2.3). All three models had the same values of [Fe/H], T$_{\rm eff}$, log g, and v_t to ensure a consistent comparison. The results of this test are summarised in Table 5.13.

The differences between the abundances determined using the two Y $= 0.248$ models ('Y-norm/α-enh' and 'Y-norm/α-norm'; see column three of Table 5.13), were constant throughout the sub-sample of 12 stars. Therefore we found that the effects of an α-enhancement are small and entirely systematic, with offsets ≤ 0.04 dex for all species.

[11]There are no 'Y-enh/α-enh' models in the ATLAS9 database.

Similarly, the effects of helium enhancement were systematic – that is, an offset across the test sample – for every species except Na, for which there was a 0.04 dex ($\sigma = 0.01$) range in abundance differences. This was smaller than our total uncertainty in $\log_\epsilon(\mathrm{Na})$ of 0.07 dex. As seen in Figure 5.19, which presents the quantitative effect of He-enhancement on Na abundance for the 12 stars in our sub-sample, the relative increase in Na abundance when the 'Y-enh/α-norm' model is used positively correlates with Na abundance. Notably, the maximum change in Na abundance (0.08 dex) is of the order of our uncertainties (±0.07 dex), and is significantly smaller than the mean difference in abundance between the RGB and AGB ($\Delta\log_\epsilon(\mathrm{Na})$ = 0.22 dex in our work).

We conclude that using helium enhanced 1D atmospheric models for the determination of chemical abundances of helium enriched stars in M 4 would not alter the findings of this study for the following reasons:

(i) The 'Y-enh/α-norm' model affects the Na abundance of AGB stars in the same direction and magnitude as RGB stars of similar parameters and Na abundance, so distributions are not altered.

(ii) A helium enhancement of ΔY = +0.1 dex alters $\log_\epsilon(\mathrm{Na})$ by $\lesssim 0.07$ dex, which is smaller than our uncertainty in $\log_\epsilon(\mathrm{Na})$. Therefore, a helium enhancement more appropriate to M 4 ($0.01 < \Delta\mathrm{Y} < 0.04$) would most likely not produce a measurable change in Na abundance.

(iii) A helium enhancement preferentially spreads out the high-Na stars to even higher values, making the AGB stars even more representative of SP1 RGB stars.

TABLE 5.13: The average differences in elemental abundance, for a representative sub-sample of M 4 stars, when three ATLAS9 atmospheric models of varying composition – helium-enhanced/α-normal ('Y-enh/α-norm'), helium-normal/α-normal ('Y-norm/α-norm'), and helium-normal/α-enhanced ('Y-norm/α-enh') – were used, in combination with our standard spectroscopic method of abundance determination. All three models had the following stellar parameters: [Fe/H]$= -1.5$, $T_{\mathrm{eff}} = 5000$ K, log $g = 1.5$, $v_t = 2.0$ km/s, while the T_{eff} of each star in our sub-sample (8 RGB, and 4 AGB stars) was between 4900 < T_{eff} < 5100 K. Errors are the standard deviation of abundance difference over our 12 star sub-sample.

Species	$\Delta\log_{\epsilon}(\mathrm{X})$	
	(Y-enh/α-norm – Y-norm/α-enh)	(Y-norm/α-enh – Y-norm/α-norm)
Fe I	$+0.029 \pm 0.003$	-0.023 ± 0.001
Fe II	-0.013 ± 0.004	$+0.040 \pm 0.001$
O	$+0.092 \pm 0.002$	$+0.010 \pm 0.006$
Na	$+0.050 \pm 0.012$	-0.020 ± 0.002
Mg	$+0.041 \pm 0.002$	-0.017 ± 0.001
Al	$+0.024 \pm 0.002$	-0.011 ± 0.000

5.6.3 MARCS and ⟨3D⟩ STAGGER-grid test

In this study, and our previous GC investigations using AAT/HERMES spectra (ML16 and ML18a), we have exclusively employed the ATLAS9 grid of stellar atmospheric models. As a further test of the effects of using different model atmospheres on abundance determination, we investigate the effect on chemical abundance when two other sets of atmospheric models are employed: the 1D MARCS grid, and the mean-3D STAGGER-grid. Moreover, we do this with a totally independent abundance determination code, providing a further test of the robustness of our results.

We determined non-LTE $\log_\epsilon(\mathrm{Na})$ and $\log_\epsilon(\mathrm{O})$ values for our entire M 4 sample using the 3D non-LTE BALDER code (Amarsi et al. 2018a; based on the MULTI3D code, Leenaarts and Carlsson 2009). This method was very different to that used in Section 5.2.3. Synthetic equivalent widths were calculated across a grid of Na and O abundances (in steps of 0.2 dex) by direct integration across the line, and then interpolated onto our spectroscopic stellar parameters (determined with PHOBOS V2). Abundances were evaluated by interpolating [X/Fe] values (a constant value of [Fe/H] $= -1.17$ was adopted) as a function of synthetic equivalent width onto our measured equivalent widths (from §5.2.3) for each star. Calculations were based on the Na model atom from Lind et al. (2011a), and the O model atom from Amarsi et al. (2018b).

This abundance determination was done twice for our entire M 4 stellar sample, with different grids of atmospheric models: i) the spherical 1D MARCS model atmospheres of scaled-solar chemical composition and $v_t = 2.0$ km/s (Gustafsson et al., 2008), and ii) the spatially- and temporally-averaged mean 3D (⟨3D⟩) model atmospheres of the STAGGER-grid (Magic et al., 2013). For the latter analysis (based on ⟨3D⟩ model atmospheres), several stars in our sample, including all AGB stars, required extrapolation in $\mathrm{T_{eff}}$ or log g, as they lie outside the parameter space of the STAGGER-grid.

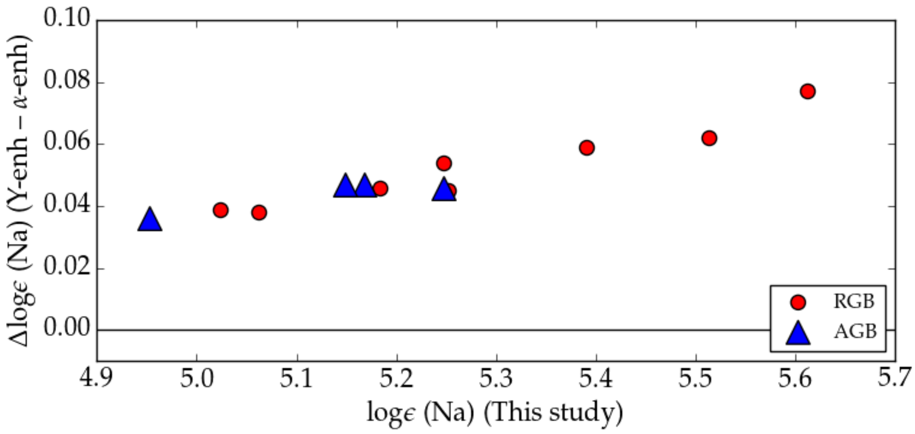

FIGURE 5.19: The star-to-star differences in Na abundance, for a representative sub-sample of 12 M 4 stars, when two ATLAS9 atmospheric models of varying composition – helium-enhanced and α-enhanced – were used, in combination with our standard spectroscopic method of abundance determination. Na abundances on the x-axis are those adopted as the final abundances in this study.

TABLE 5.14: Na and O abundances for each star in our M 4 sample, determined using the BALDER code with i) the 1D MARCS, and ii) the ⟨3D⟩ STAGGER-grid of stellar atmospheric models (see §5.6.3 for details). Abundance uncertainties reflect line-to-line scatter (1σ), and do not take atmospheric sensitivities into account. The last four lines show the cluster average abundances (for the AGB and RGB) with standard error of the mean, and standard deviation to indicate observed scatter. The final column indicates, for each star, whether extrapolation in the stellar parameters was required for the analysis based on the $\langle 3D \rangle$ STAGGER-grid. Note that the stellar parameters from Table 5.3 were used for all abundance determinations. See Appendix A, Table A.8 for complete table.

ID	Type	1D MARCS		⟨3D⟩ STAGGER		⟨3D⟩ extrapolation
		$\log_\epsilon(\mathrm{Na})$	$\log_\epsilon(\mathrm{O})$	$\log_\epsilon(\mathrm{Na})$	$\log_\epsilon(\mathrm{O})$	required?
788	AGB	4.85 ± 0.03	8.20 ± 0.06	4.85 ± 0.03	8.37 ± 0.06	Yes
3590	AGB	5.06 ± 0.07	8.04 ± 0.00	5.08 ± 0.06	8.20 ± 0.01	Yes
10092	AGB	4.88 ± 0.06	8.28 ± 0.03	4.89 ± 0.05	8.42 ± 0.03	Yes
11285	AGB	5.12 ± 0.03	8.09 ± 0.04	5.13 ± 0.02	8.19 ± 0.05	Yes
13609	AGB	4.95 ± 0.06	8.10 ± 0.03	4.96 ± 0.08	8.20 ± 0.02	Yes
⋮	⋮	⋮	⋮	⋮	⋮	⋮
Mean	AGB	5.00 ± 0.03	8.15 ± 0.02	5.03 ± 0.03	8.34 ± 0.03	
σ		0.12	0.09	0.12	0.13	
Mean	RGB	5.17 ± 0.02	8.07 ± 0.01	5.21 ± 0.02	8.20 ± 0.01	
σ		0.15	0.11	0.16	0.15	

Abundances determined using the BALDER code in combination with the MARCS grid are presented in Figure 5.20, along with the star-to-star differences in non-LTE Na abundances between those from Section 5.2.4 and those from this test. The results of this test are also presented in Table 5.14. Comparing the top panel in Figure 5.20 with Figure 5.5 shows that the spread and distribution of O and Na abundances using the MARCS grid and the BALDER code are similar to those determined with PHOBOS V2. The bottom panel, however, indicates that significant changes to the absolute Na abundances occurred. The differences between the models and methods are correlated with Na abundance, and not evolutionary status.

For Na, the average difference (in the sense of BALDER – PHOBOS, see Figure 5.20) for stars with $\log_\epsilon(\mathrm{Na}) > 5.25$ (indicated by the dashed line in Figure 5.20) was $\Delta\log_\epsilon(\mathrm{Na}) = -0.19 \pm 0.06$, which includes only one AGB star. For stars with $\log_\epsilon(\mathrm{Na}) < 5.25$, $\Delta\log_\epsilon(\mathrm{Na}) = -0.11 \pm 0.04$ for the AGB, and $\Delta\log_\epsilon(\mathrm{Na}) = -0.12 \pm 0.04$ for the RGB. This acts to reduce the 1σ spread in RGB Na abundance by 0.04 dex (to ± 0.15 dex, see Table 5.5), but does not alter the spread in AGB Na abundances. It also reduces the average difference in AGB and RGB Na abundance to $\Delta\log_\epsilon(\mathrm{Na}) = -0.17$ from -0.22.

For O, the average difference was $\Delta\log_\epsilon(\mathrm{O}) = -0.03 \pm 0.02$ for both samples, indicating no significant difference between the O abundances determined with the two methods. We again find M 4 to be homogeneous in O. It is interesting to note that Na abundance was more sensitive than O abundance to the differences in method and atmospheric models examined in this test.

Abundances determined using the ⟨3D⟩ STAGGER-grid are presented in Figure 5.21, along with the star-to-star differences in non-LTE Na abundance between the two sets of model atmospheres (the MARCS and ⟨3D⟩ STAGGER-grid), to indicate the impact of utilising atmospheric profiles computed in ⟨3D⟩ compared to 1D. The results of this test are included in Table 5.14, and stars that required extrapolation outside of the STAGGER-grid are indicated.

As with the MARCS grid results, use of the ⟨3D⟩ STAGGER-grid for Na abundance determination gives a similar distribution to our PHOBOS V2 abundances (Figure 5.5). The bottom panel of Figure 5.21 indicates that the Na abundances determined with the MARCS and ⟨3D⟩ STAGGER-grid were very similar, where the average difference was $\Delta\log_\epsilon(\mathrm{Na}) = -0.03 \pm 0.02$ for AGB stars, and $\Delta\log_\epsilon(\mathrm{Na}) = -0.05 \pm 0.01$ for RGB stars (excluding the two brightest stars in our sample, see caption of Figure 5.21). The O abundances were impacted to a much higher degree; however this was mostly due to the extrapolation that was required for several stars (all AGB stars and several RGB stars required extrapolation, particularly those with high O abundances in Figure 5.21). The average difference in O abundance between the

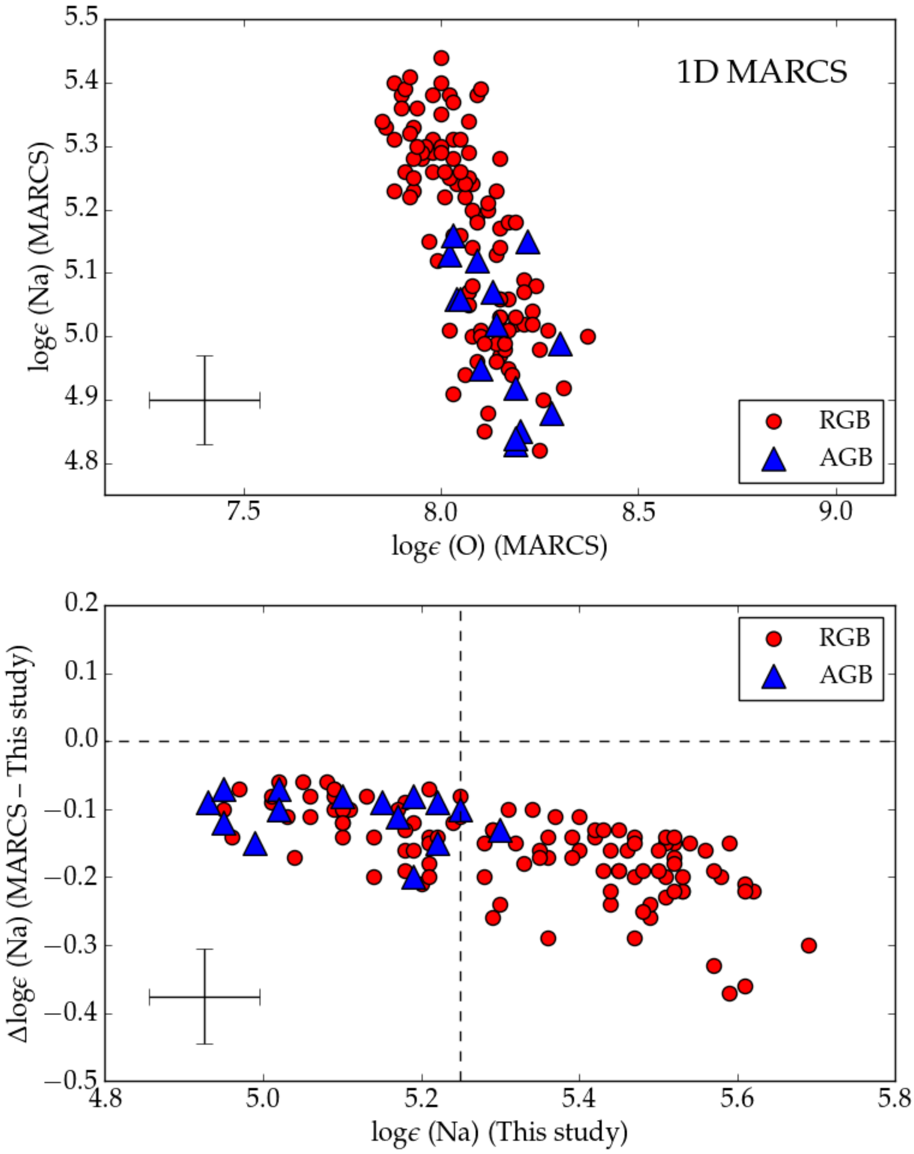

FIGURE 5.20: **Top panel:** Na and O abundances for each star in our M 4 sample, determined using the BALDER code with the 1D MARCS grid of stellar atmospheric models (see §5.6.3 for details). Error bars indicate our total abundance uncertainties (Table 5.7). **Bottom panel:** The star-to-star differences in Na abundance as determined using i) the BALDER code with the 1D MARCS grid, and ii) PHOBOS V2 with the 1D ATLAS9 grid of atmospheric models. Error bars indicate our total uncertainty in Na abundance. The dashed vertical line is at $\log_{\epsilon}(\mathrm{Na}) = 5.25$, see §5.6.3 for details. Note that the stellar parameters from Table 5.3 were used for all determinations.

MARCS and STAGGER-grid was $\Delta\log_\epsilon(\mathrm{O}) = -0.20 \pm 0.08$ for AGB stars, and $\Delta\log_\epsilon(\mathrm{O}) = +0.13 \pm 0.08$ for all RGB stars ($\Delta\log_\epsilon(\mathrm{O}) = +0.09 \pm 0.04$ excluding those that required extrapolation).

Comparing the bottom panels of Figures 5.20 and 5.21, we can see that the largest difference is between the BALDER code and PHOBOS V2, rather than between the MARCS and STAGGER-grid stellar atmospheric models. With the tests performed, however, we cannot disentangle the effects of using the ATLAS9 vs MARCS grids from the effects of using the BALDER vs PHOBOS V2 codes. For low-Na stars (including all AGB stars) there is essentially an offset when the BALDER code is used, and it compresses the range in Na by ~ 0.08 dex in high-Na RGB stars. This is independent of the choice of atmospheric model.

While the abundances of some stars are significantly different when this alternative method is employed, the overall result is unchanged, with M 4 displaying an SP2 AGB deficit using both the MARCS and ⟨3D⟩ STAGGER-grids, and different abundance determination methods. It is interesting to note that the extrapolation of ⟨3D⟩ STAGGER-grid models had a large effect on O abundance, but almost no affect on Na abundance.

5.6.4 Full-3D STAGGER-grid results

In addition to using the ⟨3D⟩ STAGGER-grid, we also conducted a test using atmospheric models from the full-3D STAGGER-grid. This grid cannot be interpolated in $T_{\rm eff}$ and log g to provide star-specific models (as with 1D grids), so only a representative test was possible. We chose three models from the STAGGER-grid, which are approximately representative of i) an upper-RGB star ($T_{\rm eff} = 4500$ K, log $g = 2.0$), ii) a lower-RGB star ($T_{\rm eff} = 5000$ K, log $g = 3.0$), and iii) an early-AGB star ($T_{\rm eff} = 5000$ K, log $g = 2.0$). For each model, we determined non-LTE stellar spectra in the region of the 568nm Na doublet feature at two representative Na abundances: [Na/Fe] = 0.0 dex ($\log_\epsilon(\mathrm{Na}) \sim 5.24$), and [Na/Fe] = 0.5 dex ($\log_\epsilon(\mathrm{Na}) \sim 5.74$).

We then computed non-LTE spectra in the same region using 1D atmopsheric models using the same stellar parameters and microphysics (those used for 1D comparisons in Magic et al., 2013), and with a range of abundances between -1.0 < [Na/Fe] < +1.2, and microturbulence values between 1.0 < v_t < 2.0 km/s. We quantified the corrections that should be applied to 1D Na abundances in order to account for 3D effects by comparing abundances between the 1D- and 3D-computed spectra at a given EW (corresponding to [Na/Fe] = 0.0 and 0.5 dex in the 3D regime).

The choice of microturbulence is vital to this test, due to the sensitivity of the corrections to v_t, which can be difficult to determine accurately (Gratton et al., 1996). We therefore interpolated the corrections based on representative v_t values for stars with $T_{\rm eff}$ and log g similar to the three

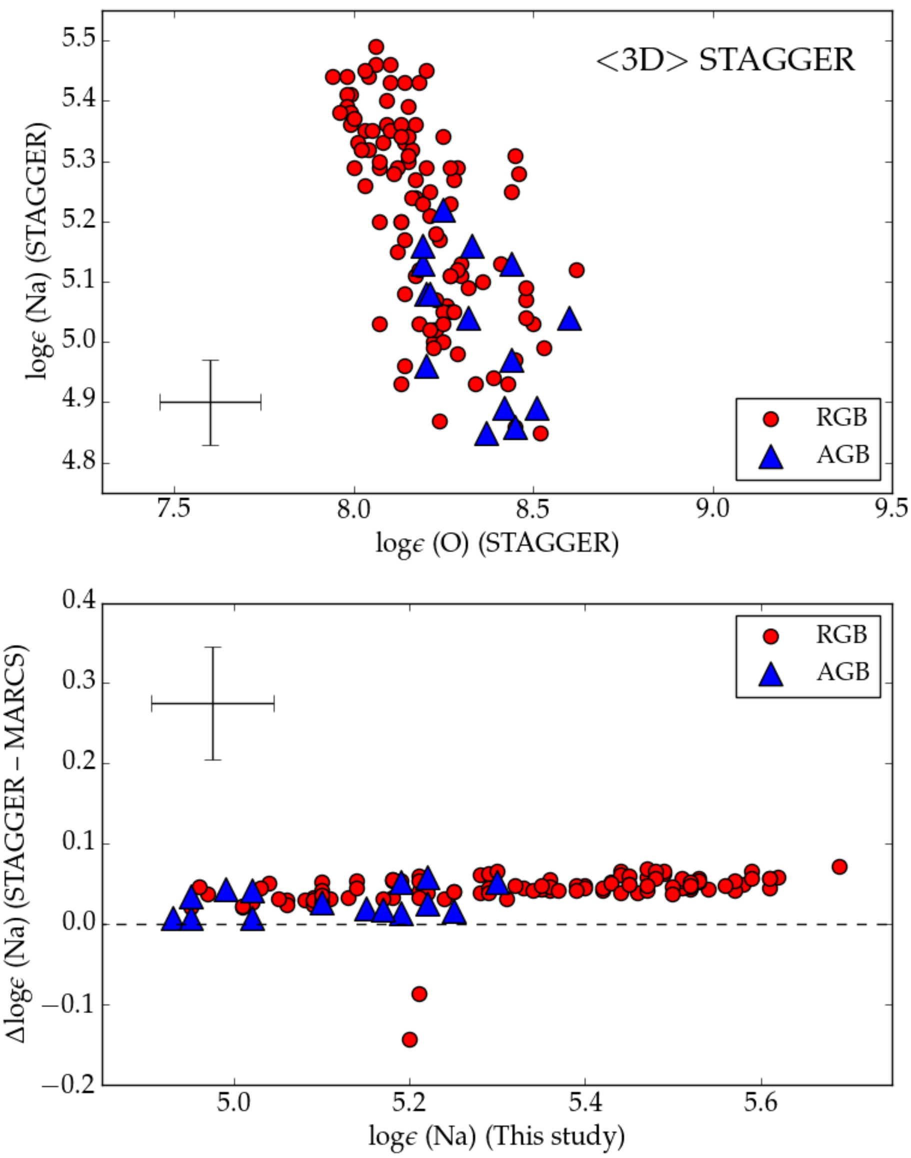

FIGURE 5.21: **Top panel:** Na and O abundances for each star in our M 4 sample, determined using the non-LTE BALDER code with the ⟨3D⟩ STAGGER-grid of stellar atmospheric models (see §5.6.3 for details). Error bars indicate our total abundance uncertainties (Table 5.7). **Bottom panel:** The star-to-star differences in Na abundance as determined using the non-LTE BALDER code with i) the 1D MARCS, and ii) the ⟨3D⟩ STAGGER-grid of atmospheric models. The two outlying stars with negative differences are the two brightest stars in our sample, and were outside the STAGGER-grid by ∼1.0 dex in log g. Error bars indicate our total uncertainty in Na abundance.

TABLE 5.15: Corrections to 1D non-LTE Na abundances in order to account for 3D non-LTE effects ('1D–3D') for three different sets of stellar parameters, representative of i) an upper-RGB star, ii) a lower-RGB star, and iii) an early-AGB star, respectively, and for two different Na abundances. These corrections were determined using the BALDER code with the 1D MARCS grid, and full-3D STAGGER-grid of atmospheric models. Corrections were interpolated in v_t based on the typical microturbulence values of representative stars in our M 4 sample.

Evolutionary	Model parameters			3D–1D correction	
Phase	$T_{\rm eff}$	log g	v_t	[Na/Fe] = 0.0	[Na/Fe] = 0.5
	(K)	(cgs)	(km/s)	(dex)	(dex)
Upper-RGB	4500	2.0	1.5	0.06	0.12
Lower-RGB	5000	3.0	1.2	0.01	0.02
Early-AGB	5000	2.0	1.6	0.03	0.04

adopted STAGGER-grid models. All spectra were determined using the non-LTE BALDER code, as in §5.6.3.

Full-3D abundance corrections, as determined with the STAGGER-grid for the three representative atmospheric models, are presented in Table 5.15.

We found that in 3D, Na abundances are quite insensitive to changes in surface gravity – a difference of Δlog g = 1.0 only changes the Na correction by 0.02 dex, far below our total uncertainty in $\log_\epsilon(\mathrm{Na})$ (± 0.07 dex). Na corrections are more sensitive to changes in effective temperature, where $\Delta T_{\rm eff}$ = 500 K alters the correction by ≤ 0.08 dex. It is important to note that significant confounding variables were unable to be accounted for in this test, including molecule (e.g. CH, NH) rearrangement due to CN processing and 'deep mixing' on the upper-RGB, and differences in electron number densities due to the intrinsic Na and Al abundance variations.

The primary effect of these corrections is that the 3D non-LTE distribution of RGB Na abundances would likely extend toward higher values, thus exacerbating the difference to the AGB stars. We conclude that Na-rich stars are not likely to be incorrectly identified as being Na-poor due to 3D non-LTE effects on the lines, and that using full-3D atmospheric models for our entire sample of stars would be unlikely to alter our primary result for M 4.

Moreover, all of the tests here suggest that while the RGB Na dispersion can be altered with different methods and atmospheric models, the AGB stars all remain Na-poor. We found that AGB stars change in $\log_\epsilon(\mathrm{Na})$ in the same direction and the same approximate magnitude as RGB stars with comparable Na abundance – we could not identify any way of systematically shifting the $\log_\epsilon(\mathrm{Na})$ values of AGB stars differently to those of RGB stars. In effect, these tests retain the relative Na distributions of the AGB and RGB that we found in Section 5.2.4.

5.7 Summary

In light of conflicting results in several spectroscopic studies targeting the AGB of M 4, we sought to i) present robust abundances for a sample of AGB and RGB stars in M 4, ii) compare these abundances to those in the recent literature to investigate whether the results agree or disagree, and iii) attempt to predict and explain the abundance distributions of AGB stars in M 4.

In Section 5.2, we analysed a sample of 15 AGB and 106 RGB stellar spectra in M 4, observed with HERMES/AAT, and originally published in ML16. We redetermined O, Na, and Fe abundances, and additionally report new Mg and Al abundances for each star. In this study, we were especially careful in our determination of stellar parameters (particularly $T_{\rm eff}$), and developed our spectroscopic code PHOBOS V2 to avoid a reliance on photometric estimates of $T_{\rm eff}$. We found M 4 to be heterogeneous in Na and Al, while our total uncertainties in O, Fe, and Mg abundances were larger than the spread in the respective values – therefore we report that M 4 is homogeneous in these species, within uncertainties. Furthermore, we found the atmospheres of our AGB sample to be lower in Na and Al, on average, compared to those of our RGB sample ($\Delta\log_\epsilon(\mathrm{Na}) = -0.22$ and $\Delta\log_\epsilon(\mathrm{Al}) = -0.14$), and with a smaller star-to-star spread in these abundances.

In Section 5.3, we presented new CN band strengths for a sample of 7 AGB and 19 RGB stars in M 4 based on independent low-resolution spectra. We identified the bimodality in CN band-strengths that was first observed by Norris (1981), and found δS3839 to correlate with our $\log_\epsilon(\mathrm{Na})$ values from §5.2. We found the average AGB band-strength to be weaker than that of our RGB sample ($\Delta\delta\mathrm{S3839} = 0.24$), and with a smaller spread in values – similar to our Na and Al results.

In Section 5.4, we compiled spectroscopic results from the literature. We used values from I99 (O, Na, Mg, Al, and Fe abundances), SB05 (CN band-strengths), Mar08 and Mar17 (O, Na, Mg, Al, and Fe abundances), and W17 (Na and Fe abundances). We compared the AGB and RGB distributions of $\log_\epsilon(\mathrm{X})$ and δS3839 values from these six studies to this study (as determined in §5.2 and §5.3). We found that all Fe abundance distributions agree well (both between studies, and between the giant branches within each study), except for Mar17 whose separately determined AGB and RGB abundances did not agree. We found a similar result for Mg. The uncertainties in the O abundances prevented us from drawing any conclusions for this element other than a formal homogeneity within M 4 stars.

A bimodality is visible in the Na abundances of I99, Mar08/Mar17, and our work (but not W17, however this is most likely due to their large uncertainties). In the abundances of every study, the AGB samples have notably lower $\log_\epsilon(\mathrm{Na})$ values, but with a bimodality still present (except W17). The Al abundances all show a similar offset between the AGB and RGB, however no bimodality could be identified, except in the results of I99 (this may be an artefact of underestimated errors and a small sample size). The CN band-strengths from SB05 and this study both show bimodality, while both AGB samples show an extreme paucity of CN-strong members.

In Section 5.5, we calculated a series of theoretical stellar evolutionary models with the MONSTAR code, using observational constraints on M 4 stars from the literature. This was done in order to establish a precise, quantitative theoretical expectation of the abundances of AGB stars in M 4. We found that in order to match the HB morphology, as determined spectroscopically by Marino et al. (2011) and Villanova et al. (2012), and using a helium enhancement for SP2 stars of ΔY = 0.03, we required a Reimers mass loss rate of $\eta = 0.44 \pm 0.03$ and initial masses of 0.827 ± 0.013 and 0.785 ± 0.013 $M_\odot$ for SP1 and SP2, respectively; which gave a cluster age of 12.4 ± 0.6 Gyr. All stellar models whose HB T_{eff} matched the observed values ascended the AGB, indicating that all post-HB stars in M 4, irrespective of Na abundance, should evolve to the AGB. We also demonstrated that at the metallicity of M 4, only stars that reach a $T_{\mathrm{eff}} \gtrsim 15,500$ K on the HB – 6000 K hotter than the bluest HB stars in M 4 – should have AGB lifetimes short enough to avoid detection, in agreement with the models of Dorman et al. (1993).

Confronted with this discordance between our observational results and the prediction of stellar theory, we investigated the robustness of our spectroscopic abundance determinations. We did this in Section 5.6 by conducted a range of tests using various stellar atmospheric models in order to determine the robustness of our elemental abundance results to uncertainties in atmospheric structure. Specifically, we i) redetermined LTE Na and Fe abundances for our entire M 4 sample using three different sets of photometric T_{eff} estimates (with individual T_{eff} differences of up to 500 K), ii) determined elemental abundances for a sub-sample of M 4 stars using a He-enhanced (ΔY = 0.10) model from the ATLAS9 grid to estimate the effect of including He variations in atmospheric models, iii) redetermined Na and O abundances independently using the non-LTE BALDER code (Amarsi et al., 2018a) in combination with atmospheric models from the 1D MARCS grid and the ⟨3D⟩ STAGGER-grid, and iv) using the full-3D STAGGER-grid, determined corrections to 1D non-LTE Na abundances to account for 3D non-LTE effects for three sets of stellar parameters. All tests indicated that Na-rich stars (on the AGB or RGB) are unlikely to be misidentified as being Na-poor.

5.8 Conclusions

A significant strength of the spectroscopic results presented in this study (§5.2–5.3) lies in the combining of two independent methods of separating the subpopulations in chemical abundance space (using both high- and low-resolution spectra). Both of our independent sets of M 4 results in this paper, namely (i) the re-analysed high-resolution spectra, with additional chemical abundances (Figure 5.6), and (ii) the new CN band strengths (Figure 5.7), support the conclusions of ML16 that AGB stars in M 4 are largely representative of SP1 stars – namely, that there is a significant paucity of SP2 AGB stars, with an SP2 AGB deficit of $\mathscr{F} \gtrsim 65\%$ – as evidenced by their Na and Al abundances, and CN band-strengths, compared to those of stars on the RGB. This adds M 4 to the list of GCs that have been reported to contain significant SP2 AGB deficits, alongside NGC 6752 (Campbell et al., 2013) and M 62 (Lapenna et al., 2015).

A comparison of these results with those from the literature (§5.4) indicate that this is unlikely to be an artefact of our method of abundance determination: spectroscopic M 4 studies that included AGB stars have consistently shown the AGB to be systematically lower in Na abundance, Al abundance, and CN band strength (typically indicative of N abundance; Cottrell and Da Costa, 1981) than the RGB – in agreement with our original findings in ML16. In stark contrast to this strong observational results, we predicted – using theoretical evolutionary models representative of M 4 stars (§5.5) – that the abundance distributions of the AGB and RGB should be *identical* for all species investigated in this study (except for CN due to extra mixing of N to the stellar surface on the RGB). In an attempt to reconcile the models and observations, we found that we were unable to significantly alter our abundance results by utilising a variety of atmospheric models (§5.6), including those with systematically offset stellar parameters, those that included a helium enhancement, different grids of 1D atmospheric models, or 3D atmospheric models.

Na, Al, and N are all products of hydrogen burning (Kippenhahn and Weigert, 1990), and are three of the species most commonly observed to vary among the stars of globular clusters (other species include He, C, O, and Mg; Gratton et al., 2004), both Galactic and extragalactic (Gratton et al., 2012; Brodie and Strader, 2006). Of these, atmospheric Na and Al abundances are not predicted to change throughout the lives of individual present-day GC stars – these abundances are typically assumed to be an intrinsic property of the star because low-mass stars do not reach temperatures high enough to activate the Ne-Na or Mg-Al H-burning chains (Norris, 1981; Iben and Renzini, 1984) – while N is observed to increase on the RGB via ‘deep mixing’ (Henkel et al., 2017).

In conclusion, with no viable mechanism to reduce these abundances in-situ between the RGB and AGB, and the prediction that all stars in M 4 should evolve through to the AGB, we can see few remaining potential explanations for the consistent observations that AGB stars in M 4 have significantly lower abundances of Na, Al, and N (inferred from CN) than RGB stars in the cluster. Avenues to consider in order to resolve this disparity are diminishing, but include investigating the effect of interstellar extinction on AGB stellar spectra (M 4 experiences large differential reddening), and exploring differences between the atmospheric structures of AGB and RGB stars. We note, however, that any solution must simultaneously account for the observed disparity in both the elemental abundance *and* CN band strength distributions, which are determined using different spectroscopic methods.

Acknowledgements

Based in part on data acquired through the AAO, via programs 09B/15, 14B/27 and 15A/21 (PI Campbell); some of these observations were conducted by Elizabeth Wylie de Boer, Richard Stancliffe, and George Angelou. Part of this work was supported by the DAAD (PPP project 57219117) with funds from the German Federal Ministry of Education and Research (BMBF). Parts of this research were conducted by the Australian Research Council Centre of Excellence for All Sky Astrophysics in 3 Dimensions (ASTRO 3D), through project number CE170100013. BTM acknowledges the financial support of the Research Training Program (RTP) scheme scholarship. SWC acknowledges federal funding from the Australian Research Council though the Future Fellowship grant entitled "Where are the Convective Boundaries in Stars?" (FT160100046). AMA acknowledges funds from the Alexander von Humboldt Foundation in the framework of the Sofja Kovalevskaja Award endowed by the Federal Ministry of Education and Research. TN acknowledges funding from the Australian Research Council (grant DP150100250). VD acknowledges support from the AAO distinguished visitor program 2016. LC gratefully acknowledges support from the Australian Research Council (grants DP150100250, FT160100402). This work was supported by computational resources provided by the Australian Government through the National Computational Infrastructure (NCI) under the National Computational Merit Allocation Scheme (project ew6). We thank Yazan Momany for providing M 4 $UBVI$ photometry, and Benjamin Hendricks for providing the M 4 reddening map. We also thank Anna Marino and Yue Wang for providing additional data that aided in the literature comparison, and Yue for helpful discussions and suggestions.

Chapter 6

Summary and Conclusions

In this thesis we conducted a systematic investigation into the asymptotic giant branches of three globular clusters – M 4, NGC 6752, and NGC 6397 – using high- and low-resolution multi-object spectroscopes on ground-based telescopes. Through four peer-reviewed journal articles (three published, one submitted), we:

(i) provided new observations of AGB and RGB stars in globular clusters,

(ii) reported parameters and abundances for our stellar samples,

(iii) discussed the implications of their relative light-elemental abundance distributions, and

(iv) provided technical analyses on the spectroscopic method and its application to AGB stars, and globular cluster giant stars in general.

In Chapter 2 (ML16) we developed a new analysis pipeline, PHOBOS V1, which employs the spectroscopic method of stellar parameter determination (using Fe I and Fe II absorption lines, see §1.4.2) in combination with the EW measurement tool ARES, the ATLAS9 grid of atmospheric models, and the LTE abundance code MOOG (see §1.4.3 for more details). We reported stellar parameters and abundances for Na, O, and Fe for a sample of AGB and RGB stars in the GC M 4. This was the first systematic study of the AGB of this cluster, and the first ever abundance study published that utilised HERMES spectra. In contrast to our expectations from stellar evolutionary theory – that the sodium and oxygen abundance distributions of the AGB and RGB of M 4 should be equivalent – we found that every star in our AGB sample showed Galactic halo-like abundances (SP1). This indicated that either every Na-enhanced (SP2) star in M 4 is evolving off the HB directly to the white dwarf phase and thereby avoiding the AGB entirely (i.e., a SP2 AGB deficit of $\mathscr{F} = 100\%$[1]), or that our abundance analysis was incorrect, potentially implying that there is a deeper issue with

[1] $\mathscr{F} = (1 - \frac{\mathscr{R}_{\rm AGB}}{\mathscr{R}_{\rm RGB}})\cdot 100\%$, where the percentages of RGB and AGB stars in a GC that are found to be members of SP2 are written as $\mathscr{R}_{RGB}$ and $\mathscr{R}_{AGB}$

using the standard spectroscopic method for low-mass AGB stars. We did not attempt to resolve this issue in this Chapter, concluding that we could not explain the observation. We returned to this GC in the final Chapter of this thesis.

In Chapter 3 (C17) we responded directly to the publication of Lapenna et al. (2016, L16), which challenged the conclusion of Campbell et al. (2013, C13) that NGC 6752 presents an SP2 AGB deficit of $\mathscr{F} = 100\%$. For a sample of AGB stars, L16 presented Fe abundances that were significantly lower, and with a larger spread in values, than had been previously reported for the cluster. They attributed this to an 'overionisation' of Fe, the cause of which they did not specify, and which is not predicted by current non-LTE theory. This resulted in a larger spread in, and generally higher, [Na/Fe] values than C13 had found. Based on this, they concluded that C13 was incorrect – that NGC 6752 has an SP2 AGB deficit of $\mathscr{F} = 30\%$, perfectly in line with theoretical expectations. In this Chapter, we re-analysed our original sample of NGC 6752 AGB stellar spectra (from VLT/FLAMES) using Fe I, Fe II, and Na I absorption lines. We were able to reproduce the overionisation that L16 reported by showing that systematic offsets in T_{eff} translate strongly into offsets in Fe abundances. With an improved T_{eff} scale using more reliable photometric estimates of stellar parameters, we found that the 'overionisation' of Fe that L16 reported was removed entirely, in line with predictions from non-LTE theory. We also demonstrated that the same offsets in T_{eff} did not significantly change the [Na/H] abundances of our AGB sample. We concluded that the original findings of C13 were sound, using both [Na/H] and [Na/Fe] – as long as reliable empirical relations between photometric colour (in this case $V - K$) and T_{eff} are adopted, or used as initial estimates for spectroscopic parameter determination.

In Chapter 4 (ML18a) we published the first set of stellar parameters and abundances for a sample of AGB stars in the GC NGC 6397. We chose to adopt photometrically estimated stellar parameters for our sample of AGB and RGB stars because some doubt had been cast over the standard spectroscopic method in recent literature (e.g., L16). We reported Fe, Na, O, Mg and Al abundances for each star. We found that our abundances from Fe I and Fe II lines agreed with previously determined metallicities for the cluster, and with non-LTE predictions – we did not find any indication of an Fe overionisation like that of L16, indicating that our adopted T_{eff} scale was reliable. In our RGB sample, we identified Na-O and Mg-Al anti-correlations, both of which have been shown in NGC 6397 previously. Following expectations from stellar evolutionary theory, and in contrast to our results for M 4 and NGC 6752 in Chapters 2 and 3, we showed that the light-element abundance distributions of our AGB sample agreed well with our RGB sample, indicating an SP2 AGB deficit of $\mathscr{F} = 0\%$. Finally we discussed how our NGC 6397 results strengthen our M 4 conclusions since we did not find an SP2 AGB deficit, despite the similarities between the methods employed in this Chapter and for the analysis of our M 4 data.

In Chapter 5 (ML18b) we returned to study M 4, in response to several publications on the topic of M 4's AGB, some of which challenged, and others that supported, our ML16 findings. We re-analysed our M 4 HERMES data using our updated PHOBOS V2 pipeline, whose iterative procedures have been significantly improved so that reliable photometric estimates of stellar parameters are no longer necessary for initial guesses. For our pre-existing sample of M 4 RGB and AGB stars, we reported more reliable stellar parameters and abundances of Na, O, and Fe. Additionally, we presented new Mg and Al abundances, and CN band-strengths using new low-resolution AAOmega spectra. Our results, both new and redetermined, supported our conclusions in ML16 of an SP2 AGB deficit in M 4. We compared our results to those of the M 4 AGB studies in the literature, and found that in all relevant studies AGB stars in M 4 appear to contain, on average, less Na and Al, and have generally weaker CN band-strengths, than RGB stars in the cluster – M 4 AGB stars are typically indicative of SP1 stars. Using theoretical stellar models, however, we established that AGB stars in M 4 *should* display an identical distribution of light-elemental abundances as RGB stars in the cluster, contrary to the observations. In order to check the robustness of our observational results, we conducted a suite of tests on our abundance results by utilising a range of stellar atmospheric models. However, we were unable to alter our primary result, indicating that our conclusion of M 4 containing a significant SP2 AGB deficit is robust, and at odds with theoretical expectations.

In conclusion, we found that the globular clusters M 4 and NGC 6752 display a significant SP2 AGB deficit, where the most Na-rich stars appear to missing on the AGB, as inferred from comparisons with abundance distributions of RGB stars in the respective clusters. These discoveries used spectra from different instruments (HERMES/AAT and FLAMES/VLT) and used different spectroscopic methods. In contrast, we found that the GC NGC 6397 does not display an SP2 AGB deficit – the distribution of Na and Al abundances in the AGB and RGB stars of the cluster were identical (within uncertainties). In this way, our study of NGC 6397 acted as a control subject for our analysis of M 4, because our NGC 6397 spectra were observed with the same instrument, and analysed using the same methods, as our M 4 spectra.

The disparity between the AGB and RGB abundances of M 4 and NGC 6752 is in disagreement with expectations from stellar evolutionary theory. We found that every star in M 4 should ascend the AGB, therefore the full range of light-elemental abundances – as seen on the RGB – should be observed on the AGB. In response to the original NGC 6752 study (C13), Cassisi et al. (2014) conducted a similar experiment with stellar models, and found that only the $\sim 30\%$ most Na-rich stars should be missing from the AGB of NGC 6752, due to the well-established expectation that HB stars with $T_{\mathrm{eff}} \gtrsim 15,000$ K become AGB-manqué stars and avoid the AGB. For both clusters, however, a very large proportion of SP2 stars appear to not be present on the AGB, in clear contradiction with theoretical expectations.

We investigated the reliability of our elemental abundances, and found that Na abundances in GC giant stars are extremely robust to many random and systematic uncertainties. Furthermore, the agreement between our Na abundances and CN band strengths reinforces our conclusions further, since the determination of molecular band strengths requires a very different method than elemental abundances, and does not include the use of atmospheric models. We could see few remaining potential explanations for the discrepancy between the robust light-elemental abundance distributions of AGB stars in M 4 and NGC 6752, and the prediction from stellar evolutionary theory that *all stars* in M 4, and *70% of stars* in NGC 6752, should ascend the AGB.

6.1 Future Work

In this thesis, we identified and fortified a discrepancy between stellar theory and observations. This gap must arise from a flaw in either low-mass stellar evolutionary theory, or the use of 1D non-LTE spectroscopic analyses for the purpose of identifying multiple populations in globular clusters using AGB stars. Specifically, *the AGB populations of M 4 and NGC 6752 show significantly less signs of containing multiple populations than the RGB populations of these clusters, which is not predicted by stellar evolutionary theory*. The source of this disparity must lie in either i) the predicted evolutionary tracks of GC stars, especially between the RGB-tip and early-AGB, ii) the determination of elemental abundances and CN band-strengths of low-mass AGB stars, or iii) a combination of these two possibilities. We find it most likely that a gap exists in our understanding of AGB stellar atmospheres that, when accounted for, would systematically increase the inferred light-elemental abundances, and the spread in those abundances, to the level observed among RGB stars in each GC. Strong evidence for this lies in our stellar models of M 4 stars which expose a 6000 K disparity in the HB effective temperatures required to produce an SP2 AGB deficit. However, the contradictory results of NGC 6397 confound this hypothesis, indicating that i) our spectroscopic methods are reliable, thus supporting the accuracy of our M 4 and NGC 6752 abundance results, and ii) that HB stars with $T_{\rm eff} \lesssim 10,500$ K indeed evolve to the AGB, thus supporting our theoretical prediction that M 4 should not contain an SP2 AGB deficit.

To investigate other possible sources of this disparity between stellar theory and observation, we propose that further observations of AGB stars in GCs should be conducted. Specifically, we recommend targeted high-resolution observation of second parameter GC pairs – those which have similar global parameters such as metallicity and age, but contain very different HB morphologies. An example of such a pair is NGC 288 and NGC 362, which Campbell et al. (2011) found to contain very different AGB distributions of CN band-strengths, a strong indicator that one of these clusters (NGC 288) displays an SP2 AGB deficit while the other does not. This may aid in disentangling the effects of metallicity and age on multiple populations as determined with AGB stars.

Another potential avenue of exploration is the atmospheres of AGB stars. As seen in Chapter 5, our initial investigation of stellar atmospheric models was unable to resolve the disparity between stellar theory and observations of GC AGB stars. We suggest a more in-depth exploration of AGB stars, including their atmospheric structure, intrinsic differences in their spectra compared to RGB stars, and the effects of interstellar reddening on their spectra compared to RGB stars. Understanding these details and their effect on atomic line formation and atmospheric molecular formation may reveal the reasons why our AGB abundances do not agree with expectation from both RGB stellar observations and evolutionary theory.

Appendix A

Supplementary Material – Online Tables

The results presented in these tables are discussed in detail in Chapters 2 - 5.

In Table A.1 we provide the full version of Table 2.1 from Chapter 2, which was previously only available online. This table includes stellar identifications, parameters, radial velocities, and chemical abundances for each star in the M 4 sample, as published in ML16.

Table A.2 was originally published with C17 as an appendix, and has been moved here for consistency. This table includes stellar identifications, parameters, and chemical abundances for each star in the NGC 6752 sample, as published in C17.

In Tables A.3 and A.4 we provide the full versions of Tables 4.1 and 4.5 from Chapter 4, which were previously only available online. Table A.3 includes stellar identifications, photometric magnitudes, and radial velocities for each star in NGC 6397, as published in ML18a; while Table A.4 includes stellar parameters and chemical abundances for each of these stars.

In Tables A.5, A.6, A.7, and A.8, we provide the full versions of Tables 5.1, 5.3, 5.5, and 5.14 from Chapter 5, which were previously only available online. Table A.5 includes stellar identifications, photometric magnitudes, and reddening values for each star in M 4, as published in ML18b, while Table A.6 includes stellar parameters (including both spectroscopic and photometric T_{eff} values) for each of these stars. Table A.7 includes chemical abundances for each star in our M 4 sample as determined using PHOBOS V2, while Table A.8 includes abundances for each stars as determined using the BALDER code with both the 1D MARCS grid, and the <3D> STAGGER-grid, of atmospheric models.

TABLE A.1: Complete version of Table 2.1 (Chapter 2). Stellar parameters, radial velocities and chemical abundances for each star in the ML16 M 4 sample. Abundance errors reflect line-to-line scatter, and do not take atmospheric sensitivities into account. Included are the stellar designations used by Mar08. We adopt the Asplund et al. (2009) solar abundance values.

Star	Type	RV (km/s)	$T_{\rm eff}$ (K)	log g (cgs)	$v_{\rm t}$ (km/s)	[Fe/H] (dex)	σ (dex)	[O/Fe] (dex)	σ (dex)	[Na/Fe] (dex)	σ (dex)	ID Mar08
25	RGB	66.6	5028	2.64	1.09	-1.14	0.12	0.30	0.12	0.43	0.13	-
907	RGB	69.4	5047	2.69	0.94	-1.18	0.11	0.42	0.12	0.37	0.11	-
1029	RGB	72.2	4936	2.45	1.41	-1.10	0.09	0.09	0.11	0.49	0.11	22089
1129	RGB	69.6	4886	2.20	1.20	-1.11	0.10	0.35	0.12	0.10	0.10	-
1474	RGB	70.4	5159	2.78	0.92	-1.06	0.11	0.12	0.12	0.39	0.12	-
2000	RGB	71.3	4918	2.38	1.08	-1.11	0.11	0.19	0.13	0.29	0.13	-
2745	RGB	76.5	4849	2.24	1.45	-1.24	0.10	0.37	0.13	0.19	0.10	-
3114	RGB	77.1	4801	2.15	0.93	-1.14	0.10	0.30	0.11	0.36	0.11	32151
3258	RGB	73.2	4741	2.19	1.26	-1.22	0.09	0.54	0.11	0.21	0.11	32121
4361	RGB	70.0	4777	2.23	1.25	-1.18	0.10	0.33	0.11	0.48	0.10	33900
4496	RGB	73.5	4758	2.05	1.21	-1.14	0.11	0.29	0.15	0.28	0.11	29222
4806	RGB	68.7	4718	2.05	1.36	-1.16	0.10	0.69	0.10	-0.11	0.10	29027
4938	RGB	76.8	4607	1.72	1.22	-1.24	0.11	0.51	0.12	0.44	0.11	34726
5965	RGB	71.4	4673	1.89	1.36	-1.11	0.11	0.14	0.13	0.55	0.15	29282
6978	RGB	68.5	4736	2.14	1.13	-1.11	0.10	0.48	0.10	0.30	0.10	30450

7076	RGB	67.6	4550	1.69	1.38	-1.17	0.11	0.67	0.13	0.12	0.11	32317
7081	RGB	70.4	4859	2.21	1.62	-1.17	0.09	0.24	0.10	0.27	0.09	33617
7298	RGB	71.4	4879	2.35	1.26	-1.14	0.10	0.43	0.11	-0.12	0.11	29272
7526	RGB	75.9	5134	2.90	1.35	-1.21	0.13	0.41	0.15	0.40	0.13	-
7634	RGB	68.4	5086	2.92	1.02	-1.11	0.12	0.52	0.12	-0.03	0.12	-
7672	RGB	67.5	5114	3.06	0.81	-1.07	0.11	0.48	0.12	0.10	0.11	-
7973	RGB	69.8	4229	1.13	1.48	-1.23	0.12	0.28	0.13	0.66	0.15	-
8099	RGB	73.6	4761	2.26	1.01	-1.05	0.12	0.37	0.14	0.01	0.12	-
8460	RGB	70.0	5075	2.80	1.03	-1.13	0.11	0.46	0.12	0.28	0.12	-
8602	RGB	71.0	4836	2.55	1.15	-1.16	0.12	0.62	0.15	-0.03	0.13	5359
8803	RGB	64.4	4356	1.26	1.26	-1.15	0.10	0.17	0.15	0.57	0.10	34006
9040	RGB	77.4	4514	1.58	1.36	-1.12	0.12	0.40	0.14	0.11	0.13	35774
9156	RGB	68.2	5040	2.73	1.14	-1.07	0.11	0.22	0.12	0.32	0.14	-
10801	RGB	69.4	4605	1.69	1.13	-1.15	0.11	0.27	0.12	0.43	0.12	34130
10928	RGB	66.3	4323	1.28	2.26	-1.22	0.08	0.64	0.08	-0.05	0.10	29693
12387	RGB	69.4	4718	2.05	0.86	-1.10	0.09	0.53	0.13	0.05	0.10	30653
13170	RGB	77.4	4859	2.39	1.00	-1.05	0.08	0.31	0.10	0.04	0.13	29848
13179	RGB	70.9	4423	1.41	1.27	-1.20	0.12	0.53	0.13	0.24	0.12	-
14037	RGB	76.8	4457	1.59	1.46	-1.12	0.08	0.45	0.11	-0.09	0.08	30598
14350	RGB	77.4	4600	1.79	1.39	-1.21	0.10	0.38	0.12	0.48	0.13	-
14377	RGB	70.6	4704	1.90	1.46	-1.13	0.09	0.42	0.11	0.38	0.10	-
15010	RGB	66.2	4504	1.60	1.10	-1.14	0.10	0.66	0.15	0.09	0.10	34240

16053	RGB	69.7	4925	2.27	1.64	-1.15	0.11	0.24	0.11	0.32	0.11	36356
16788	RGB	66.1	3954	0.36	1.44	-1.19	0.11	0.29	0.12	0.52	0.11	-
17095	RGB	71.5	4851	2.14	1.63	-1.17	0.09	0.07	0.11	0.62	0.10	31376
17461	RGB	68.2	3828	0.44	1.83	-1.23	0.11	0.55	0.11	0.18	0.11	-
22578	RGB	65.9	4688	1.98	1.53	-1.17	0.09	0.64	0.12	-0.02	0.10	29065
23196	RGB	68.9	4671	1.98	1.13	-1.16	0.10	0.53	0.15	0.37	0.12	28977
25011	RGB	70.3	4865	2.24	0.90	-1.05	0.11	0.12	0.12	0.51	0.11	30933
29983	RGB	66.3	4970	2.64	1.04	-1.13	0.11	0.43	0.13	0.46	0.11	-
31696	RGB	70.6	4313	1.29	1.39	-1.19	0.11	0.31	0.14	0.64	0.16	21191
32412	RGB	74.3	4956	2.52	1.21	-1.09	0.11	0.32	0.16	0.25	0.11	-
33040	RGB	69.1	5056	2.74	1.04	-1.10	0.11	0.50	0.13	0.10	0.11	-
33060	RGB	72.9	5112	2.92	1.17	-1.17	0.12	0.56	0.13	0.10	0.13	-
33152	RGB	74.8	4674	2.09	1.39	-1.24	0.11	0.64	0.13	0.17	0.12	-
33480	RGB	71.4	4839	2.24	1.34	-1.21	0.11	0.57	0.12	-0.09	0.11	-
33654	RGB	76.5	4505	1.64	1.29	-1.20	0.12	0.48	0.14	0.49	0.12	-
34336	RGB	70.8	5140	3.05	1.26	-1.14	0.11	0.26	0.12	0.34	0.12	-
34423	RGB	65.4	4907	2.50	1.10	-1.17	0.11	0.48	0.12	0.29	0.11	-
34725	RGB	70.0	5095	2.85	1.65	-1.15	0.11	0.52	0.12	-0.06	0.11	-
35072	RGB	70.7	4999	2.86	1.06	-1.15	0.12	0.45	0.13	0.30	0.12	-
36015	RGB	69.6	5022	2.69	0.89	-1.12	0.10	0.48	0.10	-0.03	0.10	-
36781	RGB	72.3	4817	2.20	1.20	-1.19	0.10	0.41	0.12	0.29	0.10	24590
37542	RGB	70.3	5095	2.96	1.26	-1.10	0.12	0.24	0.13	0.37	0.12	-

38229	RGB	70.3	4743	2.02	1.32	-1.17	0.11	0.25	0.12	0.34	0.11	25709
39273	RGB	73.0	4869	2.30	1.05	-1.12	0.11	0.47	0.14	0.13	0.13	26471
40856	RGB	69.6	4361	1.55	1.55	-1.22	0.11	0.73	0.12	0.05	0.11	27448
41863	RGB	66.7	5072	2.87	1.12	-1.14	0.12	0.39	0.15	0.42	0.12	-
42611	RGB	66.6	4262	1.24	1.59	-1.24	0.12	0.50	0.14	0.40	0.12	-
43859	RGB	72.9	4866	2.47	1.17	-1.19	0.11	0.33	0.15	0.19	0.11	29598
45171	RGB	77.6	5018	2.81	1.21	-1.17	0.11	0.64	0.12	0.09	0.11	-
45284	RGB	68.4	4588	1.75	1.06	-1.09	0.12	0.26	0.14	0.33	0.12	30711
45534	RGB	69.1	5150	3.03	1.18	-1.17	0.11	0.59	0.13	0.00	0.12	-
45700	RGB	70.7	5207	2.93	0.93	-1.10	0.10	0.26	0.15	0.23	0.10	-
47603	RGB	70.3	5251	3.01	1.26	-1.14	0.11	0.50	0.12	0.21	0.12	-
48035	RGB	68.0	4759	1.94	1.15	-1.11	0.12	0.27	0.12	0.06	0.13	32874
48370	RGB	68.4	5080	3.03	0.85	-1.18	0.12	0.43	0.13	0.47	0.12	-
48477	RGB	63.4	4753	2.19	1.20	-1.12	0.10	0.33	0.11	0.11	0.11	33195
48627	RGB	72.2	5212	3.13	1.09	-1.05	0.11	0.32	0.11	0.16	0.11	-
49055	RGB	74.2	4976	2.51	1.16	-1.07	0.10	0.31	0.11	0.35	0.10	33629
49190	RGB	70.1	5018	2.77	1.03	-1.14	0.11	0.53	0.11	0.00	0.14	-
49332	RGB	67.7	5136	2.95	1.02	-1.11	0.10	0.43	0.11	-0.07	0.10	-
49470	RGB	64.4	5118	2.94	1.22	-1.19	0.11	0.52	0.11	-0.01	0.12	-
57927	RGB	72.3	5109	2.91	1.28	-1.12	0.12	0.23	0.12	0.28	0.12	-
58093	RGB	66.6	4734	2.18	1.40	-1.13	0.11	0.46	0.11	-0.01	0.11	38383
59237	RGB	74.2	4839	2.35	1.48	-1.09	0.12	0.23	0.14	0.37	0.12	38896

59373	RGB	68.0	5042	2.73	1.01	-1.07	0.11	0.30	0.13	0.30	0.11	-
59950	RGB	70.1	5237	3.11	1.08	-1.02	0.07	0.14	0.08	0.33	0.08	-
62781	RGB	83.9	4982	2.70	1.20	-1.18	0.11	0.49	0.14	0.24	0.12	-
63624	RGB	69.2	4659	2.08	1.38	-1.20	0.10	0.46	0.13	0.40	0.10	42620
65008	RGB	71.1	4950	2.54	1.33	-1.20	0.10	0.34	0.12	0.35	0.10	44243
65302	RGB	66.2	4826	2.13	1.45	-1.15	0.11	0.23	0.11	0.41	0.11	44595
65790	RGB	73.2	4911	2.29	1.28	-1.11	0.11	0.13	0.15	0.36	0.11	45163
66385	RGB	70.4	4816	2.18	1.35	-1.14	0.10	0.34	0.11	0.11	0.13	45895
67398	RGB	70.8	5268	3.07	1.23	-1.05	0.11	0.37	0.12	-0.06	0.12	-
67553	RGB	65.8	5112	2.84	1.25	-1.09	0.11	0.28	0.12	0.27	0.11	-
67586	RGB	70.6	5168	2.94	1.24	-1.05	0.12	0.29	0.13	0.15	0.13	-
68085	RGB	73.1	4950	2.48	1.19	-1.07	0.11	0.26	0.12	0.43	0.11	-
68452	RGB	66.4	4982	2.32	1.34	-1.09	0.12	0.09	0.15	0.36	0.12	-
KEP10	RGB	73.7	4934	2.58	1.07	-1.16	0.11	0.63	0.11	-0.07	0.11	-
KEP14	RGB	71.9	4860	2.33	1.27	-1.19	0.11	0.37	0.11	0.29	0.12	35022
KEP16	RGB	66.8	4852	2.41	1.14	-1.21	0.11	0.65	0.11	0.04	0.11	35061
KEP17	RGB	74.0	4876	2.52	1.16	-1.27	0.10	0.63	0.11	0.03	0.10	-
KEP20	RGB	70.8	4664	2.11	1.47	-1.19	0.11	0.59	0.12	-0.05	0.11	35455
KEP21	RGB	67.4	4856	2.35	1.25	-1.18	0.11	0.31	0.12	0.46	0.12	35487
KEP22	RGB	72.9	4839	2.38	1.20	-1.23	0.11	0.45	0.14	0.41	0.11	35508
KEP29	RGB	70.6	4990	2.58	1.10	-1.11	0.10	0.43	0.11	-0.11	0.10	-
KEP31	RGB	67.3	4907	2.50	0.85	-1.21	0.12	0.56	0.12	0.24	0.13	-

KEP32	RGB	67.1	4957	2.65	0.92	-1.19	0.11	0.42	0.13	0.40	0.11	-
KEP35	RGB	69.1	4849	2.30	1.08	-1.19	0.11	0.43	0.12	0.55	0.11	36929
KEP36	RGB	77.0	4830	2.39	1.28	-1.22	0.12	0.49	0.12	0.08	0.12	36942
788	AGB	67.4	4858	1.78	1.48	-1.20	0.12	0.54	0.13	-0.07	0.12	-
3590	AGB	74.7	4860	1.81	1.47	-1.27	0.10	0.53	0.14	0.18	0.13	-
10092	AGB	73.2	4987	1.94	1.19	-1.14	0.11	0.52	0.12	-0.07	0.12	-
11285	AGB	71.3	5157	2.42	1.54	-1.12	0.09	0.35	0.11	0.11	0.10	-
13609	AGB	71.1	5198	2.31	1.39	-1.18	0.10	0.44	0.11	0.01	0.11	-
15167	AGB	69.9	4946	1.89	1.44	-1.22	0.12	0.40	0.13	0.23	0.12	-
16547	AGB	69.0	4847	1.90	1.34	-1.15	0.11	0.45	0.12	0.15	0.14	-
18573	AGB	72.2	4633	1.81	1.90	-1.20	0.09	0.57	0.14	-0.12	0.09	-
20089	AGB	75.4	5129	2.10	1.69	-1.21	0.12	0.47	0.12	0.24	0.12	-
37349	AGB	67.7	4876	1.80	1.45	-1.16	0.12	0.39	0.12	0.22	0.12	-
41504	AGB	65.9	4548	1.48	1.63	-1.21	0.11	0.52	0.16	0.25	0.11	-
43597	AGB	68.0	4720	1.66	1.78	-1.22	0.11	0.43	0.13	0.22	0.11	29397
46211	AGB	68.3	4635	1.66	1.28	-1.07	0.11	0.49	0.12	0.06	0.12	-
46676	AGB	74.0	4666	1.77	1.52	-1.22	0.11	0.62	0.16	-0.12	0.12	-
46773	AGB	73.8	4598	1.68	1.58	-1.21	0.11	0.58	0.11	0.04	0.12	-

TABLE A.2: Final stellar parameters and abundance results from Chapter 3. Abundances are presented as $\log\epsilon = \log(\mathrm{N_X}/\mathrm{N_H}) + 12$, where X represents each species. The σ values are based on line-to-line abundance scatter only. The NLTE corrections to the LTE sodium abundances are given in the third last column.

ID	Type	$T_{\rm eff}$ (K)	$\log g$ (dex)	Xi (km/s)	Fe I (dex)	σ (dex)	Fe II (dex)	σ (dex)	Na $\mathrm{I_{LTE}}$ (dex)	σ (dex)	$\mathrm{Corr}_{Na\,I}$ (dex)	Na $\mathrm{I_{NLTE}}$ (dex)	σ (dex)
22	AGB	4641	1.31	1.80	6.01	0.11	5.92	0.06	4.83	0.06	-0.08	4.75	0.05
25	AGB	4492	1.09	1.87	6.07	0.10	6.03	0.11	4.56	0.10	-0.05	4.51	0.11
31	AGB	4537	1.20	1.83	6.08	0.11	5.99	0.09	4.52	0.04	-0.05	4.47	0.03
44	AGB	4679	1.43	1.76	6.03	0.12	6.03	0.13	4.52	0.01	-0.06	4.46	0.00
52	AGB	4862	1.68	1.68	5.96	0.10	6.01	0.16	4.70	0.04	-0.08	4.61	0.03
53	AGB	4790	1.57	1.72	5.99	0.08	6.01	0.07	4.76	0.03	-0.08	4.68	0.02
59	AGB	4804	1.61	1.70	5.92	0.10	5.94	0.08	4.71	0.03	-0.08	4.62	0.02
60	AGB	4776	1.57	1.72	6.12	0.12	6.05	0.12	4.54	0.00	-0.07	4.47	0.01
61	AGB	4834	1.63	1.70	6.04	0.10	6.01	0.09	4.73	0.04	-0.08	4.65	0.02
65	AGB	4705	1.43	1.76	6.00	0.10	6.02	0.05	4.95	0.05	-0.09	4.86	0.05
75	AGB	4816	1.67	1.68	5.91	0.07	6.05	0.11	4.50	0.01	-0.07	4.44	0.00
76	AGB	4970	1.76	1.65	5.92	0.11	5.97	0.09	4.89	0.14	-0.08	4.80	0.15
78	AGB	4948	1.76	1.65	5.93	0.12	5.97	0.10	4.86	0.04	-0.09	4.77	0.02
80	AGB	4893	1.75	1.66	5.95	0.09	6.07	0.07	4.59	0.04	-0.07	4.51	0.03
83	AGB	4932	1.76	1.65	5.96	0.09	6.03	0.15	4.71	0.01	-0.09	4.63	0.00

94	AGB	4969	1.83	1.63	5.90	0.07	6.08	0.10	4.73	0.07	-0.09	4.64	0.06
97	AGB	5048	1.89	1.61	5.92	0.10	6.06	0.08	4.78	0.02	-0.09	4.69	0.03
104	AGB	4895	1.79	1.64	5.94	0.10	6.07	0.19	4.48	0.00	-0.07	4.41	0.00
201620	AGB	5019	1.83	1.63	6.01	0.11	6.01	0.04	4.84	0.01	-0.09	4.75	0.02
12	RGB	4348	1.10	1.87	6.09	0.12	5.92	0.09	5.10	0.05	-0.08	5.01	0.07
23	RGB	4404	1.19	1.84	6.09	0.10	6.12	0.02	5.12	0.08	-0.09	5.04	0.04
27	RGB	4453	1.30	1.80	6.08	0.13	6.13	0.04	4.77	0.18	-0.06	4.70	0.18
29	RGB	4362	1.13	1.86	6.07	0.11	6.07	0.17	4.67	0.04	-0.06	4.61	0.05
30	RGB	4362	1.10	1.87	6.09	0.12	5.93	0.11	5.10	0.18	-0.09	5.01	0.13
35	RGB	4490	1.37	1.78	6.09	0.12	6.05	0.05	5.39	0.13	-0.11	5.28	0.08
43	RGB	4469	1.37	1.78	6.04	0.09	5.99	0.07	5.45	0.11	-0.12	5.33	0.04
50	RGB	4436	1.27	1.81	6.11	0.12	6.08	0.16	4.95	0.06	-0.09	4.86	0.03
54	RGB	4571	1.51	1.73	6.18	0.11	6.08	0.15	4.94	0.03	-0.09	4.85	0.03
64	RGB	4467	1.36	1.78	6.07	0.09	5.98	0.11	5.39	0.15	-0.12	5.27	0.08
91	RGB	4641	1.75	1.66	5.99	0.12	6.01	0.12	5.10	0.06	-0.09	5.01	0.06
92	RGB	4672	1.73	1.66	6.12	0.11	6.02	0.13	4.72	0.11	-0.08	4.64	0.12
107	RGB	4681	1.83	1.63	6.07	0.12	5.99	0.10	5.03	0.08	-0.09	4.94	0.09
129	RGB	4738	1.94	1.60	6.03	0.12	6.08	0.20	5.04	0.05	-0.10	4.94	0.06
155	RGB	4752	2.00	1.58	6.02	0.13	6.01	0.09	4.62	0.01	-0.08	4.54	0.02
161	RGB	4852	2.07	1.55	6.14	0.09	6.05	0.10	5.23	0.06	-0.12	5.11	0.04
170	RGB	4792	2.07	1.55	6.07	0.14	6.05	0.08	5.40	0.08	-0.12	5.27	0.02
186	RGB	4832	2.13	1.54	6.02	0.15	5.99	0.13	4.63	0.06	-0.08	4.54	0.04

193	RGB	4854	2.14	1.53	6.06	0.14	6.11	0.08	4.58	0.00	-0.08	4.50	0.01
262	RGB	4873	2.25	1.50	6.03	0.09	5.92	0.04	5.17	0.04	-0.12	5.06	0.01
276	RGB	4864	2.25	1.50	5.99	0.09	6.02	0.08	5.20	0.10	-0.12	5.08	0.06
200619	RGB	4731	1.91	1.61	6.02	0.07	6.06	0.09	5.41	0.01	-0.08	5.33	0.01

TABLE A.3: Complete version of Table 4.1 (Chapter 4). NGC 6397 target details including data from Momany et al. (2003, $UBVI$ photometry and target IDs) and 2MASS (Skrutskie et al., 2006, JHK photometry – gaps in data represent targets with low quality flags), radial velocities (km/s), and Lind et al. (2011b, L11) IDs.

ID	Type	2MASS ID	L11 ID	V Mag	B Mag	U Mag	I Mag	J Mag	H Mag	K Mag	RV (km/s)
56897	AGB	17400665-5335001	-	11.83	12.76	10.59	13.11	9.76	9.25	9.13	17.17
60609	AGB	17402547-5347570	-	11.65	12.62	10.37	12.97	-	-	-	20.68
70509	AGB	17405254-5341049	-	11.98	12.90	10.75	13.17	9.95	9.48	9.31	19.38
70522	AGB	17404076-5341046	-	11.16	12.24	9.79	12.80	8.94	8.37	8.26	18.93
73216	AGB	17403510-5339572	-	11.83	12.76	10.57	13.11	-	-	-	16.00
77677	AGB	17411334-5337333	-	12.11	13.01	10.92	13.24	10.14	9.68	9.47	25.96
80621	AGB	17403507-5335244	-	10.93	12.07	9.51	12.80	-	-	-	22.30
88626	AGB	17421570-5343061	-	11.34	12.34	9.98	-	9.28	8.71	8.58	18.91
1	RGB	17415348-5333253	-	10.41	11.71	-	-	8.10	7.48	7.30	16.41
51303	RGB	17402016-5342018	-	10.03	11.38	10.87	-	7.18	6.43	6.28	18.95
63530	RGB	17403892-5345252	-	10.34	11.65	8.85	12.76	7.82	7.14	6.97	25.52
72403	RGB	17404812-5340173	-	10.71	11.94	9.25	12.71	8.34	7.66	7.56	17.66
78315	RGB	17402792-5337093	-	10.71	11.94	9.24	12.83	8.27	7.59	7.47	14.71
90214	RGB	17414840-5340354	-	10.72	11.98	9.24	12.81	8.33	7.69	7.55	20.89
4713	RGB	17421338-5323369	-	12.18	13.18	10.81	-	10.03	9.46	9.36	23.41
10500	RGB	17404013-5330589	-	11.53	12.59	10.19	13.10	9.28	8.67	8.55	20.74

11294	RGB	17404627-5328593	-	12.52	13.43	11.30	13.71	10.48	9.97	9.80	24.09
47857	RGB	17400217-5346314	-	12.59	13.53	11.36	13.76	10.59	10.08	9.95	20.60
50306	RGB	17401283-5343118	10737	12.64	13.57	11.39	13.84	10.57	10.01	9.94	20.85
50691	RGB	17402051-5342443	-	12.09	13.07	10.81	13.44	10.00	9.39	9.31	19.17
50865	RGB	17400727-5342321	-	11.17	12.27	9.79	12.85	8.91	8.36	8.22	28.69
52638	RGB	17400658-5340283	8952	12.54	13.48	11.31	13.76	10.46	9.91	9.85	18.24
52830	RGB	17401526-5340149	-	11.48	12.56	10.14	13.09	9.26	8.70	8.54	19.23
53189	RGB	17400552-5339493	-	12.20	13.18	10.94	13.52	10.07	9.51	9.40	20.32
53514	RGB	17401170-5339263	-	12.65	13.59	11.42	13.88	10.55	9.99	9.95	22.29
53724	RGB	17395249-5339111	5644	11.91	12.91	10.61	13.32	9.75	9.17	9.03	17.35
56692	RGB	17395992-5335191	-	12.22	13.17	10.96	13.53	10.10	9.55	9.45	16.76
56909	RGB	17393096-5334586	-	12.63	13.55	11.41	13.80	10.62	10.06	9.94	19.70
59968	RGB	17410477-5348277	-	11.52	12.59	10.19	13.03	9.50	8.88	8.76	20.56
60842	RGB	17404572-5347455	-	12.29	13.25	11.04	13.49	10.34	9.84	9.69	20.06
62839	RGB	17404903-5346017	-	12.64	13.58	11.41	13.79	10.64	10.10	9.99	21.00
63725	RGB	17410282-5345153	-	11.78	12.82	10.47	13.20	9.68	9.18	8.99	20.27
64858	RGB	17403378-5344202	-	12.22	13.19	10.95	13.51	10.14	9.60	9.50	12.25
64898	RGB	17405228-5344177	-	12.27	13.24	11.01	13.54	10.22	9.72	9.58	23.26
65146	RGB	17404476-5344058	-	11.65	12.69	10.32	13.09	9.51	8.95	8.81	19.53
67328	RGB	17404661-5342414	-	12.62	13.54	11.39	13.78	10.60	10.12	9.93	20.44
67793	RGB	17403068-5342258	17163	12.12	13.09	10.84	13.44	10.00	9.46	9.35	14.71
68173	RGB	17410347-5342121	-	12.62	13.57	11.38	13.83	10.56	10.07	9.93	21.65

68813	RGB	17404024-5341526	-	12.58	13.52	11.35	13.77	10.43	9.91	9.80	18.54
70613	RGB	17402849-5341018	-	12.60	13.53	11.36	13.80	10.56	10.03	9.92	19.32
70878	RGB	17403681-5340546	-	12.62	13.54	11.40	13.79	10.63	10.06	9.98	14.42
71843	RGB	17403275-5340313	-	11.99	12.99	10.70	13.39	9.88	9.30	9.17	9.10
72149	RGB	17402687-5340236	-	12.53	13.48	11.29	13.74	10.45	9.91	9.82	16.61
73589	RGB	17405736-5339473	-	10.99	12.17	9.54	12.91	8.63	8.03	7.89	23.83
73660	RGB	17404777-5339454	-	11.53	12.60	10.18	13.10	-	-	-	13.83
73832	RGB	17410346-5339398	-	11.53	12.61	10.18	13.12	9.31	8.71	8.59	9.82
74162	RGB	17404350-5339310	-	11.42	12.50	10.06	13.04	9.20	8.60	8.51	16.21
74293	RGB	17405400-5339270	-	12.30	13.24	11.06	13.55	10.24	9.72	9.56	24.29
74668	RGB	17410910-5339144	-	11.18	12.32	9.78	12.95	8.88	8.26	8.14	15.25
76048	RGB	17402864-5338323	16405	11.78	12.81	10.44	13.30	9.60	8.99	8.84	13.96
76528	RGB	17410415-5338161	-	12.60	13.55	11.37	13.82	10.53	10.06	9.90	19.48
77708	RGB	17410896-5337324	-	12.34	13.31	11.09	13.63	10.26	9.72	9.57	18.22
78490	RGB	17405674-5337019	-	12.51	13.45	11.26	13.74	10.44	9.90	9.76	22.56
79170	RGB	17404680-5336326	-	12.61	13.53	11.37	13.82	10.52	10.02	9.90	20.26
79458	RGB	17411610-5336187	-	12.33	13.31	11.09	13.59	10.29	9.74	9.59	20.89
87538	RGB	17421217-5344440	-	11.59	12.64	10.25	13.06	9.53	8.93	8.80	23.81
88524	RGB	17414264-5343174	-	11.93	12.94	10.65	13.30	9.88	9.32	9.20	18.56

TABLE A.4: Complete version of Table 4.5 (Chapter 4). Stellar parameters, and derived chemical abundances for each star in NGC 6397. Abundance uncertainties reflect line-to-line scatter (1σ), and do not take atmospheric sensitivities into account. We adopt the Asplund et al. (2009) solar abundance values.

ID	Type	$T_{\rm eff}$ (K)	log g (cgs)	$v_{\rm t}$ (km/s)	[Fe I/H]	[Fe II/H]	[O/H]	[Na/H]	[Mg/H]	[Al/H]
56897	AGB	4978	1.80	1.64	-2.13 ± 0.06	-2.00 ± 0.02	-1.64 ± 0.01	-1.92 ± 0.01	-1.84 ± 0.04	-1.32 ± 0.03
60609	AGB	4905	1.70	1.67	-2.23 ± 0.07	-2.06 ± 0.01	-1.45 ± 0.04	-1.98 ± 0.01	-2.02 ± 0.01	-1.37 ± 0.01
70509	AGB	5017	1.88	1.61	-2.18 ± 0.06	-2.07 ± 0.04	-1.49 ± 0.04	-2.15 ± 0.01	-1.79 ± 0.05	-1.53 ± 0.04
70522	AGB	4739	1.42	1.76	-2.24 ± 0.05	-2.06 ± 0.03	-1.63 ± 0.02	-1.94 ± 0.04	-1.99 ± 0.08	-1.48 ± 0.06
73216	AGB	4968	1.80	1.64	-2.16 ± 0.05	-2.04 ± 0.00	-1.39 ± 0.06	-2.29 ± 0.04	-1.73 ± 0.05	-1.67 ± 0.03
77677	AGB	5058	1.95	1.59	-2.19 ± 0.06	-2.02 ± 0.01	-1.37 ± 0.01	-2.29 ± 0.05	-1.80 ± 0.04	-1.66 ± 0.05
80621	AGB	4551	1.22	1.83	-2.28 ± 0.05	-2.10 ± 0.04	-1.50 ± 0.02	-2.00 ± 0.00	-2.08 ± 0.01	-1.46 ± 0.02
88626	AGB	4885	1.56	1.72	-2.14 ± 0.10	-2.03 ± 0.04	-1.71 ± 0.05	-1.89 ± 0.03	-1.97 ± 0.02	-1.32 ± 0.02
1	RGB	4458	1.01	1.89	-2.16 ± 0.06	-2.06 ± 0.03	-1.40 ± 0.05	-2.22 ± 0.01	-1.90 ± 0.05	-1.72 ± 0.03
51303	RGB	4174	0.67	2.00	-2.21 ± 0.07	-1.99 ± 0.02	-1.42 ± 0.00	-1.77 ± 0.01	-2.10 ± 0.06	-1.33 ± 0.04
63530	RGB	4337	0.91	1.93	-2.24 ± 0.08	-2.03 ± 0.04	-1.34 ± 0.01	-2.07 ± 0.03	-1.94 ± 0.04	-1.40 ± 0.03
72403	RGB	4497	1.16	1.85	-2.20 ± 0.05	-2.07 ± 0.03	-1.57 ± 0.02	-2.30 ± 0.07	-1.86 ± 0.00	-1.68 ± 0.06
78315	RGB	4445	1.13	1.86	-2.24 ± 0.06	-2.02 ± 0.03	-1.37 ± 0.05	-2.06 ± 0.06	-2.08 ± 0.06	-1.45 ± 0.03
90214	RGB	4467	1.14	1.85	-2.19 ± 0.07	-2.07 ± 0.03	-1.38 ± 0.03	-2.28 ± 0.06	-1.85 ± 0.02	-1.78 ± 0.03
4713	RGB	4849	1.94	1.60	-2.14 ± 0.06	-1.94 ± 0.03	-1.52 ± 0.03	-2.24 ± 0.08	-1.86 ± 0.02	-1.64 ± 0.01

10500	RGB	4704	1.61	1.70	-2.15 ± 0.07	-2.01 ± 0.05	-1.44 ± 0.05	-2.46 ± 0.10	-1.80 ± 0.05	-1.68 ± 0.00
11294	RGB	4983	2.14	1.53	-2.13 ± 0.06	-1.97 ± 0.05	-1.68 ± 0.03	-1.77 ± 0.06	-1.96 ± 0.01	-1.24 ± 0.02
47857	RGB	5017	2.18	1.52	-2.13 ± 0.10	-2.04 ± 0.04	-1.38 ± 0.01	-2.15 ± 0.03	-1.77 ± 0.05	-1.61 ± 0.08
50306	RGB	4973	2.18	1.52	-2.10 ± 0.06	-1.98 ± 0.05	-1.43 ± 0.06	-1.95 ± 0.00	-1.87 ± 0.05	-1.43 ± 0.10
50691	RGB	4884	1.92	1.60	-2.12 ± 0.04	-1.99 ± 0.05	-1.58 ± 0.02	-1.92 ± 0.00	-1.92 ± 0.10	-1.35 ± 0.02
50865	RGB	4688	1.45	1.75	-2.18 ± 0.07	-1.99 ± 0.03	-1.24 ± 0.02	-2.25 ± 0.09	-1.72 ± 0.02	-1.73 ± 0.06
52638	RGB	4968	2.14	1.53	-2.13 ± 0.07	-2.04 ± 0.02	-1.40 ± 0.02	-1.96 ± 0.08	-1.79 ± 0.10	-1.45 ± 0.05
52830	RGB	4711	1.59	1.71	-2.20 ± 0.06	-2.03 ± 0.03	-1.38 ± 0.04	-2.14 ± 0.04	-1.81 ± 0.04	-1.74 ± 0.05
53189	RGB	4869	1.96	1.59	-2.19 ± 0.06	-2.02 ± 0.03	-1.45 ± 0.04	-2.13 ± 0.04	-1.72 ± 0.01	-1.59 ± 0.01
53514	RGB	4964	2.18	1.52	-2.15 ± 0.08	-2.04 ± 0.03	-1.72 ± 0.01	-1.95 ± 0.02	-1.85 ± 0.07	-1.39 ± 0.06
53724	RGB	4805	1.81	1.64	-2.12 ± 0.06	-2.00 ± 0.00	-1.33 ± 0.06	-2.39 ± 0.05	-1.76 ± 0.03	-1.78 ± 0.08
56692	RGB	4912	1.98	1.58	-2.11 ± 0.13	-2.01 ± 0.00	-1.60 ± 0.02	-2.02 ± 0.06	-1.90 ± 0.06	-1.42 ± 0.05
56909	RGB	5004	2.19	1.51	-2.13 ± 0.07	-1.99 ± 0.03	-1.73 ± 0.05	-1.88 ± 0.03	-1.93 ± 0.09	-1.32 ± 0.03
59968	RGB	4823	1.66	1.69	-2.05 ± 0.08	-2.01 ± 0.02	-1.47 ± 0.05	-1.95 ± 0.03	-1.87 ± 0.05	-1.37 ± 0.04
60842	RGB	5025	2.06	1.56	-2.09 ± 0.08	-2.03 ± 0.00	-1.49 ± 0.03	-2.39 ± 0.04	-1.79 ± 0.05	-1.62 ± 0.07
62839	RGB	5005	2.20	1.51	-2.16 ± 0.07	-2.02 ± 0.01	-1.61 ± 0.06	-1.99 ± 0.01	-1.89 ± 0.05	-1.26 ± 0.08
63725	RGB	4831	1.77	1.65	-2.09 ± 0.07	-1.99 ± 0.04	-1.43 ± 0.03	-2.16 ± 0.01	-1.69 ± 0.00	-1.74 ± 0.07
64858	RGB	4933	1.99	1.58	-2.11 ± 0.06	-1.96 ± 0.04	-1.78 ± 0.04	-1.72 ± 0.06	-1.98 ± 0.04	-1.22 ± 0.04
64898	RGB	4950	2.02	1.57	-2.15 ± 0.07	-1.99 ± 0.05	-1.68 ± 0.01	-1.88 ± 0.04	-2.00 ± 0.04	-1.39 ± 0.05
65146	RGB	4802	1.70	1.67	-2.22 ± 0.08	-2.03 ± 0.02	-1.46 ± 0.03	-2.45 ± 0.02	-1.87 ± 0.03	-1.77 ± 0.04
67328	RGB	5002	2.18	1.52	-2.12 ± 0.08	-1.97 ± 0.01	-1.60 ± 0.03	-1.88 ± 0.05	-1.99 ± 0.03	-1.25 ± 0.04
67793	RGB	4892	1.94	1.60	-2.15 ± 0.06	-2.00 ± 0.03	-1.52 ± 0.04	-1.91 ± 0.02	-1.89 ± 0.03	-1.44 ± 0.06

68173	RGB	4965	2.17	1.52	-2.17 ± 0.08	-2.02 ± 0.04	-1.48 ± 0.01	-2.04 ± 0.04	-1.82 ± 0.04	-1.44 ± 0.02
68813	RGB	4924	2.14	1.53	-2.12 ± 0.08	-2.02 ± 0.04	-1.56 ± 0.04	-1.92 ± 0.05	-1.90 ± 0.06	-1.47 ± 0.06
70613	RGB	4991	2.17	1.52	-2.14 ± 0.09	-2.03 ± 0.06	-1.68 ± 0.03	-1.96 ± 0.07	-1.92 ± 0.00	-1.20 ± 0.04
70878	RGB	5032	2.20	1.51	-2.12 ± 0.06	-2.04 ± 0.04	-1.69 ± 0.01	-2.08 ± 0.02	-1.84 ± 0.03	-1.58 ± 0.06
71843	RGB	4850	1.86	1.62	-2.16 ± 0.08	-2.03 ± 0.00	-1.69 ± 0.06	-1.87 ± 0.04	-1.85 ± 0.02	-1.53 ± 0.06
72149	RGB	4955	2.13	1.53	-2.11 ± 0.06	-2.00 ± 0.01	-1.50 ± 0.03	-2.29 ± 0.06	-1.73 ± 0.02	-1.60 ± 0.04
73589	RGB	4552	1.30	1.80	-2.24 ± 0.05	-2.04 ± 0.02	-1.64 ± 0.01	-1.85 ± 0.02	-2.12 ± 0.09	-1.30 ± 0.05
73660	RGB	4673	1.59	1.71	-2.12 ± 0.07	-2.02 ± 0.03	-1.58 ± 0.01	-2.29 ± 0.08	-1.63 ± 0.09	-1.63 ± 0.04
73832	RGB	4710	1.61	1.70	-2.20 ± 0.05	-2.02 ± 0.02	-1.77 ± 0.04	-1.84 ± 0.02	-1.93 ± 0.06	-1.49 ± 0.06
74162	RGB	4727	1.57	1.71	-2.20 ± 0.07	-2.01 ± 0.01	-1.51 ± 0.04	-2.04 ± 0.04	-1.86 ± 0.03	-1.50 ± 0.06
74293	RGB	4945	2.03	1.57	-2.13 ± 0.07	-2.01 ± 0.01	-1.60 ± 0.04	-1.79 ± 0.01	-1.79 ± 0.05	-1.46 ± 0.05
74668	RGB	4610	1.41	1.77	-2.22 ± 0.05	-2.00 ± 0.05	-1.45 ± 0.07	-2.07 ± 0.06	-1.82 ± 0.04	-1.53 ± 0.06
76048	RGB	4761	1.73	1.66	-2.19 ± 0.07	-2.06 ± 0.02	-1.51 ± 0.04	-1.85 ± 0.02	-1.92 ± 0.03	-1.42 ± 0.07
76528	RGB	4960	2.16	1.52	-2.13 ± 0.07	-2.02 ± 0.05	-1.57 ± 0.02	-2.02 ± 0.01	-1.85 ± 0.10	-1.32 ± 0.03
77708	RGB	4900	2.03	1.57	-2.12 ± 0.07	-1.96 ± 0.01	-1.50 ± 0.02	-2.07 ± 0.05	-1.99 ± 0.07	-1.43 ± 0.06
78490	RGB	4941	2.11	1.54	-2.10 ± 0.04	-2.00 ± 0.04	-1.51 ± 0.05	-2.30 ± 0.03	-1.82 ± 0.03	-1.69 ± 0.04
79170	RGB	4978	2.17	1.52	-2.10 ± 0.07	-1.97 ± 0.01	-1.47 ± 0.01	-1.94 ± 0.05	-1.95 ± 0.01	-1.32 ± 0.07
79458	RGB	4910	2.03	1.57	-2.16 ± 0.08	-1.98 ± 0.04	-1.46 ± 0.03	-2.11 ± 0.01	-1.81 ± 0.03	-1.47 ± 0.04
87538	RGB	4823	1.69	1.68	-2.02 ± 0.04	-2.00 ± 0.01	-1.39 ± 0.06	-2.26 ± 0.01	-1.67 ± 0.01	-1.65 ± 0.01
88524	RGB	4890	1.86	1.62	-2.07 ± 0.09	-2.04 ± 0.01	-1.50 ± 0.05	-2.03 ± 0.02	-1.76 ± 0.04	-1.61 ± 0.04

TABLE A.5: Complete version of Table 5.1 (Chapter 5). M 4 target details including data from Momany et al. (2003, $UBVI$ photometry and target IDs) and 2MASS (Skrutskie et al., 2006, JHK photometry), and differential reddening corrections. Gaps in 2MASS data represent targets with low quality flags. Stars for which no reddening value is listed were outside the reddening map of Hendricks et al. (2012), and were corrected according to the average reddening value of $\mathrm{E}(B-V) = -0.37$.

ID	Type	2MASS ID	V	B	U	I	J	H	K	$\mathrm{E}(B-V)$
788	AGB	16235772-2622557	12.21	13.43	14.14	10.69	9.64	9.00	8.82	-
3590	AGB	16232184-2630495	12.48	13.64	14.37	10.92	-	-	-	0.36
10092	AGB	16233067-2629390	12.61	13.74	14.39	11.09	-	-	-	0.36
11285	AGB	16233195-2631457	12.84	13.90	14.42	11.40	10.35	9.77	9.58	0.36
13609	AGB	16233477-2631349	12.76	13.81	14.25	11.31	10.21	9.65	9.48	0.37
15167	AGB	16230063-2618065	12.43	13.63	14.39	10.87	9.79	9.16	8.94	-
16547	AGB	16233846-2629235	12.42	13.64	14.47	10.83	-	-	-	0.36
18573	AGB	16234085-2631215	12.18	13.52	14.52	10.50	-	-	-	0.35
20089	AGB	16234268-2631209	12.72	13.79	14.32	11.28	10.25	9.62	9.54	0.34
37349	AGB	16233741-2638238	12.25	13.46	14.27	10.66	9.62	8.95	8.77	-
41504	AGB	16235375-2634426	11.80	13.17	14.27	10.12	8.93	8.22	8.00	-
43597	AGB	16233020-2633241	12.20	13.53	14.60	10.47	9.25	8.54	8.32	0.41
46211	AGB	16233614-2632015	11.82	13.16	14.17	10.10	8.88	8.12	7.95	0.36
46676	AGB	16232988-2631490	12.05	13.37	14.38	10.35	9.11	8.37	8.18	0.36
46773	AGB	16234740-2631463	11.81	13.17	14.25	10.11	8.92	8.15	7.97	0.36

25	RGB	16235874-2624289	13.78	14.91	15.49	12.38	11.37	10.79	10.59	-
907	RGB	16240898-2622404	14.21	15.31	15.81	12.82	11.85	11.25	11.10	-
1029	RGB	16231690-2629479	13.14	14.36	15.28	11.54	10.34	9.61	9.47	0.36
1129	RGB	16242452-2622132	12.96	14.16	14.88	11.46	10.49	9.84	9.66	-
1474	RGB	16242595-2621299	14.35	15.42	15.90	12.98	12.08	11.53	11.33	-
2000	RGB	16240321-2620238	13.41	14.61	15.27	11.92	10.87	10.22	10.07	-
2745	RGB	16232008-2632415	13.56	14.74	15.46	11.97	10.80	10.12	9.95	0.36
3114	RGB	16232089-2631368	13.38	14.59	15.41	11.75	-	-	-	0.36
3258	RGB	16232114-2631377	13.45	14.67	15.49	11.84	-	-	-	0.36
4361	RGB	16232302-2630336	13.51	14.69	15.48	11.93	-	-	-	0.36
4496	RGB	16232305-2633322	13.17	14.42	15.28	11.52	10.32	9.59	9.41	0.38
4806	RGB	16232354-2633412	13.16	14.40	15.18	11.48	10.29	9.58	9.39	0.38
4938	RGB	16232402-2630005	12.86	14.14	15.17	11.16	9.89	9.13	8.99	0.35
5965	RGB	16232530-2633291	12.88	14.17	15.17	11.18	9.91	9.20	8.98	0.39
6978	RGB	16232674-2632388	13.34	14.59	15.44	11.69	10.47	9.78	9.59	0.40
7076	RGB	16232694-2631313	12.56	13.93	15.06	-	9.51	8.76	8.57	0.37
7081	RGB	16232700-2630444	13.36	14.57	15.38	11.76	10.59	9.86	9.68	0.36
7298	RGB	16232708-2633297	13.42	14.64	15.32	11.76	10.54	9.86	9.67	0.42
7526	RGB	16235232-2624350	14.71	15.80	16.26	-	12.24	11.65	11.49	-
7634	RGB	16233113-2624216	14.72	15.85	16.49	13.19	-	-	-	-
7672	RGB	16234090-2624169	14.85	15.94	16.55	13.42	12.38	11.79	11.62	-
7973	RGB	16231868-2623432	11.58	13.21	-	9.55	8.15	7.14	6.96	-

8099	RGB	16232982-2623253	13.10	14.40	15.46	11.42	10.19	9.45	9.26	-
8460	RGB	16234732-2622300	14.37	15.47	16.14	12.92	11.86	11.27	11.09	-
8602	RGB	16233893-2622094	13.58	14.78	15.60	12.01	10.87	10.21	10.05	-
8803	RGB	16232912-2630297	11.87	13.37	14.92	9.97	8.59	7.81	7.51	0.37
9040	RGB	16232950-2629116	12.32	13.68	14.88	10.59	9.32	8.57	8.35	0.35
9156	RGB	16233768-2620381	14.09	15.26	16.02	12.55	11.43	10.76	10.60	-
10801	RGB	16233144-2630247	12.54	13.87	14.98	10.82	9.58	8.80	8.60	0.37
10928	RGB	16233142-2633110	11.80	13.27	14.67	9.96	8.63	7.79	7.64	0.39
12387	RGB	16233310-2632306	13.14	14.40	15.23	11.50	-	-	-	0.37
13170	RGB	16233412-2633039	13.52	14.75	15.48	11.87	-	-	-	0.37
13179	RGB	16230438-2623429	11.89	13.36	14.75	10.08	8.78	7.97	7.78	-
14037	RGB	16233520-2632323	12.05	13.49	14.72	10.23	-	-	-	0.37
14350	RGB	16233565-2631227	12.65	13.98	15.06	10.95	-	-	-	0.36
14377	RGB	16233563-2631544	12.81	14.09	15.03	11.15	-	-	-	0.36
15010	RGB	16233657-2630200	12.37	13.74	14.86	10.63	-	-	-	0.36
16053	RGB	16233795-2628413	13.57	14.76	15.52	12.01	-	-	-	0.35
16788	RGB	16233846-2633192	10.86	12.77	15.13	-	6.97	5.98	5.63	0.39
17095	RGB	16233892-2632035	13.29	14.52	15.37	11.68	10.46	9.79	9.59	0.37
17461	RGB	16233927-2633059	10.77	12.71	-	-	6.98	5.93	5.68	0.38
22578	RGB	16234592-2633389	12.98	14.27	15.08	11.31	10.10	9.42	9.24	0.37
23196	RGB	16234692-2633439	13.02	14.31	15.22	11.36	10.14	9.44	9.26	0.37
25011	RGB	16235015-2632194	13.49	14.70	15.46	11.92	10.77	10.12	9.91	0.35

29983	RGB	16230273-2635364	13.97	15.13	15.82	12.42	11.31	10.68	10.46	-
31696	RGB	16231655-2632095	11.70	13.21	14.79	9.85	8.50	7.68	7.45	0.36
32412	RGB	16231204-2630540	13.63	14.82	15.61	12.05	10.86	10.19	9.98	0.39
33040	RGB	16231206-2629436	14.36	15.47	16.08	12.85	11.74	11.08	10.93	0.39
33060	RGB	16230905-2629405	14.75	15.84	16.38	13.28	12.18	11.56	11.40	0.43
33152	RGB	16230267-2629282	13.09	14.41	15.43	11.34	10.04	9.29	9.07	-
33480	RGB	16225800-2628463	12.87	14.09	14.87	11.21	10.04	9.35	9.15	-
33654	RGB	16225010-2628247	12.33	13.75	15.09	10.52	9.22	8.33	8.13	-
34336	RGB	16230601-2626522	14.95	16.03	16.63	13.42	12.26	11.62	11.46	-
34423	RGB	16231153-2626407	13.93	15.12	15.91	12.33	11.10	10.44	10.25	-
34725	RGB	16231503-2625546	14.60	15.70	16.24	13.07	11.93	11.32	11.11	-
35072	RGB	16231729-2624578	14.22	15.37	16.09	12.65	11.47	10.80	10.58	-
36015	RGB	16233621-2640002	14.14	15.27	-	12.63	11.61	10.98	10.84	-
36781	RGB	16234000-2639029	13.44	14.67	-	11.88	10.79	10.11	9.94	-
37542	RGB	16233491-2638086	14.49	15.59	16.14	13.00	11.98	11.35	11.18	-
38229	RGB	16234091-2637234	12.96	14.24	15.11	11.31	10.16	9.45	9.28	-
39273	RGB	16233151-2636183	13.49	14.70	15.38	11.87	10.73	10.05	9.90	-
40856	RGB	16234879-2635093	11.73	13.24	-	9.86	8.57	7.71	7.53	-
41863	RGB	16232827-2634278	14.71	15.83	16.40	13.17	-	-	-	0.42
42611	RGB	16234980-2633589	11.61	13.19	14.83	9.69	8.34	7.51	7.23	-
43859	RGB	16233337-2633148	13.68	14.89	15.65	12.05	10.86	10.19	10.01	0.39
45171	RGB	16232774-2632320	14.58	15.71	16.26	13.02	11.91	11.24	11.11	0.39

45284	RGB	16232437-2632284	12.49	13.86	15.04	10.73	9.44	8.66	8.46	0.38
45534	RGB	16233885-2632207	14.98	16.05	16.45	13.51	12.37	11.77	11.65	0.37
45700	RGB	16233329-2632160	14.72	15.79	16.27	13.23	-	-	-	0.36
47603	RGB	16235567-2631234	14.93	15.99	16.31	13.58	-	-	-	0.34
48035	RGB	16233948-2631114	12.72	13.99	14.82	11.07	9.86	9.13	8.93	0.37
48370	RGB	16233796-2631022	14.98	16.05	16.57	13.52	-	-	-	0.36
48477	RGB	16232741-2630595	13.12	14.39	15.30	11.45	10.23	9.50	9.36	0.37
48627	RGB	16233055-2630554	14.99	16.06	16.56	13.52	-	-	-	0.37
49055	RGB	16232115-2630440	13.90	15.06	15.77	12.34	11.17	10.48	10.36	0.36
49190	RGB	16232611-2630402	14.11	15.25	15.81	12.56	11.44	10.76	10.60	0.36
49332	RGB	16234173-2630361	14.80	15.87	16.31	13.34	-	-	-	0.35
49470	RGB	16234676-2630324	14.80	15.89	16.34	13.33	12.18	11.61	11.51	0.34
57927	RGB	16232938-2626276	14.63	15.67	16.22	13.01	11.80	11.15	11.00	0.39
58093	RGB	16232265-2626221	12.75	14.03	15.02	11.02	9.74	8.99	8.79	-
59237	RGB	16233885-2625427	13.14	14.36	15.26	11.55	10.33	9.64	9.46	0.36
59373	RGB	16234351-2625375	14.23	15.36	15.99	12.74	11.58	10.92	10.76	-
59950	RGB	16233129-2625157	14.71	15.80	16.39	13.22	12.05	11.43	11.28	0.40
62781	RGB	16242323-2637155	14.35	15.50	15.99	12.85	11.94	11.29	11.13	-
63624	RGB	16235835-2635390	12.59	13.91	14.84	10.94	9.85	9.11	8.97	-
65008	RGB	16240571-2633009	13.75	14.91	15.51	12.24	11.23	10.59	10.42	-
65302	RGB	16241589-2632274	13.00	14.24	15.02	11.45	10.42	9.75	9.58	-
65790	RGB	16240120-2631326	13.40	14.59	15.27	11.88	10.81	10.17	9.98	-

66385	RGB	16240429-2630278	12.99	14.22	14.93	11.43	10.38	9.71	9.52	-
67398	RGB	16242276-2628364	15.00	16.03	16.40	13.61	12.73	12.15	12.01	-
67553	RGB	16240060-2628207	14.17	15.26	15.77	12.76	11.79	11.16	11.01	-
67586	RGB	16242964-2628168	14.22	15.28	15.81	12.77	11.83	11.25	11.10	-
68085	RGB	16241470-2627167	13.33	14.50	15.21	11.83	10.81	10.14	9.95	-
68452	RGB	16241966-2626351	13.28	14.44	15.15	11.78	10.77	10.13	9.96	-
KEP10	RGB	16231791-2630059	13.85	15.03	13.30	-	11.30	10.61	10.52	0.35
KEP14	RGB	16234788-2629482	13.56	14.78	13.04	-	10.96	10.31	10.11	0.33
KEP16	RGB	16234175-2629466	13.78	15.00	13.27	-	11.15	10.48	10.34	0.34
KEP17	RGB	16232252-2629422	14.04	15.26	13.64	-	11.38	10.71	10.60	0.36
KEP20	RGB	16234279-2629276	12.66	13.98	12.10	-	9.83	9.08	8.92	0.33
KEP21	RGB	16235026-2629258	13.38	14.60	12.97	-	10.82	10.18	9.99	0.34
KEP22	RGB	16232499-2629249	13.72	14.95	13.39	-	11.05	10.37	10.18	0.35
KEP29	RGB	16234975-2628517	13.95	15.11	13.27	-	11.47	10.85	10.68	0.31
KEP31	RGB	16233750-2628396	14.06	15.25	13.49	-	-	-	-	0.35
KEP32	RGB	16232141-2628335	14.33	15.52	13.93	-	11.71	11.10	10.86	0.37
KEP35	RGB	16234308-2628074	13.51	14.73	13.18	-	10.93	10.25	10.07	0.34
KEP36	RGB	16235300-2628065	13.50	14.73	12.85	-	10.90	10.23	10.08	0.31

TABLE A.6: Complete version of Table 5.3 (Chapter 5). Stellar parameters for each star in the ML18b M 4 sample. Spectroscopic effective temperatures ($T_{\rm eff,sp}$), microturbulence values (v_t), and uncertainties were determined using PHOBOS V2, while log g values were calculated based in the empirical relation from Alonso et al. (1999). These were adopted as our final parameters. $T_{\rm eff,ph}$ values are the effective temperatures estimated from photometric colour-$T_{\rm eff}$ relations, were used in the PHOBOS test, and are included for comparison.

Star ID	Evolutionary phase	$T_{\rm eff,sp}$ (K)	log g (cgs)	v_t (km/s)	$T_{\rm eff,ph}$ (K)
788	AGB	4877 ± 52	1.71	1.56 ± 0.07	4937
3590	AGB	4929 ± 36	1.84	1.68 ± 0.06	4975
10092	AGB	4944 ± 29	1.90	1.45 ± 0.04	5051
11285	AGB	5137 ± 69	2.08	1.73 ± 0.19	5154
13609	AGB	5131 ± 67	2.05	1.21 ± 0.10	5166
15167	AGB	4941 ± 52	1.83	1.62 ± 0.08	4895
16547	AGB	4838 ± 62	1.77	1.82 ± 0.11	4855
18573	AGB	4625 ± 64	1.57	1.87 ± 0.11	4610
20089	AGB	5095 ± 65	2.01	1.50 ± 0.14	5111
37349	AGB	4914 ± 51	1.74	1.73 ± 0.07	4893
41504	AGB	4550 ± 51	1.37	1.79 ± 0.06	4593
43597	AGB	4689 ± 52	1.61	1.78 ± 0.07	4671
46211	AGB	4541 ± 52	1.37	1.48 ± 0.06	4550
46676	AGB	4614 ± 51	1.51	1.66 ± 0.06	4561
46773	AGB	4513 ± 50	1.35	1.63 ± 0.05	4550
25	RGB	5015 ± 60	2.49	1.30 ± 0.09	5156
907	RGB	5059 ± 71	2.68	1.26 ± 0.12	5234
1029	RGB	4865 ± 51	2.16	1.70 ± 0.08	4756
1129	RGB	4911 ± 53	2.12	1.41 ± 0.08	5029
1474	RGB	5182 ± 64	2.79	1.26 ± 0.10	5345
2000	RGB	4985 ± 58	2.33	1.32 ± 0.08	4993
2745	RGB	4808 ± 44	2.30	1.41 ± 0.06	4816
3114	RGB	4802 ± 58	2.23	1.30 ± 0.08	4875
3258	RGB	4824 ± 81	2.27	1.34 ± 0.12	4840
4361	RGB	4814 ± 90	2.29	1.50 ± 0.15	4898
4496	RGB	4724 ± 61	2.10	1.33 ± 0.07	4752
4806	RGB	4821 ± 89	2.15	1.45 ± 0.12	4750
4938	RGB	4612 ± 58	1.92	1.43 ± 0.07	4599
5965	RGB	4620 ± 72	1.93	1.40 ± 0.12	4675
6978	RGB	4761 ± 74	2.19	1.26 ± 0.10	4793

7076	RGB	4527 ± 75	1.75	1.42 ± 0.09	4536
7081	RGB	4873 ± 80	2.26	1.66 ± 0.12	4767
7298	RGB	4920 ± 63	2.30	1.47 ± 0.10	4875
7526	RGB	5174 ± 92	2.94	1.19 ± 0.17	5154
7634	RGB	5054 ± 66	2.89	1.07 ± 0.11	5043
7672	RGB	5088 ± 65	2.95	1.01 ± 0.11	5163
7973	RGB	4162 ± 55	1.11	1.73 ± 0.06	4130
8099	RGB	4677 ± 54	2.05	1.31 ± 0.07	4641
8460	RGB	5065 ± 74	2.75	1.10 ± 0.12	5114
8602	RGB	4877 ± 62	2.35	1.29 ± 0.08	4877
8803	RGB	4348 ± 49	1.36	1.57 ± 0.06	4296
9040	RGB	4541 ± 79	1.66	1.65 ± 0.10	4501
9156	RGB	5012 ± 60	2.62	1.14 ± 0.09	4928
10801	RGB	4633 ± 78	1.80	1.49 ± 0.10	4581
10928	RGB	4373 ± 88	1.35	2.33 ± 0.39	4426
12387	RGB	4760 ± 50	2.11	1.24 ± 0.07	4776
13170	RGB	4842 ± 51	2.30	1.28 ± 0.07	4831
13179	RGB	4427 ± 55	1.42	1.47 ± 0.05	4407
14037	RGB	4442 ± 49	1.49	1.57 ± 0.06	4478
14350	RGB	4597 ± 81	1.83	1.64 ± 0.10	4639
14377	RGB	4756 ± 80	1.98	1.52 ± 0.11	4721
15010	RGB	4540 ± 51	1.68	1.47 ± 0.06	4583
16053	RGB	4913 ± 67	2.36	1.38 ± 0.11	4890
16788	RGB	3778 ± 89	0.43	1.87 ± 0.08	3860
17095	RGB	4801 ± 47	2.19	1.64 ± 0.06	4765
17461	RGB	3852 ± 118	0.49	1.92 ± 0.12	3878
22578	RGB	4649 ± 79	1.99	1.61 ± 0.12	4700
23196	RGB	4678 ± 65	2.02	1.38 ± 0.08	4682
25011	RGB	4822 ± 57	2.28	1.27 ± 0.08	4796
29983	RGB	4911 ± 66	2.52	1.20 ± 0.09	4931
31696	RGB	4263 ± 53	1.23	1.67 ± 0.06	4307
32412	RGB	4887 ± 73	2.37	1.23 ± 0.10	4857
33040	RGB	4988 ± 74	2.71	1.28 ± 0.12	5057
33060	RGB	5170 ± 93	2.95	1.19 ± 0.18	5262
33152	RGB	4632 ± 54	2.02	1.46 ± 0.07	4543
33480	RGB	4827 ± 59	2.04	1.53 ± 0.09	4760
33654	RGB	4443 ± 57	1.61	1.54 ± 0.06	4397
34336	RGB	5053 ± 71	2.98	1.11 ± 0.11	4996
34423	RGB	4892 ± 61	2.49	1.31 ± 0.09	4799
34725	RGB	5065 ± 66	2.84	1.41 ± 0.12	4989
35072	RGB	4836 ± 73	2.58	1.21 ± 0.11	4863
36015	RGB	5049 ± 59	2.65	0.89 ± 0.09	5080

36781	RGB	4841 ± 55	2.27	1.28 ± 0.08	4872
37542	RGB	5104 ± 56	2.82	1.27 ± 0.10	5108
38229	RGB	4728 ± 62	2.02	1.32 ± 0.08	4738
39273	RGB	4891 ± 63	2.32	1.28 ± 0.09	4839
40856	RGB	4387 ± 52	1.33	1.65 ± 0.06	4348
41863	RGB	5091 ± 91	2.90	1.05 ± 0.17	5164
42611	RGB	4182 ± 59	1.14	1.71 ± 0.07	4240
43859	RGB	4863 ± 58	2.38	1.19 ± 0.09	4854
45171	RGB	5031 ± 81	2.82	1.28 ± 0.14	5023
45284	RGB	4431 ± 53	1.66	1.43 ± 0.07	4534
45534	RGB	5128 ± 86	3.02	1.08 ± 0.14	5107
45700	RGB	5192 ± 78	2.95	0.92 ± 0.14	5165
47603	RGB	5248 ± 73	3.05	1.38 ± 0.12	5120
48035	RGB	4692 ± 63	1.91	1.37 ± 0.08	4682
48370	RGB	5065 ± 80	3.00	1.04 ± 0.14	5163
48477	RGB	4649 ± 63	2.05	1.30 ± 0.08	4693
48627	RGB	5155 ± 81	3.04	1.10 ± 0.15	5181
49055	RGB	4911 ± 59	2.49	1.19 ± 0.09	4882
49190	RGB	4967 ± 72	2.60	1.21 ± 0.11	4914
49332	RGB	5061 ± 73	2.92	0.92 ± 0.13	5122
49470	RGB	5174 ± 60	2.97	1.36 ± 0.10	5023
57927	RGB	5035 ± 72	2.84	1.28 ± 0.13	4847
58093	RGB	4687 ± 59	1.92	1.46 ± 0.07	4595
59237	RGB	4746 ± 57	2.10	1.48 ± 0.07	4743
59373	RGB	4971 ± 61	2.65	1.08 ± 0.09	4972
59950	RGB	5093 ± 46	2.90	1.08 ± 0.07	5121
62781	RGB	4933 ± 73	2.68	1.21 ± 0.12	5128
63624	RGB	4597 ± 59	1.80	1.37 ± 0.07	4740
65008	RGB	4994 ± 62	2.47	1.37 ± 0.10	5037
65302	RGB	4760 ± 69	2.05	1.42 ± 0.09	4921
65790	RGB	4897 ± 60	2.28	1.37 ± 0.08	4955
66385	RGB	4662 ± 56	2.00	1.19 ± 0.07	4895
67398	RGB	5142 ± 70	3.04	1.07 ± 0.12	5403
67553	RGB	5143 ± 73	2.71	1.27 ± 0.11	5215
67586	RGB	5089 ± 68	2.70	1.07 ± 0.11	5280
68085	RGB	4972 ± 66	2.29	1.40 ± 0.10	4999
68452	RGB	5007 ± 74	2.29	1.51 ± 0.11	5053
KEP10	RGB	4960 ± 65	2.49	1.21 ± 0.10	4953
KEP14	RGB	4807 ± 59	2.30	1.32 ± 0.08	4801
KEP16	RGB	4921 ± 62	2.45	1.37 ± 0.09	4825
KEP17	RGB	4785 ± 61	2.48	1.12 ± 0.09	4871
KEP20	RGB	4535 ± 59	1.79	1.49 ± 0.06	4578

KEP21	RGB	4855 ± 59	2.26	1.47 ± 0.09	4848
KEP22	RGB	4852 ± 61	2.39	1.34 ± 0.09	4794
KEP29	RGB	4986 ± 60	2.55	1.27 ± 0.09	4903
KEP31	RGB	4966 ± 63	2.58	1.22 ± 0.10	4883
KEP32	RGB	5026 ± 65	2.72	1.22 ± 0.09	4912
KEP35	RGB	4838 ± 77	2.30	1.27 ± 0.10	4834
KEP36	RGB	4808 ± 60	2.28	1.38 ± 0.09	4754

TABLE A.7: Complete version of Table 5.5 (Chapter 5). Chemical abundances for each star in the ML18b M 4 sample. Abundance uncertainties reflect line-to-line scatter (1σ), and do not take atmospheric sensitivities into account. O, Na, and Al abundances were corrected for non-LTE effects.

ID	Type	$\log_\epsilon(\mathrm{Fe\,I})$	$\log_\epsilon(\mathrm{Fe\,II})$	$\log_\epsilon(\mathrm{O})$	$\log_\epsilon(\mathrm{Na})$	$\log_\epsilon(\mathrm{Mg})$	$\log_\epsilon(\mathrm{Al})$
788	AGB	6.24 ± 0.08	6.24 ± 0.03	8.26 ± 0.05	4.93 ± 0.01	6.79 ± 0.03	5.56 ± 0.02
788	AGB	6.24 ± 0.08	6.24 ± 0.03	8.26 ± 0.05	4.93 ± 0.01	6.79 ± 0.03	5.56 ± 0.02
3590	AGB	6.27 ± 0.06	6.29 ± 0.04	8.07 ± 0.02	5.15 ± 0.03	6.73 ± 0.04	5.67 ± 0.03
10092	AGB	6.33 ± 0.04	6.35 ± 0.01	8.29 ± 0.04	4.95 ± 0.02	6.72 ± 0.03	5.53 ± 0.03
11285	AGB	6.32 ± 0.07	6.31 ± 0.04	8.10 ± 0.02	5.19 ± 0.02	6.80 ± 0.02	5.71 ± 0.06
13609	AGB	6.32 ± 0.09	6.38 ± 0.06	8.12 ± 0.06	5.02 ± 0.11	6.76 ± 0.05	5.57 ± 0.05
15167	AGB	6.31 ± 0.08	6.27 ± 0.05	8.10 ± 0.04	5.17 ± 0.00	6.76 ± 0.01	5.63 ± 0.02
16547	AGB	6.32 ± 0.10	6.29 ± 0.05	8.17 ± 0.05	5.10 ± 0.02	6.71 ± 0.00	5.60 ± 0.02
18573	AGB	6.32 ± 0.08	6.26 ± 0.03	8.21 ± 0.07	5.02 ± 0.07	6.81 ± 0.06	5.82 ± 0.02
20089	AGB	6.30 ± 0.08	6.34 ± 0.07	8.25 ± 0.08	5.25 ± 0.00	6.78 ± 0.05	5.70 ± 0.02
37349	AGB	6.35 ± 0.08	6.30 ± 0.05	8.05 ± 0.06	5.22 ± 0.06	6.80 ± 0.02	5.66 ± 0.04
41504	AGB	6.27 ± 0.09	6.33 ± 0.05	8.16 ± 0.08	5.22 ± 0.04	6.77 ± 0.03	5.61 ± 0.02
43597	AGB	6.33 ± 0.08	6.31 ± 0.07	8.05 ± 0.04	5.30 ± 0.01	6.76 ± 0.02	5.63 ± 0.04
46211	AGB	6.32 ± 0.09	6.38 ± 0.04	8.35 ± 0.01	5.19 ± 0.04	6.72 ± 0.06	5.53 ± 0.05
46676	AGB	6.28 ± 0.09	6.24 ± 0.02	8.22 ± 0.07	4.95 ± 0.05	6.74 ± 0.02	5.54 ± 0.02
46773	AGB	6.24 ± 0.08	6.32 ± 0.05	8.22 ± 0.07	4.99 ± 0.08	6.71 ± 0.06	5.55 ± 0.04

8803	RGB	6.36 ± 0.08	6.29 ± 0.05	8.00 ± 0.12	5.59 ± 0.01	6.78 ± 0.05	5.76 ± 0.04
10928	RGB	6.31 ± 0.08	6.30 ± 0.07	8.21 ± 0.01	5.10 ± 0.04	6.71 ± 0.04	5.55 ± 0.04
14037	RGB	6.37 ± 0.07	6.33 ± 0.03	8.14 ± 0.07	5.04 ± 0.03	6.77 ± 0.03	5.67 ± 0.04
16788	RGB	6.34 ± 0.09	6.39 ± 0.02	8.39 ± 0.07	5.20 ± 0.02	6.77 ± 0.06	5.65 ± 0.09
17461	RGB	6.31 ± 0.09	6.34 ± 0.01	8.15 ± 0.07	5.21 ± 0.00	6.86 ± 0.03	5.77 ± 0.02
25	RGB	6.26 ± 0.09	6.34 ± 0.04	8.00 ± 0.05	5.52 ± 0.10	6.85 ± 0.02	5.86 ± 0.07
907	RGB	6.23 ± 0.09	6.32 ± 0.03	7.99 ± 0.05	5.42 ± 0.04	6.76 ± 0.02	5.86 ± 0.07
1029	RGB	6.35 ± 0.08	6.24 ± 0.03	8.10 ± 0.01	5.58 ± 0.09	6.81 ± 0.03	5.90 ± 0.02
1129	RGB	6.31 ± 0.07	6.38 ± 0.04	8.02 ± 0.07	5.24 ± 0.01	6.83 ± 0.06	5.81 ± 0.03
1474	RGB	6.32 ± 0.07	6.44 ± 0.02	7.90 ± 0.03	5.54 ± 0.08	6.83 ± 0.03	5.89 ± 0.01
2000	RGB	6.40 ± 0.09	6.41 ± 0.07	8.01 ± 0.02	5.46 ± 0.10	6.82 ± 0.03	5.84 ± 0.02
2745	RGB	6.28 ± 0.07	6.32 ± 0.05	8.12 ± 0.09	5.21 ± 0.02	6.81 ± 0.03	5.79 ± 0.04
3114	RGB	6.34 ± 0.09	6.38 ± 0.03	8.09 ± 0.03	5.43 ± 0.06	6.73 ± 0.04	5.84 ± 0.03
3258	RGB	6.34 ± 0.08	6.36 ± 0.04	8.07 ± 0.08	5.33 ± 0.12	6.74 ± 0.03	5.74 ± 0.04
4361	RGB	6.29 ± 0.09	6.33 ± 0.05	8.03 ± 0.02	5.53 ± 0.03	6.67 ± 0.04	5.77 ± 0.03
4496	RGB	6.36 ± 0.09	6.43 ± 0.01	8.12 ± 0.10	5.36 ± 0.03	6.84 ± 0.04	5.68 ± 0.04
4806	RGB	6.44 ± 0.09	6.39 ± 0.04	8.24 ± 0.01	5.06 ± 0.04	6.82 ± 0.05	5.65 ± 0.03
4938	RGB	6.33 ± 0.08	6.36 ± 0.03	8.17 ± 0.05	5.44 ± 0.04	6.76 ± 0.05	5.81 ± 0.03
5965	RGB	6.38 ± 0.08	6.44 ± 0.07	7.94 ± 0.08	5.69 ± 0.13	6.73 ± 0.03	5.89 ± 0.03
6978	RGB	6.38 ± 0.09	6.43 ± 0.04	8.17 ± 0.03	5.47 ± 0.05	6.75 ± 0.04	5.81 ± 0.03
7076	RGB	6.34 ± 0.09	6.36 ± 0.06	8.34 ± 0.01	5.21 ± 0.03	6.66 ± 0.04	5.64 ± 0.05
7081	RGB	6.36 ± 0.07	6.28 ± 0.03	7.97 ± 0.05	5.36 ± 0.01	6.76 ± 0.04	5.89 ± 0.05

7298	RGB	6.35 ± 0.09	6.29 ± 0.03	8.08 ± 0.04	5.01 ± 0.04	6.75 ± 0.05	5.64 ± 0.03
7526	RGB	6.39 ± 0.10	6.41 ± 0.01	7.94 ± 0.04	5.52 ± 0.09	6.82 ± 0.06	5.83 ± 0.04
7634	RGB	6.36 ± 0.08	6.40 ± 0.01	8.22 ± 0.03	5.09 ± 0.01	6.73 ± 0.03	5.62 ± 0.04
7672	RGB	6.40 ± 0.08	6.40 ± 0.02	8.17 ± 0.06	5.25 ± 0.02	6.81 ± 0.04	5.73 ± 0.01
7973	RGB	6.25 ± 0.09	6.26 ± 0.06	8.15 ± 0.05	5.57 ± 0.07	6.73 ± 0.05	5.79 ± 0.04
8099	RGB	6.35 ± 0.07	6.33 ± 0.10	8.21 ± 0.01	5.21 ± 0.06	6.73 ± 0.00	5.75 ± 0.01
8460	RGB	6.35 ± 0.09	6.38 ± 0.08	8.11 ± 0.02	5.42 ± 0.07	6.78 ± 0.03	5.75 ± 0.03
8602	RGB	6.36 ± 0.08	6.35 ± 0.05	8.13 ± 0.09	5.11 ± 0.09	6.80 ± 0.04	5.60 ± 0.05
9040	RGB	6.36 ± 0.08	6.32 ± 0.07	8.12 ± 0.07	5.28 ± 0.03	6.71 ± 0.05	5.61 ± 0.03
9156	RGB	6.42 ± 0.08	6.37 ± 0.02	7.90 ± 0.03	5.51 ± 0.13	6.79 ± 0.02	5.75 ± 0.04
10801	RGB	6.37 ± 0.09	6.31 ± 0.04	7.94 ± 0.05	5.49 ± 0.04	6.70 ± 0.03	5.80 ± 0.05
12387	RGB	6.36 ± 0.07	6.33 ± 0.04	8.17 ± 0.10	5.19 ± 0.03	6.78 ± 0.03	5.72 ± 0.04
13170	RGB	6.41 ± 0.07	6.42 ± 0.04	8.14 ± 0.05	5.22 ± 0.14	6.80 ± 0.02	5.90 ± 0.05
13179	RGB	6.35 ± 0.08	6.35 ± 0.03	8.20 ± 0.06	5.29 ± 0.06	6.75 ± 0.01	5.75 ± 0.02
14350	RGB	6.30 ± 0.09	6.28 ± 0.07	8.03 ± 0.08	5.49 ± 0.12	6.75 ± 0.08	5.78 ± 0.03
14377	RGB	6.40 ± 0.10	6.31 ± 0.06	8.02 ± 0.07	5.53 ± 0.07	6.77 ± 0.03	5.75 ± 0.03
15010	RGB	6.35 ± 0.08	6.33 ± 0.03	8.32 ± 0.11	5.18 ± 0.04	6.74 ± 0.02	5.61 ± 0.06
16053	RGB	6.41 ± 0.08	6.37 ± 0.02	8.04 ± 0.03	5.51 ± 0.06	6.75 ± 0.06	5.73 ± 0.03
17095	RGB	6.32 ± 0.07	6.33 ± 0.07	7.90 ± 0.06	5.53 ± 0.02	6.75 ± 0.02	5.73 ± 0.02
22578	RGB	6.30 ± 0.08	6.38 ± 0.07	8.35 ± 0.07	5.03 ± 0.01	6.77 ± 0.04	5.58 ± 0.04
23196	RGB	6.34 ± 0.09	6.39 ± 0.04	8.16 ± 0.11	5.44 ± 0.08	6.67 ± 0.00	5.79 ± 0.02
25011	RGB	6.35 ± 0.08	6.41 ± 0.03	8.04 ± 0.05	5.62 ± 0.00	6.80 ± 0.05	5.90 ± 0.03

29983	RGB	6.34 ± 0.09	6.38 ± 0.08	8.11 ± 0.07	5.57 ± 0.01	6.77 ± 0.02	5.80 ± 0.01
31696	RGB	6.25 ± 0.08	6.30 ± 0.04	8.12 ± 0.10	5.61 ± 0.12	6.73 ± 0.08	5.75 ± 0.02
32412	RGB	6.35 ± 0.10	6.38 ± 0.10	8.06 ± 0.11	5.40 ± 0.05	6.78 ± 0.02	5.81 ± 0.03
33040	RGB	6.28 ± 0.10	6.33 ± 0.05	8.24 ± 0.07	5.18 ± 0.03	6.71 ± 0.02	5.66 ± 0.05
33060	RGB	6.35 ± 0.10	6.46 ± 0.03	8.09 ± 0.05	5.21 ± 0.04	6.86 ± 0.08	5.76 ± 0.02
33152	RGB	6.26 ± 0.08	6.21 ± 0.05	8.13 ± 0.05	5.18 ± 0.02	6.67 ± 0.04	5.69 ± 0.04
33480	RGB	6.28 ± 0.09	6.18 ± 0.02	8.15 ± 0.06	4.95 ± 0.05	6.71 ± 0.05	5.49 ± 0.05
33654	RGB	6.27 ± 0.09	6.26 ± 0.05	8.22 ± 0.08	5.47 ± 0.02	6.83 ± 0.05	5.80 ± 0.02
34336	RGB	6.37 ± 0.08	6.36 ± 0.06	7.96 ± 0.03	5.43 ± 0.02	6.78 ± 0.08	5.87 ± 0.06
34423	RGB	6.31 ± 0.09	6.29 ± 0.04	8.11 ± 0.04	5.35 ± 0.03	6.79 ± 0.04	5.81 ± 0.02
34725	RGB	6.36 ± 0.08	6.32 ± 0.05	8.21 ± 0.05	5.06 ± 0.05	6.80 ± 0.04	5.68 ± 0.04
35072	RGB	6.22 ± 0.10	6.27 ± 0.07	8.24 ± 0.06	5.32 ± 0.03	6.70 ± 0.06	5.78 ± 0.02
36015	RGB	6.40 ± 0.08	6.41 ± 0.10	8.11 ± 0.03	5.13 ± 0.01	6.77 ± 0.01	5.63 ± 0.03
36781	RGB	6.33 ± 0.08	6.39 ± 0.08	8.11 ± 0.06	5.39 ± 0.00	6.83 ± 0.05	5.81 ± 0.05
37542	RGB	6.41 ± 0.08	6.37 ± 0.03	7.94 ± 0.02	5.56 ± 0.00	6.76 ± 0.03	5.86 ± 0.03
38229	RGB	6.34 ± 0.09	6.28 ± 0.04	7.89 ± 0.05	5.45 ± 0.06	6.69 ± 0.04	5.80 ± 0.03
39273	RGB	6.35 ± 0.10	6.35 ± 0.10	8.20 ± 0.08	5.28 ± 0.09	6.85 ± 0.04	5.74 ± 0.03
40856	RGB	6.30 ± 0.09	6.25 ± 0.04	8.26 ± 0.04	5.14 ± 0.03	6.81 ± 0.04	5.58 ± 0.05
41863	RGB	6.38 ± 0.11	6.48 ± 0.06	8.01 ± 0.08	5.59 ± 0.01	6.79 ± 0.05	5.91 ± 0.02
42611	RGB	6.23 ± 0.10	6.31 ± 0.06	8.31 ± 0.03	5.36 ± 0.01	6.73 ± 0.08	5.79 ± 0.03
43859	RGB	6.33 ± 0.09	6.36 ± 0.08	8.01 ± 0.10	5.29 ± 0.01	6.76 ± 0.06	5.82 ± 0.02
45171	RGB	6.32 ± 0.11	6.36 ± 0.08	8.25 ± 0.05	5.17 ± 0.03	6.87 ± 0.04	5.77 ± 0.03

45284	RGB	6.23 ± 0.08	6.35 ± 0.06	8.21 ± 0.09	5.30 ± 0.01	6.83 ± 0.07	5.72 ± 0.03
45534	RGB	6.33 ± 0.10	6.36 ± 0.01	8.23 ± 0.07	5.08 ± 0.03	6.81 ± 0.07	5.71 ± 0.03
45700	RGB	6.39 ± 0.09	6.39 ± 0.02	7.96 ± 0.10	5.40 ± 0.06	6.78 ± 0.05	5.82 ± 0.05
47603	RGB	6.34 ± 0.08	6.30 ± 0.03	8.12 ± 0.04	5.31 ± 0.01	6.77 ± 0.07	5.76 ± 0.03
48035	RGB	6.31 ± 0.10	6.38 ± 0.04	8.14 ± 0.02	5.14 ± 0.09	6.77 ± 0.02	5.63 ± 0.04
48370	RGB	6.25 ± 0.10	6.37 ± 0.03	8.02 ± 0.05	5.51 ± 0.00	6.78 ± 0.01	5.85 ± 0.02
48477	RGB	6.29 ± 0.09	6.30 ± 0.03	8.22 ± 0.05	5.19 ± 0.08	6.80 ± 0.04	5.87 ± 0.03
48627	RGB	6.40 ± 0.10	6.43 ± 0.05	8.07 ± 0.01	5.34 ± 0.01	6.75 ± 0.00	5.80 ± 0.05
49055	RGB	6.37 ± 0.09	6.37 ± 0.04	8.07 ± 0.06	5.52 ± 0.02	6.81 ± 0.06	5.85 ± 0.02
49190	RGB	6.28 ± 0.10	6.26 ± 0.07	8.17 ± 0.03	5.09 ± 0.10	6.84 ± 0.06	5.80 ± 0.03
49332	RGB	6.35 ± 0.09	6.41 ± 0.02	8.18 ± 0.06	5.05 ± 0.02	6.82 ± 0.06	5.80 ± 0.04
49470	RGB	6.37 ± 0.07	6.29 ± 0.05	8.04 ± 0.02	5.09 ± 0.02	6.85 ± 0.03	5.79 ± 0.01
57927	RGB	6.32 ± 0.10	6.36 ± 0.04	7.95 ± 0.03	5.39 ± 0.02	6.82 ± 0.02	5.87 ± 0.05
58093	RGB	6.34 ± 0.09	6.23 ± 0.03	8.13 ± 0.02	5.10 ± 0.05	6.78 ± 0.03	5.57 ± 0.04
59237	RGB	6.34 ± 0.09	6.31 ± 0.06	8.04 ± 0.07	5.51 ± 0.06	6.81 ± 0.03	5.75 ± 0.02
59373	RGB	6.38 ± 0.09	6.41 ± 0.04	8.07 ± 0.07	5.45 ± 0.06	6.81 ± 0.03	5.84 ± 0.02
59950	RGB	6.35 ± 0.07	6.36 ± 0.03	8.00 ± 0.04	5.52 ± 0.01	6.76 ± 0.05	5.84 ± 0.04
62781	RGB	6.27 ± 0.11	6.37 ± 0.02	8.20 ± 0.01	5.25 ± 0.01	6.81 ± 0.04	5.78 ± 0.02
63624	RGB	6.26 ± 0.10	6.31 ± 0.05	8.08 ± 0.08	5.48 ± 0.07	6.80 ± 0.06	5.79 ± 0.06
65008	RGB	6.32 ± 0.10	6.36 ± 0.07	7.92 ± 0.02	5.44 ± 0.04	6.80 ± 0.07	5.78 ± 0.03
65302	RGB	6.29 ± 0.11	6.37 ± 0.06	7.99 ± 0.05	5.48 ± 0.00	6.77 ± 0.02	5.84 ± 0.04
65790	RGB	6.36 ± 0.09	6.40 ± 0.05	7.94 ± 0.11	5.50 ± 0.01	6.73 ± 0.05	5.84 ± 0.04

66385	RGB	6.26 ± 0.09	6.29 ± 0.04	8.24 ± 0.05	5.18 ± 0.16	6.80 ± 0.05	5.72 ± 0.04
67398	RGB	6.36 ± 0.09	6.40 ± 0.04	8.25 ± 0.03	5.09 ± 0.08	6.81 ± 0.07	5.87 ± 0.06
67553	RGB	6.40 ± 0.10	6.40 ± 0.02	7.97 ± 0.03	5.47 ± 0.01	6.82 ± 0.03	5.90 ± 0.04
67586	RGB	6.36 ± 0.08	6.41 ± 0.04	8.03 ± 0.05	5.37 ± 0.12	6.78 ± 0.07	5.77 ± 0.04
68085	RGB	6.39 ± 0.10	6.43 ± 0.02	7.94 ± 0.06	5.61 ± 0.03	6.84 ± 0.02	5.87 ± 0.04
68452	RGB	6.35 ± 0.10	6.33 ± 0.05	7.85 ± 0.05	5.50 ± 0.01	6.85 ± 0.04	5.87 ± 0.05
KEP10	RGB	6.34 ± 0.09	6.38 ± 0.08	8.14 ± 0.01	5.02 ± 0.02	6.78 ± 0.04	5.61 ± 0.02
KEP14	RGB	6.28 ± 0.09	6.36 ± 0.01	8.14 ± 0.04	5.35 ± 0.09	6.76 ± 0.02	5.71 ± 0.01
KEP16	RGB	6.36 ± 0.09	6.31 ± 0.04	8.21 ± 0.03	5.10 ± 0.02	6.82 ± 0.03	5.72 ± 0.02
KEP17	RGB	6.20 ± 0.08	6.29 ± 0.00	8.26 ± 0.06	4.97 ± 0.02	6.75 ± 0.06	5.63 ± 0.04
KEP20	RGB	6.26 ± 0.09	6.31 ± 0.05	8.32 ± 0.06	4.96 ± 0.05	6.73 ± 0.08	5.61 ± 0.01
KEP21	RGB	6.30 ± 0.09	6.25 ± 0.08	7.99 ± 0.03	5.52 ± 0.05	6.84 ± 0.08	5.78 ± 0.03
KEP22	RGB	6.28 ± 0.09	6.29 ± 0.02	8.11 ± 0.08	5.45 ± 0.01	6.74 ± 0.05	5.84 ± 0.04
KEP29	RGB	6.38 ± 0.09	6.35 ± 0.05	8.06 ± 0.03	5.01 ± 0.01	6.82 ± 0.07	5.59 ± 0.06
KEP31	RGB	6.30 ± 0.10	6.34 ± 0.04	8.07 ± 0.03	5.29 ± 0.08	6.72 ± 0.05	5.70 ± 0.03
KEP32	RGB	6.36 ± 0.08	6.32 ± 0.05	7.95 ± 0.07	5.47 ± 0.01	6.75 ± 0.02	5.81 ± 0.05
KEP35	RGB	6.28 ± 0.11	6.29 ± 0.04	8.15 ± 0.06	5.61 ± 0.04	6.83 ± 0.05	5.72 ± 0.01
KEP36	RGB	6.31 ± 0.09	6.24 ± 0.04	8.16 ± 0.03	5.10 ± 0.01	6.77 ± 0.02	5.70 ± 0.03

TABLE A.8: Complete version of Table 5.14 (Chapter 5). Na and O abundances for each star in the ML18b M 4 sample, determined using the non-LTE BALDER code with i) the 1D MARCS, and ii) the <3D> STAGGER-grid of stellar atmospheric models. Abundance uncertainties reflect line-to-line scatter (1σ), and do not take atmospheric sensitivities into account. The final column indicates, for each star, whether extrapolation outside the parameter space of the <3D> STAGGER-grid was required. Note that the stellar parameters from Table A.6 were used for all abundance determinations.

ID	Type	1D MARCS		<3D> STAGGER		<3D> extrapolation
		$\log_\epsilon(\mathrm{Na})$	$\log_\epsilon(\mathrm{O})$	$\log_\epsilon(\mathrm{Na})$	$\log_\epsilon(\mathrm{O})$	required?
788	AGB	4.85 ± 0.03	8.20 ± 0.06	4.85 ± 0.03	8.37 ± 0.06	Yes
3590	AGB	5.06 ± 0.07	8.04 ± 0.00	5.08 ± 0.06	8.20 ± 0.01	Yes
10092	AGB	4.88 ± 0.06	8.28 ± 0.03	4.89 ± 0.05	8.42 ± 0.03	Yes
11285	AGB	5.12 ± 0.03	8.09 ± 0.04	5.13 ± 0.02	8.19 ± 0.05	Yes
13609	AGB	4.95 ± 0.06	8.10 ± 0.03	4.96 ± 0.08	8.20 ± 0.02	Yes
15167	AGB	5.06 ± 0.05	8.05 ± 0.02	5.08 ± 0.04	8.21 ± 0.02	Yes
16547	AGB	5.02 ± 0.06	8.14 ± 0.03	5.04 ± 0.05	8.32 ± 0.03	Yes
18573	AGB	4.92 ± 0.01	8.19 ± 0.07	4.97 ± 0.03	8.44 ± 0.07	Yes
20089	AGB	5.15 ± 0.06	8.22 ± 0.04	5.16 ± 0.05	8.33 ± 0.03	Yes
37349	AGB	5.13 ± 0.10	8.02 ± 0.07	5.16 ± 0.09	8.19 ± 0.07	Yes
41504	AGB	5.07 ± 0.03	8.13 ± 0.08	5.13 ± 0.02	8.44 ± 0.08	Yes
43597	AGB	5.16 ± 0.05	8.03 ± 0.03	5.22 ± 0.04	8.25 ± 0.02	Yes
46211	AGB	4.99 ± 0.04	8.30 ± 0.02	5.04 ± 0.03	8.60 ± 0.02	Yes

46676	AGB	4.83 ± 0.01	8.19 ± 0.08	4.86 ± 0.00	8.45 ± 0.08	Yes
46773	AGB	4.84 ± 0.00	8.19 ± 0.08	4.89 ± 0.01	8.51 ± 0.08	Yes
25	RGB	5.35 ± 0.00	8.00 ± 0.05	5.40 ± 0.01	8.09 ± 0.05	Yes
907	RGB	5.28 ± 0.03	7.95 ± 0.05	5.32 ± 0.03	8.02 ± 0.05	No
1029	RGB	5.38 ± 0.01	8.02 ± 0.00	5.43 ± 0.01	8.14 ± 0.01	No
1129	RGB	5.12 ± 0.06	7.99 ± 0.06	5.15 ± 0.05	8.12 ± 0.06	No
1474	RGB	5.40 ± 0.02	7.88 ± 0.05	5.44 ± 0.01	7.94 ± 0.05	No
2000	RGB	5.29 ± 0.00	7.98 ± 0.01	5.33 ± 0.01	8.08 ± 0.01	No
2745	RGB	5.07 ± 0.05	8.07 ± 0.08	5.11 ± 0.04	8.17 ± 0.08	No
3114	RGB	5.24 ± 0.03	8.04 ± 0.05	5.30 ± 0.02	8.15 ± 0.05	No
3258	RGB	5.16 ± 0.01	8.03 ± 0.05	5.20 ± 0.02	8.13 ± 0.05	No
4361	RGB	5.31 ± 0.06	7.98 ± 0.03	5.36 ± 0.06	8.09 ± 0.03	No
4496	RGB	5.19 ± 0.05	8.09 ± 0.09	5.25 ± 0.04	8.21 ± 0.08	No
4806	RGB	4.95 ± 0.03	8.17 ± 0.03	4.98 ± 0.02	8.29 ± 0.04	No
4938	RGB	5.20 ± 0.05	8.12 ± 0.04	5.27 ± 0.05	8.28 ± 0.04	Yes
5965	RGB	5.38 ± 0.01	7.90 ± 0.08	5.46 ± 0.01	8.06 ± 0.08	Yes
6978	RGB	5.28 ± 0.04	8.15 ± 0.01	5.34 ± 0.03	8.25 ± 0.01	No
7076	RGB	5.01 ± 0.05	8.27 ± 0.01	5.07 ± 0.04	8.48 ± 0.01	Yes
7081	RGB	5.22 ± 0.06	7.92 ± 0.05	5.26 ± 0.06	8.03 ± 0.06	No
7298	RGB	4.91 ± 0.02	8.03 ± 0.05	4.93 ± 0.01	8.13 ± 0.05	No
7526	RGB	5.36 ± 0.00	7.94 ± 0.05	5.41 ± 0.01	7.99 ± 0.05	No
7634	RGB	5.02 ± 0.05	8.19 ± 0.04	5.06 ± 0.04	8.26 ± 0.04	No

7672	RGB	5.17 ± 0.03	8.15 ± 0.04	5.21 ± 0.02	8.21 ± 0.03	No
7973	RGB	5.24 ± 0.00	8.08 ± 0.05	5.28 ± 0.01	8.46 ± 0.05	Yes
8099	RGB	5.06 ± 0.02	8.17 ± 0.02	5.11 ± 0.01	8.30 ± 0.03	No
8460	RGB	5.29 ± 0.01	8.07 ± 0.04	5.33 ± 0.00	8.14 ± 0.04	No
8602	RGB	5.00 ± 0.01	8.08 ± 0.07	5.03 ± 0.02	8.18 ± 0.06	No
8803	RGB	5.23 ± 0.07	7.93 ± 0.11	5.29 ± 0.07	8.29 ± 0.11	Yes
9040	RGB	5.07 ± 0.05	8.07 ± 0.06	5.13 ± 0.04	8.30 ± 0.06	Yes
9156	RGB	5.36 ± 0.03	7.90 ± 0.02	5.41 ± 0.04	7.98 ± 0.01	No
10801	RGB	5.23 ± 0.06	7.88 ± 0.05	5.29 ± 0.05	8.07 ± 0.05	Yes
10928	RGB	4.97 ± 0.09	8.15 ± 0.02	5.03 ± 0.08	8.50 ± 0.02	Yes
12387	RGB	5.06 ± 0.08	8.15 ± 0.09	5.11 ± 0.08	8.27 ± 0.09	No
13170	RGB	5.08 ± 0.04	8.08 ± 0.03	5.12 ± 0.05	8.18 ± 0.03	No
13179	RGB	5.03 ± 0.04	8.15 ± 0.04	5.09 ± 0.03	8.48 ± 0.04	Yes
14037	RGB	4.88 ± 0.05	8.12 ± 0.07	4.93 ± 0.04	8.43 ± 0.07	Yes
14350	RGB	5.26 ± 0.00	7.98 ± 0.06	5.32 ± 0.00	8.16 ± 0.06	Yes
14377	RGB	5.31 ± 0.03	8.03 ± 0.07	5.36 ± 0.03	8.17 ± 0.07	Yes
15010	RGB	4.98 ± 0.05	8.25 ± 0.09	5.04 ± 0.04	8.48 ± 0.09	Yes
16053	RGB	5.30 ± 0.03	8.00 ± 0.02	5.35 ± 0.03	8.10 ± 0.02	No
16788	RGB	5.00 ± 0.05	8.37 ± 0.07	4.85 ± 0.07	8.52 ± 0.06	Yes
17095	RGB	5.33 ± 0.09	7.86 ± 0.07	5.39 ± 0.08	7.98 ± 0.07	No
17461	RGB	5.03 ± 0.02	8.15 ± 0.07	4.94 ± 0.03	8.39 ± 0.07	Yes
22578	RGB	4.92 ± 0.06	8.31 ± 0.07	4.97 ± 0.05	8.45 ± 0.07	Yes

23196	RGB	5.23 ± 0.02	8.14 ± 0.11	5.29 ± 0.01	8.27 ± 0.11	No
25011	RGB	5.40 ± 0.07	8.00 ± 0.05	5.46 ± 0.07	8.10 ± 0.05	No
29983	RGB	5.38 ± 0.06	8.09 ± 0.07	5.43 ± 0.05	8.18 ± 0.07	No
31696	RGB	5.25 ± 0.02	8.07 ± 0.09	5.31 ± 0.01	8.45 ± 0.09	Yes
32412	RGB	5.25 ± 0.03	8.02 ± 0.11	5.29 ± 0.02	8.12 ± 0.11	No
33040	RGB	5.09 ± 0.08	8.21 ± 0.07	5.12 ± 0.07	8.29 ± 0.07	No
33060	RGB	5.14 ± 0.08	8.08 ± 0.06	5.17 ± 0.07	8.14 ± 0.06	No
33152	RGB	5.01 ± 0.08	8.10 ± 0.06	5.07 ± 0.07	8.23 ± 0.06	No
33480	RGB	4.85 ± 0.01	8.11 ± 0.07	4.87 ± 0.00	8.24 ± 0.08	No
33654	RGB	5.18 ± 0.09	8.17 ± 0.08	5.25 ± 0.09	8.44 ± 0.08	No
34336	RGB	5.30 ± 0.05	7.96 ± 0.04	5.35 ± 0.04	8.03 ± 0.04	No
34423	RGB	5.20 ± 0.05	8.08 ± 0.02	5.24 ± 0.04	8.17 ± 0.02	No
34725	RGB	4.98 ± 0.01	8.16 ± 0.06	5.00 ± 0.00	8.22 ± 0.06	No
35072	RGB	5.18 ± 0.04	8.19 ± 0.05	5.23 ± 0.04	8.27 ± 0.05	No
36015	RGB	5.05 ± 0.04	8.07 ± 0.02	5.08 ± 0.03	8.14 ± 0.02	No
36781	RGB	5.22 ± 0.07	8.06 ± 0.07	5.27 ± 0.06	8.17 ± 0.07	No
37542	RGB	5.39 ± 0.07	7.91 ± 0.04	5.44 ± 0.07	7.98 ± 0.04	No
38229	RGB	5.26 ± 0.03	7.91 ± 0.03	5.32 ± 0.03	8.04 ± 0.03	No
39273	RGB	5.13 ± 0.00	8.14 ± 0.09	5.17 ± 0.01	8.24 ± 0.09	No
40856	RGB	4.94 ± 0.05	8.18 ± 0.05	4.99 ± 0.05	8.53 ± 0.05	Yes
41863	RGB	5.44 ± 0.06	8.00 ± 0.09	5.49 ± 0.05	8.06 ± 0.09	No
42611	RGB	5.08 ± 0.07	8.24 ± 0.03	5.12 ± 0.07	8.62 ± 0.03	Yes

43859	RGB	5.15 ± 0.06	7.97 ± 0.10	5.20 ± 0.05	8.07 ± 0.10	No
45171	RGB	5.07 ± 0.03	8.21 ± 0.05	5.11 ± 0.02	8.27 ± 0.06	No
45284	RGB	5.06 ± 0.07	8.15 ± 0.08	5.13 ± 0.07	8.41 ± 0.08	No
45534	RGB	5.02 ± 0.06	8.21 ± 0.05	5.05 ± 0.06	8.27 ± 0.05	No
45700	RGB	5.29 ± 0.01	7.95 ± 0.11	5.33 ± 0.01	8.01 ± 0.11	No
47603	RGB	5.21 ± 0.07	8.12 ± 0.03	5.24 ± 0.06	8.16 ± 0.03	No
48035	RGB	5.00 ± 0.00	8.10 ± 0.03	5.05 ± 0.01	8.25 ± 0.04	Yes
48370	RGB	5.37 ± 0.06	8.03 ± 0.03	5.43 ± 0.06	8.10 ± 0.03	No
48477	RGB	5.03 ± 0.01	8.19 ± 0.03	5.09 ± 0.00	8.32 ± 0.02	No
48627	RGB	5.24 ± 0.05	8.06 ± 0.01	5.28 ± 0.04	8.11 ± 0.02	No
49055	RGB	5.34 ± 0.05	8.07 ± 0.06	5.39 ± 0.05	8.15 ± 0.06	No
49190	RGB	4.99 ± 0.03	8.14 ± 0.02	5.02 ± 0.05	8.22 ± 0.02	No
49332	RGB	4.99 ± 0.03	8.16 ± 0.03	5.02 ± 0.02	8.23 ± 0.03	No
49470	RGB	5.01 ± 0.06	8.02 ± 0.03	5.03 ± 0.05	8.07 ± 0.03	No
57927	RGB	5.25 ± 0.05	7.93 ± 0.01	5.29 ± 0.04	8.00 ± 0.01	No
58093	RGB	4.96 ± 0.02	8.09 ± 0.01	5.00 ± 0.01	8.25 ± 0.02	Yes
59237	RGB	5.28 ± 0.04	8.03 ± 0.07	5.34 ± 0.03	8.15 ± 0.07	No
59373	RGB	5.31 ± 0.02	8.05 ± 0.08	5.36 ± 0.01	8.13 ± 0.08	No
59950	RGB	5.38 ± 0.07	7.98 ± 0.02	5.44 ± 0.06	8.04 ± 0.02	No
62781	RGB	5.14 ± 0.06	8.15 ± 0.02	5.18 ± 0.05	8.23 ± 0.03	No
63624	RGB	5.22 ± 0.03	8.01 ± 0.09	5.29 ± 0.03	8.20 ± 0.09	Yes
65008	RGB	5.28 ± 0.04	7.93 ± 0.03	5.32 ± 0.03	8.02 ± 0.03	No

65302	RGB	5.29 ± 0.08	8.00 ± 0.03	5.34 ± 0.07	8.13 ± 0.02	No
65790	RGB	5.31 ± 0.08	7.88 ± 0.11	5.36 ± 0.08	7.99 ± 0.11	No
66385	RGB	5.04 ± 0.06	8.23 ± 0.04	5.10 ± 0.07	8.36 ± 0.04	Yes
67398	RGB	5.02 ± 0.02	8.23 ± 0.03	5.05 ± 0.04	8.28 ± 0.04	No
67553	RGB	5.33 ± 0.06	7.93 ± 0.04	5.38 ± 0.05	7.99 ± 0.04	No
67586	RGB	5.26 ± 0.03	8.01 ± 0.05	5.30 ± 0.04	8.07 ± 0.05	No
68085	RGB	5.41 ± 0.06	7.92 ± 0.05	5.45 ± 0.05	8.03 ± 0.05	No
68452	RGB	5.34 ± 0.07	7.85 ± 0.06	5.38 ± 0.06	7.96 ± 0.06	Yes
KEP10	RGB	4.96 ± 0.06	8.14 ± 0.02	4.99 ± 0.05	8.22 ± 0.03	No
KEP14	RGB	5.18 ± 0.01	8.09 ± 0.02	5.23 ± 0.00	8.19 ± 0.02	No
KEP16	RGB	5.01 ± 0.03	8.17 ± 0.02	5.03 ± 0.03	8.25 ± 0.02	No
KEP17	RGB	4.90 ± 0.06	8.26 ± 0.05	4.93 ± 0.05	8.34 ± 0.05	No
KEP20	RGB	4.82 ± 0.03	8.25 ± 0.05	4.86 ± 0.02	8.45 ± 0.05	Yes
KEP21	RGB	5.30 ± 0.05	7.94 ± 0.02	5.35 ± 0.04	8.05 ± 0.02	No
KEP22	RGB	5.26 ± 0.06	8.05 ± 0.09	5.31 ± 0.06	8.15 ± 0.09	No
KEP29	RGB	4.94 ± 0.03	8.06 ± 0.04	4.96 ± 0.02	8.14 ± 0.04	No
KEP31	RGB	5.16 ± 0.00	8.05 ± 0.04	5.20 ± 0.01	8.13 ± 0.05	No
KEP32	RGB	5.32 ± 0.07	7.92 ± 0.05	5.37 ± 0.07	8.00 ± 0.05	No
KEP35	RGB	5.39 ± 0.04	8.10 ± 0.04	5.45 ± 0.04	8.20 ± 0.04	No
KEP36	RGB	4.99 ± 0.05	8.11 ± 0.03	5.02 ± 0.04	8.21 ± 0.03	No

Bibliography

AAO Software Team (2015). *2dfdr: Data reduction software*. Astrophysics Source Code Library.

Alonso, A., S. Arribas, and C. Martínez-Roger (1999). "The effective temperature scale of giant stars (F0-K5). II. Empirical calibration of T_{eff} versus colours and [Fe/H]". In: *A&AS* 140, pp. 261–277. DOI: 10.1051/aas:1999521.

Amarsi, A. M., M. Asplund, R. Collet, and J. Leenaarts (2015). "The Galactic chemical evolution of oxygen inferred from 3D non-LTE spectral-line-formation calculations". In: *MNRAS* 454, pp. L11–L15. DOI: 10.1093/mnrasl/slv122.

Amarsi, A. M., K. Lind, M. Asplund, P. S. Barklem, and R. Collet (2016a). "Non-LTE line formation of Fe in late-type stars - III. 3D non-LTE analysis of metal-poor stars". In: *MNRAS* 463, pp. 1518–1533. DOI: 10.1093/mnras/stw2077.

Amarsi, A. M., M. Asplund, R. Collet, and J. Leenaarts (2016b). "Non-LTE oxygen line formation in 3D hydrodynamic model stellar atmospheres". In: *MNRAS* 455, pp. 3735–3751. DOI: 10.1093/mnras/stv2608.

Amarsi, A. M., T. Nordlander, P. S. Barklem, M. Asplund, R. Collet, and K. Lind (2018a). "Effective temperature determinations of late-type stars based on 3D non-LTE Balmer line formation". In: *ArXiv e-prints*.

Amarsi, A. M., P. S. Barklem, M. Asplund, R. Collet, and O. Zatsarinny (2018b). "Inelastic O+H collisions and the OI 777nm solar centre-to-limb variation". In: *ArXiv e-prints*.

Arp, H. C., W. A. Baum, and A. R. Sandage (1952). "The HR diagrams for the globular clusters M 92 and M 3." In: *AJ* 57, pp. 4–5. DOI: 10.1086/106674.

Asplund, M. (2005). "New Light on Stellar Abundance Analyses: Departures from LTE and Homogeneity". In: *ARA&A* 43, pp. 481–530. DOI: 10.1146/annurev.astro.42.053102.134001.

Asplund, M., N. Grevesse, A. J. Sauval, and P. Scott (2009). "The Chemical Composition of the Sun". In: *ARA&A* 47, pp. 481–522. DOI: 10.1146/annurev.astro.46.060407.145222.

Baade, W. (1944). "The Resolution of Messier 32, NGC 205, and the Central Region of the Andromeda Nebula." In: *ApJ* 100, p. 137. DOI: 10.1086/144650.

Baraffe, I., G. Chabrier, F. Allard, and P. H. Hauschildt (1997). "Evolutionary models for metal-poor low-mass stars. Lower main sequence of globular clusters and halo field stars". In: *A&A* 327, pp. 1054–1069.

Bastian, N., H. J. G. L. M. Lamers, S. E. de Mink, S. N. Longmore, S. P. Goodwin, and M. Gieles (2013). "Early disc accretion as the origin of abundance anomalies in globular clusters". In: *MNRAS* 436, pp. 2398–2411. DOI: `10.1093/mnras/stt1745`.

Bastian, N., I. Cabrera-Ziri, and M. Salaris (2015). "A general abundance problem for all self-enrichment scenarios for the origin of multiple populations in globular clusters". In: *MNRAS* 449, pp. 3333–3346. DOI: `10.1093/mnras/stv543`.

Bellazzini, M. (2008). "The Tip of the Red Giant Branch". In: *Mem. Societa Astronomica Italiana* 79, p. 440.

Bergemann, M. and T. Nordlander (2014). "Non-LTE radiative transfer in cool stars. Theory and applications to the abundance analysis for 24 chemical elements". In: *ArXiv e-prints*.

Bergemann, M., K. Lind, R. Collet, Z. Magic, and M. Asplund (2012). "Non-LTE line formation of Fe in late-type stars - I. Standard stars with 1D and <3D> model atmospheres". In: *MNRAS* 427, pp. 27–49. DOI: `10.1111/j.1365-2966.2012.21687.x`.

Bragaglia, A., E. Carretta, R. Gratton, V. D'Orazi, S. Lucatello, and C. Sneden (2013). "Reading the book: from "chemical anomalies" to "standard composition" of globular clusters". In: *ArXiv e-prints*.

Briley, M. M., J. E. Hesser, and R. A. Bell (1991). "C and N abundances among 47 Tucanae main-sequence stars". In: *Astrophys. J.* 373, pp. 482–496. DOI: `10.1086/170068`.

Brodie, J. P. and J. Strader (2006). "Extragalactic Globular Clusters and Galaxy Formation". In: *ARAA* 44, pp. 193–267. DOI: `10.1146/annurev.astro.44.051905.092441`.

Campbell, S. W. and J. C. Lattanzio (2008). "Evolution and nucleosynthesis of extremely metal-poor and metal-free low- and intermediate-mass stars. I. Stellar yield tables and the CEMPs". In: *A&A* 490, pp. 769–776. DOI: `10.1051/0004-6361:200809597`.

Campbell, S. W., J. C. Lattanzio, and L. M. Elliott (2006). "Are there radical cyanogen abundance differences between galactic globular cluster RGB and AGB stars?. Possibly a Vital Clue to the Globular Cluster Abundance Anomaly Problem". In: *MmSAI* 77, p. 864.

Campbell, S. W., D. Yong, E. C. Wylie-de Boer, R. J. Stancliffe, J. C. Lattanzio, G. C. Angelou, F. Grundahl, and C. Sneden (2010). "The case of the disappearing CN-strong AGB stars in Galactic Globular Clusters - preliminary results". In: *MmSAI* 81, p. 1004.

— (2011). "AGB Stars in Galactic Globular Clusters: Are They Really Chemically Distinct from Their Fellow RGB and HB Stars?" In: *Why Galaxies Care about AGB Stars II: Shining Examples and Common Inhabitants*. Ed. by F. Kerschbaum, T. Lebzelter, and R. F. Wing. Vol. 445. Astronomical Society of the Pacific Conference Series, p. 63.

Campbell, S. W., D. Yong, E. C. Wylie-de Boer, R. J. Stancliffe, J. C. Lattanzio, G. C. Angelou, V. D'Orazi, S. L. Martell, F. Grundahl, and C. Sneden (2012). "Cyanogen in NGC 1851 Red Giant Branch and Asymptotic Giant Branch Stars: Quadrimodal Distributions". In: *ApJL* 761, L2, p. L2. DOI: 10.1088/2041-8205/761/1/L2.

Campbell, S. W., V. D'Orazi, D. Yong, T. N. Constantino, J. C. Lattanzio, R. J. Stancliffe, G. C. Angelou, E. C. Wylie-de Boer, and F. Grundahl (2013). "Sodium content as a predictor of the advanced evolution of globular cluster stars". In: *Nature* 498, pp. 198–200. DOI: 10.1038/nature12191.

Campbell, S. W., T. N. Constantino, V. D'Orazi, C. Meakin, D. Stello, J. Christensen-Dalsgaard, C. Kuehn, G. M. De Silva, W. D. Arnett, J. C. Lattanzio, and B. T. MacLean (2016). "Towards 21st century stellar models: Star clusters, supercomputing and asteroseismology". In: *Astronomische Nachrichten* 337, p. 788. DOI: 10.1002/asna.201612373.

Campbell, S. W., B. T. MacLean, V. D'Orazi, L. Casagrande, G. M. de Silva, D. Yong, P. L. Cottrell, and J. C. Lattanzio (2017). "NGC 6752 AGB stars revisited. I. Improved AGB temperatures remove apparent overionisation of Fe I". In: *A&A* 605, A98, A98. DOI: 10.1051/0004-6361/201731101.

Cannon, R. D., B. F. W. Croke, R. A. Bell, J. E. Hesser, and R. A. Stathakis (1998). "Carbon and nitrogen abundance variations on the main sequence of 47 Tucanae". In: *MNRAS* 298, pp. 601–624. DOI: 10.1046/j.1365-8711.1998.01671.x.

Carbon, D. F., W. Romanishin, G. E. Langer, D. Butler, E. Kemper, C. F. Trefzger, R. P. Kraft, and N. B. Suntzeff (1982). "Carbon and nitrogen abundances in giant stars of the metal-poor globular cluster M92". In: *ApJS* 49, pp. 207–258. DOI: 10.1086/190796.

Carretta, E., A. Bragaglia, R. G. Gratton, S. Lucatello, and Y. Momany (2007). "Na-O anticorrelation and horizontal branches. II. The Na-O anticorrelation in the globular cluster NGC 6752". In: *Astron. Astrophys.* 464, pp. 927–937. DOI: 10.1051/0004-6361:20065208.

Carretta, E., A. Bragaglia, R. Gratton, V. D'Orazi, and S. Lucatello (2009a). "Intrinsic iron spread and a new metallicity scale for globular clusters". In: *A&A* 508, pp. 695–706. DOI: 10.1051/0004-6361/200913003.

Carretta, E., A. Bragaglia, R. G. Gratton, S. Lucatello, G. Catanzaro, F. Leone, M. Bellazzini, R. Claudi, V. D'Orazi, Y. Momany, S. Ortolani, E. Pancino, G. Piotto, A. Recio-Blanco, and E. Sabbi (2009b). "Na-O anticorrelation and HB. VII. The chemical composition of first and second-generation stars in 15 globular clusters from GIRAFFE spectra". In: *A&A* 505, pp. 117–138. DOI: 10.1051/0004-6361/200912096.

Carretta, E., A. Bragaglia, R. Gratton, and S. Lucatello (2009c). "Na-O anticorrelation and HB. VIII. Proton-capture elements and metallicities in 17 globular clusters from UVES spectra". In: *A&A* 505, pp. 139–155. DOI: 10.1051/0004-6361/200912097.

Carretta, E., A. Bragaglia, R. G. Gratton, A. Recio-Blanco, S. Lucatello, V. D'Orazi, and S. Cassisi (2010). "Properties of stellar generations in globular clusters and relations with global parameters". In: *A&A* 516, A55, A55. DOI: 10.1051/0004-6361/200913451.

Carretta, E., A. Bragaglia, R. G. Gratton, S. Lucatello, and V. D'Orazi (2012). "Chemical Tagging of Three Distinct Populations of Red Giants in the Globular Cluster NGC 6752". In: *Astrophys. J.* 750, L14, p. L14. DOI: 10.1088/2041-8205/750/1/L14.

Carretta, E., R. G. Gratton, A. Bragaglia, V. D'Orazi, and S. Lucatello (2013). "An aluminium tool for multiple stellar generations in the globular clusters 47 Tucanae and M 4". In: *A&A* 550, A34, A34. DOI: 10.1051/0004-6361/201220470.

Casagrande, L., I. Ramírez, J. Meléndez, M. Bessell, and M. Asplund (2010). "An absolutely calibrated T_{eff} scale from the infrared flux method. Dwarfs and subgiants". In: *A&A* 512, A54, A54. DOI: 10.1051/0004-6361/200913204.

Casagrande, L., L. Portinari, I. S. Glass, D. Laney, V. Silva Aguirre, J. Datson, J. Andersen, B. Nordström, J. Holmberg, C. Flynn, and M. Asplund (2014). "Towards stellar effective temperatures and diameters at 1 per cent accuracy for future surveys". In: *MNRAS* 439, pp. 2060–2073. DOI: 10.1093/mnras/stu089.

Cassisi, S., M. Salaris, A. Pietrinferni, J. S. Vink, and M. Monelli (2014). "On the missing second generation AGB stars in NGC 6752". In: *A&A* 571, A81, A81. DOI: 10.1051/0004-6361/201424540.

Castellani, V. and A. Renzini (1968). "On the Evolution of the Horizontal Branch Stars of Metal-Poor Globular Clusters". In: *Ap&SS* 2, pp. 310–314. DOI: 10.1007/BF00650907.

Castelli, F. and R. L. Kurucz (2004). "New Grids of ATLAS9 Model Atmospheres". In: *ArXiv Astrophysics e-prints (astro-ph/0405087)*.

Castelli, F., R. G. Gratton, and R. L. Kurucz (1997). "Notes on the convection in the ATLAS9 model atmospheres." In: *A&A* 318, pp. 841–869.

Catelan, M. (2009). "Horizontal branch stars: the interplay between observations and theory, and insights into the formation of the Galaxy". In: *Astrophysics and Space Science* 320, pp. 261–309. DOI: 10.1007/s10509-009-9987-8.

Catelan, M., J. A. de Freitas Pacheco, and J. E. Horvath (1996). "The Helium-Core Mass at the Helium Flash in Low-Mass Red Giant Stars: Observations and Theory". In: *ApJ* 461, p. 231. DOI: 10.1086/177051.

Chantereau, W., C. Charbonnel, and G. Meynet (2016). "Evolution of long-lived globular cluster stars. III. Effect of the initial helium spread on the position of stars in a synthetic Hertzsprung-Russell diagram". In: *A&A* 592, A111, A111. DOI: 10.1051/0004-6361/201628418.

Charbonnel, C. and W. Chantereau (2016). "Evolution of long-lived globular cluster stars. II. Sodium abundance variations on the asymptotic giant branch as a function of globular cluster age and metallicity". In: *A&A* 586, A21. DOI: 10.1051/0004-6361/201527576.

Charbonnel, C., W. Chantereau, T. Decressin, G. Meynet, and D. Schaerer (2013). "Why the globular cluster NGC 6752 contains no sodium-rich second-generation AGB stars". In: *A&A* 557, L17, p. L17. DOI: 10.1051/0004-6361/201322422.

Charbonnel, C., W. Chantereau, M. Krause, F. Primas, and Y. Wang (2014). "Are there any first-generation stars in globular clusters today?" In: *A&A* 569, L6, p. L6. DOI: 10.1051/0004-6361/201424804.

Clayton, D. D. (1983). *Principles of Stellar Evolution and Nucleosynthesis*. University of Chicago Press, Chicago.

Constantino, T., S. Campbell, P. Gil-Pons, and J. Lattanzio (2014). "On the Necessity of Composition-dependent Low-temperature Opacity in Models of Metal-poor Asymptotic Giant Branch Stars". In: *ApJ* 784, 56, p. 56. DOI: 10.1088/0004-637X/784/1/56.

Constantino, T., S. W. Campbell, J. Christensen-Dalsgaard, J. C. Lattanzio, and D. Stello (2015). "The treatment of mixing in core helium burning models - I. Implications for asteroseismology". In: *MNRAS* 452, pp. 123–145. DOI: 10.1093/mnras/stv1264.

Constantino, T., S. W. Campbell, J. C. Lattanzio, and A. van Duijneveldt (2016). "The treatment of mixing in core helium burning models - II. Constraints from cluster star counts". In: *MNRAS* 456, pp. 3866–3885. DOI: 10.1093/mnras/stv2939.

Constantino, T., S. W. Campbell, and J. C. Lattanzio (2017). "The treatment of mixing in core helium-burning models - III. Suppressing core breathing pulses with a new constraint on overshoot". In: *MNRAS* 472, pp. 4900–4909. DOI: 10.1093/mnras/stx2321.

Cottrell, P. L. and G. S. Da Costa (1981). "Correlated cyanogen and sodium anomalies in the globular clusters 47 TUC and NGC 6752". In: *ApJL* 245, pp. L79–L82. DOI: 10.1086/183527.

Cristallo, S., O. Straniero, R. Gallino, L. Piersanti, I. Domínguez, and M. T. Lederer (2009). "Evolution, Nucleosynthesis, and Yields of Low-Mass Asymptotic Giant Branch Stars at Different Metallicities". In: *ApJ* 696, pp. 797–820. DOI: 10.1088/0004-637X/696/1/797.

Da Costa, G. S., J. Norris, and J. V. Villumsen (1986). "The blue stragglers of Omega Centauri". In: *ApJ* 308, pp. 743–754. DOI: 10.1086/164547.

Dalessandro, E., M. Salaris, F. R. Ferraro, A. Mucciarelli, and S. Cassisi (2013). "The horizontal branch in the UV colour-magnitude diagrams - II. The case of M3, M13 and M79". In: *MNRAS* 430, pp. 459–471. DOI: 10.1093/mnras/sts644.

D'Antona, F., V. Caloi, J. Montalbán, P. Ventura, and R. Gratton (2002). "Helium variation due to self-pollution among Globular Cluster stars. Consequences on the horizontal branch morphology". In: *A&A* 395, pp. 69–75. DOI: 10.1051/0004-6361:20021220.

D'Antona, F., M. Bellazzini, V. Caloi, F. F. Pecci, S. Galleti, and R. T. Rood (2005). "A Helium Spread among the Main-Sequence Stars in NGC 2808". In: *ApJ* 631, pp. 868–878. DOI: 10.1086/431968.

De Silva, G. M., B. K. Gibson, J. Lattanzio, and M. Asplund (2009). "O and Na abundance patterns in open clusters of the Galactic disk". In: *A&A* 500, pp. L25–L28. DOI: 10.1051/0004-6361/200912279.

De Silva, G. M., K. C. Freeman, J. Bland-Hawthorn, S. Martell, E. W. de Boer, M. Asplund, S. Keller, S. Sharma, D. B. Zucker, T. Zwitter, B. Anguiano, C. Bacigalupo, D. Bayliss, M. A. Beavis, M. Bergemann, S. Campbell, R. Cannon, D. Carollo, L. Casagrande, A. R. Casey, G. Da Costa, V. D'Orazi, A. Dotter, L. Duong, A. Heger, M. J. Ireland, P. R. Kafle, J. Kos, J. Lattanzio, G. F. Lewis, J. Lin, K. Lind, U. Munari, D. M. Nataf, S. O'Toole, Q. Parker, W. Reid, K. J. Schlesinger, A. Sheinis, J. D. Simpson, D. Stello, Y.-S. Ting, G. Traven, F. Watson, R. Wittenmyer, D. Yong, and M. Žerjal (2015). "The GALAH survey: scientific motivation". In: *MNRAS* 449, pp. 2604–2617. DOI: 10.1093/mnras/stv327.

Decressin, T., G. Meynet, C. Charbonnel, N. Prantzos, and S. Ekström (2007). "Fast rotating massive stars and the origin of the abundance patterns in galactic globular clusters". In: *A&A* 464, pp. 1029–1044. DOI: 10.1051/0004-6361:20066013.

Doherty, C. L., P. Gil-Pons, L. Siess, J. C. Lattanzio, and H. H. B. Lau (2015). "Super- and massive AGB stars - IV. Final fates - initial-to-final mass relation". In: *MNRAS* 446, pp. 2599–2612. DOI: 10.1093/mnras/stu2180.

D'Orazi, V. and A. F. Marino (2010). "Lithium Abundances in Red Giants of M4: Evidence for Asymptotic Giant Branch Star Pollution in Globular

Clusters?” In: *ApJL* 716, pp. L166–L169. DOI: 10.1088/2041-8205/716/2/L166.

Dorman, B., R. T. Rood, and R. W. O’Connell (1993). “Ultraviolet Radiation from Evolved Stellar Populations. I. Models”. In: *ApJ* 419, p. 596. DOI: 10.1086/173511.

Dupree, A. K., J. Strader, and G. H. Smith (2011). “Direct Evidence for an Enhancement of Helium in Giant Stars in Omega Centauri”. In: *ApJ* 728, 155, p. 155. DOI: 10.1088/0004-637X/728/2/155.

Eddington, A. S. (1926). *The Internal Constitution of the Stars*.

Eggleton, P. P., D. S. P. Dearborn, and J. C. Lattanzio (2006). “Deep Mixing of ^{3}He: Reconciling Big Bang and Stellar Nucleosynthesis”. In: *Science* 314, p. 1580. DOI: 10.1126/science.1133065.

Fenner, Y., S. Campbell, A. I. Karakas, J. C. Lattanzio, and B. K. Gibson (2004). “Modelling self-pollution of globular clusters from asymptotic giant branch stars”. In: *MNRAS* 353, pp. 789–795. DOI: 10.1111/j.1365-2966.2004.08108.x.

Fitzpatrick, E. L. and D. Massa (2007). “An Analysis of the Shapes of Interstellar Extinction Curves. V. The IR-through-UV Curve Morphology”. In: *ApJ* 663, pp. 320–341. DOI: 10.1086/518158.

Freeman, K. C. (2012). “The HERMES Project: Reconstructing Galaxy Formation”. In: *Galactic Archaeology: Near-Field Cosmology and the Formation of the Milky Way*. Ed. by W. Aoki, M. Ishigaki, T. Suda, T. Tsujimoto, and N. Arimoto. Vol. 458. Astronomical Society of the Pacific Conference Series, p. 393.

Freeman, K. C. and J. Norris (1981). “The chemical composition, structure, and dynamics of globular clusters”. In: *ARAA* 19, pp. 319–356. DOI: 10.1146/annurev.aa.19.090181.001535.

García-Hernández, D. A., S. Mészáros, M. Monelli, S. Cassisi, P. B. Stetson, O. Zamora, M. Shetrone, and S. Lucatello (2015). “Clear Evidence for the Presence of Second-generation Asymptotic Giant Branch Stars in Metal-poor Galactic Globular Clusters”. In: *ApJL* 815, L4, p. L4. DOI: 10.1088/2041-8205/815/1/L4.

González Hernández, J. I. and P. Bonifacio (2009). “A new implementation of the infrared flux method using the 2MASS catalogue”. In: *A&A* 497, pp. 497–509. DOI: 10.1051/0004-6361/200810904.

Gratton, R., C. Sneden, and E. Carretta (2004). “Abundance Variations Within Globular Clusters”. In: *ARA&A* 42, pp. 385–440. DOI: 10.1146/annurev.astro.42.053102.133945.

Gratton, R. G. and C. Sneden (1988). “Abundances in extremely metal-poor stars”. In: *A&A* 204, pp. 193–218.

Gratton, R. G., E. Carretta, and F. Castelli (1996). "Abundances of light elements in metal-poor stars. I. Atmospheric parameters and a new T_eff_ scale". In: *A&A* 314, pp. 191–203.

Gratton, R. G., E. Carretta, K. Eriksson, and B. Gustafsson (1999). "Abundances of light elements in metal-poor stars. II. Non-LTE abundance corrections". In: *A&A* 350, pp. 955–969.

Gratton, R. G., P. Bonifacio, A. Bragaglia, E. Carretta, V. Castellani, M. Centurion, A. Chieffi, R. Claudi, G. Clementini, F. D'Antona, S. Desidera, P. François, F. Grundahl, S. Lucatello, P. Molaro, L. Pasquini, C. Sneden, F. Spite, and O. Straniero (2001). "The O-Na and Mg-Al anticorrelations in turn-off and early subgiants in globular clusters". In: *A&A* 369, pp. 87–98. DOI: 10.1051/0004-6361:20010144.

Gratton, R. G., E. Carretta, R. Claudi, S. Lucatello, and M. Barbieri (2003a). "Abundances for metal-poor stars with accurate parallaxes. I. Basic data". In: *A&A* 404, pp. 187–210. DOI: 10.1051/0004-6361:20030439.

Gratton, R. G., A. Bragaglia, E. Carretta, G. Clementini, S. Desidera, F. Grundahl, and S. Lucatello (2003b). "Distances and ages of NGC 6397, NGC 6752 and 47 Tuc". In: *A&A* 408, pp. 529–543. DOI: 10.1051/0004-6361:20031003.

Gratton, R. G., A. Bragaglia, E. Carretta, F. de Angeli, S. Lucatello, Y. Momany, G. Piotto, and A. Recio Blanco (2005). "Precise reddening and metallicity of NGC 6752 from FLAMES spectra". In: *A&A* 440, pp. 901–908. DOI: 10.1051/0004-6361:20053019.

Gratton, R. G., V. D'Orazi, A. Bragaglia, E. Carretta, and S. Lucatello (2010a). "The connection between missing AGB stars and extended horizontal branches". In: *A&A* 522, A77, A77. DOI: 10.1051/0004-6361/201015405.

Gratton, R. G., E. Carretta, A. Bragaglia, S. Lucatello, and V. D'Orazi (2010b). "The second and third parameters of the horizontal branch in globular clusters". In: *A&A* 517, A81, A81. DOI: 10.1051/0004-6361/200912572.

Gratton, R. G., E. Carretta, and A. Bragaglia (2012). "Multiple populations in globular clusters. Lessons learned from the Milky Way globular clusters". In: *A&A Rev.* 20, p. 50. DOI: 10.1007/s00159-012-0050-3.

Gratton, R. G., S. Lucatello, A. Sollima, E. Carretta, A. Bragaglia, Y. Momany, V. D'Orazi, M. Salaris, S. Cassisi, and P. B. Stetson (2015). "The Na-O anticorrelation in horizontal branch stars. V. NGC 6723". In: *A&A* 573, A92, A92. DOI: 10.1051/0004-6361/201424393.

Gratton, R.G. (1988). In: *Rome Obs. Preprint Ser., 29*.

Gray, D. F. (2005). *The Observation and Analysis of Stellar Photospheres*.

Greggio, L. and A. Renzini (1990). "Clues on the hot star content and the ultraviolet output of elliptical galaxies". In: *ApJ* 364, pp. 35–64. DOI: `10.1086/169384`.

Grevesse, N. and A. J. Sauval (1998). "Standard Solar Composition". In: *SSRv* 85, pp. 161–174. DOI: `10.1023/A:1005161325181`.

Grundahl, F., M. Catelan, W. B. Landsman, P. B. Stetson, and M. I. Andersen (1999). "Hot Horizontal-Branch Stars: The Ubiquitous Nature of the "Jump" in Strömgren u, Low Gravities, and the Role of Radiative Levitation of Metals". In: *ApJ* 524, pp. 242–261. DOI: `10.1086/307807`.

Gruyters, P., L. Casagrande, A. P. Milone, S. T. Hodgkin, A. Serenelli, and S. Feltzing (2017). "First evidence of multiple populations along the AGB from Strömgren photometry". In: *A&A* 603, A37, A37. DOI: `10.1051/0004-6361/201630341`.

Gustafsson, B., R. A. Bell, K. Eriksson, and A. Nordlund (1975). "A grid of model atmospheres for metal-deficient giant stars. I". In: *A&A* 42, pp. 407–432.

Gustafsson, B., B. Edvardsson, K. Eriksson, U. G. Jørgensen, Å. Nordlund, and B. Plez (2008). "A grid of MARCS model atmospheres for late-type stars. I. Methods and general properties". In: *A&A* 486, pp. 951–970. DOI: `10.1051/0004-6361:200809724`.

Habing, H.J. and H. Olofsson (2004). *Asymptotic Giant Branch Stars*. Astronomy and Astrophysics Library. Springer. ISBN: 9780387008806. URL: `http://books.google.com.au/books?id=KpRH1mAl7HIC`.

Hansen, B. M. S., J. Brewer, G. G. Fahlman, B. K. Gibson, R. Ibata, M. Limongi, R. M. Rich, H. B. Richer, M. M. Shara, and P. B. Stetson (2002). "The White Dwarf Cooling Sequence of the Globular Cluster Messier 4". In: *ApJL* 574, pp. L155–L158. DOI: `10.1086/342528`.

Hansen, C. J., S. D. Kawaler, and V. Trimble (2004). *Stellar interiors : physical principles, structure, and evolution*.

Harris, W. E. (1996). "A Catalog of Parameters for Globular Clusters in the Milky Way". In: *AJ* 112, p. 1487. DOI: `10.1086/118116`.

Heger, A., C. L. Fryer, S. E. Woosley, N. Langer, and D. H. Hartmann (2003). "How Massive Single Stars End Their Life". In: *ApJ* 591, pp. 288–300. DOI: `10.1086/375341`.

Heijmans, J., M. Asplund, S. Barden, M. Birchall, D. Carollo, J. Bland-Hawthorn, J. Brzeski, S. Case, V. Churilov, M. Colless, R. Dean, G. De Silva, T. Farrell, K. Fiegert, K. Freeman, L. Gers, M. Goodwin, D. Gray, R. Heald, A. Heng, D. Jones, C. Kobayashi, U. Klauser, Y. Kondrat, J. Lawrence, S. Lee, D. Mathews, D. Mayfield, S. Miziarski, G. J. Monnet, R. Muller, N. Pai, R. Patterson, E. Penny, D. Orr, A. Sheinis, K. Shortridge, S. Smedley, G. Smith, D. Stafford, N. Staszak, M. Vuong, L. Waller, D. Whittard, E.

Wylie de Boer, P. Xavier, J. Zheng, R. Zhelem, and D. Zucker (2012). "Integrating the HERMES spectrograph for the AAT". In: *Society of Photo-Optical Instrumentation Engineers (SPIE) Conference Series*. Vol. 8446. Society of Photo-Optical Instrumentation Engineers (SPIE) Conference Series. DOI: 10.1117/12.925806.

Hendricks, B., P. B. Stetson, D. A. VandenBerg, and M. Dall'Ora (2012). "A New Reddening Law for M4". In: *AJ* 144, 25, p. 25. DOI: 10.1088/0004-6256/144/1/25.

Henkel, K., A. I. Karakas, and J. C. Lattanzio (2017). "A phenomenological modification of thermohaline mixing in globular cluster red giants". In: *MNRAS* 469, pp. 4600–4612. DOI: 10.1093/mnras/stx1187.

Herwig, F. (2005). "Evolution of Asymptotic Giant Branch Stars". In: *ARAA* 43, pp. 435–479. DOI: 10.1146/annurev.astro.43.072103.150600.

Herwig, F., T. Bloecker, D. Schoenberner, and M. El Eid (1997). "Stellar evolution of low and intermediate-mass stars. IV. Hydrodynamically-based overshoot and nucleosynthesis in AGB stars." In: *A&A* 324, pp. L81–L84.

Hesser, J. E., F. D. A. Hartwick, and R. D. McClure (1977). "Cyanogen strengths and ultraviolet excesses of evolved stars in 17 globular clusters from DDO photometry." In: *ApJS* 33, pp. 471–493. DOI: 10.1086/190438.

Hinkel, N. R., P. A. Young, M. D. Pagano, S. J. Desch, A. D. Anbar, V. Adibekyan, S. Blanco-Cuaresma, J. K. Carlberg, E. Delgado Mena, F. Liu, T. Nordlander, S. G. Sousa, A. Korn, P. Gruyters, U. Heiter, P. Jofré, N. C. Santos, and C. Soubiran (2016). "A Comparison of Stellar Elemental Abundance Techniques and Measurements". In: *ApJS* 226, 4, p. 4. DOI: 10.3847/0067-0049/226/1/4.

Hubeny, I. and D. Mihalas (2014). *Theory of Stellar Atmospheres*.

Iben, I. and A. Renzini (1984). "Single star evolution I. Massive stars and early evolution of low and intermediate mass stars". In: *Physics Reports* 105, pp. 329–406. DOI: 10.1016/0370-1573(84)90142-X.

Iben Jr., I. (1965). "Stellar Evolution. I. The Approach to the Main Sequence." In: *ApJ* 141, p. 993. DOI: 10.1086/148193.

— (1967). "Stellar Evolution Within and off the Main Sequence". In: *ARAA* 5, p. 571. DOI: 10.1146/annurev.aa.05.090167.003035.

— (1971). "Globular Cluster Stars: Results of Theoretical Evolution and Pulsation Studies Compared with the Observations". In: *PASP* 83, p. 697. DOI: 10.1086/129210.

— (1975). "Thermal pulses; p-capture, alpha-capture, s-process nucleosynthesis; and convective mixing in a star of intermediate mass". In: *ApJ* 196, pp. 525–547. DOI: 10.1086/153433.

Iben Jr., I. and R. T. Rood (1970). "Metal-Poor Stars. III. on the Evolution of Horizontal-Branch Stars". In: *ApJ* 161, p. 587. DOI: 10.1086/150563.

Ivans, I. I., C. Sneden, R. P. Kraft, N. B. Suntzeff, V. V. Smith, G. E. Langer, and J. P. Fulbright (1999). "Star-to-Star Abundance Variations among Bright Giants in the Mildly Metal-poor Globular Cluster M4". In: *AJ* 118, pp. 1273–1300. DOI: 10.1086/301017.

Ivans, I. I., R. P. Kraft, C. Sneden, G. H. Smith, R. M. Rich, and M. Shetrone (2001). "New Analyses of Star-to-Star Abundance Variations among Bright Giants in the Mildly Metal-poor Globular Cluster M5". In: *AJ* 122, pp. 1438–1463. DOI: 10.1086/322108.

Johnson, C. I., I. McDonald, C. A. Pilachowski, M. Mateo, J. I. Bailey III, M. J. Cordero, A. A. Zijlstra, J. D. Crane, E. Olszewski, S. A. Shectman, and I. Thompson (2015). "AGB Sodium Abundances in the Globular Cluster 47 Tucanae (NGC 104)". In: *AJ* 149, 71, p. 71. DOI: 10.1088/0004-6256/149/2/71.

Johnson, H. L. and W. W. Morgan (1953). "Fundamental stellar photometry for standards of spectral type on the revised system of the Yerkes spectral atlas". In: *ApJ* 117, p. 313. DOI: 10.1086/145697.

Karakas, A. I., Y. Fenner, A. Sills, S. W. Campbell, and J. C. Lattanzio (2006). "The Chemical Evolution of Helium in Globular Clusters: Implications for the Self-Pollution Scenario". In: *ApJ* 652, pp. 1240–1245. DOI: 10.1086/508504.

Karakas, A. I., A. F. Marino, and D. M. Nataf (2014). "Nucleosynthesis in Helium-enriched Asymptotic Giant Branch Models: Implications for Heavy Element Enrichment in ω Centauri". In: *ApJ* 784, 32, p. 32. DOI: 10.1088/0004-637X/784/1/32.

Kippenhahn, R. and A. Weigert (1990). *Stellar Structure and Evolution*, p. 192.

Kraft, R. P. (1979). "On the nonhomogeneity of metal abundances in stars of globular clusters and satellite subsystems of the Galaxy". In: *ARAA* 17, pp. 309–343. DOI: 10.1146/annurev.aa.17.090179.001521.

— (1994). "Abundance differences among globular-cluster giants: Primordial versus evolutionary scenarios". In: *PASP* 106, pp. 553–565. DOI: 10.1086/133416.

Kraft, R. P., C. Sneden, G. H. Smith, M. D. Shetrone, G. E. Langer, and C. A. Pilachowski (1997). "Proton Capture Chains in Globular Cluster Stars.II.Oxygen, Sodium, Magnesium, and Aluminum Abundances in M13 Giants Brighter Than the Horizontal Branch". In: *AJ* 113, p. 279. DOI: 10.1086/118251.

Kurucz, R. (1993). "ATLAS9 Stellar Atmosphere Programs and 2 km/s grid." In: *CD-ROM No. 13., Smithsonian Astrophysical Observatory, Cambridge, Mass.* 13.

Lada, C. J. and E. A. Lada (2003). "Embedded Clusters in Molecular Clouds". In: *ARAA* 41, pp. 57–115. DOI: 10.1146/annurev.astro.41.011802.094844.

Lambert, D. L. (1992). "Observational Effects of Nucleosynthesis in Evolved Stars". In: *Elements and the Cosmos*. Ed. by M. G. Edmunds and R. Terlevich, p. 92.

Langer, G. E., R. P. Kraft, and E. D. Friel (1985). "Bimodal cyanogen distributions in moderately metal-poor globular clusters. I - Carbon and nitrogen abundances for six M5 giants". In: *PASP* 97, pp. 373–381. DOI: 10.1086/131547.

Lapenna, E., A. Mucciarelli, B. Lanzoni, F. R. Ferraro, E. Dalessandro, L. Origlia, and D. Massari (2014). "Non-local Thermodynamical Equilibrium Effects on the Iron Abundance of Asymptotic Giant Branch Stars in 47 Tucanae". In: *ApJ* 797, 124, p. 124. DOI: 10.1088/0004-637X/797/2/124.

Lapenna, E., A. Mucciarelli, F. R. Ferraro, L. Origlia, B. Lanzoni, D. Massari, and E. Dalessandro (2015). "Chemical Analysis of Asymptotic Giant Branch Stars in M62". In: *ApJ* 813, 97, p. 97. DOI: 10.1088/0004-637X/813/2/97.

Lapenna, E., C. Lardo, A. Mucciarelli, M. Salaris, F. R. Ferraro, B. Lanzoni, D. Massari, P. B. Stetson, S. Cassisi, and A. Savino (2016). "Lost and Found: Evidence of Second-generation Stars Along the Asymptotic Giant Branch of the Globular Cluster NGC 6752". In: *ApJL* 826, L1, p. L1. DOI: 10.3847/2041-8205/826/1/L1.

Lardo, C., M. Salaris, A. Savino, P. Donati, P. B. Stetson, and S. Cassisi (2017). "Multiple populations along the asymptotic giant branch of the globular cluster M4". In: *MNRAS* 466, pp. 3507–3512. DOI: 10.1093/mnras/stw3374.

Larson, R. B. (2003). "The physics of star formation". In: *Reports on Progress in Physics* 66, pp. 1651–1697. DOI: 10.1088/0034-4885/66/10/R03.

Lattanzio, J. C. (1986). "The asymptotic giant branch evolution of 1.0-3.0 solar mass stars as a function of mass and composition". In: *Astrophys. J.* 311, pp. 708–730. DOI: 10.1086/164810. URL: http://adsabs.harvard.edu/cgi-bin/nph-bib_query?bibcode=1986ApJ...311..708L\&db_key=AST.

Lattanzio, J. C., C. A. Frost, R. C. Cannon, and P. R. Wood (1997). "Hot Bottom Burning Nucleosynthesis in 6M_{solar} Stellar Models". In: *Nuclear Physics A* 621, pp. 435–438. DOI: 10.1016/S0375-9474(97)00286-8.

Lee, H.-c., Y.-W. Lee, and B. K. Gibson (2002). "Horizontal-Branch Morphology and the Photometric Evolution of Old Stellar Populations". In: *AJ* 124, pp. 2664–2676. DOI: 10.1086/344066.

Lee, Y.-W., P. Demarque, and R. Zinn (1994). "The horizontal-branch stars in globular clusters. 2: The second parameter phenomenon". In: *ApJ* 423, pp. 248–265. DOI: 10.1086/173803.

Leenaarts, J. and M. Carlsson (2009). "MULTI3D: A Domain-Decomposed 3D Radiative Transfer Code". In: *The Second Hinode Science Meeting: Beyond Discovery-Toward Understanding*. Ed. by B. Lites, M. Cheung, T. Magara, J. Mariska, and K. Reeves. Vol. 415. Astronomical Society of the Pacific Conference Series, p. 87.

Lewis, I. J., R. D. Cannon, K. Taylor, K. Glazebrook, J. A. Bailey, I. K. Baldry, J. R. Barton, T. J. Bridges, G. B. Dalton, T. J. Farrell, P. M. Gray, A. Lankshear, C. McCowage, I. R. Parry, R. M. Sharples, K. Shortridge, G. A. Smith, J. Stevenson, J. O. Straede, L. G. Waller, J. D. Whittard, J. K. Wilcox, and K. C. Willis (2002). "The Anglo-Australian Observatory 2dF facility". In: *MNRAS* 333, pp. 279–299. DOI: `10.1046/j.1365-8711.2002.05333.x`.

Lind, K., F. Primas, C. Charbonnel, F. Grundahl, and M. Asplund (2009). "Signatures of intrinsic Li depletion and Li-Na anti-correlation in the metal-poor globular cluster NGC 6397". In: *A&A* 503, pp. 545–557. DOI: `10.1051/0004-6361/200912524`.

Lind, K., M. Asplund, P. S. Barklem, and A. K. Belyaev (2011a). "Non-LTE calculations for neutral Na in late-type stars using improved atomic data". In: *A&A* 528, A103, A103. DOI: `10.1051/0004-6361/201016095`.

Lind, K., C. Charbonnel, T. Decressin, F. Primas, F. Grundahl, and M. Asplund (2011b). "Tracing the evolution of NGC 6397 through the chemical composition of its stellar populations". In: *A&A* 527, A148, A148. DOI: `10.1051/0004-6361/201015356`.

Lind, K., M. Bergemann, and M. Asplund (2012). "Non-LTE line formation of Fe in late-type stars - II. 1D spectroscopic stellar parameters". In: *MNRAS* 427, pp. 50–60. DOI: `10.1111/j.1365-2966.2012.21686.x`.

Lovisi, L., A. Mucciarelli, B. Lanzoni, F. R. Ferraro, R. Gratton, E. Dalessandro, and R. Contreras Ramos (2012). "Chemical and Kinematical Properties of Blue Straggler Stars and Horizontal Branch Stars in NGC 6397". In: *ApJ* 754, 91, p. 91. DOI: `10.1088/0004-637X/754/2/91`.

Lugaro, M., F. Herwig, J. C. Lattanzio, R. Gallino, and O. Straniero (2003). "s-Process Nucleosynthesis in Asymptotic Giant Branch Stars: A Test for Stellar Evolution". In: *ApJ* 586, pp. 1305–1319. DOI: `10.1086/367887`.

MacLean, B. T., G. M. De Silva, and J. Lattanzio (2015). "O, Na, Ba and Eu abundance patterns in open clusters". In: *MNRAS* 446, pp. 3556–3561. DOI: `10.1093/mnras/stu2348`.

MacLean, B. T., S. W. Campbell, G. M. De Silva, J. Lattanzio, V. D'Orazi, J. D. Simpson, and Y. Momany (2016). "An extreme paucity of second population AGB stars in the 'normal' globular cluster M4". In: *MNRAS* 460, pp. L69–L73. DOI: `10.1093/mnrasl/slw073`.

MacLean, B. T., S. W. Campbell, G. M. De Silva, J. Lattanzio, V. D'Orazi, P. L. Cottrell, Y. Momany, and L. Casagrande (2018a). "AGB subpopulations in the nearby globular cluster NGC 6397". In: *MNRAS* 475, pp. 257–265. DOI: 10.1093/mnras/stx3217.

MacLean, B. T., S. W. Campbell, A. M. Amarsi, T. Nordlander, P. L. Cottrell, G. M. De Silva, J. Lattanzio, T. Constantino, V. D'Orazi, and L. Casagrande (2018b). "On the AGB stars of M 4: A robust disagreement between spectroscopic observations and theory". In: *MNRAS, Submitted*.

Magic, Z., R. Collet, W. Hayek, and M. Asplund (2013). "The Stagger-grid: A grid of 3D stellar atmosphere models. II. Horizontal and temporal averaging and spectral line formation". In: *A&A* 560, A8, A8. DOI: 10.1051/0004-6361/201322252.

Malavolta, L., G. Piotto, L. R. Bedin, C. Sneden, V. Nascimbeni, and V. Sommariva (2015). "The M 4 Core Project with HST - IV. Internal kinematics from accurate radial velocities of 2771 cluster members". In: *MNRAS* 454, pp. 2621–2635. DOI: 10.1093/mnras/stv2158.

Mallia, E. A. (1975). "The asymptotic giant branch in NGC 6397". In: *MNRAS* 170, 57P–60P. DOI: 10.1093/mnras/170.1.57P.

— (1978). "Spectra of asymptotic giant branch stars in four southern globular clusters." In: *A&A* 70, pp. 115–123.

Marcolini, A., B. K. Gibson, A. I. Karakas, and P. Sánchez-Blázquez (2009). "The chemical evolution of globular clusters - I. Reactive elements and non-metals". In: *MNRAS* 395, pp. 719–735. DOI: 10.1111/j.1365-2966.2009.14591.x.

Marigo, P. and B. Aringer (2009). "Low-temperature gas opacity. ÆSOPUS: a versatile and quick computational tool". In: *Astron. Astrophys.* 508, pp. 1539–1569. DOI: 10.1051/0004-6361/200912598.

Marín-Franch, A., A. Aparicio, G. Piotto, A. Rosenberg, B. Chaboyer, A. Sarajedini, M. Siegel, J. Anderson, L. R. Bedin, A. Dotter, M. Hempel, I. King, S. Majewski, A. P. Milone, N. Paust, and I. N. Reid (2009). "The ACS Survey of Galactic Globular Clusters. VII. Relative Ages". In: *ApJ* 694, pp. 1498–1516. DOI: 10.1088/0004-637X/694/2/1498.

Marino, A. F., S. Villanova, G. Piotto, A. P. Milone, Y. Momany, L. R. Bedin, and A. M. Medling (2008). "Spectroscopic and photometric evidence of two stellar populations in the Galactic globular cluster NGC 6121 (M 4)". In: *A&A* 490, pp. 625–640. DOI: 10.1051/0004-6361:200810389.

Marino, A. F., S. Villanova, A. P. Milone, G. Piotto, K. Lind, D. Geisler, and P. B. Stetson (2011). "Sodium-Oxygen Anticorrelation Among Horizontal Branch Stars in the Globular Cluster M4". In: *ApJL* 730, L16, p. L16. DOI: 10.1088/2041-8205/730/2/L16.

Marino, A. F., A. P. Milone, D. Yong, G. Da Costa, M. Asplund, L. R. Bedin, H. Jerjen, D. Nardiello, G. Piotto, A. Renzini, and M. Shetrone (2017).

"Spectroscopy and Photometry of Multiple Populations along the Asymptotic Giant Branch of NGC 2808 and NGC 6121 (M4)". In: *ApJ* 843, 66, p. 66. DOI: `10.3847/1538-4357/aa7852`.

Martell, S. L., J. P. Smolinski, T. C. Beers, and E. K. Grebel (2011). "Building the Galactic halo from globular clusters: evidence from chemically unusual red giants". In: *A&A* 534, A136, A136. DOI: `10.1051/0004-6361/201117644`.

Mashonkina, L. I., T. N. Sitnova, and Y. V. Pakhomov (2016). "Influence of departures from LTE on calcium, titanium, and iron abundance determinations in cool giants of different metallicities". In: *AstL* 42, pp. 606–615. DOI: `10.1134/S1063773716080028`.

McClure, R. D. (1973). "The David Dunlap Observatory (ddo) Photometric System for Classification of Late-Type Stars". In: *Spectral Classification and Multicolour Photometry*. Ed. by C. Fehrenbach and B. E. Westerlund. Vol. 50. IAU Symposium, p. 162.

— (1979). "Observational evidence for abundance variations in stellar populations". In: *Mem. Societa Astronomica Italiana* 50, pp. 15–35.

McClure, R. D. and J. Norris (1977). "A CH star in the globular cluster M22, and the nature of CH and CN anomalies". In: *ApJL* 217, pp. L101–L104. DOI: `10.1086/182548`.

McDonald, I. and A. A. Zijlstra (2015). "Mass-loss on the red giant branch: the value and metallicity dependence of Reimers' η in globular clusters". In: *MNRAS* 448, pp. 502–521. DOI: `10.1093/mnras/stv007`.

McWilliam, A. (1997). "Abundance Ratios and Galactic Chemical Evolution". In: *ARAA* 35, pp. 503–556. DOI: `10.1146/annurev.astro.35.1.503`.

Meléndez, J. and B. Barbuy (2009). "Both accurate and precise gf-values for Fe II lines". In: *A&A* 497, pp. 611–617. DOI: `10.1051/0004-6361/200811508`.

Meylan, G. and M. Mayor (1986). "Studies of dynamical properties of globular clusters. II - The rotation, velocity dispersion and mass of Omega Centauri and 47 Tucanae". In: *A&A* 166, pp. 122–142.

Miglio, A., W. J. Chaplin, K. Brogaard, M. N. Lund, B. Mosser, G. R. Davies, R. Handberg, A. P. Milone, A. F. Marino, D. Bossini, Y. P. Elsworth, F. Grundahl, T. Arentoft, L. R. Bedin, T. L. Campante, J. Jessen-Hansen, C. D. Jones, J. S. Kuszlewicz, L. Malavolta, V. Nascimbeni, and E. L. Sandquist (2016). "Detection of solar-like oscillations in relics of the Milky Way: asteroseismology of K giants in M4 using data from the NASA K2 mission". In: *MNRAS* 461, pp. 760–765. DOI: `10.1093/mnras/stw1555`.

Milone, A. P. (2013). "Three parameters for the horizontal-branch morphology in globular clusters". In: *Mem. Societa Astronomica Italiana* 84, p. 79.

Milone, A. P. (2015). "Helium and multiple populations in the massive globular cluster NGC 6266 (M 62)". In: *MNRAS* 446, pp. 1672–1684. DOI: 10.1093/mnras/stu2198.

Milone, A. P., L. R. Bedin, G. Piotto, J. Anderson, I. R. King, A. Sarajedini, A. Dotter, B. Chaboyer, A. Marín-Franch, S. Majewski, A. Aparicio, M. Hempel, N. E. Q. Paust, I. N. Reid, A. Rosenberg, and M. Siegel (2008). "The ACS Survey of Galactic Globular Clusters. III. The Double Subgiant Branch of NGC 1851". In: *ApJ* 673, pp. 241–250. DOI: 10.1086/524188.

Milone, A. P., A. F. Marino, G. Piotto, L. R. Bedin, J. Anderson, A. Aparicio, S. Cassisi, and R. M. Rich (2012a). "A Double Main Sequence in the Globular Cluster NGC 6397". In: *ApJ* 745, 27, p. 27. DOI: 10.1088/0004-637X/745/1/27.

Milone, A. P., G. Piotto, L. R. Bedin, I. R. King, J. Anderson, A. F. Marino, A. Bellini, R. Gratton, A. Renzini, P. B. Stetson, S. Cassisi, A. Aparicio, A. Bragaglia, E. Carretta, F. D'Antona, M. Di Criscienzo, S. Lucatello, M. Monelli, and A. Pietrinferni (2012b). "Multiple Stellar Populations in 47 Tucanae". In: *ApJ* 744, 58, p. 58. DOI: 10.1088/0004-637X/744/1/58.

Milone, A. P., A. F. Marino, G. Piotto, L. R. Bedin, J. Anderson, A. Aparicio, A. Bellini, S., F. D'Antona, F. Grundahl, M. Monelli, and D. Yong (2013). "A WFC3/HST View of the Three Stellar Populations in the Globular Cluster NGC 6752". In: *ApJ* 767, 120, p. 120. DOI: 10.1088/0004-637X/767/2/120.

Milone, A. P., A. F. Marino, L. R. Bedin, G. Piotto, S. Cassisi, A. Dieball, J. Anderson, H. Jerjen, M. Asplund, A. Bellini, K. Brogaard, A. Dotter, M. Giersz, D. C. Heggie, C. Knigge, R. M. Rich, M. van den Berg, and R. Buonanno (2014). "The M 4 Core Project with HST - II. Multiple stellar populations at the bottom of the main sequence". In: *MNRAS* 439, pp. 1588–1595. DOI: 10.1093/mnras/stu030.

Milone, A. P., A. F. Marino, G. Piotto, L. R. Bedin, J. Anderson, A. Renzini, I. R. King, A. Bellini, T. M. Brown, S. Cassisi, F. D'Antona, H. Jerjen, D. Nardiello, M. Salaris, R. P. v. d. Marel, E. Vesperini, D. Yong, A. Aparicio, A. Sarajedini, and M. Zoccali (2015a). "The Hubble Space Telescope UV Legacy Survey of galactic globular clusters - II. The seven stellar populations of NGC 7089 (M2)". In: *MNRAS* 447, pp. 927–938. DOI: 10.1093/mnras/stu2446.

Milone, A. P., A. F. Marino, G. Piotto, A. Renzini, L. R. Bedin, J. Anderson, S. Cassisi, F. D'Antona, A. Bellini, H. Jerjen, A. Pietrinferni, and P. Ventura (2015b). "The Hubble Space Telescope UV Legacy Survey of Galactic Globular Clusters. III. A Quintuple Stellar Population in NGC 2808". In: *ApJ* 808, 51, p. 51. DOI: 10.1088/0004-637X/808/1/51.

Milone, A. P., A. F. Marino, L. R. Bedin, J. Anderson, D. Apai, A. Bellini, P. Bergeron, A. J. Burgasser, A. Dotter, and J. M. Rees (2017). "The HST large programme on ω Centauri - I. Multiple stellar populations at the bottom of the main sequence probed in NIR-Optical". In: *MNRAS* 469, pp. 800–812. DOI: 10.1093/mnras/stx836.

Mochejska, B. J., J. Kaluzny, I. Thompson, and W. Pych (2002). "Clusters Ages Experiment: Hot Subdwarfs and Luminous White Dwarf Candidates in the Field of the Globular Cluster M4". In: *AJ* 124, pp. 1486–1496. DOI: 10.1086/342015.

Momany, Y., G. Piotto, A. Recio-Blanco, L. R. Bedin, S. Cassisi, and G. Bono (2002). "A New Feature along the Extended Blue Horizontal Branch of NGC 6752". In: *Astrophys. J.* 576, pp. L65–L68. DOI: 10.1086/343125.

Momany, Y., S. Cassisi, G. Piotto, L. R. Bedin, S. Ortolani, F. Castelli, and A. Recio-Blanco (2003). "Why hot horizontal branch stars can appear redder than red giants". In: *A&A* 407, pp. 303–309. DOI: 10.1051/0004-6361:20030827.

Monelli, M., A. P. Milone, P. B. Stetson, A. F. Marino, S. Cassisi, A. del Pino Molina, M. Salaris, A. Aparicio, M. Asplund, F. Grundahl, G. Piotto, A. Weiss, R. Carrera, M. Cebrián, S. Murabito, A. Pietrinferni, and L. Sbordone (2013). "The SUMO project I. A survey of multiple populations in globular clusters". In: *MNRAS* 431, pp. 2126–2149. DOI: 10.1093/mnras/stt273.

Mucciarelli, A. (2011). "Microturbulent velocity from stellar spectra: a comparison between different approaches". In: *A&A* 528, A44, A44. DOI: 10.1051/0004-6361/201015814.

Mucciarelli, A., E. Lapenna, D. Massari, F. R. Ferraro, and B. Lanzoni (2015). "The Origin of the Spurious Iron Spread in the Globular Cluster NGC 3201". In: *ApJ* 801, 69, p. 69. DOI: 10.1088/0004-637X/801/1/69.

Mucciarelli, A., E. Lapenna, F. R. Ferraro, and B. Lanzoni (2018). "The chemical composition of NGC5824, a globular cluster without iron spread but with an extreme Mg-Al anticorrelation". In: *ArXiv e-prints*.

Nardiello, D., A. P. Milone, G. Piotto, A. F. Marino, A. Bellini, and S. Cassisi (2015). "Observing multiple stellar populations with VLT/FORS2. Main sequence photometry in outer regions of NGC 6752, NGC 6397, and NGC 6121 (M 4)". In: *A&A* 573, A70, A70. DOI: 10.1051/0004-6361/201424117.

Nordlander, T. and K. Lind (2017). "Non-LTE aluminium abundances in late-type stars". In: *A&A* 607, A75, A75. DOI: 10.1051/0004-6361/201730427.

Nordlander, T., A. M. Amarsi, K. Lind, M. Asplund, P. S. Barklem, A. R. Casey, R. Collet, and J. Leenaarts (2017). "3D NLTE analysis of the most iron-deficient star, SMSS0313-6708". In: *A&A* 597, A6, A6. DOI: 10.1051/0004-6361/201629202.

Norris, J. (1974). "Advanced evolution in globular clusters. II - The ultraviolet-bright stars in omega Centauri". In: *ApJ* 194, pp. 109–123. DOI: 10.1086/153228.

— (1981). "The cyanogen distribution of M4 and the possible connection between horizontal branch morphology and chemical inhomogeneity". In: *ApJ* 248, pp. 177–188. DOI: 10.1086/159141.

Norris, J. and G. H. Smith (1983). "The AL I-cyanogen correlation in the spectra of globular cluster red giants and the origin of intracluster heavy element variations". In: *ApJ* 272, pp. 635–645. DOI: 10.1086/161326.

Norris, J. and R. Zinn (1977). "The weak-G-band effect in M13, M92, NGC 6397, and M15." In: *ApJ* 215, pp. 74–88. DOI: 10.1086/155336.

Norris, J., P. L. Cottrell, K. C. Freeman, and G. S. Da Costa (1981). "The abundance spread in the giants of NGC 6752". In: *ApJ* 244, pp. 205–220. DOI: 10.1086/158698.

Osborn, W. (1971). "Two new CN-strong globular cluster stars". In: *The Observatory* 91, pp. 223–224.

Osorio, Y. and P. S. Barklem (2016). "Mg line formation in late-type stellar atmospheres. II. Calculations in a grid of 1D models". In: *A&A* 586, A120, A120. DOI: 10.1051/0004-6361/201526958.

Pasquini, L., G. Avila, A. Blecha, C. Cacciari, V. Cayatte, M. Colless, F. Damiani, R. de Propris, H. Dekker, P. di Marcantonio, T. Farrell, P. Gillingham, I. Guinouard, F. Hammer, A. Kaufer, V. Hill, M. Marteaud, A. Modigliani, G. Mulas, P. North, D. Popovic, E. Rossetti, F. Royer, P. Santin, R. Schmutzer, G. Simond, P. Vola, L. Waller, and M. Zoccali (2002). "Installation and commissioning of FLAMES, the VLT Multifibre Facility". In: *The Messenger* 110, pp. 1–9.

Pasquini, L., J. Alonso, G. Avila, P. Barriga, P. Biereichel, B. Buzzoni, C. Cavadore, C. Cumani, H. Dekker, B. Delabre, A. Kaufer, H. Kotzlowski, V. Hill, J.-L. Lizon, W. Nees, P. Santin, R. Schmutzer, A. V. Kesteren, and M. Zoccali (2003). "Installation and first results of FLAMES, the VLT multifibre facility". In: *Instrument Design and Performance for Optical/Infrared Ground-based Telescopes*. Ed. by M. Iye and A. F. M. Moorwood. Vol. 4841. Proc. SPIE, pp. 1682–1693. DOI: 10.1117/12.458915.

Peterson, C. J. (1974). "Distribution of Orbital Eccentricities of the Globular Clusters". In: *ApJL* 190, p. L17. DOI: 10.1086/181492.

Piotto, G., L. R. Bedin, J. Anderson, I. R. King, S. Cassisi, A. P. Milone, S. Villanova, A. Pietrinferni, and A. Renzini (2007). "A Triple Main Sequence in the Globular Cluster NGC 2808". In: *ApJL* 661, pp. L53–L56. DOI: 10.1086/518503.

Ramírez, I. and J. Meléndez (2005). “The Effective Temperature Scale of FGK Stars. II. T_{eff}:Color:[Fe/H] Calibrations”. In: *ApJ* 626, pp. 465–485. DOI: 10.1086/430102.

Reimers, D. (1975). “Circumstellar absorption lines and mass loss from red giants”. In: *Memoires of the Societe Royale des Sciences de Liege* 8, pp. 369–382.

Renzini, A. and A. Buzzoni (1986). “Global properties of stellar populations and the spectral evolution of galaxies”. In: *Spectral Evolution of Galaxies*. Ed. by C. Chiosi and A. Renzini. Vol. 122. Astrophysics and Space Science Library, pp. 195–231. DOI: 10.1007/978-94-009-4598-2_19.

Renzini, A., A. Bragaglia, F. R. Ferraro, R. Gilmozzi, S. Ortolani, J. B. Holberg, J. Liebert, F. Wesemael, and R. C. Bohlin (1996). “The White Dwarf Distance to the Globular Cluster NGC 6752 (and Its Age) with the Hubble Space Telescope”. In: *ApJL* 465, p. L23. DOI: 10.1086/310128.

Renzini, A., F. D’Antona, S. Cassisi, I. R. King, A. P. Milone, P. Ventura, J. Anderson, L. R. Bedin, A. Bellini, T. M. Brown, G. Piotto, R. P. van der Marel, B. Barbuy, E. Dalessandro, S. Hidalgo, A. F. Marino, S. Ortolani, M. Salaris, and A. Sarajedini (2015). “The Hubble Space TelescopeUV Legacy Survey of Galactic Globular Clusters - V. Constraints on formation scenarios”. In: *MNRAS* 454, pp. 4197–4207. DOI: 10.1093/mnras/stv2268.

Rosenberg, A., G. Piotto, I. Saviane, and A. Aparicio (2000). “Photometric catalog of nearby globular clusters. I. A large homogeneous (V,I) color-magnitude diagram data-base”. In: *A&AS* 144, pp. 5–38. DOI: 10.1051/aas:2000341.

Ruffoni, M. P., E. A. Den Hartog, J. E. Lawler, N. R. Brewer, K. Lind, G. Nave, and J. C. Pickering (2014). “Fe I oscillator strengths for the Gaia-ESO survey”. In: *MNRAS* 441, pp. 3127–3136. DOI: 10.1093/mnras/stu780.

Salaris, M., S. Degl’Innocenti, and A. Weiss (1997). “The Age of the Oldest Globular Clusters”. In: *ApJ* 479, pp. 665–672. DOI: 10.1086/303909.

Salaris, M., S. Cassisi, and A. Pietrinferni (2016). “On the red giant branch mass loss in 47 Tucanae: Constraints from the horizontal branch morphology”. In: *A&A* 590, A64, A64. DOI: 10.1051/0004-6361/201628181.

Sandage, A. (1986). “The population concept, globular clusters, subdwarfs, ages, and the collapse of the Galaxy”. In: *ARAA* 24, pp. 421–458. DOI: 10.1146/annurev.aa.24.090186.002225.

Sandage, A. and G. Wallerstein (1960). “Color-Magnitude Diagram for Disk Globular Cluster NGC 6356 Compared with Halo Clusters.” In: *ApJ* 131, p. 598. DOI: 10.1086/146872.

Sandage, A. and R. Wildey (1967). “The Anomalous Color-Magnitude Diagram of the Remote Globular Cluster NGC 7006”. In: *ApJ* 150, p. 469. DOI: 10.1086/149350.

Sandage, A. R. (1953). “The color-magnitude diagram for the globular cluster M 3.” In: *AJ* 58, pp. 61–75. DOI: 10.1086/106822.

Sandquist, E. L., M. Bolte, P. B. Stetson, and J. E. Hesser (1996). “CCD Photometry of the Globular Cluster M5. I. The Color-Magnitude Diagram and Luminosity Functions”. In: *ApJ* 470, p. 910. DOI: 10.1086/177920.

Saunders, W., T. Bridges, P. Gillingham, R. Haynes, G. A. Smith, J. D. Whittard, V. Churilov, A. Lankshear, S. Croom, D. Jones, and C. Boshuizen (2004). “AAOmega: a scientific and optical overview”. In: *Ground-based Instrumentation for Astronomy*. Ed. by A. F. M. Moorwood and M. Iye. Vol. 5492. Proc. SPIE, pp. 389–400. DOI: 10.1117/12.550871.

Schiavon, R. P., O. Zamora, R. Carrera, S. Lucatello, A. C. Robin, M. Ness, S. L. Martell, V. V. Smith, D. A. García-Hernández, A. Manchado, R. Schönrich, N. Bastian, C. Chiappini, M. Shetrone, J. T. Mackereth, R. A. Williams, S. Mészáros, C. Allende Prieto, F. Anders, D. Bizyaev, T. C. Beers, S. D. Chojnowski, K. Cunha, C. Epstein, P. M. Frinchaboy, A. E. García Pérez, F. R. Hearty, J. A. Holtzman, J. A. Johnson, K. Kinemuchi, S. R. Majewski, D. Muna, D. L. Nidever, D. C. Nguyen, R. W. O’Connell, D. Oravetz, K. Pan, M. Pinsonneault, D. P. Schneider, M. Schultheis, A. Simmons, M. F. Skrutskie, J. Sobeck, J. C. Wilson, and G. Zasowski (2017). “Chemical tagging with APOGEE: discovery of a large population of N-rich stars in the inner Galaxy”. In: *MNRAS* 465, pp. 501–524. DOI: 10.1093/mnras/stw2162.

Schlegel, D. J., D. P. Finkbeiner, and M. Davis (1998). “Maps of Dust Infrared Emission for Use in Estimation of Reddening and Cosmic Microwave Background Radiation Foregrounds”. In: *ApJ* 500, pp. 525–553. DOI: 10.1086/305772.

Schönberg, M. and S. Chandrasekhar (1942). “On the Evolution of the Main-Sequence Stars.” In: *ApJ* 96, p. 161. DOI: 10.1086/144444.

Schröder, K.-P. and M. Cuntz (2005). “A New Version of Reimers’ Law of Mass Loss Based on a Physical Approach”. In: *Astrophys. J.* 630, pp. L73–L76. DOI: 10.1086/491579.

Schwarzschild, M. (1970). “Stellar Evolution in Globular Clusters”. In: *QJRAS* 11, p. 12.

Sharp, R., W. Saunders, G. Smith, V. Churilov, D. Correll, J. Dawson, T. Farrel, G. Frost, R. Haynes, R. Heald, A. Lankshear, D. Mayfield, L. Waller, and D. Whittard (2006). “Performance of AAOmega: the AAT multi-purpose fiber-fed spectrograph”. In: *Society of Photo-Optical Instrumentation Engineers (SPIE) Conference Series*. Vol. 6269. Proc. SPIE, 62690G. DOI: 10.1117/12.671022.

Sheinis, A., B. Anguiano, M. Asplund, C. Bacigalupo, S. Barden, M. Birchall, J. Bland-Hawthorn, J. Brzeski, R. Cannon, D. Carollo, S. Case, A. Casey, V. Churilov, C. Warrick, R. Dean, G. De Silva, V. D'Orazi, L. Duong, T. Farrell, K. Fiegert, K. Freeman, F. Gabriella, L. Gers, M. Goodwin, D. Gray, A. Green, R. Heald, J. Heijmans, M. Ireland, D. Jones, P. Kafle, S. Keller, U. Klauser, Y. Kondrat, J. Kos, J. Lawrence, S. Lee, S. Mali, S. Martell, D. Mathews, D. Mayfield, S. Miziarski, R. Muller, N. Pai, R. Patterson, E. Penny, D. Orr, K. Schlesinger, S. Sharma, K. Shortridge, J. Simpson, S. Smedley, G. Smith, D. Stafford, N. Staszak, M. Vuong, L. Waller, E. W. de Boer, P. Xavier, J. Zheng, R. Zhelem, D. Zucker, and T. Zwitter (2015). "First light results from the High Efficiency and Resolution Multi-Element Spectrograph at the Anglo-Australian Telescope". In: *Journal of Astronomical Telescopes, Instruments, and Systems* 1.3, 035002, p. 035002. DOI: 10.1117/1.JATIS.1.3.035002.

Simpson, J. D., G. De Silva, S. L. Martell, C. A. Navin, and D. B. Zucker (2017). "ESO 452-SC11: the lowest mass globular cluster with a potential chemical inhomogeneity". In: *MNRAS* 472, pp. 2856–2868. DOI: 10.1093/mnras/stx2174.

Sitnova, T., G. Zhao, L. Mashonkina, Y. Chen, F. Liu, Y. Pakhomov, K. Tan, M. Bolte, S. Alexeeva, F. Grupp, J.-R. Shi, and H.-W. Zhang (2015). "Systematic Non-LTE Study of the -2.6 < [Fe/H] < 0.2 F and G dwarfs in the Solar Neighborhood. I. Stellar Atmosphere Parameters". In: *ApJ* 808, 148, p. 148. DOI: 10.1088/0004-637X/808/2/148.

Skrutskie, M. F., R. M. Cutri, R. Stiening, M. D. Weinberg, S. Schneider, J. M. Carpenter, C. Beichman, R. Capps, T. Chester, J. Elias, J. Huchra, J. Liebert, C. Lonsdale, D. G. Monet, S. Price, P. Seitzer, T. Jarrett, J. D. Kirkpatrick, J. E. Gizis, E. Howard, T. Evans, J. Fowler, L. Fullmer, R. Hurt, R. Light, E. L. Kopan, K. A. Marsh, H. L. McCallon, R. Tam, S. Van Dyk, and S. Wheelock (2006). "The Two Micron All Sky Survey (2MASS)". In: *AJ* 131, pp. 1163–1183. DOI: 10.1086/498708.

Smith, G. H. (1987). "The chemical inhomogeneity of globular clusters". In: *PASP* 99, pp. 67–90. DOI: 10.1086/131958.

— (2015). "A Comparison Between the Patterns of CN, O, and Na Inhomogeneities on the Red Giant Branch of Messier 71 Using Data from the Literature". In: *PASP* 127, p. 1204. DOI: 10.1086/684099.

Smith, G. H. and M. M. Briley (2005). "CN Abundance Inhomogeneities in the Globular Cluster Messier 4 (NGC 6121): Results Based on Merged Data Sets from the Literature". In: *PASP* 117, pp. 895–910. DOI: 10.1086/444485.

Smith, G. H. and J. E. Norris (1993). "CN variations among asymptotic giant branch and horizontal branch stars in the intermediate metallicity globular clusters M5, M4, and NGC 6752". In: *AJ* 105, pp. 173–183. DOI: 10.1086/116418.

Smith, G. H., A. K. Dupree, and J. Strader (2014). "A Study of the λ10830 He I Line Among Red Giants in Messier 13". In: *PASP* 126, p. 901. DOI: 10.1086/678542.

Sneden, C. (1999). "Abundances in Globular Clusters". In: *Astrophysics and Space Science* 265, pp. 145–152. DOI: 10.1023/A:1002122502384.

Sneden, C., R. P. Kraft, M. D. Shetrone, G. H. Smith, G. E. Langer, and C. F. Prosser (1997). "Star-To-Star Abundance Variations Among Bright Giants in the Metal-Poor Globular Cluster M15". In: *AJ* 114, p. 1964. DOI: 10.1086/118618.

Sneden, C., I. I. Ivans, and R. P. Kraft (2000). "Do AGB stars differ chemically from RGB stars in globular clusters ?" In: *Mem.Soc.Ast.It.* 71, pp. 657–665.

Sneden, C. A. (1973). "Carbon and Nitrogen Abundances in Metal-Poor Stars." PhD thesis. The University of Texas at Austin.

Sousa, S. G. (2014). "ARES+MOOG - a practical overview of an EW method to derive stellar parameters". In: *ArXiv e-prints*.

Sousa, S. G., N. C. Santos, V. Adibekyan, E. Delgado-Mena, and G. Israelian (2015). "ARES v2: new features and improved performance". In: *A&A* 577, A67, A67. DOI: 10.1051/0004-6361/201425463.

Spruit, H. C. (2015). "The growth of helium-burning cores". In: *A&A* 582, L2, p. L2. DOI: 10.1051/0004-6361/201527171.

Stetson, P. B. (2000). "Homogeneous Photometry for Star Clusters and Resolved Galaxies. II. Photometric Standard Stars". In: *PASP* 112, pp. 925–931. DOI: 10.1086/316595.

Suntzeff, N. B. and V. V. Smith (1991). "Carbon isotopic abundances in giant stars in the CN-bimodal globular clusters NGC 6752 and M4". In: *ApJ* 381, pp. 160–172. DOI: 10.1086/170638.

Sweigart, A. V. (1997). "Effects of Helium Mixing on the Evolution of Globular Cluster Stars". In: *ApJL* 474, pp. L23–L26. DOI: 10.1086/310414.

Sweigart, A. V. and M. Catelan (1998). "The Second-Parameter Effect in Metal-rich Globular Clusters". In: *ApJL* 501, pp. L63–L66. DOI: 10.1086/311443.

Sweigart, A. V. and P. G. Gross (1978). "Evolutionary sequences for red giant stars". In: *ApJS* 36, pp. 405–437. DOI: 10.1086/190506.

Takeda, Y. (2003). "Oxygen line formation in late-F through early-K disk/halo stars. Infrared O I triplet and [O I] lines". In: *A&A* 402, pp. 343–359. DOI: 10.1051/0004-6361:20030217.

Tody, D. (1986). "The IRAF Data Reduction and Analysis System". In: *Instrumentation in Astronomy VI*. Ed. by D. L. Crawford. Vol. 627. Proc. SPIE, p. 733.

Valcarce, A. A. R., M. Catelan, J. Alonso-García, C. Cortés, and J. R. De Medeiros (2014). "Constraints on Helium Enhancement in the Globular Cluster M4 (NGC 6121): The Horizontal Branch Test". In: *ApJ* 782, 85, p. 85. DOI: `10.1088/0004-637X/782/2/85`.

Valcarce, A. A. R., M. Catelan, J. Alonso-García, R. Contreras Ramos, and S. Alves (2016). "Level of helium enhancement among M3's horizontal branch stars". In: *A&A* 589, A126, A126. DOI: `10.1051/0004-6361/201526387`.

Vassiliadis, E. and P. R. Wood (1993). "Evolution of low- and intermediate-mass stars to the end of the asymptotic giant branch with mass loss". In: *ApJ* 413, pp. 641–657. DOI: `10.1086/173033`.

Ventura, P., F. D'Antona, I. Mazzitelli, and R. Gratton (2001). "Predictions for Self-Pollution in Globular Cluster Stars". In: *ApJL* 550, pp. L65–L69. DOI: `10.1086/319496`.

Villanova, S., D. Geisler, G. Piotto, and R. G. Gratton (2012). "The Helium Content of Globular Clusters: NGC 6121 (M4)". In: *ApJ* 748, 62, p. 62. DOI: `10.1088/0004-637X/748/1/62`.

Wang, Y., F. Primas, C. Charbonnel, M. Van der Swaelmen, G. Bono, W. Chantereau, and G. Zhao (2016). "Sodium abundances of AGB and RGB stars in Galactic globular clusters. I. Analysis and results of NGC 2808". In: *A&A* 592, A66, A66. DOI: `10.1051/0004-6361/201628502`.

— (2017). "Sodium abundances of AGB and RGB stars in Galactic globular clusters. II. Analysis and results of NGC 104, NGC 6121, and NGC 6809". In: *A&A* 607, A135, A135. DOI: `10.1051/0004-6361/201730976`.

Woosley, S. E., A. Heger, and T. A. Weaver (2002). "The evolution and explosion of massive stars". In: *Reviews of Modern Physics* 74, pp. 1015–1071. DOI: `10.1103/RevModPhys.74.1015`.

Yong, D., F. Grundahl, D. L. Lambert, P. E. Nissen, and M. D. Shetrone (2003). "Mg isotopic ratios in giant stars of the globular cluster NGC 6752". In: *A&A* 402, pp. 985–1001. DOI: `10.1051/0004-6361:20030296`.

Yong, D., F. Grundahl, P. E. Nissen, H. R. Jensen, and D. L. Lambert (2005). "Abundances in giant stars of the globular cluster NGC 6752". In: *A&A* 438, pp. 875–888. DOI: `10.1051/0004-6361:20052916`.

Yong, D., J. Meléndez, F. Grundahl, I. U. Roederer, J. E. Norris, A. P. Milone, A. F. Marino, P. Coelho, B. E. McArthur, K. Lind, R. Collet, and M. Asplund (2013). "High precision differential abundance measurements in globular clusters: chemical inhomogeneities in NGC 6752". In: *MNRAS* 434, pp. 3542–3565. DOI: `10.1093/mnras/stt1276`.

Yong, D., F. Grundahl, and J. E. Norris (2015). "CNO abundances in the globular clusters NGC 1851 and NGC 6752". In: *MNRAS* 446, pp. 3319–3329. DOI: `10.1093/mnras/stu2334`.

Zinn, R. (1973). "The G-Band Anomaly of the Asymptotic-Branch Stars in M92". In: *ApJ* 182, pp. 183–188. DOI: 10.1086/152129.

— (1974). "Advanced Evolution in Globular Clusters. the Ultraviolet-Bright Stars in Eight Globular Clusters". In: *ApJ* 193, pp. 593–606. DOI: 10.1086/153197.

— (1977). "A spectroscopic survey of the giant branch of M5". In: *ApJ* 218, pp. 96–104. DOI: 10.1086/155661.